Universitat Ramon Llull

TESI DOCTORAL

Títol **Graph theory applied to transmission path problems in vibroacoustics**

Realitzada per **Àngels Aragonès Martín**

en el Centre **Escola Tècnica Superior d'Enginyeria Electrònica i Informàtica La Salle**

i en el Departament d'**Enginyeria.**

Dirigida per **Dr. Oriol Guasch Fortuny**

C. Claravall, 1-3
08022 Barcelona
Tel. 936 022 200
Fax 936 022 249
E-mail: urlsc@sec.url.es
www.url.es

GRAPH THEORY APPLIED TO TRANSMISSION PATH PROBLEMS IN VIBROACOUSTICS

by

ÀNGELS ARAGONÈS MARTÍN

Grup de Recerca en Tecnologies Mèdia

Enginyeria i Arquitectura La Salle

Universitat Ramon Llull

Submitted in accordance with the requirements for the Degree of

Doctor of Philosophy

Supervised by:

Dr. Oriol Guasch Fortuny

Àngels Aragonès Martín: *Graph theory applied to transmission path problems in vibroacoustics,* PhD program: Information Technologies and its Management, April 2015

Als meus pares, Coia i Josep Maria.

ABSTRACT

A fundamental aspect when solving a vibroacoustic problem in a mechanical system is that of finding out how energy flows from a given source to any part of the system. This would help making decisions to undertake actions for diminishing, for example, the noise or vibration levels at a given system area. The dynamic behavior of a mechanical system can be estimated using different numerical methods, each of them targeting a certain frequency range. Whereas at low frequencies deterministic methods such as the Finite Element Method (FEM) or the Boundary Element Method (BEM) can be applied, statistical methods like Statistical Energy Analysis (SEA) become unavoidable at high frequencies. In addition, a large variety of approaches such as the hybrid FE-SEA, the Energy Distribution (ED) models or the Statistical modal Energy distribution Analysis (SmEdA), among many others, have been recently proposed to tackle with the so-called mid-frequency problem. However, although numerical methods can predict the pointwise or averaged vibroacoustic response of a system, they do not directly provide information on how energy flows throughout the system. Therefore, some kind of post-processing is required to determine energy transmission paths.

The energy transmitted through a particular path linking a source subsystem, where external energy is being input, and a target subsystem, can be computed numerically. Yet, identifying which paths dominate the whole energy transmission from source to target usually relies on the engineer's expertise and judgement. Thus, an approach for the automatic identification of those paths would prove very useful. Graph theory provides a way out to this problem, since powerful path algorithms for graphs are available. In this thesis, a link between vibroacoustic models and graph theory is proposed, which allows one to address energy transmission path problems in a straightforward manner.

The dissertation starts focusing on SEA models. It is first shown that performing a transmission path analysis (TPA) in SEA makes sense. Then a graph that accurately represents the SEA model is defined. Given that the energy transmission between sources and targets is justified by the contribution of a limited group of dominant paths in many cases of practical interest, an algorithm to find them is presented. Thereafter, an enhanced algorithm is devised to include the stochastic nature of SEA loss factors in the ranking of paths. Next, it is discussed how transmission path analysis can be extended to the mid frequency range. The graph approach for path computation becomes adapted for some ED models, as well as for SmEdA. Finally, we outline another possible application of graph theory to vibroacoustics. A graph cut algorithm strategy is implemented to achieve energy reduction at a target subsystem with the sole modification of a reduced set of loss factors. The set is found by computing cuts in the graph separating source and receiver subsystems.

ACKNOWLEDGEMENTS

En primer lloc, voldria encapçalar aquesta llista d'agraïments amb el tutor i director de la meva tesi, el Dr. Oriol Guasch, per haver confiat en mi i per haver-me donat l'oportunitat de començar a fer recerca. Per transmetre'm la passió per aquest ofici i per ensenyar-me, entre moltes altres coses, com n'és d'important estimar la feina que fas. També li vull agrair les tones de paciència que ha tingut amb mi durant tots aquests anys. (Espero que no renunciï a tenir més dones doctorands, després d'això.) Però sobretot, li vull agrair que es mostrés tan comprensiu en els moments més delicats, sóc conscient que no tothom ho hauria fet.

Voldria continuar pel Dr. Francesc Alías, el Xuti, per haver estat el meu padrí en l'ombra. Per no tenir mai un no quan es tractava d'escoltar-me i per tots els consells que segur que m'han portat a millor port. Si la qualitat humana es pogués quantificar, en Xuti sobrepassaria tots els límits.

La família de La Salle no s'acaba aquí i en la majoria de famílies hi ha un germà gran disposat a tot, malgrat els martiris freqüents. Ramon, gràcies per ser tan "espectacular" i no haver fallat mai.

Durant tots aquests anys, hi ha hagut molts mals dies encara que ara mateix només recordi els moments bons. Gràcies Marc Freixes, Raúl, Alan i les teves carmanyoles de fruita, Marc Arnela, Rosa i Xavi Sevillano per tos els riures que han estat un al·licient més per venir a treballar i sobretot per haver-me aguantat durant els moments en els que estava més insuportable. Costarà trobar companys que us estiguin a l'alçada. No em vull oblidar els que ja no corren per aquí: Ester Creixell, Carlos García i Xavi Valero, tots heu deixat empremta, ni als nous fitxatges: Ale i Patricia, estic segura que mantindreu el pavelló ben alt.

Gràcies també al Joan Navarro per haver estat sempre disposat a donar un cop de mà, a l'Àlex Barco pels seus ànims en els moments més indicats i al Marcos Hervás per les pauses reconstituents plenes de rialles.

Gràcies a la Lisa Kinnear per revisar algun dels textos d'aquest manuscrit. A la Tero, la Regina i el Xavi de la biblioteca, i l'Andrea del Pozo i la Cristina Costa del rectorat, per haver-me fet la vida més fàcil. A la Lidia, la Carmen, el Gus, la May, la Lucía i el Carlos pels cafès que m'han fet posar de bon humor tantes vegades i per l'afecte que em demostren cada dia.

I would like to thank Dr. Laurent Maxit for giving me the opportunity of going to Lyon. Many thanks to all the colleagues at the LVA for their warm welcome. I want to give special thanks to Thibault Lafont and Antonio Pereira for helping me in the fight with the French bureaucracy. But, above all, I want to thank Valentin and Youssef for making of Lyon a home away from home. My time in France would have never been so nice without you and I hope we can enlarge our list of good memories together.

Per sort, també hi ha vida fora de la recerca. Vull agrair al Diego tot el suport que m'ha donat des de gairebé l'inici dels temps, per ser dels pocs capaços de fer-me reaccionar quan més convenia. A l'Uri Bielsa, per totes les cerveses que hem utilitzat de vàlvula d'escapament i per totes les que vindran. Al Sergio, per ser un amic incondicional i per les nits de festa que feien emprendre els dilluns amb més ganes.

A tu, Lluís, mai et podré agrair tot el que fas per mi, no es pot escriure en un paper. Gràcies per ser el millor company de viatge, per fer-me llevar cada dia de bon humor i amb un somriure, per creure en mi quan jo no n'era capaç i per donar-me forces per continuar. Les condicions no eren les òptimes i malgrat tot ens n'hem sortit. Ben aviat estaràs escrivint els agraïments de la teva tesi i oblidarem tot el que hem suat.

Per últim i més important, vull agrair a la meva família que m'hagi donat suport des del principi, malgrat no sabessin molt bé on m'estava posant. Vull donar les gràcies als meus pares Josep Maria i Coia, per haver-me aplanat tant el camí i per haver-me donat l'oportunitat de triar a cada moment el que volia fer. En especial, vull agrair al meu pare que ens hagi inculcat des de petites la importància de l'esforç i d'aconseguir les coses per nosaltres mateixes. A la mare per haver-me transmès l'afany de la feina ben feta i la curiositat per saber. A la Marta, per ser el meu referent i posar-me el llistó tan alt. I al meu cunyat Marc i la meva neboda Rut, per aportar la calma enmig del caos. No hi ha cap altre equip al que preferiria pertànyer.

FUNDING

This research has been financially supported by the Generalitat de Catalunya (SUR/ECO) under the pre-doctoral FI grants No. 2012 FI_B 01219, No. 2013 FI_B1 00062 and No. 2014 FI_B2 00141.

The author also would like to acknowledge the Labex CeLyA of Université de Lyon, operated by the French National Research Agency, for being invited for a short stay at INSA-Lyon, under the supervision of Dr. Laurent Maxit.

CONTENTS

LIST OF FIGURES

LIST OF TABLES

LIST OF ALGORITHMS

ACRONYMS

ASMA Asymptotical Scaled Modal Analysis

BEM Boundary Element Method

CLF Coupling Loss Factor

CPP Coupling Power Proportionality

DFDS Direct Field Dynamic Stiffness

DMF Dual Modal Formulation

ED Energy Distribution

EEPS Elasticized Expanded PolyStyrene

EIC Energy Influence Coefficient

ENR Energy Noise Reduction

FE-SEA Finite Element - Statistical Energy Analysis

FEM Finite Element Method

ILF Internal Loss Factor

MIMO Multiple Input Multiple Output

MISO Multiple Input Single Output

NCT Noise Control Treatment

NVH Noise, Vibration and Harshness

SEA Statistical Energy Analysis

SISO Single Input Single Output

SmEdA Statistical modal Energy distribution Analysis

TLF Total Loss Factor

TPA Transmission Path Analysis

1 INTRODUCTION

1.1 BACKGROUND

Over the last decades, vibroacoustics has become a necessary aspect to consider in many type of industries. For instance, in the automotive industry, attention is increasingly paid to improving the passengers comfort. This implies reducing the noise and vibration levels in the passengers cabin. The same could be applied to trains, planes and ships.

In the building industry, the standards regarding the admissible noise levels in dwelling have customarily been raised due to increasing social awareness. Furthermore, not only noise and vibration issues are a concern to human well-being but also they may affect the endurance of the operating life of structures, i.e. excessive vibrations can cause damages in the structure itself.

In all of these situations, it is important to know the behaviour of the mechanical systems in order to solve noise and vibration problems such as the aforementioned. The dynamic characteristics of the mechanical system can be obtained by means of a vibroacoustic analysis, which shall be conducted experimentally or numerically. The experimental approaches are all based on measurements over the built-up system. For instance, to obtain the vibration modes of a system, one may perform experimental modal analysis whereas a Transmission Path Analysis (TPA) provides information on how the energy is transmitted throughout the system. On the other hand, the numerical methods, which will be described next, predict the response of the system according to some input parameters. Usually, both approaches are combined and the experimental methods are used to validate and adjust the predictions obtained by the numerical methods. In this thesis, we will focus on numerical approaches.

Typically, the dynamic vibroacoustic response of a system is to be analysed over a wide frequency range. For example, the human hearing range extends from 20 Hz to 20 kHz. Thus, a noise problem analysis should consider all this frequency span.

However, the dynamic characteristics of a system are not uniform throughout the whole range. Typically, one may distinguish between low frequency, mid-frequency and high frequency behaviour. The analysis in each of these frequency

regimes has to be tackled in a different way. Therefore, specific analysis methods are implemented depending on the target frequency range.

On the one hand, the vibration in the low frequency range is characterized by a small number of modes, which are well-separated. Moreover, since the characteristic wavelength of the modes is large, the response is not affected by small variations of the physical parameters. Accordingly, deterministic approaches can be used. The most common methods in the low frequency range are element based methods such as the Finite Element Method (FEM) or the Boundary Element Method (BEM).

On the other hand, the response at high frequencies is driven by a high population of modes which overlap one another. In this case, the large number of modes make computationally unaffordable the methods used in low frequency. In addition, the wavelength is short and thus, the numerical predictions become very sensitive to uncertainty. As a consequence, deterministic approaches make no sense and statistical methods such as Statistical Energy Analysis (SEA) become necessary.

Finally, the mid-frequency range covers a gap where neither low frequency nor high frequency requisites are fulfilled. Deterministic methods cannot account for a certain degree of uncertainty whereas there is not enough number of modes for obtaining accurate results from a statistical analysis. The approaches for mid frequencies thus combine characteristics of the previous methods. For instance, the hybrid FE-SEA method applies a deterministic or statistical treatment to every component of the system respectively, according to their frequency behaviour. Alternatively, methods such as Energy Distribution (ED) analysis or Statistical modal Energy distribution Analysis (SmEdA) aim at relaxing the Statistical Energy Analysis requirements to be applicable in the mid-frequency range.

1.2 THESIS OBJECTIVES

The numerical methods mentioned in the preceding section provide a description of the system response in a certain frequency range. However, in some situations, this data does not suffice to solve noise and vibration problems and further exploitation of the results is needed. A useful approach is that of identifying the energy transmission paths in the system, i.e. how the energy is transmitted from a certain source to any target substructure of the system. Transmission path analysis is a well-established technique at high frequencies. The vibration modes are mostly local and the system can be divided in subsystems. As a consequence, the definition of a power flow between subsystems makes sense. One of the issues of this thesis is determining if TPA can be extended to lower frequencies, i.e. to the mid-frequency range.

There are several experimental approaches to perform a transmission path analysis in a system. However, a computational method to identify them is still needed. Graph theory is the most appropriate mathematical framework when it

comes to path computation since very efficient algorithms have been developed to that purpose. Therefore, the main purpose of this dissertation is to apply graph theory to obtain the energy transmission paths in a vibroacoustic system. To that end, a link between graph theory and the numerical methods used in vibroacoustics should be established by defining a graph for representing each vibroacoustic model. Next, graph theory algorithms should be adapted to identify the energy transmission paths in the system.

In conclusion, the main objectives of this thesis can be summarized as follows.

- Determining in which cases it is possible to establish a link between graph theory and numerical methods for mid and high frequency vibroacoustic analysis.
- Adapting graph theory algorithms for computing energy transmission paths in SEA, ED and SmEdA models.
- Attempting to exploit graph theory to implement automatic methods for vibroacoustic energy reduction in mechanical systems.

1.3 OUTLINE

The dissertation is organised in eight chapters whose contents are introduced in what follows.

Chapter 2 Vibroacoustics and graph theory provides the basic theoretical concepts for the understanding of the thesis discussion. First, the numerical methods used in vibroacoustics are reviewed. Special emphasis is given to Statistical Energy Analysis, Energy Distribution Analysis and Statistical modal Energy distribution Analysis, since the graph theory approach proposed in this thesis deals with these kinds of models. Then, the potential of TPA is introduced. Next, we provide some basis of graph theory. Finally, the first link between graph theory and vibroacoustic models, in this case SEA models, is established by defining a SEA graph.

Chapter 3 Finding the dominant energy transmission paths in Statistical Energy Analysis justifies the existence, in some cases, of a finite group of dominant paths which govern the energy transmission in a SEA system. In addition, it presents the MPS algorithm which is adapted to obtain the mentioned group of paths in a SEA graph. The algorithm is applied to a numerical example consisting of a simplified building model.

Chapter 4 Ranking paths in Statistical Energy Analysis models with non-deterministic loss factors considers the stochastic nature of the loss factors in a SEA system when determining the group of the most dominant energy transmission paths. This implies some variations on the definition of the graph and the implementation of the algorithm. The approach is applied

to two test cases, consisting of a building and a satellite's mock-up, and the results are compared with those obtained from a deterministic analysis.

Chapter 5 Conditions for transmission path analysis in Energy Distribution models presents a first attempt to extend graph theory TPA to mid-frequency methods. The mathematical requirements to perform the analysis are discussed. The ED graph is defined and the algorithm to obtain the most dominant energy transmission paths in an ED model is applied to a small benchmark system composed by 6 steel plates.

Chapter 6 A graph theory approach to identify resonant and non-resonant transmission paths in Statistical modal Energy distribution Analysis particularizes the path ranking approach for SmEdA models. The SmEdA matrix is proven to fulfill the requirements to perform TPA so a SmEdA graph can be defined. The method is evaluated on two simple systems, comprising two cavities separated by an homogeneous and a ribbed plate, respectively, and a more realistic case consisting of a shipbuilding.

Chapter 7 A graph cut strategy for transmission path problems in Statistical Energy Analysis presents a method to reduce the energy in SEA subsystems based on the fact that when the transmission paths connecting two subsystems are cut, the subsystems become isolated. To that end, graph cut algorithms are adapted to the SEA graph. The results are used to find the minimum number of modifications to apply in the system in order to obtain the desired energy reduction. The method is tested in two different simplified building models.

Chapter 8 closes the thesis with the conclusions and proposes some future work lines.

2

VIBROACOUSTICS AND GRAPH THEORY

Summary. This chapter provides the theoretical bases of the several topics viewed in this thesis. First of all, in Section 2.1, a review of the numerical methods used to solve vibroacoustic problems is done. Next, in Sections 2.2 to 2.4, the three methods that will be considered in this thesis are revisited in detail. They are the Statistical Energy Analysis (SEA), the Energy Distribution (ED) Analysis and the Statistical modal Energy distribution Analysis respectively (SmEdA). In Section 2.5, the notion of energy transmission paths is introduced and the importance of practicing a transmission path analysis in noise and vibration problems is justified. The main contribution of this thesis is the application of graph theory to solve some NVH problems. Thus, Section 2.6 presents the basic graph theory concepts needed to understand the developments in the following chapters. Finally, Section 2.7 shows how graph theory can be easily linked to SEA, one of the numerical methods presented earlier. This result will be used in the following chapters as a reference to establish connections between graph theory and other numerical methods.

2.1 INTRODUCTION TO MODELLING IN VIBROACOUSTICS

2.1.1 *Low and high frequency numerical methods*

The vibroacoustic behaviour of a physical system can be modelled using several numerical methods. The most common criterium to classify them is according to the frequency range, i.e. low frequency, mid frequency and high frequency methods. As a first approximation, to determine the frequency range, the characteristic physical dimension of the system may be compared to the dominant wavelength in the dynamic response. Therefore, when the wavelength is larger or comparable to the dimensions of the system, it is considered a low frequency response. On the contrary, when the wavelength is considerably smaller, the problem is set at high frequencies. Finally, the mid frequency range corresponds to two possible situations. First, the intermediate case where the wavelength is neither comparable to the system dimensions nor small enough to be considered high frequency. Second, the case when some components show low frequency behavior and some others show high frequency behavior.

Each frequency range has its own characteristics and that is the reason why each method has a limited scope of validity [Deckers et al., 2014]. In the low frequency range, deterministic approaches can be used to predict the vibration modes because there are few modes and they are well-separated. The most applied techniques are the Finite Element Method (FEM) and the Boundary Element Method (BEM). These are element-based methods because they consist in dividing the problem domain or its boundary into a large set of small elements. The problem unknowns are approximated by polynomials inside every element. The size of the element is chosen to guarantee the accuracy of the approximations, typically, between 6 and 10 elements per wavelength are needed [Ihlenburg, 1998]. As the frequency increases and hence the wavelength shortens, more elements increasing the matrix system dimensions become necessary. As a result, the increase of the computational cost limits the application of these methods to low frequencies. (See e.g. [Hughes, 2000; Petyt, 2010; Wu, 2000] for a detailed description of these methods.)

In the high frequency range, the opposite situation is found: the modal density and the modal overlap are high. In addition, since the wavelength is short, the system behaviour becomes more sensitive to small variations in the physical parameters. Therefore, taking into account that in a real context such variations are unavoidable, determining the response of a single system becomes meaningless and average responses shall be computed instead. Consequently, statistical approaches such as the Statistical Energy Analysis (SEA) [Lyon and DeJong, 1998] are the most used methods. In SEA, the system is divided into a small group of subsystems and the spatially averaged energy level is computed for each of them. The number of degrees of freedom in SEA corresponds to the number of subsystems, which makes the computational cost fairly affordable. However, the assumptions that are made to allow ensemble averaging are only fulfilled at high frequencies. Consequently, statistical methods are restricted to this frequency range. The SEA method will be reviewed in detail in Section 2.2.

2.1.2 *The mid frequency problem*

As mentioned above, there is a frequency gap where none of the above mentioned methods can be used for the correct description of the system response. Two situations are possible. On the one hand, the characteristics of the response may fall in between those that would distinguish a low or high frequency response respectively. On the other hand, the system may not present a uniform dynamic behaviour. In other words, some elements of the system are small in comparison with the characteristic wavelength whereas others are large. The mid-frequency methods appear to fill this frequency gap.

In recent years, several strategies have been followed to tackle the mid-frequency problem. They can be sorted in three groups. The first includes the methods which try to extend the applicability of low frequency methods to higher frequencies. For instance, the Wave Based Methods (WBM) which

adopt exact solutions of the governing partial differential equations as basis functions, instead of the polynomial bases of finite elements [Deckers et al., 2014; Desmet, 1998]. Another option could be the scaling procedure proposed in the asymptotical scaled modal analysis (ASMA) in [De Rosa and Franco, 2008]. Finally, there is a group of methods which aim at enhancing the performance of the element-based approaches such as optimised solvers, domain decomposition methods or multipole methods (see [Deckers et al., 2014] and references therein).

The second category is made up of approaches that try to extend the statistical methods to lower frequencies. For instance, proposing alternatives to compute the SEA parameters like the Energy Distribution Methods [Mace and Shorter, 2000] or attempting to relax the SEA assumptions which restrict the validity of SEA to a limited number of cases. For example, the Statistical modal Energy distribution Analysis (SmEdA) no longer requires the modal energy equipartition imposed by SEA [Maxit and Guyader, 2001a, 2003]. These methods will be viewed in detail in Sections 2.3 and 2.4.

The last class consists in combining statistical and deterministic approaches, to deal with the cases where there is a mix of dynamic behaviour, as described before. In such cases, hybrid strategies are proposed. One of them is the FE/SEA approaches which uses FE for the deterministic components and SEA for the highly random components [Cotoni et al., 2005; Langley and Cordioli, 2009].

The main difficulty of these methods is that of coupling FE and SEA in the same model, since both methods are quite different. On the one hand, SEA relies on the conservation of energy whereas FE relies on dynamic equilibrium. On the other, SEA is a statistical method while FE is deterministic. Probably the most extended hybrid FE-SEA method is that in [Shorter and Langley, 2005] that bases the coupling between FE and SEA on wave concepts. This method provides an average response over an ensemble of systems where the randomness is concentrated only in the parts modelled using SEA.

In a nutshell, the method goes as follows. FE is used to model the deterministic components and SEA is used for the random components, modelling them as SEA subsystems. Before explaining how to make the FE-SEA coupling possible, a distinction has to be made. The response of a SEA subsystem can be divided in two parts: The direct field, which corresponds to the initial generated waves and the reverberant field which corresponds to the waves resulting on the first and subsequent boundary reflections. The direct field of each SEA subsystem is represented by the direct field dynamic stiffness (DFDS) matrix. The uncertainties in the system are associated to the wave reflections on boundaries and interior scattering devices, i.e. to the reverberant field. Therefore, the DFDS matrices are deterministic across the ensemble.

The first step of the hybrid FE-SEA method is to identify which parts of the system can be modelled as SEA subsystems leaving the rest for a general FE model. The DFDS matrices of the SEA subsystems are added to the FE model to include the degrees of freedom associated to the boundaries of the SEA subsystem resulting in an augmented FE model. The coupling between

the SEA part and the FE model can be made thanks to a reciprocity statement which states that the force that the reverberant field exerts on its surrounding boundaries is proportional to the resistive part of the DFDS matrix and to the energy of the reverberant field [Cotoni et al., 2007]. This statement allows one to define equations relating the energy at the SEA subsystems with the dynamics of the FE model, and thus, makes it possible to determine the coupling between both parts.

As a conclusion, thanks to this method, a model whose frequency behaviour cannot be classified as uniform throughout the system can have the best adapted treatment for every component. In addition, the use of a hybrid method implies a reduction of the computational cost respect to the use of a pure FE model [Cotoni et al., 2007].

2.2 STATISTICAL ENERGY ANALYSIS

The Statistical Energy Analysis was developed in the early 1960s partly motivated by the need to predict the vibrational response of satellite launch vehicles and their payloads. These are really huge systems formed by many components each of which has different characteristics and a high amount of vibration modes in the frequency range of study. Thus, at that time and for the reasons stated before, an alternative had to be proposed.

The first works considered as the origins of SEA were made independently by R.H. Lyon and P. W. Smith, Jr [Lyon and DeJong, 1998]. The former determined two features about the power flow between two lightly coupled linear oscillators when excited by independent white noise sources. First, it is proportional to the difference between their uncoupled energies and second, the flow is directed from the oscillator with higher energy to the one with lower energy.

Meanwhile, Smith computed the response of an oscillator excited by a broad-band diffuse field. He reached the conclusion that the response of the system is bounded when the radiation damping of the oscillator is higher than its internal damping and that this boundary value is independent of the value of the radiation damping.

In fact, as a result of their joint work, it was discovered that the boundary value is set by the equality between the resonator energy and the average modal energy of the sound field [Lyon and DeJong, 1998]. In other words, that given two resonators excited by independent white noise sources, the power flows from one to the other until an equilibrium state is reached. In the case that the coupling between the resonators is stronger than their respective internal dampings, the energy is equally distributed. From these first initial conclusions, SEA has evolved to how it is known nowadays, as described in the following section.

2.2.1 *Principles and validity scope of Statistical Energy Analysis*

Statistical Energy Analysis is used to predict the vibroacoustic behaviour of a mechanical system at high frequencies. The system consists of a group of coupled elements, normally, structures, cavities or ducts. To model it with SEA, it is divided in several subsystems which correspond to groups of vibration modes with similar characteristics.

In a first approximation, the subsystems may correspond to physical elements, for instance, a cavity can be represented by a subsystem. However, since depending on the type of physical element, different kinds of vibration modes may be present, e.g. a beam may have compression, flexure and torsion modes, the same physical element can be modelled by several subsystems, one per each type of mode. Thus, a beam of rectangular cross section can be assigned up to 4 subsystems, representing the compression, flexure in both directions and torsion modes. A plate can be assigned, up to 3 subsystems which correspond to flexure, in-plane compression and in-plane shear modes and finally, a cavity will be described by a unique subsystem. Nevertheless, in a realistic context, the substructuring of a SEA model can be more complex. Thus, some techniques have been implemented to ensure that the resulting subsystems fulfill the SEA assumptions that will be described below [Díaz-Cereceda et al., 2015; Totaro and Guyader, 2006].

Therefore, the system will comprise several groups of similar vibration modes, where energy coupling can only occur between modes of different groups. In addition, since the number of modes at high frequency is reasonably large, instead of working with specific quantities for every single mode, the subsystem is assigned an average energy value and the couplings between subsystems are characterized by power flows. This is one of the advantages of SEA, the system has as many degrees of freedom as subsystems are defined, which is much less than the d.o.f. of a FEM or BEM model.

In order to make this definition of the system which consists in dividing it in subsystems and establishing the power flows, SEA lays on the following principles [Burroughs et al., 1997]:

- The power flow between two subsystems is proportional to the difference of their energy densities or modal energies. This is known as the Coupling Power Proportionality (CPP) condition. A discussion about CPP can be found in [Mace, 1994].

- The energy is stored in resonance modes. Thus, the amount of energy a subsystem is able to keep is proportional to the number of modes it has.

- The energy always flows from the subsystem with higher energy to the one with lower energy.

- The injected power in a subsystem is either transferred to other subsystems or dissipated in the same subsystem.

- From a wave approach point of view, every point in a subsystem has the same average energy level, in other words, the energy density is homogeneous and isotropic all over the subsystem. This is known as the diffuse field assumption. From a modal point of view, it is equivalent to state that modal energy equipartition exists, which means that the subsystem energy is uniformly shared amongst the modes. In other words, that the average modal energy is equal for all the modes in a subsystem.

In addition, to simplify the formulation and the development of the models, it is also assumed that:

- The excitation forces are uncorrelated white noises to ensure that all the modes in the subsystem are equally excited. Typically, for the plates a rain-on-the-roof excitation is used.
- The energy can only be input in the subsystems, never in the couplings between subsystems. Usually, the couplings will be considered conservative. However, more complex approaches deal with the inclusion of non-conservative couplings in the system [Beshara and Keane, 1996; Díaz-Cereceda, 2013; Sheng et al., 1998].
- All the modes in the same subsystem and the same frequency band have the same damping loss factor.
- There is no coupling between the modes of the same subsystem.

As seen, SEA is a statistical method and it deals with average values of energy. On the one hand, the energy is averaged in frequency, i.e a unique energy value is considered for a whole frequency band. On the other hand, the energy is supposed to be equally partitioned amongst all the modes in the subsystem, thus, there is an average modal energy value. That is why a high number of modes is needed, otherwise the average value would not be representative. Other approaches suggest an alternative when the number of modes is insufficient, which is making an ensemble average. In any case, dealing with an statistical method such SEA requires that the system fulfills some conditions in order to guarantee the validity of the results [Lafont et al., 2014; Le Bot and Cotoni, 2010]. These conditions can be established from two points of view: the modal approach or the wave approach. Although the conditions determined from the former are related which those obtained from the latter, the correspondence is not straightforward. This topic has been discussed in [Lafont et al., 2014] and is summarized as follows.

- As introduced, the first requirement is to have a high population of modes. Formally, it is quantified by the mode count N

$$N = n\Delta\omega, \tag{2.1}$$

  where n is the modal density and $\Delta\omega$ is the width of the frequency band. The expressions to compute the modal density change depending on the

type of subsystem [Craik, 1996; Lyon and DeJong, 1998]. To consider that the population of modes is large enough, it is recommended that

$$N \gg 1. \tag{2.2}$$

Otherwise, the ensemble averaging should be chosen [Le Bot and Cotoni, 2010].

- Besides a high population of modes, it is necessary that the mode amplitudes are uncorrelated random variables. To that end, the modes should be close in frequency one to the other and none of them should dominate over the rest so that the result is a smooth frequency response. The modal overlap factor measures the amount of overlapping between consecutive modes in the frequency response. It is computed as

$$M = n\eta\omega, \tag{2.3}$$

where η is the damping loss factor and ω is the band central frequency [Hopkins, 2007; Le Bot and Cotoni, 2010]. To guarantee the validity of SEA

$$M \gg 1. \tag{2.4}$$

- The diffuse field assumption is ensured as long as the waves are reflected enough times before being attenuated in order to guarantee that the wave intensity is the same in all directions. Thus, it is desirable that the attenuation capability of the system is really low. This can be quantified by means of the attenuation factor of wave per meter, $m = \eta\omega/c_g$, where c_g is the wave group speed. It can be normalized to the mean free path of the subsystem l, giving

$$\bar{m} = \frac{\eta\omega}{c_g} l. \tag{2.5}$$

The normalized attenuation factor $\bar{m}$ is considered low when

$$\bar{m} \ll 1. \tag{2.6}$$

- The subsystems should be weakly coupled, otherwise, energy equipartition between subsystems takes place and it makes no sense to separate them in different subsystems. Although there is not a common universally accepted definition for weak coupling [Langley, 1989; Mace, 2003], the coupling can be considered weak when

$$\eta_{ij} \ll \eta_i, \tag{2.7}$$

which is known as the Smith criterion [Smith, 1979].

All in all, SEA is a useful method to work with high frequency models but the system must fulfill some conditions which in some cases may be quite restrictive.

2.2.2 *Formulation of Statistical Energy Analysis*

The SEA model can be built once the conditions of validity of SEA are guaranteed in the system. The parameters needed at each frequency band of study are the loss factors. There are three types of loss factors:

COUPLING LOSS FACTOR The coupling loss factor (CLF) η_{ij} is the ratio of energy transferred from subsystem i to subsystem j in a radian cycle.

INTERNAL LOSS FACTOR The internal or damping loss factor (ILF) η_{id} is the ratio of energy lost as heat in subsystem i in a radian cycle.

TOTAL LOSS FACTOR The total loss factor (TLF) η_i is the total energy lost in subsystem i in a radian cycle,

$$\eta_i = \eta_{id} + \sum_{j,j\neq i}^{N} \eta_{ij}, \tag{2.8}$$

where N is the total number of subsystems.

The obtention of the coupling and internal loss factors can be done analytically, by means of measurements, or by using numerical methods. The analytical methods are used in simple cases of coupled beams, plats and shells. Theoretical expressions can be found for point, line and area connections based on the wave transmission analysis [Langley and Heron, 1990; Langley and Shorter, 2003; Lyon and DeJong, 1998]. However, when the system gets more complex, numerical methods based on finite element analysis have to be used [Craik, 1996; De Rosa and Franco, 2010; Fredö, 1997; Lyon and DeJong, 1998; Maxit and Guyader, 2001a; Thite and Mace, 2007]. Alternatively, experimental techniques such as experimental SEA can also be employed [Fahy, 1998].

In some cases, the modal densities are easier to obtain than the coupling loss factors. Thanks to the CPP, there exists a proportionality relation between the coupling loss factors of a pair of subsystems in both directions. Known as the *consistency relationship*, it states that

$$n_i \eta_{ij} = n_j \eta_{ji}. \tag{2.9}$$

Thus, having the modal density, once η_{ij} is obtained, η_{ji} can be directly computed [Craik, 1996; Lyon and DeJong, 1998].

Therefore, once the division in subsystems is made and the parameters are obtained, the formulation of SEA allows computing the energy level at every subsystem. Towards this end, the power balance equations are stated for every subsystem,

$$W_i + \sum_{j,j\neq i}^{N} W_{ji} = W_{id} + \sum_{j,j\neq i}^{N} W_{ij} \quad \forall i, j = 1, \ldots, N. \tag{2.10}$$

Where W_i is the external power input, W_{id} is the power lost due to internal dissipation mechanisms, N is the number of subsystems in the system and W_{ij}

is the power flow from subsystem i to subsystem j. Hence, the left hand term represents the power inputs to the subsystem and the right hand term, the power outputs.
The dissipated power W_{id} is defined as

$$W_{id} = \omega \eta_{id} E_i, \tag{2.11}$$

where ω is the central frequency of the band and E_i the energy at subsystem i. Analogously, the transmitted power is given by

$$W_{ij} = \omega \eta_{ij} E_i. \tag{2.12}$$

Thus, the net power flow between two subsystems can be obtained considering

$$\Delta W_{ij} = W_{ij} - W_{ji} = \omega \eta_{ij} \left(E_i - \frac{n_i}{n_j} E_j \right), \tag{2.13}$$

where use of the consistency relationship has been made. Note from (2.13) that the power flow between two subsystems is indeed proportional to the difference between their energy densities.
Replacing (2.11) and (2.12) in (2.10) yields

$$W_i = \omega \eta_{id} E_i + \omega \sum_{j, j \neq i}^{N} \left(\eta_{ij} E_i - \eta_{ji} E_j \right), \tag{2.14}$$

which can be expressed in matrix form as

$$\begin{pmatrix} \eta_1 & -\eta_{21} & -\eta_{31} & \cdots & -\eta_{N1} \\ -\eta_{12} & \eta_2 & -\eta_{32} & \cdots & -\eta_{N2} \\ -\eta_{13} & -\eta_{23} & \eta_3 & \cdots & -\eta_{N3} \\ \vdots & \vdots & \vdots & \ddots & \vdots \\ -\eta_{1N} & -\eta_{2N} & -\eta_{3N} & \cdots & \eta_N \end{pmatrix} \begin{pmatrix} E_1 \\ E_2 \\ E_3 \\ \vdots \\ E_N \end{pmatrix} = \frac{1}{\omega} \begin{pmatrix} W_1 \\ W_2 \\ W_3 \\ \vdots \\ W_N \end{pmatrix}. \tag{2.15}$$

The matrix in (2.15) is the loss factor matrix, termed as $\boldsymbol{\mathcal{H}}$. Therefore, the system of equations can be expressed as

$$\boldsymbol{\mathcal{H}} \boldsymbol{E} = \frac{1}{\omega} \boldsymbol{W} \equiv \boldsymbol{E}_0, \tag{2.16}$$

with $\boldsymbol{E}$ standing for the unknown vector of subsystem energies and $\boldsymbol{W}$ standing for the external power inputs (Which has been rewritten as an external energy input vector $\boldsymbol{E}_0 \equiv \boldsymbol{W}/\omega$).

To conclude, a reference to the graphical representation of a SEA system will be made. Figure 2.1 illustrates an example of the diagram corresponding to a SEA system consisting of 4 subsystems. There are two kinds of elements, the blocks and the arrows. The blocks represent the SEA subsystems from 1 to 4. On the other hand, there are three types of arrows: directed arrows connecting pairs

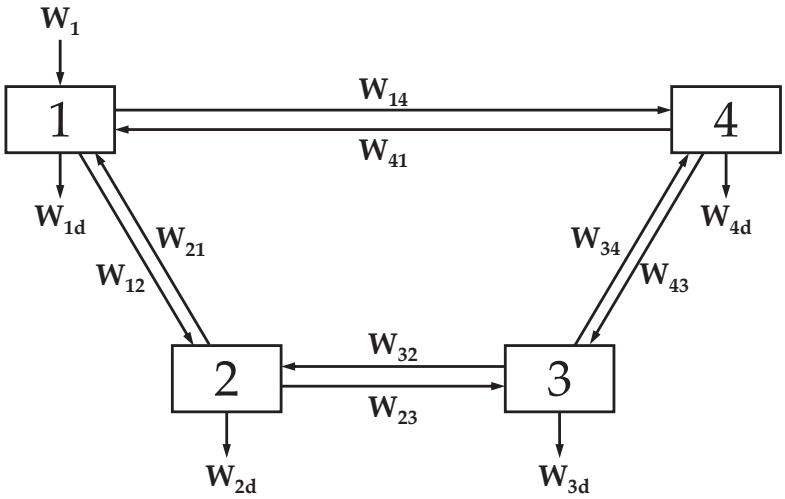

Figure 2.1: Example of SEA diagram

of subsystems and symbolizing the power flow between them, non-connecting arrows pointing to subsystems representing external input power, and non-connecting arrows leaving subsystems and standing for internally dissipated power. For instance, the arrow from 1 to 4 stands for the power flow W_{14}, whereas W_1 is the power injected in 1 and W_{4d} the power dissipated in 4. Typically, the SEA modelling only considers direct couplings since at this frequency band resonant transmission is predominant. However, non-resonant paths are to be considered, they can be included in the model as virtual couplings [Craik, 1996].

2.3 ENERGY DISTRIBUTION MODELS

The approach being presented in this thesis will be firstly implemented on SEA models but will be later extended to mid-frequency methods, specifically, Energy Distribution models and SmEdA models. In this section, a description of the Energy Distribution analysis is given.

The energy distribution (ED) models aim at giving a general description of the dynamic behaviour of a system in terms of vibroacoustic energy. To that end, the system is split into a set of subsystems and the so called Energy Influence Coefficients (EIC) are computed to characterize the energy sharing between them [Fredö, 1997; Mace and Shorter, 2000]. The main purpose is to obtain the frequency averaged subsystem energies when some part of the system is submitted to a broadband excitation. The EICs can be computed either from theoretical modal developments [Guyader et al., 1982], numerical approaches using the finite element method [Fredö, 1997; Mace and Shorter, 2000; Zhang and Sainsbury, 1999] or scaling procedures [De Rosa and Franco, 2010], or by resorting to experimental procedures relying on the power injection method [Bies and Hamid, 1980; Guasch, 2011; Hopkins, 2009; R. Ming, 2005]. Note that SEA is a particular case of ED method with additional stronger restrictions.

In an ED model, the EIC's matrix $\boldsymbol{A}$ is used to relate the subsystem energies $\boldsymbol{E}$ with the external input powers $\boldsymbol{P}_{in}$, so that (see e.g. [Mace and Shorter, 2000])

$$\boldsymbol{E} = \boldsymbol{A}\boldsymbol{P}_{in}. \tag{2.17}$$

The external excitations in (2.17) are assumed to be random and stationary, and uncorrelated between subsystems. Moreover, the input power and subsystem energies are time and frequency averaged over the considered frequency band. The EIC between two subsystems i and j, A_{ij}, consequently represents the time and frequency averaged energy at i, resulting from a unit input power at subsystem j. The EIC matrix $\boldsymbol{A}$ can be directly obtained from experiments, or from numerical or analytical modelling.

Let us next consider the inverse of the EIC matrix $\boldsymbol{X} := \boldsymbol{A}^{-1}$. It follows that

$$\boldsymbol{X}\boldsymbol{E} = \boldsymbol{P}_{in}. \tag{2.18}$$

Equation (2.18) is similar to the structure of a SEA matrix system $\boldsymbol{\mathcal{H}}\boldsymbol{E} = \boldsymbol{P}_{in}$ ($\boldsymbol{\mathcal{H}}$ standing for ω times the SEA matrix of loss factors, ω being the radial frequency). However, $\boldsymbol{X}$ is much more general than $\boldsymbol{\mathcal{H}}$, and does not need to fulfill the SEA hypotheses. The question of which conditions the inverse EIC matrix $\boldsymbol{X}$ should satisfy to become an SEA loss factor matrix has been addressed by various authors, starting with the numerical analysis in [C.H Hodges, P. Nash and J. Woodhouse, 1987]. In [Mace, 2003, 2005], a distinction was made between the so called *quasi-SEA* and *proper-SEA* matrices. $\boldsymbol{X}$ was said to be a quasi-SEA matrix if it satisfies the two necessary conditions of energy conservation and consistency. If in addition, all indirect coupling loss factors between subsystems are zero, then $\boldsymbol{X}$ was said to be a proper-SEA matrix. It is to be noted that a proper-SEA matrix is not yet a SEA matrix, given that X_{ij} may not comply with some of the ideal properties a SEA coupling loss factor should have. In the most general case, $\boldsymbol{X}$ does not even have to be SEA-like because the coupling power proportionality (CPP) hypothesis will not necessarily be satisfied.

2.4 STATISTICAL MODAL ENERGY DISTRIBUTION ANALYSIS

Statistical modal Energy distribution Analysis (SmEdA), originally proposed in [Maxit and Guyader, 2001a,b, 2003], can be envisaged as a particular case of ED method, in which SEA hypotheses are relaxed to extend its range of applicability to mid frequencies. However, SmEdA has a clear distinctive feature with respect to most ED methods in the sense that power balance equations are not established between subsystems but rather between the resonant modes of different subsystems. These modes can be extracted from the modal bases of uncoupled subsystems, which can be computed using FEM, thanks to the dual modal formulation (DMF) [Maxit and Guyader, 2001b]. This offers the possibility of considering subsystems with complex geometries and varying properties.

Moreover, circumventing SEA energy equipartition allows one to deal with locally excited subsystems with low modal overlap [Maxit and Guyader, 2003], as well as to evaluate the spatial distribution of energy density within subsystems [Totaro and Guyader, 2012]. Recently, SmEdA has been extended to incorporate the contribution of non-resonant transmission through condensation of the DMF equations. This has resulted in the appearance of indirect coupling between modes in non-physically connected subsystems, standard non-resonant paths in SEA being recovered as a particular case [Maxit et al., 2014].

2.4.1 *Resonant transmission in a two-subsystem SmEdA model*

An introduction to SmEdA will be next presented to describe its general performance. For the sake of simplicity, the SmEdA modal energy equations for a system simply made of two coupled subsystems will be addressed first.

As for SEA, the prerequisites of weak coupling and of dominant reverberant field will be assumed, so that the vibratory behaviour of the two coupled subsystems can be solely described in terms of the energy transmission between resonant modes (i.e., modes having their modal frequencies within the frequency band of excitation). Numerical tests [Maxit, 2000; Maxit and Guyader, 2001b] have shown that this assumption is compliant if the substructuring into subsystems is done well along mechanical impedance mismatch and if the boundary conditions at the coupling surfaces are correctly imposed to determine the subsystem modes. This can be achieved by describing the stiff subsystem by its uncoupled free modes (i.e., assuming free displacements on the coupling surface) while describing the soft one by its uncoupled blocked modes (i.e., imposition of null displacements on the coupling surface).

For illustrative purposes, consider that the two subsystems consist of an acoustic cavity (subsystem 1) coupled to a vibrating structure (subsystem 2). The cavity is therefore the soft subsystem and becomes characterized by means of its blocked modes (i.e., its boundary is assumed to be composed of rigid walls) whereas the vibrating structure is the stiff subsystem and its free modes (i.e. in vacuo modes) should be used instead. According to the dual modal formulation (see [Maxit and Guyader, 2001a] for the case of two coupled mechanical subsystems and [Maxit et al., 2014] for a cavity-structure problem), the acoustic pressure field (stress field in a general case) is the appropriate one to describe subsystem 1, whereas the displacement field is adequate for subsystem 2. Denoting by $\hat{P}$ and $\hat{Q}$ the sets of resonant modes in subsystems 1 and 2, respectively containing N_p and N_q modes, the acoustic pressure at point M in the cavity and

the displacement at point N on the structure can be estimated using the modal expansions

$$p(M,t) = \sum_{p\in\hat{P}} \xi_p(t)\,\tilde{p}_p(M), \tag{2.19a}$$

$$u(N,t) = \sum_{q\in\hat{Q}} \zeta_q(t)\,\tilde{u}_q(N), \tag{2.19b}$$

where ξ_p and ζ_q denote modal amplitudes, $\tilde{p}_p$ stands for the spatial acoustic pressure distribution of the p-th cavity mode, and $\tilde{u}_q$ represents the displacement spatial shape of the q-th structure mode.

Following the DMF approach, expressions (2.19a)-(2.19b) are to be introduced in the weak formulation of the coupled problem. Taking advantage of the orthogonality of the uncoupled modes, presuming viscous damping and making the change of variables $\xi_p = \chi'_p$, $\forall p \in \hat{P}$ (with the prime symbol indicating time derivative), the following modal equations of motion can be derived (see [Maxit and Guyader, 2001a] for details)

$$\chi''_p(t) + \omega_p\eta_p\chi'_p(t) + \omega_p^2\chi_p(t) - \sum_{q\in\hat{Q}} W_{pq}\zeta'_q(t) = Q_p(t), \quad \forall p \in \hat{P}, \tag{2.20a}$$

$$\zeta''_q(t) + \zeta_q\eta_q\zeta'_q(t) + \omega_q^2\zeta_q(t) - \sum_{p\in\hat{P}} W_{pq}\chi'_p(t) = 0, \qquad \forall q \in \hat{Q}. \tag{2.20b}$$

In (2.20a)-(2.20b), ω_p, ω_q denote the modal angular frequencies and η_p, η_q the modal damping loss factors. The mode shapes are supposed to be normalized to a unit modal mass for the free subsystem and to a unit modal stiffness for the blocked subsystem. Q_p represents the modal source strength at mode p due to external excitation and W_{pq} corresponds to the modal interaction work between p and q. For each pair of modes, the latter is defined as the integral over the coupling surface, S_C, of the product between a displacement mode shape of the free subsystem and a stress mode shape of the blocked subsystem. For the cavity-structure example the modal interaction work would be $W_{pq} = \int_{S_C} \tilde{p}_p\tilde{u}_q dS$.

The form of equations (2.20a)-(2.20b) allows one to interpret mode interactions as oscillators coupled by gyroscopic elements (which introduce opposite sign coupling forces proportional to the oscillator velocities [Maxit and Guyader, 2001a]). A schematic representation of this modal coupling is proposed in Fig. 2.2. Note that a mode in one subsystem is coupled to all modes in the other subsystem but it is not coupled with the modes in its own subsystem. The number of back and forth modal energy direct couplings (the former symbolized with black lines in Fig. 2.2) is $2N_PN_Q$, which strongly increases with the number of modes considered in each subsystem. Moreover, energy may obviously go back and forth between subsystem modes resulting in transmission paths of high order, the total number of them being infinite.

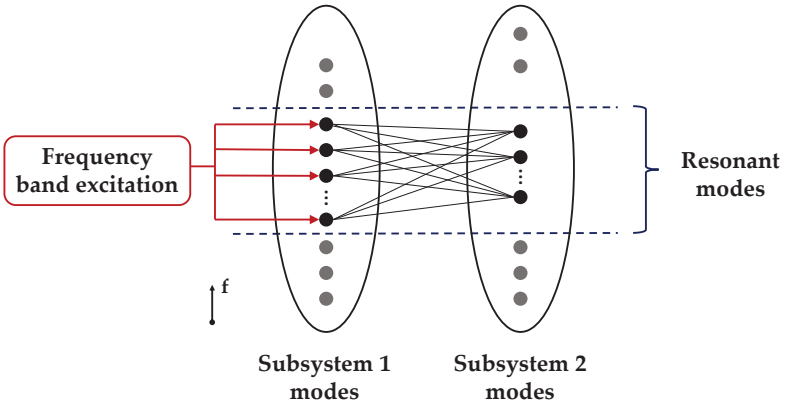

Figure 2.2: Sketch for the the modal coupling between two coupled subsystems.

SmEdA equations describe the power balance between the modes in different subsystems and are obtained from the principle of energy conservation for each mode in a subsystem. For the p-th mode in subsystem 1, they result in

$$\Pi^p_{inj} = \Pi^p_{diss} + \sum_{q \in \hat{Q}} \Pi_{pq}, \quad \forall p \in \hat{P}, \tag{2.21}$$

where Π^p_{inj} is the time-averaged injected power by the generalized force Q_p, Π^p_{diss} is the time-averaged power dissipated by the internal damping of mode p and Π_{pq} is the time-averaged power flow exchanged between the resonant mode p of subsystem 1 and the resonant mode q of subsystem 2. The various powers appearing in (2.21) can be evaluated from the previously established relations for one single oscillator and/or two coupled oscillators, using the same assumptions as in SEA (e.g., white noise force spectra and uncorrelated modal interaction forces [Lyon and DeJong, 1998]). It follows that

$$\Pi^p_{inj} \approx \frac{\pi}{4} \bar{S}_{Q_p}, \qquad \Pi^p_{diss} \approx \omega_p \eta_p E_p, \qquad \Pi_{pq} \approx \beta_{pq} \left(E_p - E_q \right), \tag{2.22}$$

where $\bar{S}_{Q_p}$ is the power spectral density of the modal source strength, E_p is the time averaged energy of mode p, and β_{pq} is called the modal coupling factor given by (see [Maxit and Guyader, 2003]),

$$\beta_{pq} = W^2_{pq} \left[\frac{\omega_p \eta_p \omega_q^2 + \omega_q \eta_q \omega_p^2}{\left(\omega_p^2 - \omega_q^2 \right)^2 + \left(\omega_p \eta_p + \omega_q \eta_q \right) \left(\omega_p \eta_p \omega_q^2 + \omega_q \eta_q \omega_p^2 \right)} \right]. \tag{2.23}$$

The power balance equation for any resonant mode of subsystem 2 will be analogous to that of subsystem 1 in (2.21) (though for simplicity it will be supposed that no external force is acting on subsystem 2). The $N_p + N_q$ equations for all modes in subsystems 1 and 2 can be combined in the linear matrix system

$$\begin{pmatrix} \boldsymbol{\beta_{11}} & -\boldsymbol{\beta_{12}} \\ -\boldsymbol{\beta_{12}}^\top & \boldsymbol{\beta_{22}} \end{pmatrix} \begin{pmatrix} \boldsymbol{E_1} \\ \boldsymbol{E_2} \end{pmatrix} = \begin{pmatrix} \boldsymbol{\Pi_1} \\ \boldsymbol{0} \end{pmatrix}, \tag{2.24}$$

with unknown modal energies $\boldsymbol{E_1} = \left(E_p\right)_{N_P \times 1}$ and $\boldsymbol{E_2} = \left(E_q\right)_{N_Q \times 1}$, external input power at subsystem 1 modes $\boldsymbol{\Pi_1} = \left(\Pi^p_{inj}\right)_{N_P \times 1}$, coupling loss factor matrix $\boldsymbol{\beta_{12}} = \left(\beta_{pq}\right)_{N_P \times N_Q}$ and diagonal loss factor matrices $\boldsymbol{\beta_{11}} = \text{diag}\left(\omega_p \eta_p + \sum_{q \in \hat{Q}} \beta_{pq}\right)_{N_P \times N_P}$ and $\boldsymbol{\beta_{22}} = \text{diag}\left(\omega_q \eta_q + \sum_{p \in \hat{P}} \beta_{pq}\right)_{N_Q \times N_Q}$. Inversion of (2.24) results in the SmEdA system modal energies. From the summation of all modal energies in a subsystem its overall energy can be obtained and then related to a spatial mean square velocity in the case of a vibrating plate, or to a mean square acoustic pressure in the case of a cavity, following standard SEA formulations [Craik, 1996; Hopkins, 2007; Lyon and DeJong, 1998].

2.4.2 *General matrix formulation for an N-subsystem SmEdA model*

Generalization of the above SmEdA matrix system formulation for a model consisting of N subsystems is straightforward and yields

$$\begin{pmatrix} \boldsymbol{\beta_{11}} & -\boldsymbol{\beta_{12}} & -\boldsymbol{\beta_{13}} & \cdots & -\boldsymbol{\beta_{1N}} \\ -\boldsymbol{\beta_{12}}^\top & \boldsymbol{\beta_{22}} & -\boldsymbol{\beta_{23}} & \cdots & -\boldsymbol{\beta_{2N}} \\ -\boldsymbol{\beta_{13}}^\top & -\boldsymbol{\beta_{23}}^\top & \boldsymbol{\beta_{33}} & \cdots & -\boldsymbol{\beta_{3N}} \\ \vdots & \vdots & \vdots & \ddots & \vdots \\ -\boldsymbol{\beta_{1N}}^\top & -\boldsymbol{\beta_{2N}}^\top & -\boldsymbol{\beta_{3N}}^\top & \cdots & \boldsymbol{\beta_{NN}} \end{pmatrix} \begin{pmatrix} \boldsymbol{E_1} \\ \boldsymbol{E_2} \\ \boldsymbol{E_3} \\ \vdots \\ \boldsymbol{E_N} \end{pmatrix} = \begin{pmatrix} \boldsymbol{\Pi_1} \\ \boldsymbol{\Pi_2} \\ \boldsymbol{\Pi_3} \\ \vdots \\ \boldsymbol{\Pi_N} \end{pmatrix}, \tag{2.25}$$

with $\boldsymbol{E_i} = \left(E_i\right)_{I \times 1}$ standing for the vector of modal energies of the i-th subsystem where an external power $\boldsymbol{\Pi_i} = \left(\Pi^i_{inj}\right)_{I \times 1}$ is being input. In order to lighten forthcoming expressions, system (2.25) will be simply rewritten as

$$\boldsymbol{\beta E} = \boldsymbol{\Pi}. \tag{2.26}$$

2.5 TRANSMISSION PATH ANALYSIS

Vibroacoustic analysis may be used to solve noise and vibration problems. Generally, these situations consist of a vibroacoustic source that generates an excessive energy level in another part of the system, normally termed target or receiver. Consider for instance, a car where the vibrations produced by the engine generate an uncomfortable noise in the passenger compartment. Therefore, some parts of the system will have to be modified to reduce the energy level at the target up to an acceptable value.

The purpose of the methods described in the previous sections is to predict the vibroacoustic response of a system at any frequency band. Depending on the method, they provide as a result, quantities such as the acoustic pressure, velocity, displacement or energy, i.e. in the car example, the pressure level in the passenger compartment can be known.

This allows one to have somewhat of a picture of the vibroacoustic behaviour of the system but does not directly provide a solution to the mentioned problems. Some postprocessing of the results must be done to find which modifications should be implemented in the system to obtain the desired energy levels at the target.

There is a wide range of adjustments to apply in a system, from changing the dimensions and materials to apply extra absorbent materials or damping elements in the junctions. However, the restrictions imposed by other design criteria will limit the flexibility of the system to be modified. As a consequence, the applied solutions will often be a compromise between the improvements in the system response and the required modifications. Taking into account that after the modifications, the behaviour of the rest of the system is also altered.

The roughest approach to solve this problem is by using Monte Carlo experiments, whose object is to define thousands of different scenarios where the parameters are randomly and slightly modified within admissible values and to keep the one which offers the best results [Dinsmore and Unglenieks, 2005]. In some cases, genetic algorithms can be used to improve the solutions [He et al., 2005]. Although the solution provided by this method may be good, it implies a high computational cost without ensuring the optimal resolution of the problem.

Alternatively, a more refined method combines optimization algorithms with sensitivity analysis. The former consists on maximizing or minimizing an objective function whereas the second analyses which are the parameters in the system that when modified, alter in a higher degree the results. This procedure has been applied to SEA models [Bartosch and Eggner, 2007; Büssow and Petersson, 2007; Chavan and Manik, 2005]. For instance, in [Büssow and Petersson, 2007] the subsystem energy was expressed by means of a Taylor expansion in terms of the coupling loss factor. The objective was to minimize the energy function of a certain subsystem. Next, the sensitivity analysis was done to assess which were the most influential coupling loss factors in the variation of energy.

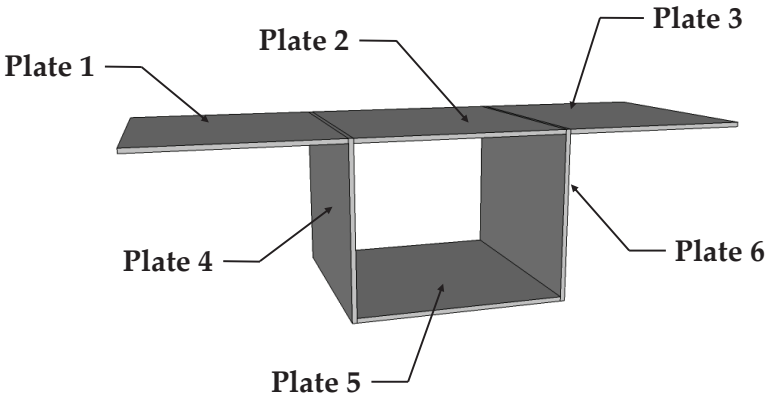

Figure 2.3: SEA system example

All these techniques look for the solution that provides the best results but they do not try to find out the origin of the problem. A different way to tackle

the problem is by determining how energy is transmitted from the vibroacoustic sources to the targets. In other terms, to identify the energy transmission paths. The experimental methods that traditionally have followed this approach are known as Transmission Path Analysis (TPA) techniques.

The TPA methods can be classified into 1-step processes or 2-step processes. The 2-step methods consist of two steps of measurements. In the first step, the system is characterized in its static state whereas in the second one, the measurements are carried out under operational conditions. The 1-step methods, on the other hand, only use operational data and thus, just one phase is needed. The first TPA techniques date from the late 1970's and were 1-step methods based on partial and multiple coherence analysis [Bendat, 1976a,b; Dodds and Robson, 1975; Potter, 1977]. The problem with 1-step methods is the separation of partially correlated sources. For this reason, in the 1980's, the 2-step TPA approaches appeared. The most relevant is a 2-step method commonly known as classical TPA. The aim of this method is knowing how the operational loads acting on a system influence the response of some selected degrees of freedom of the system [Stahel et al., 1980; Tschudi, 1991; Verheij, 1982]. Other approaches are based on the transmissibility concept, which consist in decomposing the response at a selected degree of freedom in terms of the responses of the rest of degrees of freedom [Guasch, 2009; Guasch and Magrans, 2004; Magrans, 1981].

However, the energy transmission paths can also be obtained computationally. At mid frequencies, there were some proposals to determine the energy flows in an energy flow model [Lenzi et al., 2010]. Yet, it is at high frequencies and more precisely in SEA models where more efforts have been made. The first definitions of the contribution of an energy transmission path between two subsystems were made in [Craik, 1979, 1996]. Furthermore, later works proved that the energy level in a subsystem can be recovered by adding the contribution of all the paths heading such subsystem [Craik, 1996; Magrans, 1993]. This aspect will be shown later, but first, let us describe in detail how the contribution of an energy transmission path is computed. To this end, the plate system in Fig. 2.3 is used. The SEA model is built considering only flexural waves. The source set at Plate 1 and the target at Plate 6. The energy contribution to the target subsystem of the path starting at Plate 1 followed by Plate 2 and ending at Plate 6 will be computed step by step, following the same procedure as in [Craik, 1996]. Figure 2.4 contains the SEA diagram corresponding to this system where the path to be computed is marked in yellow.

First, it is supposed that energy in subsystem 4 is only input from subsystem 1. Note that this assumption is equivalent to assume that, except for 1 and 4, all the subsystems are blocked, so their energy is null. This description coincides with the concept of direct transmissibility which has also been used to compute transmission path analysis in SEA systems [Guasch, 2011; Magrans, 1993]. Therefore, the power balance equation becomes

$$\omega E_1 \eta_{14} = \omega E_4 \eta_4, \tag{2.27}$$

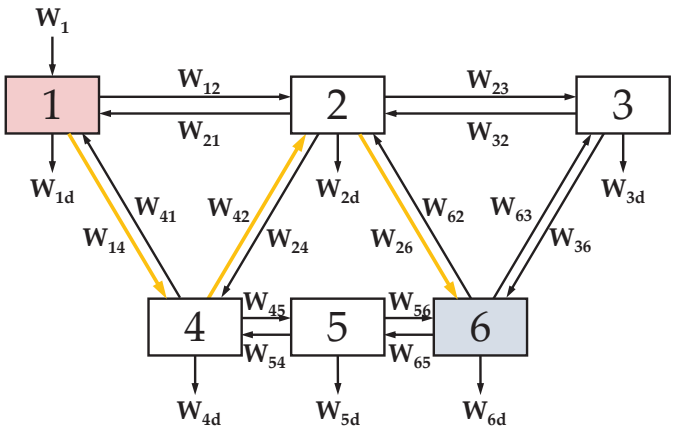

Figure 2.4: Example of energy transmission path

which can be rewritten as

$$E_4 = \frac{\eta_{14}}{\eta_4} E_1. \tag{2.28}$$

Hence, the contribution of the direct path from subsystem 1 to subsystem 4 is η_{14}/η_4, since this is the portion of E_1 that arrives to E_4. The direct path between two subsystems is also known as a first order path. The next step in the path is subsystem 2, so again, the energy is supposed to be input only from subsystem 4. The power balance equation is expressed for subsystem 2 and E_2 is isolated,

$$E_2 = \frac{\eta_{42}}{\eta_2} E_4. \tag{2.29}$$

Analogously for subsystem 6, the only energy input is assumed to be from subsystem 2, so

$$E_6 = \frac{\eta_{26}}{\eta_6} E_2, \tag{2.30}$$

Next, if (2.28) is replaced in (2.29) and the result is replaced in (2.30), the energy in subsystem 6 can be computed in terms of E_1 as

$$E_6 = \frac{\eta_{42}\eta_{26}}{\eta_2\eta_4} E_4 = \frac{\eta_{14}\eta_{42}\eta_{26}}{\eta_4\eta_2\eta_6} E_1. \tag{2.31}$$

Therefore, it can be observed from (2.31), that the contribution of a path is the product of the contributions of the first order paths composing the path. Thus, in general, Craik's definition of the contribution of a k-th order path P_{ij}^k, from subsystem i to subsystem j is given by

$$w\left(P_{ij}^n\right) = \frac{\eta_{ih_1}}{\eta_{h_1}} \frac{\eta_{h_1h_2}}{\eta_{h_2}} \cdots \frac{\eta_{h_{n-1}j}}{\eta_j}. \tag{2.32}$$

Considering that the system is weakly coupled, i.e. $\eta_{ij} \ll \eta_i$, it can be observed that the weight of a first order path η_{ij}/η_j will always be less than unity, and so, the higher the order of the path, the lower its contribution. Thus, the contribution of very long paths will tend to zero. This suggests that there will be paths whose

contribution is negligible in comparison to others that will provide the target with a high amount of energy.

To study this point in depth, let us recover the previously mentioned relation between the subsystem energy and the total contribution of the paths heading a subsystem. To do it, an alternative form to solve the system of equations in (2.16) other than computing the inverse of $\boldsymbol{\mathcal{H}}$ is presented. First of all, every row in the system of equations in (2.15) is divided by the corresponding diagonal element of $\boldsymbol{\mathcal{H}}$,

$$\begin{pmatrix} 1 & -\eta_{21}/\eta_1 & -\eta_{31}/\eta_1 & \cdots & -\eta_{N1}/\eta_1 \\ -\eta_{12}/\eta_2 & 1 & -\eta_{32}/\eta_2 & \cdots & -\eta_{N2}/\eta_2 \\ -\eta_{13}/\eta_3 & -\eta_{23}/\eta_3 & 1 & \cdots & -\eta_{N3}/\eta_3 \\ \vdots & \vdots & \vdots & \ddots & \vdots \\ -\eta_{1N}/\eta_N & -\eta_{2N}/\eta_N & -\eta_{3N}/\eta_N & \cdots & 1 \end{pmatrix} \begin{pmatrix} E_1 \\ E_2 \\ E_3 \\ \vdots \\ E_N \end{pmatrix} = \frac{1}{\omega} \begin{pmatrix} W_1/\eta_1 \\ W_2/\eta_2 \\ W_3/\eta_3 \\ \vdots \\ W_N/\eta_N \end{pmatrix}. \quad (2.33)$$

Let us redefine matrix $\boldsymbol{\mathcal{H}}$ and vector $\boldsymbol{E}_0$ respectively as $\boldsymbol{\mathcal{H}}' = \operatorname{diag}(1/\eta_i)\,\boldsymbol{\mathcal{H}}$ and $\boldsymbol{E}_0' = \operatorname{diag}(1/\eta_i)\,\boldsymbol{E}_0$ and define the matrix $\boldsymbol{\mathcal{S}}$ such that $\boldsymbol{\mathcal{H}}' = (\boldsymbol{I} - \boldsymbol{\mathcal{S}})$. The solution of the system of equations in (2.33), can be obtained by means of a Neumann series expansion as

$$\boldsymbol{E} = (\boldsymbol{I} - \boldsymbol{\mathcal{S}})^{-1}\,\boldsymbol{E}_0' = \left(\sum_{n=0}^{\infty} \boldsymbol{\mathcal{S}}^n\right) \boldsymbol{E}_0', \quad (2.34)$$

as long as the spectral radius of $\boldsymbol{\mathcal{S}}$ is less than unity and thus the series converges, which in SEA will always be the case, as it will be proven in subsequent chapters. Note that the elements of $\boldsymbol{\mathcal{S}}$ are defined as

$$\mathcal{S}_{ij} = \begin{cases} 0 & \text{if } i = j \\ \frac{\eta_{ji}}{\eta_i} & \text{if } i \neq j \end{cases} \quad (2.35)$$

so that the element $\mathcal{S}_{ij}$ corresponds to the first order energy transmission path from subsystem i to subsystem j as defined in (2.32). In addition, it was proven in [Magrans, 1993] that the n-th power of matrix $\boldsymbol{\mathcal{S}}$ has as elements the contributions of the n-th order paths between every pair of subsystems. Making use again of the example in Figure 2.3, the $\boldsymbol{\mathcal{S}}$ matrix for that SEA system becomes

$$\boldsymbol{\mathcal{S}} = \begin{pmatrix} 0 & \eta_{21}/\eta_1 & 0 & \eta_{41}/\eta_1 & 0 & 0 \\ \eta_{12}/\eta_2 & 0 & \eta_{32}/\eta_2 & \eta_{42}/\eta_2 & 0 & \eta_{62}/\eta_2 \\ 0 & \eta_{23}/\eta_3 & 0 & 0 & 0 & \eta_{63}/\eta_3 \\ \eta_{14}/\eta_4 & \eta_{24}/\eta_4 & 0 & 0 & \eta_{54}/\eta_4 & 0 \\ 0 & 0 & 0 & \eta_{45}/\eta_5 & 0 & \eta_{65}/\eta_6 \\ 0 & \eta_{26}/\eta_6 & \eta_{36}/\eta_6 & 0 & \eta_{56}/\eta_6 & 0 \end{pmatrix} \quad (2.36)$$

and contains the weights of all the first order paths in the system. For example, $\mathcal{S}_{32}$ corresponds to the weight of the first order path from subsystem 2 to

subsystem 3, i.e. $\mathcal{S}_{32} = \eta_{23}/\eta_3 = w\left(P_{23}^1\right)$. On the other hand, if two subsystems are not directly connected, like 1 and 5, the corresponding element is null, $\mathcal{S}_{51} = 0$. In addition, note that the diagonal elements are also zero since a first order transmission path from a subsystem to itself has no physical sense.

Next, $\boldsymbol{\mathcal{S}}^2$ is computed to obtain the contribution of the second order paths.

$$\boldsymbol{\mathcal{S}}^2 = \begin{pmatrix} \frac{\eta_{12}\eta_{21}}{\eta_1\eta_2} + \frac{\eta_{14}\eta_{41}}{\eta_1\eta_4} & \frac{\eta_{24}\eta_{41}}{\eta_1\eta_4} & \frac{\eta_{32}\eta_{21}}{\eta_2\eta_1} & \frac{\eta_{42}\eta_{21}}{\eta_2\eta_1} & \frac{\eta_{54}\eta_{41}}{\eta_4\eta_1} & \frac{\eta_{62}\eta_{21}}{\eta_2\eta_1} \\ \frac{\eta_{14}\eta_{42}}{\eta_4\eta_2} & \frac{\eta_{21}\eta_{12}}{\eta_1\eta_2} + \frac{\eta_{23}\eta_{32}}{\eta_3\eta_2} + \frac{\eta_{24}\eta_{42}}{\eta_4\eta_2} + \frac{\eta_{26}\eta_{62}}{\eta_6\eta_2} & \frac{\eta_{36}\eta_{62}}{\eta_6\eta_2} & \frac{\eta_{41}\eta_{12}}{\eta_1\eta_2} & \frac{\eta_{54}\eta_{42}}{\eta_4\eta_2} & \frac{\eta_{63}\eta_{32}}{\eta_3\eta_2} \\ \frac{\eta_{12}\eta_{23}}{\eta_2\eta_3} & \frac{\eta_{26}\eta_{63}}{\eta_6\eta_3} & \frac{\eta_{32}\eta_{23}}{\eta_2\eta_3} + \frac{\eta_{36}\eta_{63}}{\eta_6\eta_3} & \frac{\eta_{42}\eta_{23}}{\eta_2\eta_3} & \frac{\eta_{56}\eta_{63}}{\eta_6\eta_3} & \frac{\eta_{62}\eta_{23}}{\eta_2\eta_3} \\ \frac{\eta_{12}\eta_{24}}{\eta_2\eta_4} & \frac{\eta_{21}\eta_{14}}{\eta_1\eta_4} & \frac{\eta_{32}\eta_{24}}{\eta_2\eta_4} & \frac{\eta_{41}\eta_{14}}{\eta_1\eta_4} + \frac{\eta_{42}\eta_{24}}{\eta_2\eta_4} + \frac{\eta_{45}\eta_{54}}{\eta_5\eta_4} & 0 & \frac{\eta_{62}\eta_{24}}{\eta_2\eta_4} + \frac{\eta_{65}\eta_{54}}{\eta_5\eta_4} \\ \frac{\eta_{14}\eta_{45}}{\eta_4\eta_5} & \frac{\eta_{24}\eta_{45}}{\eta_4\eta_5} & \frac{\eta_{36}\eta_{65}}{\eta_6\eta_5} & 0 & \frac{\eta_{54}\eta_{45}}{\eta_4\eta_5} + \frac{\eta_{56}\eta_{65}}{\eta_6\eta_5} & 0 \\ \frac{\eta_{12}\eta_{26}}{\eta_2\eta_6} & \frac{\eta_{23}\eta_{36}}{\eta_3\eta_6} & \frac{\eta_{32}\eta_{26}}{\eta_2\eta_6} & \frac{\eta_{42}\eta_{26}}{\eta_2\eta_6} + \frac{\eta_{45}\eta_{56}}{\eta_5\eta_6} & 0 & \frac{\eta_{62}\eta_{26}}{\eta_2\eta_6} + \frac{\eta_{63}\eta_{36}}{\eta_3\eta_6} + \frac{\eta_{65}\eta_{56}}{\eta_5\eta_6} \end{pmatrix} \tag{2.37}$$

Note that in contrast to (2.36), the diagonal elements of (2.37) are non-null which shows that the existence of transmission paths starting and finishing at the same subsystem is possible. In addition, note also that when two subsystems are connected by more than one path, the corresponding element in matrix $\boldsymbol{\mathcal{S}}^2$ includes the contribution of all of them as a summation. For example, the second order paths departing from subsystem 4 to subsystem 6 are $P_{46,1}^2 = 4 \to 2 \to 6$ and $P_{46,2}^2 = 4 \to 5 \to 6$ and so, their total contribution is $\mathcal{S}_{64}^2 = w\left(P_{46,1}^2\right) + w\left(P_{46,2}^2\right) = \frac{\eta_{42}\eta_{26}}{\eta_2\eta_6} + \frac{\eta_{45}\eta_{56}}{\eta_5\eta_6}$.

Therefore, observing the powers of $\boldsymbol{\mathcal{S}}$ and the number of terms in the sums of each element, one can determine the number of paths between every pair of subsystems. However, there is a direct way to count paths of a certain order between subsystems and it is by binarizing matrix $\boldsymbol{\mathcal{S}}$ [Guasch and Cortés, 2009],

$$\mathcal{S}_{b,ij} = \begin{cases} 0 & \text{if } S_{ij} = 0 \\ 1 & \text{if } S_{ij} \neq 0 \end{cases} \tag{2.38}$$

Therefore, following the definition in (2.38), the $\boldsymbol{\mathcal{S}_b}$ corresponding to (2.36) becomes

$$\boldsymbol{\mathcal{S}_b} = \begin{pmatrix} 0 & 1 & 0 & 1 & 0 & 0 \\ 1 & 0 & 1 & 1 & 0 & 1 \\ 0 & 1 & 0 & 0 & 0 & 1 \\ 1 & 1 & 0 & 0 & 1 & 0 \\ 0 & 0 & 0 & 1 & 0 & 1 \\ 0 & 1 & 1 & 0 & 1 & 0 \end{pmatrix}. \tag{2.39}$$

In the same way that the powers of $\boldsymbol{\mathcal{S}}$ contain the path contributions, the i-th power of $\boldsymbol{\mathcal{S}}_b$ contains the number of i-th order paths between every pair of subsystems. Thus,

$$\boldsymbol{\mathcal{S}}_b^2 = \begin{pmatrix} 2 & 1 & 1 & 1 & 1 & 1 \\ 1 & 4 & 1 & 1 & 2 & 1 \\ 1 & 1 & 2 & 1 & 1 & 1 \\ 1 & 1 & 1 & 3 & 0 & 2 \\ 1 & 2 & 1 & 0 & 2 & 0 \\ 1 & 1 & 1 & 2 & 0 & 3 \end{pmatrix}. \tag{2.40}$$

Next, if the order is increased to e.g. 10, it can be observed that the number of paths grows significantly,

$$\boldsymbol{\mathcal{S}}_b^{10} = \begin{pmatrix} 3754 & 5933 & 3753 & 4605 & 3277 & 4605 \\ 5933 & 9672 & 5933 & 7045 & 5442 & 7045 \\ 3753 & 5933 & 3754 & 4605 & 3277 & 4605 \\ 4605 & 7045 & 4605 & 5919 & 3768 & 5918 \\ 3277 & 5442 & 3277 & 3768 & 3118 & 3768 \\ 4605 & 7045 & 4605 & 5918 & 3768 & 5919 \end{pmatrix}, \tag{2.41}$$

which makes a big difference from the number of 2nd order paths. Therefore, from the example above, it can be observed that as the path order grows, the number of paths between two subsystems becomes larger. However, since the path contribution is the product of several quantities less than unity, their contribution diminishes with increasing length. Thus, in spite of their increase in number, as the paths get longer, their contribution becomes insignificant, i.e. as $i \to \infty \Rightarrow \boldsymbol{\mathcal{S}}^i \to 0$.

Consequently, beyond a certain power of $\boldsymbol{\mathcal{S}}$, the contribution of the paths to the total energy is little and thus, they can be neglected. In other words, the series in (2.34) can be truncated without incurring significant error in the value of $\boldsymbol{E}$. To put it another way, in some situations, it follows that there is a limited group of paths whose contribution represents a big portion of the total energy at the target subsystem whereas the rest of the paths can be ignored. When the former group is relatively small, such paths are known as dominant energy transmission paths.

Obtaining the group of the most dominant energy transmission paths not only at high frequencies, i.e. in a SEA system, but also at mid frequencies, will be the main subject of study in this thesis.

2.6 GRAPH THEORY

In the previous section we have introduced the importance of finding a method that permits obtaining the energy transmission paths in a vibroacoustic model

in a straightforward way. As one may suppose, path problems are not exclusive to this framework, they are also relevant for instance in logistics, to compute the best delivery routes or in telecommunications, to design communication networks. There is a discipline included in the branch of discrete mathematics devoted to the study of this kind of problems which is graph theory.

The origins of graph theory date back to 1735 with the resolution of the so-called problem of *The Seven Bridges of Königsberg* by Leonhard Euler. However, it was not until 1878 that the term *graph* was first coined [Gross et al., 2013]. From then on, significant advances on graph theory have been achieved largely due to its interest to computer engineering and new technology frameworks. Nowadays, graphs have an even wider range of applications as a tool for calculation and optimization.

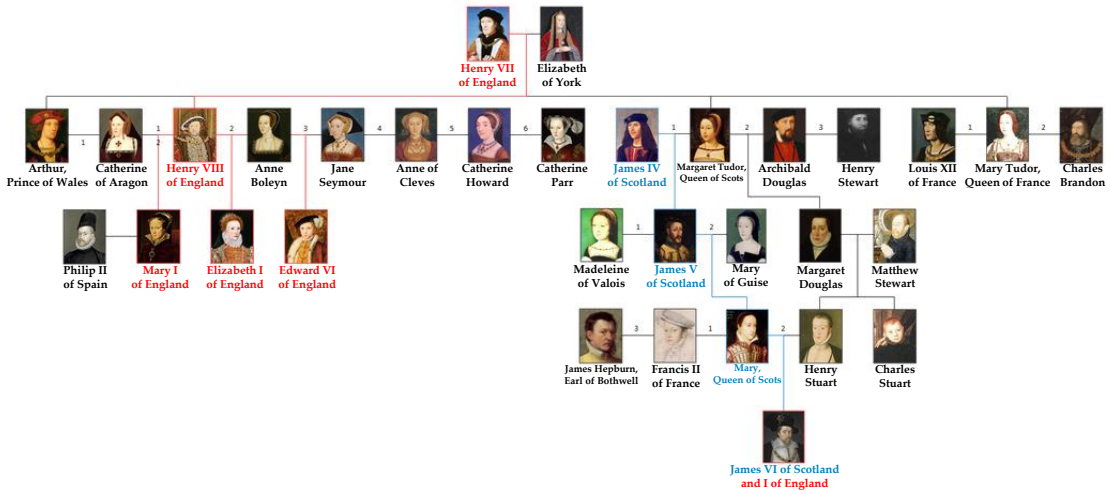

(a)

(b)

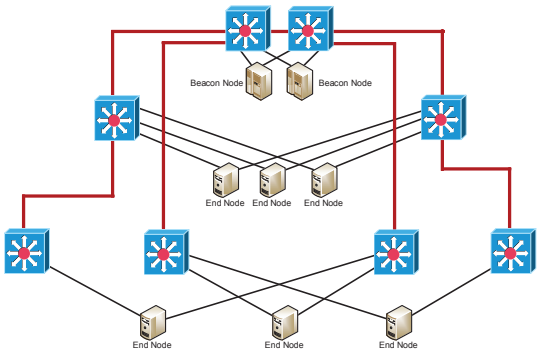

(c)

Figure 2.5: Examples of potential graphs. (b) Railway network. (c) Communications redundancy network. (a) Henry VIII of England's family tree [Wikipedia contributors, 2015]

Typically, one thinks of a graph as a set of points plotted in a plane or a 3d-space and a set of lines or arrows which are connecting some of the points. In fact, conceptually, a graph consists of a group of elements which are pairwise related. For example, the members of a family in a genealogic tree like in Figure 2.5a, a railway network like the one depicted in Figure 2.5b or a telecommunications network such as for instance, the one shown in Figure 2.5c. Throughout this section we will focus on the example of the railway network to support the explanations about several graph theory concepts.

Amongst all the cities that appear in the map, we have selected some of them arbitrarily to build the graph in Figure 2.6. In it, there is a dot for every selected city or train station in the network and a segment for every direct connection between stations. Note that the position of the points in the graph is irrelevant since the only necessary information is if they are connected or not. As we will see later, other types of information such as distances or costs can be included by adding attributes to the arcs.

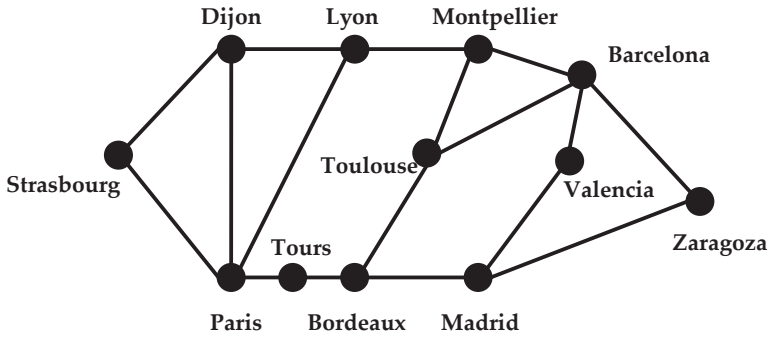

Figure 2.6: Graph corresponding to the railway network in Figure 2.6.

Let us give now a formal definition of a graph and of some of the basic concepts of graph theory which are necessary for the comprehension of the later chapters.

GRAPH A *graph* is a pair of sets $G = (U, E)$ where $U = \{u_1, u_2, \ldots, u_n\}$ is a set of items called *nodes* or *vertices* and $E \subset U \times U$ is a subset whose elements (u_i, u_j) are called *arcs* or *edges*. Every edge joins the two nodes, u_i and u_j, that compose it.

Thus, the graph in Fig. 2.6 has 12 nodes, which are $U = \{$Strasbourg, Dijon, Paris, $\ldots$, Zaragoza$\}$, and 17 arcs, $E = \{$(Strasbourg, Dijon), (Strasbourg, Paris), $\ldots$, (Barcelona, Valencia)$\}$.

Some of the characteristics of a graph depend on the characteristics of its arcs. Below, some definitions concerning to the arcs can be found.

DIRECTED AND UNDIRECTED GRAPHS A graph whose arcs have a definite direction, i.e. $(u_i, u_j) \neq (u_j, u_i)$, is called a *directed* graph or a *digraph*. Conversely, a graph where $(u_i, u_j) \equiv (u_j, u_i)$ is named *undirected* graph.

HEAD AND TAIL OF AN ARC Given a directed arc (u_i, u_j), the initial node u_i is known as the *tail* of the arc and the terminal node u_j as the *head* of the arc. The set of edges between u_i and its adjacent (neighbours) nodes is denoted as $\mathcal{E}_i$. We will distinguish between $\mathcal{E}_i^+$, corresponding to edges $(u_j, u_i) \in \mathcal{E}_i$ such that u_i is the head of the edge, and $\mathcal{E}_i^-$ whose edges are such that u_i is their tail node.

LOOPS AND REFLEXIVE GRAPHS An arc (u_i, u_i) whose *tail* and *head* correspond to the same node u_i is known as a *loop*. A graph where there exists a loop for every node is called a *reflexive* graph. Conversely, a graph where none of the nodes has a loop is called *anti-reflexive*.

SYMMETRIC GRAPH A graph is said to be *symmetric* if for every arc $(u_i, u_j) \in E$ exists an arc $(u_j, u_i) \in E$.

SIMPLE GRAPH A graph which is anti-reflexive and symmetric is called a *simple* graph.

Figure 2.7 contains some examples of graphs distinguished by the characteristics mentioned above. The first graph in Figure 2.7a is an example of undirected graph with a loop in node A and a loop in node B. It is not a reflexive graph since not all the nodes have a loop. In the second graph (Fig. 2.7b), the arcs have a defined direction. For example, there is a connection from A to B but not in the opposite direction. By contrast, B and C are connected in both directions. Note that there may be more than one arc between every pair of nodes. The third graph, in 2.7c, is a simple graph, it does not contain any loop and for every arc, there is another one in the opposite direction.

Throughout this work only simple directed graphs will be considered, thus, for the sake of simplicity, some of the following definitions will be particularized for this type of graphs and we will refer to *simple graphs* only as *graphs* unless otherwise indicated.

Besides the graphical plot, a graph may be also represented by a matrix which contains exactly the same information. The following concepts are linked to this matrix and the uses it may have [Carré, B.A., 1979; Gross et al., 2013].

ADJACENT NODES Two different nodes u_i and u_j are considered *adjacent* if there exists an arc connecting them, i.e. if $(u_i, u_j) \in E$ or $(u_j, u_i) \in E$.

ADJACENCY MATRIX Given a graph with N nodes, its adjacency matrix is an $N \times N$ matrix whose elements are defined by

$$\mathcal{A}_{ij} = \begin{cases} 1 & \text{if} \quad (u_i, u_j) \in E \\ 0 & \text{if} \quad (u_i, u_j) \notin E. \end{cases} \tag{2.42}$$

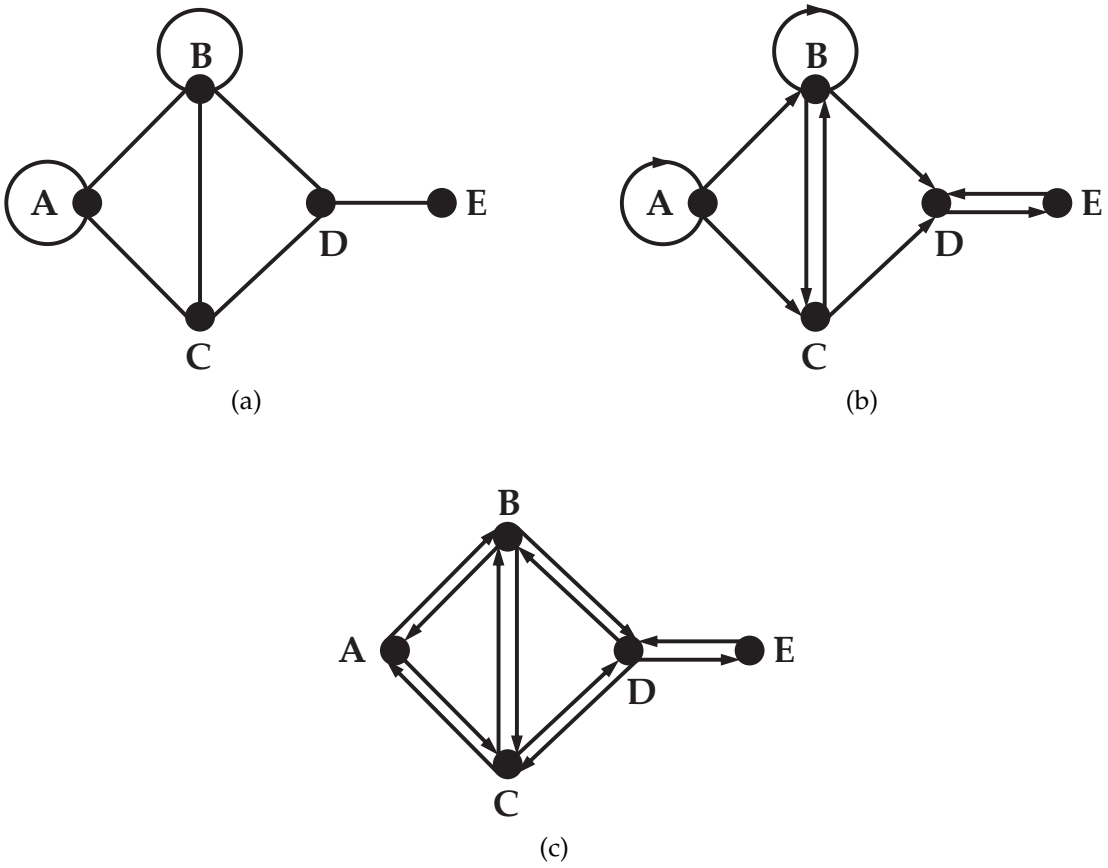

Figure 2.7: Some types of graphs (a) Undirected graph with loops. (b) Digraph with loops. (c) Simple graph.

WEIGHTED GRAPHS AND WEIGHTING MATRIX A *weighted* graph is such that its arcs (u_i, u_j) are assigned a weight $w_{u_i u_j}$. The weights can be gathered in a *weighting matrix* defined as

$$\mathcal{W}(i,j) = \begin{cases} w_{u_i u_j} & \text{if} \quad (u_i, u_j) \in E \\ 0 & \text{if} \quad (u_i, u_j) \notin E. \end{cases} \tag{2.43}$$

PATH A *path* is a finite concatenation of arcs, expressed as

$$p^n_{u_{i_0} u_{i_n}} = \left\{ (u_{i_0}, u_{i_1}) (u_{i_1}, u_{i_2}) (u_{i_2}, u_{i_3}) \dots (u_{i_{n-1}}, u_{i_n}) \right\}, \tag{2.44}$$

or, alternatively,

$$p^n_{u_{i_0} u_{i_n}} = \left\{ u_{i_0}, u_{i_1}, u_{i_2}, u_{i_3} \dots u_{i_{n-1}}, u_{i_n} \right\}. \tag{2.45}$$

ORDER OF A PATH Given a path $p^n_{u_{i_0} u_{i_n}}$, the number of concatenated arcs n is called the *order* of the path.

HEAD AND TAIL OF A PATH Given a path $p^n_{u_{i_0} u_{i_n}}$, the initial node u_{i_0} is called the *tail* or the *source* of the path whereas the terminal node u_{i_n} is called the *head* or the *target* of the path.

OPEN PATHS AND CYCLES A path whose tail and head correspond to different nodes is an *open* path whereas a path whose tail and head correspond to the same node is a *closed* path or *cycle*.

PATH ALGEBRA A *path algebra* is a set P provided with two binary operations: the join operation $(\vee)$ and the multiplication $(\cdot)$. They fulfill the following properties,

1. The join operation is idempotent, commutative and associative
2. The multiplication is associative, and distributive over the join operation.
3. The set P contains a zero element $\emptyset$ such that $\emptyset \vee x = x$ and $\emptyset \cdot x = \emptyset$ and a unit element e such that $e \cdot x = x = x \cdot e$, for all $x \in P$.

Path algebras can be used to formulate and solve path problems in a graph.

WEIGHT OF A PATH The weight of a path is computed as the weight of all the arcs forming the path. For instance,

$$w_a\left(p^n_{u_{i_0}u_{i_n}}\right) = w_{u_{i_0}u_{i_1}} w_{u_{i_1}u_{i_2}} w_{u_{i_2}u_{i_3}} \dots w_{u_{i_{n-1}}u_{i_n}}, \tag{2.46}$$

or

$$w_b\left(p^n_{u_{i_0}u_{i_n}}\right) = w_{u_{i_0}u_{i_1}} + w_{u_{i_1}u_{i_2}} + w_{u_{i_2}u_{i_3}} + \dots + w_{u_{i_{n-1}}u_{i_n}}. \tag{2.47}$$

CONCATENATION OF PATHS Given the paths p_{ij} and q_{jl}, respectively linking node u_i with u_j and node u_j with u_l, the concatenated path $p_{ij} \circ q_{jl}$ from u_i to u_l according to (2.46) will have weight

$$w\left(p_{ij} \circ q_{jl}\right) = w\left(p_{ij}\right) w\left(q_{jl}\right) = \prod_p w_{ij} \prod_q w_{jl} = \prod_{p+q} w_{il}. \tag{2.48}$$

and according to (2.47) will have weight

$$w\left(p_{ij} \circ q_{jl}\right) = w\left(p_{ij}\right) + w\left(q_{jl}\right) = \sum_p w_{ij} \sum_q w_{jl} = \sum_{p+q} w_{il}. \tag{2.49}$$

CONNECTED AND STRONGLY CONNECTED GRAPHS A graph is said to be *connected* if for any two nodes u_i and u_j there exists a path from u_i to u_j, or a path from u_j to u_i. If both paths exist the graph is said to be *strongly connected*.

The significance of adding weights to the arcs and defining paths in the graph may be illustrated using again the example of the railway network. Let us suppose one wants to travel from Strasbourg to Barcelona. Having a glance to the map in Fig. 2.5b, it can be observed that there are several possible routes connecting both cities although a priori, one cannot determine which is the best one. There might be many preference criteria to determine which is the best

route, for instance the quickest journey, the cheapest one, the one that have less train changes or even a compromise solution which takes into account all the previous ones. The method to answer these questions may be found using graph theory.

Let us imagine that one wants to find the quickest route between the two mentioned cities. The weights of the arcs in Fig. 2.6 could be defined as the journey times for every segment, for instance, $w_{Lyon,\ Paris} = 118\text{min}$. Then, the weight of all the possible routes from Strasbourg to Barcelona could be computed using (2.47). In other words, a path algebra can be defined such that $P = \mathbb{R} \cup \{\infty\}$, $x \vee y := \min\{x, y\}$, $x \cdot y := x + y$, $\emptyset := \infty$ and $e := 0$. It seems obvious that defining a graph is not necessary to compute the time that a journey between two cities will take. However, if a path or a group of paths fulfilling a certain requirement is to be found, as in this case the quickest; one would have to find all the possible combinations of routes, compute the cost of each one, and then, find the one with the required characteristics.

The advantage on using graph theory is that there exist many algorithms focused on computing paths in a graph. Following any criterium or even more than one, the path algorithms are used to obtain results such as the shortest (or the longest) path between two nodes, the one with maximum (or minimum) weight, an ordered list of paths fulfilling a certain requirement, etc. For example, one of these groups of algorithms are the so called *k shortest path algorithms* which aim at finding the first k shortest paths from a source node to a target node in a graph.

Therefore, using a k shortest paths algorithm, one may compute an ordered list of the k cheapest routes from Strasbourg to Barcelona, being k a value fixed by the user. The results would be obtained straightforwardly and most importantly, the optimum solution would be found. Some of these algorithms will be reviewed in depth in the following chapters.

To finish the overview on graph theory, the idea of dividing a graph in subgraphs is introduced.

SUBGRAPH Given a graph $G = (U_G, E_G)$, a graph $H = (U_H, E_H)$ whose nodes $U_H \subset U_G$ and whose arcs $E_H \subset E_G$ is said to be a subgraph of G.

$s-t$ CUT Given $G = (U, E)$, let $s \in U$ and $t \in U$, with $s \neq t$ and let U_s and U_t form a partition of U such that $U_s \cup U_t = U$, $U_s \cap U_t = \emptyset$, $s \in U_s$ and $t \in U_t$. Then, the set of all arcs that has an endpoint in U_s and the other in U_t is expressed as $\langle U_s, U_t \rangle$ an called *$s-t$ cut*.

MINIMUM $s-t$ CUT An $s-t$ cut such that $\langle U_s, U_t \rangle$ has the minimum weight is a *minimum $s-t$ cut*.

From a more practical point of view, to obtain an $s-t$ cut means to find a way to isolate the node t from s and viceversa. In other words, if the arcs in $\langle U_s, U_t \rangle$ are deleted, all the paths that connect s and t disappear. In the example of Figure 2.6, if Strasbourg is set as s and Barcelona as t, one of the possible

$s-t$ cuts is $\langle U_s, U_t\rangle = \{(\text{Lyon}, \text{Montpellier}), (\text{Tours}, \text{Bordeaux})\}$. Therefore, if all the connections included in $\langle U_s, U_t\rangle$ were interrupted, and assuming that there are no alternatives other than the ones included in the graph, travelling from Strasbourg to Barcelona would become impossible.

As an example, two $s-t$ cuts are found in the graph of Fig. 2.8, where s is placed at node C and t at node F. The $s-t$ cuts are depicted in Figures 2.9 and 2.10. The nodes belonging to U_s are colored in yellow and the nodes belonging to U_t are colored in blue. The elements of $\langle U_s, U_t\rangle$ are represented by red dashed lines.

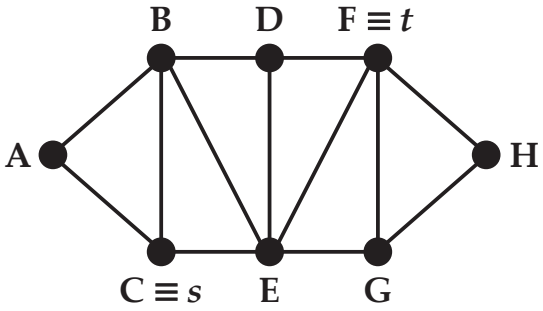

Figure 2.8: Graph where s is placed at node C and t at node F

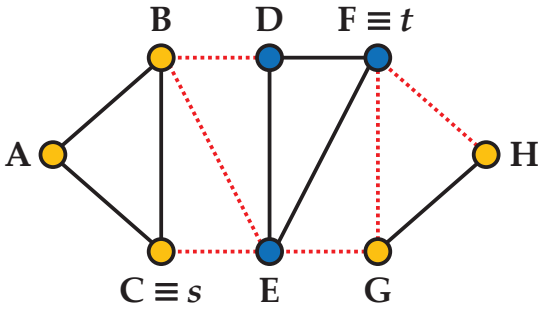

Figure 2.9: $s-t$ cut i: First example of $s-t$ cut in the graph of Fig. 2.8

The first $s-t$ cut, in Fig. 2.9, is expressed as

$$
\begin{aligned}
U_s^i &= \{A, B, C, G, H\}, & E_s^i &= \{(A,B),(A,C),(B,C),(G,H)\}\\
U_t^i &= \{D, E, F\}, & E_t^i &= \{(D,E),(D,F),(E,F)\}\\
\langle U_s, U_t\rangle^i &= \{(B,D),(B,E),(C,E),(E,G),(F,G),(F,H)\}.
\end{aligned}
$$

The graph is divided into two subgraphs, $G_s^i = (U_s^i, E_s^i)$ and $G_t^i = (U_t^i, E_t^i)$ and the arcs in $\langle U_s, U_t\rangle$ have an endpoint in U_s^i and the other in U_t^i. This specific example is included to highlight a characteristic of the $s-t$ cuts that might be not directly intuited. As it can be observed, the nodes G and H are not connected with the rest of the nodes in U_s^i. In other words, the subgraphs resulting from the $s-t$ cut do not have to be strongly connected. Some other examples will be seen in Chapter 7.

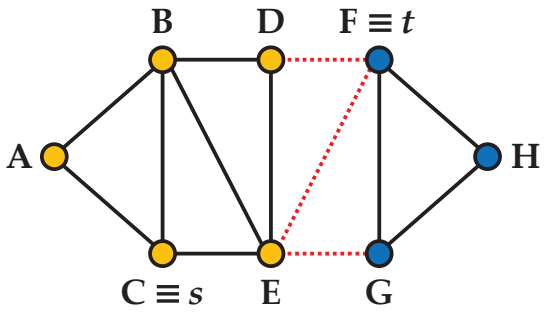

Figure 2.10: $s-t$ cut ii: Second example of $s-t$ cut in the graph of Fig. 2.8 and minimum $s-t$ cut.

The second example of $s-t$ cut to be examined is shown in Figure 2.10 and expressed as

$$U_s^{ii} = \{A, B, C, D, E\}, \quad E_s^{ii} = \{(A,B),(A,C),(B,C),(B,D),(B,E),(C,E),(D,E)\}$$
$$U_t^{ii} = \{F, G, H\}, \quad E_t^{ii} = \{(F,G),(F,H),(G,H)\}$$
$$\langle U_s, U_t \rangle^{ii} = \{(D,F),(E,F),(E,G)\}.$$

The graph is split again in two subgraphs $G_s^{ii} = (U_s^{ii}, E_s^{ii})$ although in this case both are strongly connected. Assuming an equal weight for all the arcs, the minimum number of arcs necessary to isolate C from F is 3. Therefore, the $s-t$ cut in Figure 2.10 becomes a minimum $s-t$ cut.

2.7 USE OF GRAPH THEORY TO OBTAIN THE ENERGY TRANSMISSION PATHS IN A SEA MODEL

In Section 2.5, the worth of obtaining the energy transmission paths in a vibroacoustic system has been proved. Besides a review of some experimental procedures, the analytical definition of an energy transmission path in a SEA system has been given. In addition, the decomposition of the subsystem energies in terms of transmission paths has been justified thanks to the series development in 2.34. However, a direct method to obtain such paths and to work with them is still missing.

As we have seen in Section 2.6, graph theory is a powerful tool for path computation. We recall that in simple terms, a graph is a set of elements which share some pairwise connections. On the other hand, in Section 2.2, it has been explained that the definition of a SEA model consists in dividing the system in subsystems and establishing power flows between them. Observing the SEA diagrams in Figures 2.1 and 2.4, the conceptual similarities between a graph and a SEA system become evident.

This thesis proposes the definition of a graph which accurately represents a vibroacoustic system so that graph algorithms can be used to solve problems related to energy transmission paths. In this section, the approach is introduced for SEA systems yet in subsequent chapters analogous definitions will be given

for Energy Distribution and SmEdA models. The graph that represents the SEA system is called SEA graph and is defined as follows [Guasch and Cortés, 2009].

THE SEA GRAPH A SEA graph, $G_{\text{SEA}} = \{U_{\text{SEA}}, E_{\text{SEA}}\}$ is a simple digraph such that every node u_i in U_{SEA} corresponds to a SEA subsystem and such that directed arcs $(u_i, u_j), (u_j, u_i) \in E_{\text{SEA}}$ exist between subsystems u_i and u_j, whenever they are coupled in the SEA model.

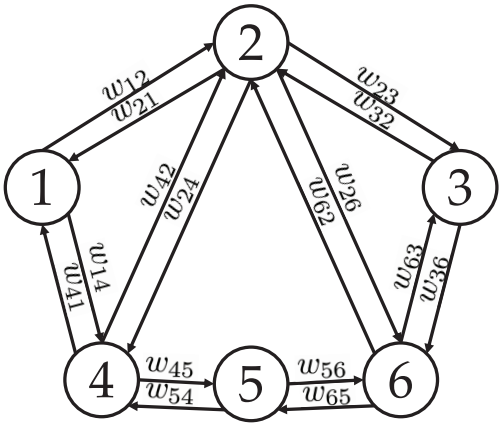

Figure 2.11: SEA graph corresponding to the system in Figure 2.3

Thus, the SEA graph that corresponds to the SEA system in Figure 2.3 is the one depicted in Figure 2.11. The choice of the arc weights as well as the path algebras, w_{ij} will depend on the problem that has to be solved [Guasch and Cortés, 2009]. The considered problems in this work can be classified into two general types. First, the case where the most dominant energy transmission paths between a source subsystem and a target subsystem have to be found. In this case, the arc weights w_{ij} are identified with the contribution of the first order paths between subsystem i and subsystem j, i.e.

$$\mathcal{W}(i,j) = w_{ij} = \begin{cases} \frac{\eta_{ij}}{\eta_j} & \text{if} \quad (u_i, u_j) \in E_{\text{SEA}} \\ 0 & \text{if} \quad (u_i, u_j) \notin E_{\text{SEA}}. \end{cases} \tag{2.50}$$

Therefore the weighting matrix $\boldsymbol{\mathcal{W}}$ coincides with the transposed of the generating matrix $\boldsymbol{\mathcal{S}}^{\top}$ in the Neumann series solution of the SEA algebraic matrix system defined in (2.34) and (2.35).

In addition, the weight of a path in a SEA graph is defined to coincide with the Craik's definition of a SEA path,

$$w\left(p^n_{u_{i_0}u_{i_n}}\right) = w_{u_{i_0}u_{i_1}} w_{u_{i_1}u_{i_2}} w_{u_{i_2}u_{i_3}} \dots w_{u_{i_{n-1}}u_{i_n}} = \frac{\eta_{i_0 h_1}}{\eta_{h_1}} \frac{\eta_{h_1 h_2}}{\eta_{h_2}} \dots \frac{\eta_{h_{n-1} h_n}}{\eta_{h_n}}. \tag{2.51}$$

The second type of problem, which will be discussed in Chapter 7, uses the energy transmission paths from a different point of view. The proposed situation consists of a system where there is a vibroacoustic source and a target subsystem

where energy has to be minimized. An ideal situation would be that of totally isolating the source from the target, so the energy cannot be transmitted from the former to the latter. In other words, to suppress all the energy transmission paths from the source to the target.

As explained in Section 2.6, algorithms which permit the form to find the minimum cuts to separate two nodes in a graph exist. The isolation of two nodes in a graph is equivalent to cut all the paths connecting those nodes. Therefore, as described with more detail in Chapter 7, the obtention of the minimum cuts between the source and the target in the SEA graph will provide the modifications to apply in the SEA system. In this case, the important detail is not the path weight but its existence.

Therefore, in Chapter 7, in addition to the weighting matrix $\boldsymbol{\mathcal{W}}$ defined in (2.50), we will also be interested in the boolean adjacency matrix $\boldsymbol{\mathcal{W}_b}$ obtained by weighting with zeros and ones the undirected SEA graph $B_{SEA} = (U^u_{SEA}, E^u_{SEA})$ induced by the binary counterpart of $\boldsymbol{\mathcal{S}}$, $\boldsymbol{\mathcal{S}_b}$ in (2.38) (see also [Guasch and Cortés, 2009]). $\boldsymbol{\mathcal{W}_b}$ is a symmetric matrix with elements

$$\mathcal{W}_b(i,j) = \begin{cases} 1 & \text{if} \quad (u_i, u_j) \in E^u_{SEA} \\ 0 & \text{if} \quad (u_i, u_j) \notin E^u_{SEA}. \end{cases} \tag{2.52}$$

Note that $U^u_{SEA} = U_{SEA}$ but that E^u_{SEA} contains half the elements of E_{SEA}.

In conclusion, a graph which accurately represents the SEA system is defined. Accordingly, the problem of computing energy transmission path problems in a SEA system can be posed in the graph theory framework. This permits a direct and easier resolution of the different mentioned problems by making use of the graph algorithms. In addition, since SEA has a limited scope of validity, in Chapters 5 and 6, the approach will be applied to other techniques that relax SEA requirements. In this way, the approach will be extended to lower frequencies.

2.8 CONCLUSIONS

In this chapter, an overview of the numerical methods used to solve vibroacoustic problems is given. The methods can be classified according to the frequency range where they are valid. At low frequencies, deterministic methods such as Finite Element Analysis are applied since there is a low population of modes and they are well separated. At high frequencies, the characteristics of the response are exactly the opposite and they require the use of statistical methods such as Statistical Energy Analysis. At the mid-frequency range, the intermediate situation asks for alternative approaches such as the hybrid FE-SEA method. Special emphasis is provided to Statistical Energy Analysis and two mid-frequency methods, specifically Energy Distribution Analysis and Statistical modal Energy distribution Analysis, since the approach proposed in this thesis will be applied to these kinds of models.

Next, the importance of transmission path analysis has been discussed and the need of a method to identify energy transmission paths in a vibroacoustic system has been introduced. To fill this gap, this thesis proposes the application of graph theory to obtain the mentioned transmission paths. To that end, a brief introduction to graph theory is given.

Finally, the connection between graph theory and the vibroacoustic models is established by the definition of the SEA graph, i.e. a graph which represents the SEA system. In subsequent chapters, algorithms to compute energy transmission paths in SEA systems will be implemented using the SEA graph and the approach will be extended to the cited mid-frequency methods.

3

FINDING THE DOMINANT ENERGY TRANSMISSION PATHS IN STATISTICAL ENERGY ANALYSIS

Summary. A key issue for noise, vibration and harshness purposes, when modelling the vibroacoustic behaviour of a system, is that of determining how energy is transmitted from a given source, where external energy is being input, to a target where energy is to be reduced. In many situations of practical interest, a high percentage of the transmitted energy is driven by a limited set of dominant paths. For instance, this is at the core of the existence of transmission loss regulations between dwellings. In this chapter, it is shown that in the case of a system modelled with statistical energy analysis (SEA), the problem of ranking dominant paths can be posed as a variation of the so called K shortest path problem in graph theory. An algorithm for the latter is then modified and adapted to obtain the sorted set of K dominant energy transmission paths in a SEA model. A numerical example to show its potential for practical applications is included.

This chapter is based on the following work

- O. Guasch and À. Aragonès. Finding the dominant energy transmission paths in statistical energy analysis. *Journal of Sound and Vibration*, 330(10): 2325 – 2338, 2011 [Guasch and Aragonès, 2011]
- O. Guasch and À. Aragonès. Ranking energy paths in a SEA model. In *Proceedings of 20th International Congress on Acoustics ICA 2010, Sidney, Australia, 2010*, 2010 [Guasch and Aragonès, 2010]

3.1 INTRODUCTION

As introduced in Chapter 2, an important problem for noise and vibration control, is that of ranking the energy transmission paths from a source subsystem s, where external energy is being input, to a target subsystem t. As quoted in [Craik, 1996], p. 161, "In many cases it is useful to know not only how much sound is transmitted, but also the transmission paths taken and the relative importance of these paths. This can be used to identify areas for remedial work or redesign".

Knowing whether energy transmission takes place via a small set of dominant paths carrying a high percentage of the overall energy or not, certainly constitutes

a question of practical interest. For instance, transmission loss regulations such as EN 12354-1 (ISO 15712-1) are based on a first order approach to SEA, and on the assumption that energy transmission between adjacent dwellings is mainly carried out through the direct path linking them, plus second order flanking paths [Craik, 1996; Galbrun, 2008].

Therefore, having a procedure to rank all existing energy transmission paths between rooms would turn very useful to analyse those cases in which the regulation is known to fail (see e.g., [Galbrun, 2008]). Providing a systematic procedure to determine the set of say, K ranked dominant energy transmission paths in a SEA model will be the main goal of this chapter.

The problem of finding the maximum energy transmission path in a SEA model is in fact analogous to the problem of finding the shortest path in a graph. The latter is a classical problem in graph theory and a large amount of literature can be found on it (see e.g., [Denardo and Fox, 1979; Deo and Pang, 1979; Dijkstra, 1959; Ford and Fulkerson, 1956; Yen, 1970] among hundreds).

With some slight modifications, several of the algorithms in these references can be generalized to find extremal paths in graphs weighted with very different path algebras [Carré, B.A., 1979]. Most of these algorithms rely on the Optimality principle which states that the there is an extremal path formed by extremal sub-paths [Martins et al., 1999]. The shortest path problem will be important for our purposes, given that its application constitutes a prior step to find the solution of the K shortest path problem.

Finding the set of K shortest paths in a graph is also a classical issue of graph theory. Although it has not been so extensively studied as the shortest path problem, again a vast amount of literature exists on it, given that applications can be found in many areas of science (see e.g., [Dreyfus, 1969; Eppstein, 1998] and references therein). A distinction must be made between two variations of the problem, namely that of finding the set of simple paths (i.e., the paths are loopless) and that of finding paths with repeated vertices. In the first case, fulfilment of the Optimality Principle [Martins et al., 1999] cannot be guaranteed so that the loopless constraint makes the problem harder. It will be shown that the SEA problem of finding the K dominant energy transmission paths corresponds to a problem of the second type, given that loop paths are obviously allowed to transmit energy from a source s to a target t, in a SEA model.

Again, several algorithms exist for the solution of the unconstrained path problem [Azevedo et al., 1993; Dreyfus, 1969; Eppstein, 1998; Martins, 1984; Martins et al., 1999; Miaou and Chin, 1991]. In this work use will be made of deviation path algorithms. In particular, we will adapt the MPS algorithm in [Martins et al., 1999] to compute the set of K dominant energy paths between source and receiver in a SEA model, although other options could have been chosen. The MPS is a very efficient algorithm [Santos, 2006] with theoretical computational cost $\mathcal{O}(N_E \log N + KN)$, N standing for the number of subsystems (vertices) in the SEA graph and N_E for the number of edges.

The chapter is organised as follows. In Section 3.2 we state the problem we would like to solve. In Section 3.4, the chosen MPS K shortest path algorithm is described and modified to find the set of K dominant energy transmission paths between s and t. A numerical example to test the performance and usefulness of the algorithm in practical cases is presented in Section 3.5. The considered case is that of energy transmission between subsystems in the SEA model of a building. Conclusions close the chapter in Section 3.6.

3.2 PROBLEM STATEMENT

3.2.1 *Energy transmission paths in statistical energy analysis*

The contribution of an energy transmission path can be computed using Craik's definition in (2.51). It expresses the ratio between the energy at the target and the energy at the source that has been transmitted through the particular path under consideration being $P_{st} = \{s, h_1, h_2, \ldots, h_{n-1}, t\}$. In other words, the product $w(P_{st})\, E_s$, with an arbitrary path, provides the energy at the target that has been transmitted through P_{st} [Craik, 1996]. If the energy at the target is to be expressed in terms of the external energy input at the source, W_s, then it suffices to take the product $w(P_{st})\, W_s/(\eta_s \omega)$ (ω standing for the radian frequency).

Consequently, the higher the value of $w(P_{st})$ in (2.51), the higher the energy transmitted along this particular path. In general, we will refer to paths carrying most energy from the source to the target as dominant transmission paths. Actually, the energy at the target can be recovered from the infinite summation of the energy contributions of all paths linking s and t. However, transmission path analysis in SEA is mainly of interest in those cases where the number of dominant paths is moderate, i.e., the energy at the target can be basically justified from the contributions of a finite and relatively small number of paths [Craik, 1996].

In this chapter, a systematic and efficient way to compute and rank the set of say, K, dominant paths in a SEA system will be presented.

3.2.2 *Problem definition in the framework of graph theory*

In Section 2.7, the link between SEA and graph theory has been established by defining a graph that accurately represents the SEA model. In the SEA graph, the nodes correspond to the SEA subsystems and the arcs to the first order paths between those subsystems. The weighting matrix of the SEA graph contains the contributions of the first order paths between every subsystem pair, as defined in (2.50). Thus, the problem of computing the dominant energy transmission paths can be solved using graph theory.

However, first and foremost, the condition to state that a path dominates over another must be established. The aim is to obtain the highest energy contribution

paths which in graph theory terms, equals to the maximum weight paths. Given two paths p_{ij} and q_{ij}, the dominance condition states that

$$p_{st} > q_{st} \Longleftrightarrow w\left(p_{st}\right) > w\left(q_{st}\right), \tag{3.1}$$

in other words, p_{st} dominates over q_{st} if $w\left(p_{st}\right)$ is greater than $w\left(q_{st}\right)$. Although the condition in 3.1 is trivial, more complex ones could be established as we will see in the next chapter. The first dominant path between u_i and u_j (the path transmitting maximum energy) will be denoted by p^*_{ij}.

The problem of determining the set of K dominant energy transmission paths in a SEA model (K being a finite positive integer number) can be stated as follows:

Problem 1. *Given two nodes s and t in a SEA graph G_{SEA} (s usually being identified with a source subsystem where external energy is being input, and t with a target subsystem where energy is to be reduced), we intend to find the set $\mathcal{P}_{st,K} = \{p_{st,1}, p_{st,2} \dots p_{st,K}\} \subseteq \mathcal{P}_{st}$ such that*

- $w(p_{st,k}) \geq w(p_{st,k+1})\ \forall k \in \{1, \dots K-1\}$,
- $w(p_{st,K}) \geq w(q_{st})\ \forall q_{st} \in \mathcal{P}_{st} - \mathcal{P}_{st,K}$,
- *$p_{st,k}$ is found just before $p_{st,k+1} \forall k \in \{1, \dots K-1\}$.*

In other words, we would like to find a set of K paths such that the k-th path in the set transmits more energy than the $k+1$ path (first item), such that any path in the set transmits more energy than any path not belonging to the set (second item), and such that all paths in the set are computed in order i.e., first the maximum energy transmission path p^*_{st} is found, then the second dominant path, then the third one and so on until the K-th path (third item).

Problem 1 is well-posed in the sense that it can be shown that the set $\mathcal{P}_{st,K}$ of K dominant paths exists, that each one of the K paths, $p_{st,k}$, involves a finite number of nodes (subsystems), and that each $p_{st,k}$ transmits a finite amount of energy (see Theorem 1 and Corollary 1 in Section 3.3).

3.3 EXISTENCE OF A SET OF k FINITE DOMINANT ENERGY PATHS

Theorem 1. *Consider a SEA digraph $G_{SEA} = (U_{SEA}, E_{SEA})$ with adjacency matrix $\boldsymbol{\mathcal{W}}$ given by the transpose of the generating matrix $\boldsymbol{\mathcal{S}}$ of the Neumann series solution of the SEA system, i.e. $\boldsymbol{\mathcal{W}} = \boldsymbol{\mathcal{S}}^\top$. There exists a finite and maximum energy transmission path from the source s to the target t in G_{SEA}.*

Proof. The proof relies on that of theorem 1 in [Martins et al., 1999], but adapted to the SEA framework (see also the reasoning in [Carré, B.A., 1979], section 3.3.3, page 97). If no approximation is made (no loss factor neglected), a SEA digraph will be strongly connected. Therefore, for every $u_i \in U_{\text{SEA}}$ it will follow that $\mathcal{P}_{si} \neq \emptyset$ and $\mathcal{P}_{it} \neq \emptyset$, which implies the existence of $p_{si} \in \mathcal{P}_{si}$

and $p_{it} \in \mathcal{P}_{it}$, such that $p_{st} = p_{si} \circ p_{it}$ is a path from the source s to the target t. Consider also that $u_i \in \mathcal{C}$, $\mathcal{C}$ being a cycle in G_{SEA} with weight $w(\mathcal{C}) = \prod_{\mathcal{C}} w_{ij}$. Denote by $\mathcal{C}^n$ the n cycle $\mathcal{C}$ concatenation $\mathcal{C} \circ \ldots \circ \mathcal{C}^{(n}$ (i.e., n turns around $\mathcal{C}$). Then $p_{st}(n) := p_{si} \circ \mathcal{C}^n \circ p_{it}$ is also a path from s to $t \; \forall \; n \geq 0$. If we define the limiting path $p_{st}^{\infty} := \lim_{n\to\infty} p_{st}(n)$, its weight will be given by

$$\begin{aligned} w(p_{st}^{\infty}) &= w[\lim_{n\to\infty} p_{st}(n)] = \lim_{n\to\infty} w[p_{st}(n)] = \lim_{n\to\infty} w[p_{si} \circ \mathcal{C}^n \circ p_{it}] \\ &= \lim_{n\to\infty} [w(p_{si}) w(\mathcal{C}^n) w(p_{it})] = w(p_{st}) \lim_{n\to\infty} [w(\mathcal{C}^n)] \\ &= w(p_{st}) \lim_{n\to\infty} [w(\mathcal{C})^n] \,. \end{aligned} \tag{3.2}$$

Let us consider the following two cases:

- Super-unitary cycle: The weight of a super-unitary cycle fulfils $w(\mathcal{C}) = \prod_{\mathcal{C}} w_{ij} > 1$. Hence, from (3.2) $w(p_{st}^{\infty}) = \infty$. That is to say the most dominant (maximum) path in G_{SEA} has infinite length and infinite weight.

- Absorptive cycle: In this case $w(\mathcal{C}) = \prod_{\mathcal{C}} w_{ij} \leq 1$. From (3.2) it follows that $w(p_{st}^{\infty}) \leq w(p_{st})$. That is to say, in the case of the cycle being unitary we get $w(p_{st}^{\infty}) = w(p_{st})$, whereas for the sub-unitary cycle we get $w(p_{st}^{\infty}) = 0$. In the case a sub-unitary cycle with finite n it is straightforward to see that $w\left[p_{st}(n)\right] < w(p_{st})$. Consequently, there exists an elementary path, the loopless path p_{st}, that has a finite number of nodes and whose weight is bigger than the weight of any path consisting in the concatenation of p_{st} with a finite or infinite cycle. Hence, from all elementary paths connecting s and t, the one having maximum weight will be the predominant or maximum energy transmission path in the SEA graph, G_{SEA}.

We next note that cycles in the SEA graph G_{SEA} will always be absorptive (in other words, G_{SEA} is an absorptive graph), otherwise energy conservation would be violated. To do so let us argue by contradiction and assume that super-unitary cycles are allowed in G_{SEA}.

Assume also, and without loss of generality, that external energy is only being input at the source subsystem s. The energy at the target t can be obtained from the Neumann series expansion [Guasch and Cortés, 2009]

$$E(t) = E_0'(s) \sum_{n=1}^{\infty} \mathcal{S}^n(t,s) = \eta_s^{-1} E_0(s) \sum_{n=1}^{\infty} \mathcal{S}^n(t,s) < \infty, \tag{3.3}$$

where we have used $E_0'(s) = E_0(s)/\eta_s$, $E_0(s)$ being the external energy supplied at the source. The last inequality is mandatory because any real system will be dissipative to some extent, so that the SEA power balance equations will yield finite energy for all subsystems. Now, the summation in (3.3) precisely represents the contributions of all paths [Magrans, 1993] (finite or infinite) linking s and t, which will be logically stronger than the contribution of any individual path. If we choose in particular $p_{st}(n) = p_{si} \circ \mathcal{C}^n \circ p_{it}$ with $\mathcal{C}$ super-unitary, we get

$$E(t) = \eta_s^{-1} E_0(s) \lim_{N\to\infty} \sum_{n=1}^{N} \mathcal{S}^n(t,s) \geq \eta_s^{-1} E_0(s) \lim_{N\to\infty} w[p_{si} \circ \mathcal{C}^N \circ p_{it}] = \infty, \tag{3.4}$$

which contradicts (3.3). Thus no super-unitary cycles are admissible in G_{SEA}.

□

Corollary 1. *The problem of finding the $K \in \mathbb{Z}^+$ dominant paths in the SEA graph G_{SEA} is finite.*

Proof. It is a direct consequence of Theorem 1.

□

3.4 THE SET OF k DOMINANT PATHS IN A SEA MODEL

3.4.1 *Algorithm general description*

As it has been mentioned in the introduction, the MPS algorithm in [Martins et al., 1999] will be adapted to solve the K energy transmission path problem stated above. The MPS algorithm is based on a generalization of the algorithm in [Yen, 1971] for the K shortest loopless path problem and makes use of the idea of deviation paths introduced in [Eppstein, 1998]. A general description of the main processes of the algorithm will be next provided, while a detailed step by step application for a benchmark SEA problem will be given in next subsection, for a better comprehension.

A necessary condition for the algorithm to work properly is that there must be no edge in E_{SEA} with the source s as the head node, and no edge with the target t as the tail node. This is clearly not the case in a SEA model, but the problem can easily be solved by enlarging the SEA graph with virtual source and target nodes vs and vt, such that $w_{vs\,s} = w_{t\,vt} = 1$ (i.e., the energy attenuation of a path linking the source and the target does not change if the virtual nodes are included in the path). The algorithm is then applied to nodes vs and vt yielding the expected results.

It is also assumed that the tree $\mathcal{T}_t^* = (U_{\text{SEA}}, E_t^*)$ of all maximum energy transmission paths from any node in the graph to the target t has already been computed. The maximum path from a particular $u_i \in U_{\text{SEA}}$ to t can be computed by introducing some modifications to well-known algorithms, such as the Dijkstra algorithm [Dijkstra, 1959]. In [Carré, B.A., 1979] it is shown how the latter and several other algorithms intended to solve algebraic linear systems, can be adapted to solve extremal path problems. The procedure is explained in full detail in that reference and will be not reproduced here. Once all maximum energy transmission paths p_{it}^* have been computed, the maximum energy tree rooted at t, $\mathcal{T}_t^*$, can be build. The weight of a path $p_{it}^* \in \mathcal{T}_t^*$ will be denoted by $\pi_i \equiv w(p_{it}^*)$. A very efficient way to obtain $\mathcal{T}_t^*$ is based on the use of Fibonacci heaps [Fredman and Tarjan, 1987].

The algorithm to compute the K dominant energy transmission paths relies on the notion of deviation path. Consider for instance, the finite nth order path from source to target $p_{st} = \left\{ \left(s, u_{h_1}\right), \left(u_{h_1}, u_{h_2}\right), \ldots \left(u_{h_{n-1}}, t\right) \right\}$. Then, the mth order

path $q_{st} = \{(s, v_{h_1}), (v_{h_1}, v_{h_2}), \ldots (v_{h_{m-1}}, t)\}$ is called a deviation path from p_{st} whenever

- the subpath $q_{st} \supset q_{sh_j} = p_{sh_j} \subset p_{st}$ with $j < n, m$,
- the first arc of the subpath $q_{h_j t}$ is different from the first arc in the subpath $p_{h_j t}$, i.e., $(u_{h_j}, u_{h_{j+1}}) \neq (v_{h_j}, v_{h_{j+1}})$,
- the subpath $q_{h_{j+1}t} = q^*_{h_{j+1}t} \in \mathcal{T}^*_t$, i.e., $q_{h_{j+1}t}$ is the maximum energy transmission path from node $v_{h_{j+1}}$ to the target t.

Moreover, the node $u_{h_j} = v_{h_j}$ is termed the deviation node of q_{st} and $(v_{h_j}, v_{h_{j+1}})$ the deviation arc of q_{st} from p_{st}[1].

The key idea of the MPS algorithm applied to our SEA problem is as follows. It starts choosing the first dominant energy transmission path from the source to the target $p_1 \equiv p^*_{st} \in \mathcal{T}^*_t$. Then, a set $\mathcal{X}$ of possible candidates to be the second maximum energy transmission path p_2 is built. The candidates are computed from deviation paths of p_1. One begins considering the first node (source node s) in p_1 as a deviation node[2], and then compute the weight of all deviation paths $(u_s, u_{h_j}) \circ p^*_{h_j t} \; \forall \; (u_s, u_{h_j}) \in \mathcal{E}^-_s$. This is rather straightforward given that $w(p^*_{h_j t})$ is known from $\mathcal{T}^*_t$. Moreover, the process can be fastened using reduced weights [Eppstein, 1998] and sorting E_{SEA} in the forward star form [Martins et al., 1999], as will be explained below. From all first node s deviation paths we chose the one having maximum weight and save it in $\mathcal{X}$. Then we consider the next node in p_1 and repeat the procedure to obtain deviation paths of the type $p_{sh_1} \circ (u_{h_1}, u_{h_j}) \circ p^*_{h_j t} \; \forall \; (u_{h_1}, u_{h_j}) \in \mathcal{E}^-_{h_1}$. Again, the maximum of these paths is stored in $\mathcal{X}$. The procedure continues until all nodes of p_1 have been explored. The maximum path in $\mathcal{X}$ is selected to be the second dominant energy transmission path p_2 in the SEA graph, and is output from $\mathcal{X}$. We then begin to consider the deviation paths of p_2 and proceed in the same manner. Once all maximum deviation paths from p_2 have been computed and inserted into $\mathcal{X}$, p_3 is chosen as the maximum path in $\mathcal{X}$. Note that at this step $\mathcal{X}$ contains all maximum deviation paths from p_2 and all maximum deviation paths from p_1, different from p_2. The process continues until all desired K dominant energy transmission paths have been computed.

In order to visualize the process, a pseudo tree $\mathcal{T}^k_t$ of deviation paths is built at each kth iteration. The first pseudo tree $\mathcal{T}^1_t$ simply contains the maximum energy transmission path from the source to the target $p_1 \equiv p^*_{st} \in \mathcal{T}^*_t$. The second pseudo tree $\mathcal{T}^2_t$ contains p_1 plus all maximum deviation paths from p_1, from which p_2 is selected. $\mathcal{T}^3_t$ contains p_1, plus its deviation paths, plus the deviation paths from p_2, one of these paths corresponding to p_3, etc. $\mathcal{T}^k_t$ corresponds to a pseudo tree and not to a simple tree given that it can have

1 It should be noted that in some references the term deviation path is used to designate the subpath q_{jt} instead of the whole path q_{st}.

2 As we will use vs instead of s, we will actually start with the second node of p_1

repeated nodes (cycles are allowed in SEA graphs). However, it is important from an implementation point of view to treat all nodes in $\mathcal{T}_t^k$ as being different.

On the other hand, and as it has been mentioned above, the ranking of deviation path weights can be fastened by defining edge reduced weights. Let us denote the reduced weight for the edge (u_i, u_j) as $\bar{w}_{ij}$. For our SEA problem, we choose $\bar{w}_{ij}$ to be

$$\bar{w}_{ij} := \frac{\pi_j}{\pi_i} w_{ij}. \tag{3.5}$$

$\bar{w}_{ij}$ may be interpreted as the additional energy attenuation that a path from u_i to t experiences if $u_j \notin p_{it}^*$. This is so for if $u_j \in p_{it}^*$, then $\pi_i = w_{ij}\pi_j$ and $\bar{w}_{ij} = 1$.

It is proved in the results of the next section that the reduced weights satisfy the following interesting properties:

$$\bullet\ \bar{w}_{ij} = 1 \ \forall\ (u_i, u_j) \in E_{\text{SEA}} \cap E_t^*, \tag{3.6}$$

$$\bullet\ \bar{w}_{ij} \leq 1 \ \forall\ (u_i, u_j) \in E_{\text{SEA}}, \tag{3.7}$$

$$\bullet\ w(p_{st}) \geq w(q_{st}) \ \text{ iff } \bar{w}(p_{st}) \geq \bar{w}(q_{st}), \tag{3.8}$$

the latter being a particularization for the source and target subsystems of the results in Corollary 2, Section 3.4.1.1. Note that this property guarantees that the order is preserved, i.e., if p_{st} transmits more energy than q_{st}, then not only its weight $w(p_{st})$ will be bigger than $w(q_{st})$ but also $\bar{w}(p_{st}) \geq \bar{w}(q_{st})$. Consequently, one can sort the paths either using the path weights w, or using the reduced path weights $\bar{w}$. However, the second option is more advantageous. This is so because a deviation path of p_{st}, $p_{sh_{j-1}} \circ (u_{h_{j-1}}, u_{h_j}) \circ p_{h_j t}^*$ will have reduced weight

$$\begin{aligned} \bar{w}\left[p_{sh_{j-1}} \circ (u_{h_{j-1}}, u_{h_j}) \circ p_{h_j t}^*\right] &= \bar{w}(p_{sh_{j-1}})\bar{w}\left[(u_{h_{j-1}}, u_{h_j})\right]\bar{w}(p_{h_j t}^*) \\ &= \bar{w}(p_{sh_{j-1}})\bar{w}\left[(u_{h_{j-1}}, u_{h_j})\right] = \bar{w}(p_{st})\bar{w}\left[(u_{h_{j-1}}, u_{h_j})\right], \end{aligned} \tag{3.9}$$

where use has been made of (2.48) and (3.6). Therefore, it will suffice to compare the deviation arc weights $\bar{w}\left[(u_{h_{j-1}}, u_{h_j})\right]$ to rank the deviation paths of p_{st}.

Sorting the graph edge set E_{SEA} in the forward star form can further speed the evaluation of deviation paths. The main idea is based on the following observation: if for a deviation node u_i, the edges in $\mathcal{E}_i^-$ are adequately ranked according to their reduced weights, then only one deviation edge needs to be considered for u_i. To do so, E_{SEA} is first factorised as $E_{\text{SEA}} = \cup_{i=1}^{N} \mathcal{E}_i^-$, with the tail node u_i being smaller than u_{i+1}. Then the edges in every $\mathcal{E}_i^-$ are rearranged, the edge having maximum reduced weight being the first one in the list. Logically, this edge will be the only one taken into account when evaluating deviation arcs from u_i, so we can avoid computing all remaining edges in $\mathcal{E}_i^-$.

3.4.1.1 *Edge reduced weight properties*

The following corollaries are the analogues of theorems 8 and 9 in [Martins et al., 1999] for the SEA graph G_{SEA}, and can be proved in the same manner.

Corollary 2. *For any pair of nodes $u_i, u_j \in U_{SEA}$ $(u_i \neq u_j)$ consider two paths $p_{ij}, q_{ij} \in \mathcal{P}_{ij}$ from u_i to u_j. Then, for any tree rooted at the target t, $\mathcal{T}_t$, it follows:*

1. $w(p_{ij}) = \prod_p w_{ij} = \prod_q w_{ij} = w(q_{ij})$ iff $\bar{w}(p_{ij}) = \prod_p \bar{w}_{ij} = \prod_q \bar{w}_{ij} = \bar{w}(q_{ij})$
2. $w(p_{ij}) = \prod_p w_{ij} > \prod_q w_{ij} = w(q_{ij})$ iff $\bar{w}(p_{ij}) = \prod_p \bar{w}_{ij} > \prod_q \bar{w}_{ij} = \bar{w}(q_{ij})$

Proof. The first assertion follows directly from the definition of reduced weight $\bar{w}_{ij} = (\pi_j/\pi_i)w_{ij}$. Assuming $\bar{w}(p_{ij}) = \bar{w}(q_{ij})$ yields

$$\begin{aligned}
\prod_p \bar{w}_{ij} &= \prod_q \bar{w}_{ij}, \\
\prod_p w_{ij}\frac{\pi_j}{\pi_i} &= \prod_q w_{ij}\frac{\pi_j}{\pi_i}, \\
\prod_p \frac{\pi_j}{\pi_i}\prod_p w_{ij} &= \prod_q \frac{\pi_j}{\pi_i}\prod_q w_{ij}, \\
\frac{\pi_t}{\pi_i}\prod_p w_{ij} &= \frac{\pi_t}{\pi_i}\prod_q w_{ij}, \\
\prod_p w_{ij} &= \prod_q w_{ij}. \qquad (3.10)
\end{aligned}$$

For the second assertion we proceed analogously replacing the equality symbol "=" by ">".

□

Corollary 3. *Let $\mathcal{T}_t^* = (U_{SEA}, E_t^*)$ be the tree rooted at t of all maximum paths from any $u_i \in U_{SEA}$ to t. It follows that $\bar{w}_{ij} \leq 1$ for every edge $(u_i, u_j) \in E_{SEA}$ and that $\bar{w}_{ij} = 1$ for every edge $(u_i, u_j) \in E_{SEA} \cap E_t^*$.*

Proof. Suppose that there exists an edge $(u_i, u_j) \in E_{\text{SEA}}$ such that $\bar{w}_{ij} = (\pi_j/\pi_i)w_{ij} \geq 1$. From their definitions, π_j stands for the weight of the maximum path $p_{jt}^* \in \mathcal{T}_t^*$ linking u_j and t, whereas π_i is the analogous for the maximum path linking u_i and t. The concatenated path $(u_i, u_j) \circ p_{jt}^*$ is a path from u_i to t with weight $w\left[(u_i, u_j) \circ p_{jt}^*\right] = w_{ij}w(p_{jt}^*) = w_{ij}\pi_j$. However, the assumption $\bar{w}_{ij} = (\pi_j/\pi_i)w_{ij} \geq 1$ implies $\pi_j w_{ij} \geq \pi_i$. But $\pi_j w_{ij}$ is the weight of the path $(u_i, u_j) \circ p_{jt}^*$ from u_i to t so it cannot be bigger than π_i. Therefore $\bar{w}_{ij} \leq 1$.

On the other hand if $(u_i, u_j) \in E_{\text{SEA}} \cap E_t^*$, $(u_i, u_j) \circ p_{jt}^* \equiv p_{it}^*$ will be the maximum path from u_i to t with weight $\pi_i = w_{ij}\pi_j$. Replacing $w_{ij} = (\pi_i/\pi_j)\bar{w}_{ij}$ in this expression results in $\bar{w}_{ij} = 1$.

□

3.4.2 *Algorithm performance in a benchmark case*

In this section we will show the performance of the MPS algorithm to compute the set of K dominant energy transmission paths in a SEA benchmark model. The pseudocode for the MPS algorithm is shown in Algorithm 3.1. It corresponds to that in [Martins et al., 1999] except for slight differences.

Algorithm 3.1 *MPS algorithm to compute the set of K dominant energy transmission paths in a SEA model*

Generate virtual source vs and virtual target vt
Compute the tree of maximum energy paths to the target $\mathcal{T}_t^*$ /c Dijkstra + Fibonacci Heaps c/
Compute the reduced weights $\bar{w}_{ij} = (\pi_j/\pi_i)w_{ij}$ for all edges $(u_i, u_j) \in E_{SEA}$

Rearrange E_{SEA} in the sorted forward star form
$p_1 \leftarrow p_{st}^*$ /c Select the dominant energy path in $\mathcal{T}_t^*$ to be p_1 c/
$k \leftarrow 1$
$\mathcal{X} \leftarrow \{p_k\}$
$\mathcal{T}_t^k \leftarrow \{p_k\}$
while $k < K$ **and** $\mathcal{X} \neq \emptyset$ **do**
  $\mathcal{X} \leftarrow \mathcal{X} - \{p_k\}$
  $u_k \leftarrow$ deviation node of p_k
  for each node $u_{h_i} \in p_{u_k t}^k$ **do**
    if $\mathcal{E}_{h_i}^- - \mathcal{E}_{\mathcal{T}_t^k}^-(u_{h_i}) \neq \emptyset$ **then**
      $(u_{h_i}, x) \leftarrow$ first edge in $\mathcal{E}_{h_i}^- - \mathcal{E}_{\mathcal{T}_t^k}^-(u_{h_i})$ /c As $\mathcal{E}_{h_i}^-$ is sorted in the forward star form. Also rename node if necessary.
      $q_i \leftarrow p_{vsu_{h_i}}^k \circ (u_{h_i}, x) \circ p_{xvt}^*$
      $\mathcal{X} \leftarrow \mathcal{X} \cup \{q_i\}$
      $q_{u_{h_i}t} \leftarrow (u_{h_i}, x) \circ p_{xt}^*$
      $\mathcal{T}_t^{k+1} \leftarrow \mathcal{T}_t^k \cup \left\{q_{u_{h_i}t}\right\}$
    end if
  end for
  $k \leftarrow k + 1$
  $p_k \leftarrow$ maximum energy path in $\mathcal{X}$
end while

As a benchmark case we will consider the SEA graph G_{SEA} in Fig. 3.1. This graph consists of five subsystems, subsystem #1 being identified with the source s and subsystem #3 with the target t. The virtual source vs and target vt, respectively connected with s and t through edges of unit weight, have also been included. As explained in the previous section, they are necessary for the good performance of the MPS algorithm.

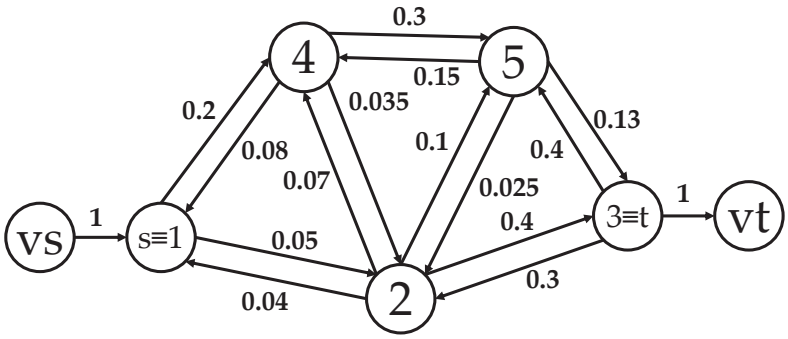

Figure 3.1: Edge weights for the benchmark SEA graph G_{SEA} used to show the MPS algorithm performance.

From a physical point of view, the SEA graph in Fig. 3.1 may represent the noise transmission between two cavities separated by a wall and connected by means of a non-rigid flanking path (see [Craik, 1996], p.152, Fig. 6.1). This example was also considered in [Guasch and Cortés, 2009], with the edge weights $w_{ij} = \eta_{ij}/\eta_j$ in Fig. 3.1, to show the information that could be obtained from the powers of the adjacency matrix of a SEA graph, weighted with different path algebras. We have chosen to work with this example to allow comparison of the hereafter derived results with those in [Guasch and Cortés, 2009]. Our goal will be to determine the four dominant energy transmission paths from s to t (read from vs to vt) in G_{SEA}.

The first step of the algorithm in Algorithm 3.1 consists in determining the tree $\mathcal{T}_t^*$ of maximum energy transmission paths from each node to the target. This can be done applying Dijkstra algorithm to the SEA graph. The result is shown in Fig. 3.2. Next, the reduced weights for the SEA graph corresponding to $\mathcal{T}_t^*$ are computed for each edge in E_{SEA}. The results are presented in Table 3.1 and we note that, as expected, the reduced weights are unity for every edge belonging to $\mathcal{T}_t^*$. The set E_{SEA} can then be factorised in the forward star form $E_{\text{SEA}} = \cup_{i=1}^{N} \mathcal{E}_i^-$ with $\mathcal{E}_s^- = \{(1,2),(1,4)\}$, $\mathcal{E}_2^- = \{(2,t),(2,5),(2,4),(2,s)\}$, $\mathcal{E}_t^- = \{(t,2),(t,5)\}$, $\mathcal{E}_4^- = \{(4,5),(4,s),(4,2)\}$ and $\mathcal{E}_5^- = \{(5,t),(5,2),(5,4)\}$.

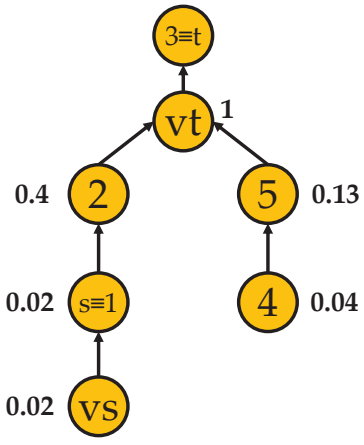

Figure 3.2: The tree $\mathcal{T}_t^*$ of maximum energy transmission paths to the target.

$(u_i, u_j) \in E_{SEA}$	π_i	π_j	w_{ij}	$\bar{w}_{ij} = \pi_j w_{ij} / \pi_i$
$(vs, s \equiv 1)$	0.02	0.02	1.0	1.0
$(s \equiv 1, 2)$	0.02	0.4	0.05	1.0
$(s \equiv 1, 4)$	0.02	0.04	0.2	0.4
$(2, s \equiv 1)$	0.4	0.02	0.04	0.002
$(2, t \equiv 3)$	0.4	1.0	0.4	1.0
$(2, 4)$	0.4	0.04	0.07	0.007
$(2, 5)$	0.4	$0.1\hat{3}$	0.1	$0.0\hat{3}$
$(t \equiv 3, 2)$	1.0	0.4	0.3	0.12
$(t \equiv 3, 5)$	1.0	$0.1\hat{3}$	0.4	$0.05\hat{3}$
$(t \equiv 3, vt)$	1.0	1.0	1.0	1.0
$(4, s \equiv 1)$	0.04	0.02	0.08	0.04
$(4, 2)$	0.04	0.4	0.035	0.35
$(4, 5)$	0.04	$0.1\hat{3}$	0.3	1.0
$(5, 2)$	$0.1\hat{3}$	0.4	0.025	0.075
$(5, t \equiv 3)$	$0.1\hat{3}$	1.0	$0.1\hat{3}$	1.0
$(5, 4)$	$0.1\hat{3}$	0.04	0.15	0.045

Table 3.1: *Reduced costs corresponding to* $\mathcal{T}_t^*$

From $\mathcal{T}_t^*$ in Fig. 3.2 we observe that the maximum energy transmission path from s to t is given by $p_{st}^* = \langle (vs, s), (s, 2), (2, t), (t, vt) \rangle$. Its weight is $w(p_{st}^*) = 0.02$, which means that if the source has energy E_s, the energy at the target that has been transmitted from the source to the target via p_{st}^* is $E_t^* = 0.02 E_s$. p_{st}^* is a second order transmission path and it was obtained in [Guasch and Cortés, 2009] from the square of the SEA graph adjacency.

p_{st}^* is next chosen as p_1 in the algorithm, input into $\mathcal{X}$, and identified with $\mathcal{T}_t^1$. The algorithm then proceeds with the first iteration ($k = 1$) to find the deviation paths from p_1. We get $\mathcal{X} = \mathcal{X} - \{p_1\} = \emptyset$ and choose vs as the first deviation node. We then initiate the *for* loop for every node in $p_{vst}^1 \equiv p_{vst}^*$, i.e., nodes $\{vs, s, 2, t, vt\}$. For $u_{h_1} = vs$ it follows $\mathcal{E}_{vs}^- - \mathcal{E}_{\mathcal{T}_t^1}^-(vs) = \emptyset$ given that the only edge living vs links it with s, and obviously $(vs, s) \in \mathcal{T}_t^1$. For $u_{h_2} = s$ we get $\mathcal{E}_s^- - \mathcal{E}_{\mathcal{T}_t^1}^-(s) = \{(s, 4)\}$ because $(s, 2) \in \mathcal{T}_t^1$. Then $(s, x) = (s, 4)$ and $q_2 = p_{vss}^k \circ (s, 4) \circ p_{4vt}^* = \langle (vs, s), (s, 4), (4, 5), (5, t), (t, vt) \rangle$. We input q_2 into $\mathcal{X}$ and begin to build $\mathcal{T}_t^2$ as $\mathcal{T}_t^2 = \mathcal{T}_t^1 \cup \{(s, 4) \circ p_{4vt}^*\}$, which is the branch in the right side of the pseudo tree in Fig. 3.3a. Next, we consider $u_{h_3} = 2$ for which $\mathcal{E}_2^- - \mathcal{E}_{\mathcal{T}_t^1}^-(2) = \{(2, 5), (2, 4), (2, s)\}$ as $(2, t) \in \mathcal{T}_t^1$. We then pick $(2, 5)$ as it is the first one in the list and will have maximum reduced weight, and build $q_3 =$

$p^k_{vs2} \circ (2,5) \circ p^*_{5vt} = \langle (vs,s),(s,2),(2,5),(5,t),(t,vt)\rangle$. q_3 is input into $\mathcal{X}$ so that by now $\mathcal{X} = \{q_2, q_3\}$ and $\{(2,5) \circ p^*_{5vt}\}$ is joined to $\mathcal{T}_t^2$ that becomes $\mathcal{T}_t^2 = \mathcal{T}_t^2 \cup \{(2,5) \circ p^*_{5vt}\} = \mathcal{T}_t^1 \cup \{(s,4) \circ p^*_{4vt}\} \cup \{(2,5) \circ p^*_{5vt}\}$. For $u_{h_4} = t$ we have $\mathcal{E}_t^- - \mathcal{E}^-_{\mathcal{T}_t^1}(t) = \{(t,2),(t,5)\}$ given that (t,vt) logically belongs to $\mathcal{T}_t^1$. $(t,2)$ is then used to build $q_4 = p^k_{vst} \circ (t,2) \circ p^*_{2vt} = \langle (vs,s),(s,2),(2,t),(t,2),(2,t),(t,vt)\rangle$ so that $\mathcal{X} = \{q_2, q_3, q_4\}$ and $\mathcal{T}_t^2 = \mathcal{T}_t^2 \cup \{(t,2) \circ p^*_{2vt}\} = \mathcal{T}_t^1 \cup \{(s,4) \circ p^*_{4vt}\} \cup \{(2,5) \circ p^*_{5vt}\} \cup \{(t,2) \circ p^*_{2vt}\}$. Finally, for $u_{h_5} = vt$ it follows that $\mathcal{E}^-_{vt} - \mathcal{E}^-_{\mathcal{T}_t^1}(vt) = \emptyset$ because vt is not a tail node. Consequently, no q_5 is found at this step and the *for* loop is left without further modifications. The final pseudo tree resulting from the $k = 1$ iteration $\mathcal{T}_t^2$ is provided in Fig. 3.3a. On the other hand, the set of candidates to be the second dominant energy transmission paths is $\mathcal{X} = \{q_2, q_3, q_4\}$. We increase k to 2 and evaluate the weights of the paths in $\mathcal{X}$, which yields $w(q2) = 0.008$, $w(q3) = 0.000\hat{6}$ and $w(q4) = 0.0024$. Hence, the second dominant energy transmission path is $p_2 = q_2$.

The algorithm then continues to find the deviation paths from p_2, the latter being output from the set of candidates $\mathcal{X}$. Note that at the end of the $k = 2$ iteration, $\mathcal{X}$ will not only contain the deviation paths of p_2, but also q_3 and q_4 that have to be considered in order to determine the third energy transmission path p_3. The pseudo tree $\mathcal{T}_t^3$ is given in Fig. 3.3b with p_3 corresponding to $q_5 = \langle (vs,s),(s,4),(4,2),(2,t),(t,vt)\rangle \equiv p_3$. Its weight is $w(p_3) = 0.0028$. In Fig. 3.3c, the pseudo tree $\mathcal{T}_t^4$ needed to find the fourth dominant energy transmission path is presented. p_4 corresponds to $q_4 = \langle (vs,s),(s,2),(2,t),(t,2),(2,t),(t,vt)\rangle$, which was found as a deviation path of p_1, in the first iteration of the algorithm. Its weight was found to be $w(p_4) = 0.0024$.

In Fig. 3.3d the four dominant energy transmission paths have been plotted alone for clarity. Neglecting the virtual source and target, it can be observed that p_1 is a second order transmission path from s to t, that p_2 and p_3 are both third order transmission paths and that p_4 corresponds to a fourth order transmission path. The energy brought through these paths from the source to the target is given by $E_t^{p_1 p_4} = E_s \sum_{i=1}^4 w(p_i) = 0.0332 E_s$.

Finally, notice that p_1, p_2 and p_4 could have been respectively obtained from the second, third and fourth powers of the SEA graph adjacency matrix weighted with $\mathfrak{P}_2$, as explained in [Guasch and Cortés, 2009]. However, this is not the case for p_3 because it is not the maximum third order path. Consequently, obtaining a set of dominant energy transmission paths directly using the SEA graph adjacency matrix powers would have required to compute all first order transmission paths, plus all second order transmission paths, plus all third order transmission paths, and so on. Then the set of dominant paths should be selected from all computed paths. This is clearly a very inefficient way to solve the problem, only feasible for very low dimensional SEA graphs. On the contrary, the MPS algorithm can be applied to really huge graphs at a very low computational cost [Santos, 2006].

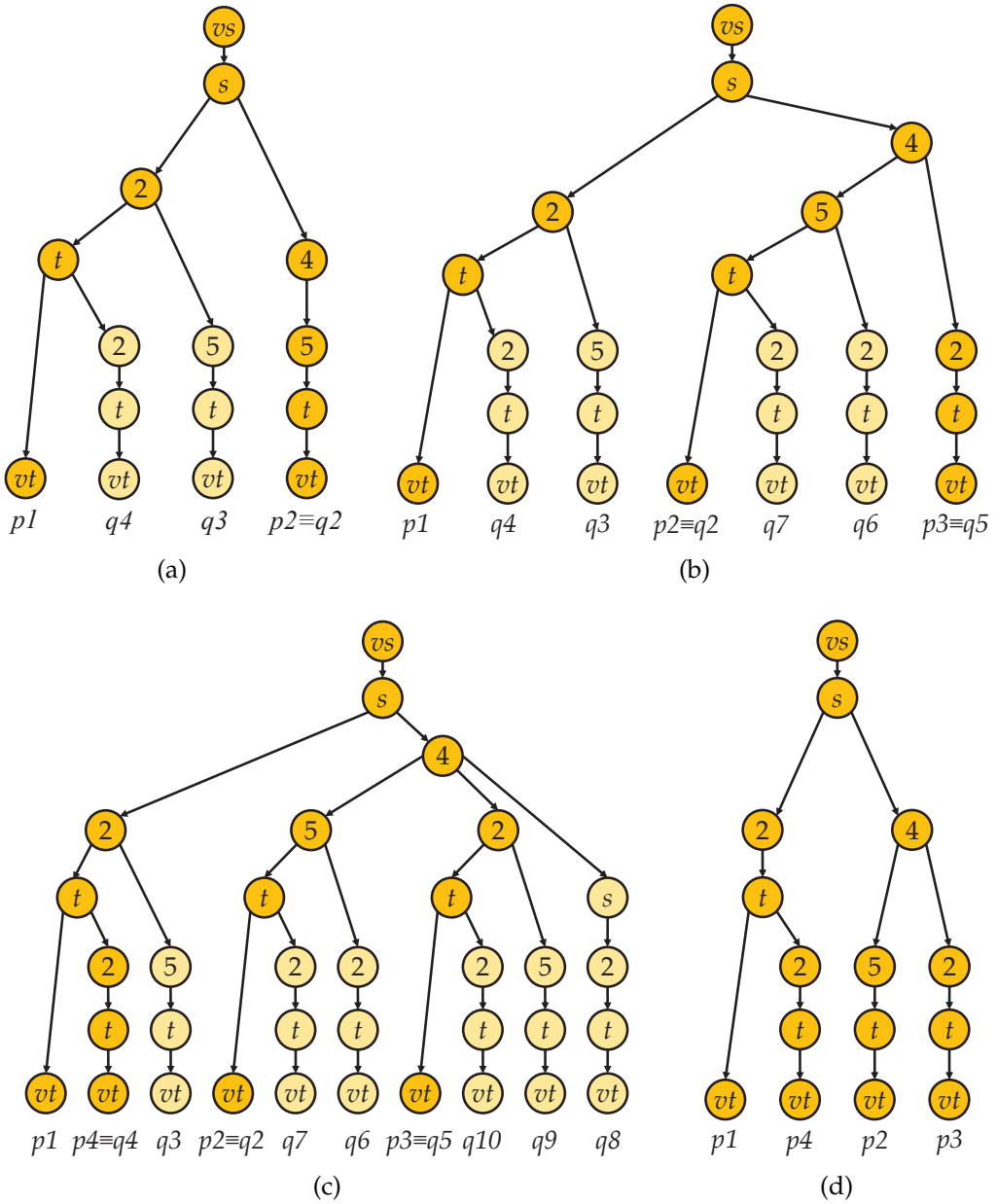

Figure 3.3: Pseudo trees $\mathcal{T}_t^k$, $k = 2...4$ and first 4 dominant transmission paths. (a) $\mathcal{T}_t^2$ (b) $\mathcal{T}_t^3$ (c) $\mathcal{T}_t^4$ (d) First 4 dominant transmission paths.

3.5 NUMERICAL EXAMPLE

3.5.1 *SEA test model description*

A more realistic example is next analysed to show some of the potentialities of the presented algorithm to determine dominant paths in a SEA model. Energy transmission in a 24 room test building model is considered for that purpose. The model consists of a two floor building with twelve identical rooms per floor, arranged in two files of six rooms each. The room dimensions together

with floor and wall material properties are provided in Table 3.2. The model is pure bending, i.e., only flexural waves have been considered, so that any wall or floor is represented by a single subsystem. The model has been built using the commercial package VA-ONE, from which the loss factor matrix has been output to generate the SEA graph G_{SEA}, with adjacency matrix weights in (2.50).

Room			Length [m]	Width [m]	Height [m]
Dimensions			4	4	2.5
Material	Thickness [m]	Density [kg/m^3]	Young modulus [GPa]	Poisson ratio	Internal Loss Factor
Walls: Hollow brick	0.07	770	3.5	0.33	0.006
Floors: Concrete	0.15	2300	28.1	0.2	0.006

Table 3.2: *Dimensions and materials used in the SEA test model*

Two different cases, hereafter designated as "cases A and B", have been analysed. Case A consists of airborne energy transmission between to adjacent rooms in the second floor, one standing for the source where external energy is being input, and the other one for the target (see Fig. 3.4a). Case B consists of structure-borne energy transmission from a wall being excited at the first floor, to the same target room in the second floor of case A (see Fig. 3.6a). The transmission path analysis using the MPS algorithm has been carried out for the SEA graph corresponding to the 1 KHz octave frequency band, for both cases A and B.

3.5.2 *Dominant energy transmission paths*

Let us first consider the results for case A, for which an external power of 1 W has been input to the source room, resulting in an energy level at the target of 118.3 dB. The computation of the first 500 sorted energy transmission paths has revealed many interesting features. For instance, 55% of the overall energy at the target is transmitted through the maximum path, which is the second order path linking the source and target cavities through their common wall. This path is plotted in Fig. 3.4a whereas the 2nd and 3rd dominant paths are respectively shown in Figs. 3.4b and c (path # 460 has been chosen arbitrarily and plotted in Fig. 3.4d).

The energy transmitted through the set of the first four dominant paths justifies 73% of the target energy and with the first 20 dominant paths 90% of the target energy is achieved (see Fig. 3.5a). In terms of energy levels this means, for instance, that the first seven transmission paths account for 117.3 dB of the overall 118.3 dB at the target (see Fig. 3.5b). Hence, if the overall contribution of

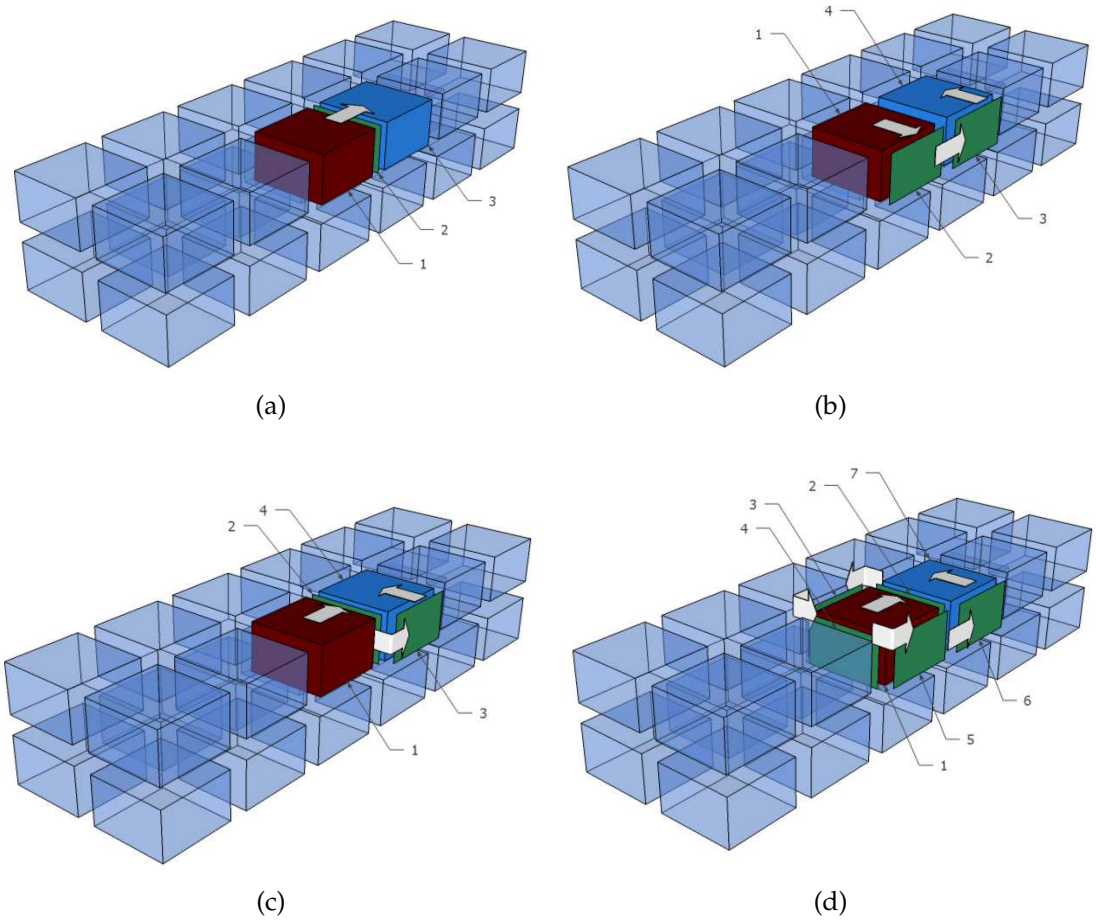

Figure 3.4: Some dominant energy transmission paths for Case A. (a) maximum energy transmission path (b) 2nd dominant energy transmission path (c) 3rd dominant energy transmission path (d) 460th dominant energy transmission path.

these paths could be reduced in say, 12 dB, a reduction of at least 9 dB could be achieved at the target (actually the reduction could be much stronger given that the subsystems in these paths will also belong to many other paths and their modification will also affect the latter, see below). Obvioulsy, and as mentioned in the Introduction, this type of behaviour makes possible the existence of in situ transmission loss regulations that only take into account direct and first order flanking paths between dwellings (e.g., EN 12354-1 (ISO 15712-1) for airborne sound transmission between adjacent rooms). However, these regulations are known to fail under many circumstances depending on the properties of the room walls, the influence of additional neighbourhood rooms, etc. (see e.g., [Craik, 2001; Galbrun, 2008] and references therein). In such cases, the MPS algorithm could prove very useful to determine in a precise way which are the drawbacks and weak points of such regulations.

On the other hand, it can be appreciated from Figs. 3.5a and b that the number of paths to be accounted for, to achieve the overall energy value at the target,

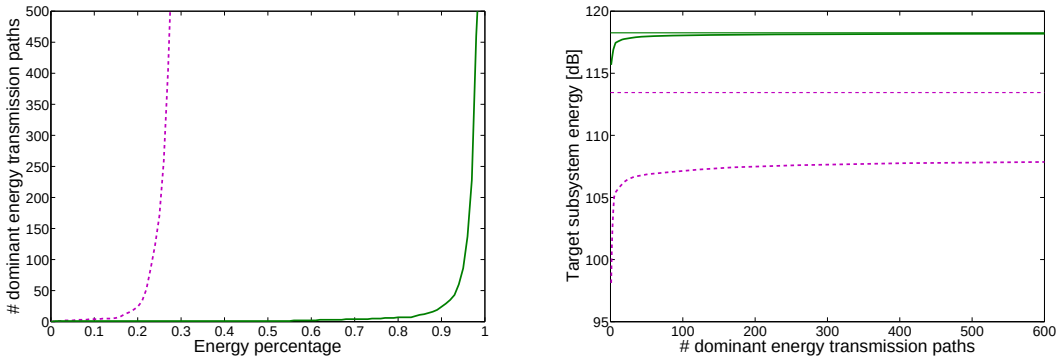

(a) (b)

Figure 3.5: # dominant paths vs energy level and percentage at the target subsystem. Continuous lines: Case A. Dashed lines: Case B. Straight lines: overall energy levels at the target. (a) # dominant paths percentage of target subsystem energy (b) Target subsystem energy level vs # dominant paths.

grows exponentially. This is not strange given that actually, an infinite number of them should be considered as stated by the Neumann series expansion of the SEA system solution [Guasch and Cortés, 2009]. However, the number of loss factors to be modified to reduce the energy at the target will not only depend on the number of dominant paths involved to reach a certain percentage of the target energy, but also on the characteristics of these paths. For instance, one may wonder about their length or if they involve a large amount of different subsystems. This information can be readily obtained from the output list of ranked paths of the MPS algorithm. For example, the analysis of the 500 sorted dominant paths for case A reveals that the longest path in the set is only made of 7 subsystems. Moreover, the 500 dominant paths only involve 32 different subsystems. This means that these paths contain a large amount of cycles and that do not separate considerably from the source and target subsystems. Hence, one could make a classification of subsystems according to the number of paths in which their appear. The loss factors of those subsystems belonging to a largest number of paths will be natural candidates to be modified, if the energy at the target subsystem was to be reduced.

In practical situations the possibility to modify the system loss factors may depend on many factors (mechanical resistance, economical restrictions, etc.) other than the pure acoustic ones. However, once made the loss factor changes it will suffice to solve the SEA matrix system with the new values to check the improvements achieved. In some situations, it will not be possible to modify a certain loss factor without changing other ones. However, these cases can be solved numerically in a quite straightforward way by an a priori definition of groups of loss factors to be modified together. If one member of the group has to be changed because it belongs to a dominant path, then the other ones get automatically changed to their allowed new values too (this procedure was

explained in [Guasch and Cortés, 2009] in the framework of a graph cut strategy to reduce energy transmission in SEA models, see also [Guasch et al., 2010] for implementation in a more realistic case).

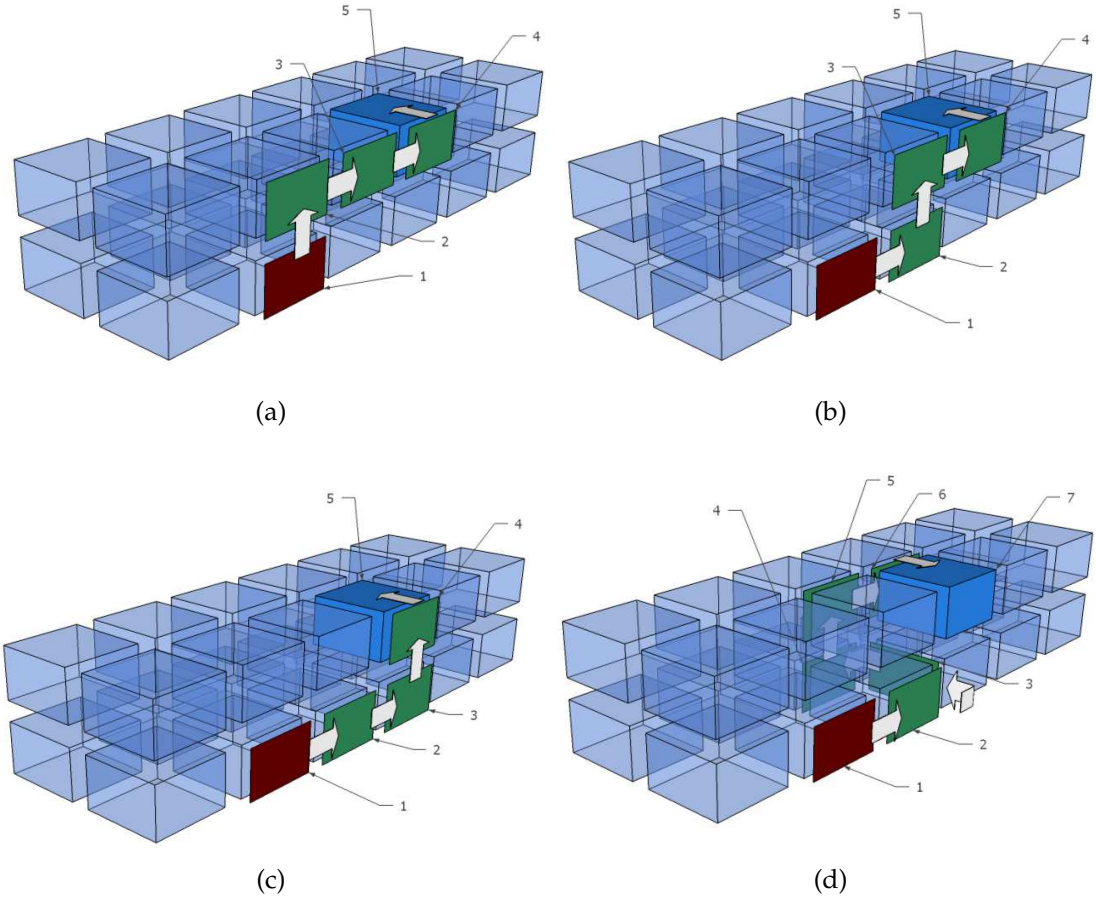

Figure 3.6: Some dominant energy transmission paths for Case B. (a) maximum energy transmission path (b) 2nd dominant energy transmission path (c) 3rd dominant energy transmission path (d) 405th dominant energy transmission path.

In what concerns case B, an external input of 1 W has been applied to the wall in the first floor (see Fig. 3.6a), which has resulted in an energy level of 113.4 dB at the target room in the second floor. The first three dominant paths have been plotted in Figs. 3.6a, 3.6b and 3.6c, whereas Fig. 3.6d corresponds to path # 405. The analysis of the first 500 dominant paths now reveals that the situation is considerably more intricate than for case A. Effectively, as observed from Figs. 3.5a only 27.5 % of the target energy is justified by means of the contributions of the first 500 ranked paths. In dBs this means that only 107 dB of the overall 113.4 dB can be obtained from these paths. It is clear that attempting some kind of regulation for such situation only involving first order flanking paths would make no sense. However, this does not mean that for case B, large energy reduction could not be achieved at the target. A quick analysis of the 500

ranked dominant paths shows that the longest path in the set now contains 9 subsystems, and that 47 different subsystems get involved in these paths. Again, by proper inspection of path intersections one could find optimum candidates for modifications in order to achieve enery reductions at the target subsystem.

Finally, on the one hand it is worthwhile mentioning that the building SEA model analysed in this section is highly symmetric, which favours the existence of many paths with similar weights, hence transmitting very close energy values. On the other hand, we note that whatever is the case A or B, it is apparent from the above results that valuable information can be derived on the energetic behaviour of a SEA model, from the MPS algorithm.

3.5.3 *Computation times*

The algorithm has been performed in a regular PC (Intel Core 2 Quad CPU q9400 @2.66 GHz). The computation times of the algorithm in every case are described in Table 3.3. As it can be observed, the highest values correspond to the execution of the MPS algorithm, which are proportional to the number of computed paths. However, the total time in both cases is less than 30 s, which cannot be considered significant.

	Tree of max. paths	Sorted Forward Star Form	MPS Algorithm	Post-processing functions	Total
Case A	21.7×10^{-3} s	1.2×10^{-3} s	23.34 s	9.6×10^{-1} s	24.32 s
Case B	20.6×10^{-3} s	1.2×10^{-3} s	23.08 s	10.1×10^{-3} s	23.97 s

Table 3.3: *Computation times of Case A and Case B.*

3.6 CONCLUSIONS

In this chapter, it has been shown how the sorted set of K dominant energy transmission paths between a source subsystem and a target subsystem in a SEA model can be obtained in a systematic and efficient way. This has been done by resorting to graph theory results. In particular, the MPS algorithm intended to solve the so called "K shortest path" problem in a graph has been adapted for our purposes, and tested in the SEA model of a building.

The presented algorithm can provide deep insight on the energetic behaviour of a SEA system and could be exploited to obtain many valuable information for noise control engineering. For instance, it can be used to assess the validity of transmission loss regulations between dwellings. The algorithm highlights the advantages of setting some SEA transmission path problems in the general framework of graph theory, and it is expected to become a helpful tool for noise, vibration and harshness analysis and design.

4

RANKING PATHS IN STATISTICAL ENERGY ANALYSIS MODELS WITH NON-DETERMINISTIC LOSS FACTORS

Summary. In Chapter 3, very efficient methods have been derived to rank the energy transmission paths in a SEA system in the framework of graph theory. However, up to date classification schemes have only considered the mean values of loss factors for path comparison, their variance being ignored. This can result in significant errors in the final results. In this work it is proposed to address this problem by defining stochastic biparametric SEA graphs whose edges are assigned both, mean and variance values. Paths between subsystems are then compared according to a proposed cost function that accounts for the stochastic nature of loss factors. For an efficient ranking of paths, the stochastic SEA graph is converted to an extended deterministic SEA graph where fast classification deterministic algorithms can be applied. The importance of non neglecting the influence of the variance in path ranking is illustrated by means of some academic numerical examples.

This chapter is based on the following work

- À. Aragonès and O. Guasch. Ranking paths in statistical energy analysis models with non-deterministic loss factors. *Mechanical Systems and Signal Processing* , 52–53:741–753, 2015a [Aragonès and Guasch, 2015a]
- À. Aragonès and O. Guasch. Considering the stochastic nature of loss factors to classify energy transmission paths in SEA. In *Proceedings of the Nineteenth International Congress on Sound and Vibration ICSV19, Vilnius, Lithuania, 2012.*, July 2012 [Aragonès and Guasch, 2012]

4.1 INTRODUCTION

The possibility to rank contributions of individual paths in an efficient way is possible by establishing a connection between SEA and graph theory as seen in Chapter 2. In Chapter 3, the deterministic MPS algorithm [Martins et al., 1999] based on deviation path computations has been adapted for this purpose.

That said however, SEA does not deal with the dynamic response of a single structure but with that of an ensemble average of structures having similar but randomly varying parameters. In fact, the importance to quantify not only the

mean energy per subsystem but also its variance, was highlighted from the very beginnings of SEA [Lyon and DeJong, 1998]. Since then, both nonparametric and parametric approaches have been followed to deal with uncertainties. Recently, some closed formulas have been derived for the former based on the Gaussian orthogonal ensemble [Cotoni et al., 2005; Langley and Cotoni, 2004] (see also the work in [Langley et al., 2013]). Analytic [Büssow and Petersson, 2007] as well as parametric methods to evaluate subsystem energy variability due to loss factor and input power uncertainties have been also developed [Culla et al., 2011]. However, in what concerns transmission paths, no classification scheme has yet considered the influence of the statistical nature of SEA on path ranking. The need of doing so was pointed out in [Davis, E.B. , 2008], where standard error propagation formulas were used to analyse the variability of paths, though this obviously not resulted in a unique list of sorted paths. Similarly, resorting to computationally expensive Monte Carlo simulations introducing variations on the loss factors of paths would neither provide a list of energy transmission paths (again only some information on the variability of path ranking could be attempted). Alternatively, a better option would be to make use of the Hurwicz criterion [Guasch and Aragonès, 2010] to find a balanced solution between the best and worst scenarios in path analysis, though once again, this does not result in a single ranking of paths.

It is precisely the aim of this chapter to provide a classification methodology that results in a unique set of sorted paths which not only takes into account the mean values of the loss factors involved in them, but also their variances. Though academic in nature, providing a possible solution to such a problem is worth exploring and could be useful to the vibroacoustic engineer decision-making process. The proposed solution follows some of the suggestions in [Loui, 1983] to tackle with the general problem of path classification with random weights in the framework of graph theory.

The strategy exposed in this work to rank paths with non-deterministic loss factors involves several steps. According to Craik's definition seen in Chapter 2 [Craik, 1990], a first order path from a source subsystem to a neighbor receiver subsystem is defined by the ratio between the coupling loss factor from the source to the receiver, and the total loss factor of the receiver. A nth order path between two arbitrary subsystems in a SEA model is built from the consecutive products of n first order paths that link the intermediate subsystems one to another. Therefore, the initial step to deal with non-deterministic paths involves gaining information on the probability density functions (pdfs) that describe the loss factors involved in a first order path. Most available information at present concerns coupling loss factor pdfs for simple element connections involving springs [Manohar and Keane, 1994], beams or plates [Fahy and Mohammed, 1992; Hopkins, 2002; Park et al., 2005; Thite and Mace, 2010; Wester and Mace, 1996], but little information is found e.g., on internal loss factors. As a consequence and as it will be shown later on, some simplifying hypotheses are to be made for them, as well as for combining loss factor pdfs in Craik's

path formula. Once it is known how to assign variances to first order paths, the following step consists in building a biparametric stochastic SEA graph in analogy to what is done for the deterministic case [Guasch and Aragonès, 2011; Guasch and Cortés, 2009]. The basic difference is that now two values (mean and variance) are assigned to each edge of the SEA graph instead of one. Next, in order to compare path weights for classification, one can no longer solely rely on their mean values but the variance information has to be incorporated somehow. As it will be shown, this can be done by defining a nonlinear cost function that combines mean and variance path values. Having done this, the final and most intricate step, consists in establishing an algorithmic strategy for the efficient comparison and classification of paths. The MPS algorithm used in Chapter 3 cannot be directly applied to the problem because stochastic graphs do not satisfy the optimality principle (i.e., a maximal transmitting path is not made of maximal transmitting subpaths, see [Guasch and Aragonès, 2011; Martins et al., 1999] and references therein). To circumvent this difficulty it is proposed to resort to the procedure in [Deng and Wong, 2006], which consists in transforming a stochastic biparametric graph into an extended uniparametric graph. This will allow applying the very efficient MPS algorithm to the extended SEA graph and to classify energy transmission paths with non-deterministic loss factors. A preliminary version of some of the herein exposed results was recently presented in [Aragonès and Guasch, 2012].

The chapter is organized as follows. In Section 4.2, the notion of stochastic SEA graph is introduced and it is shown how to weight it using information from loss factor pdfs. The nonlinear cost function to compare paths is presented and the classification problem to be solved is mathematically posed. The strategy and algorithms used to rank non-deterministic paths are described in Section 4.3. Section 4.4 contains two benchmark examples where the algorithm is applied and the results become compared with those from the pure deterministic classification scheme. Conclusions close the chapter in Section 4.5.

4.2 PROBLEM STATEMENT

4.2.1 *Deterministic and stochastic SEA graphs*

Paths are computed in SEA according to (2.51), and all group [Magrans, 1993] and individual [Guasch and Aragonès, 2011] classification schemes are based on its use. However, the weight of any arc $w_{ij} = \eta_{ij}/\eta_j$ only considers definite values for η_{ij} and η_j, without taking into account that these are SEA parameters, and thus have some uncertainty. In practice, w_{ij} should be represented with a pdf instead of a single number. As it will be shown, neglecting the stochastic character of w_{ij} could lead to significant mistakes when ranking paths.

In this chapter, it will be assumed that the pdfs describing arc weights w_{ij} are such that they can be well characterized through mean $\mu_{w_{ij}}$ and variance $\sigma^2_{w_{ij}}$ values. Therefore, instead of working with deterministic SEA graphs, biparamet-

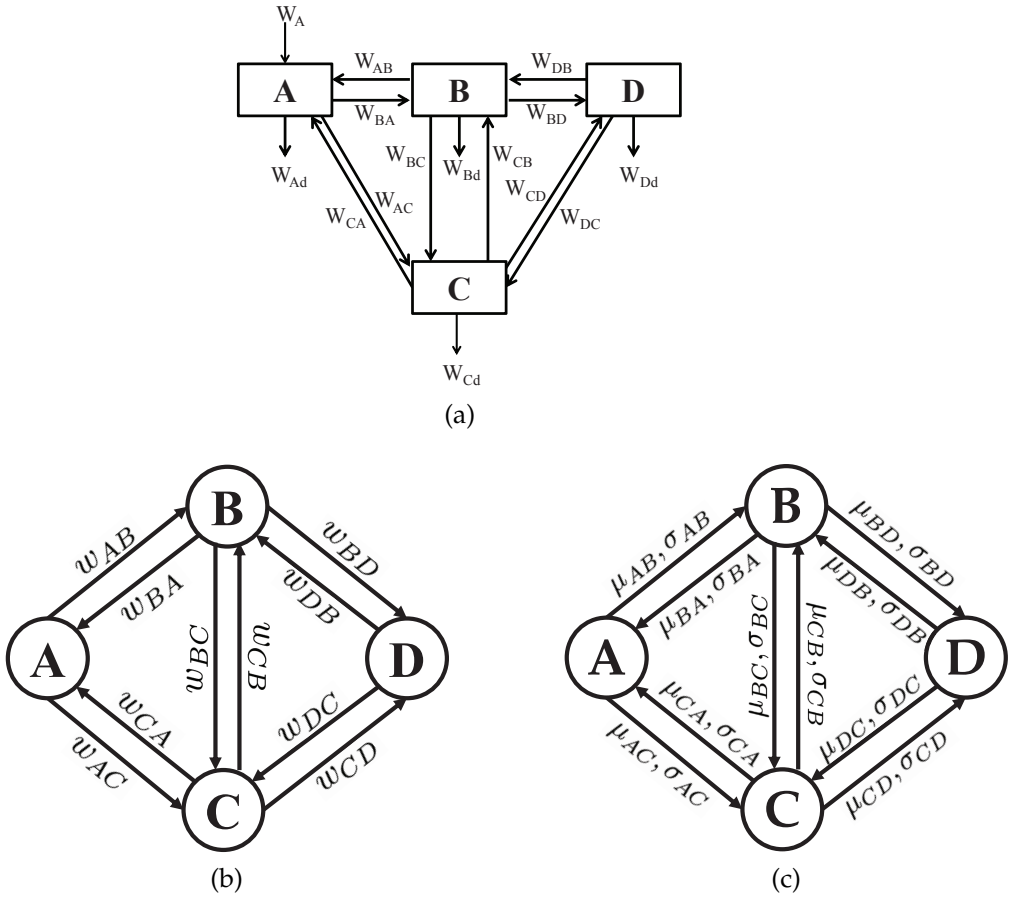

Figure 4.1: (a) Example of a SEA block diagram. (b) corresponding deterministic SEA graph. (c) corresponding stochastic SEA graph.

ric stochastic SEA graphs will be used. Observe for instance, the SEA system in Figure 4.1a, the corresponding deterministic SEA graph would be the one depicted in Figure 4.1b. However, the stochastic one with two quantities per arc shown in Figure 4.1c will be used instead. Two weighting matrices will be then necessary to characterize this new SEA graphs, one containing all arc mean values and the other one containing all arc variances.

4.2.2 *Probability density functions for the weights in a stochastic SEA graph*

No direct statistics on $w_{ij} = \eta_{ij}/\eta_j$ have been reported in literature, which makes necessary to resort to statistics on loss factors to find values for $\mu_{w_{ij}}$ and $\sigma^2_{w_{ij}}$. As shown below, this will imply assuming some simplifications.

The arc weight involves a quotient between a coupling loss factor η_{ij} and a total loss factor η_j, which in turn is made of the summation of several coupling loss factors and an internal loss factor. Existing statistics mainly concern coupling loss factors and can be classified according to the modal overlap factor M. For instance, in the case of η_{ij} between two plates and for $M < 1$, the pdfs tend to be right skewed and have a wide spread [Fahy and Mohammed, 1992; Hopkins,

2002]. However, when expressed in decibels, the coupling loss factors fit in a normal distribution so that η_{ij} can be properly represented by a lognormal pdf [Fahy and Mohammed, 1992; Hodges and Woodhouse, 1989; Hopkins, 2002]. When $M > 1$ (which is the case under the SEA hypotheses), the values of η_{ij} have a much narrower spread and can be described either by a normal or a lognormal pdf [Hopkins, 2002]. The latter will be used hereafter in this work. Besides, the following will be surmised. First, and in what concerns internal loss factors, it will be considered for simplicity that they also fit into a lognormal pdf (no existing statistical data has been found for them). Second, and though not strictly true, coupling loss factors will be treated as independent random variables. Given that the sum of independent lognormally distributed random variables can be well approximated by a lognormal [Beaulieu et al., 1995], the total loss factors will also fit into a lognormal pdf.

In order to get mean and variance values for w_{ij}, the logarithmic transformation $\tilde{w}_{ij} \equiv \log(w_{ij})$ is used. The arc weight in (2.50) then becomes

$$\tilde{w}_{ij} = \tilde{\eta}_{ij} - \tilde{\eta}_j, \tag{4.1}$$

with $\tilde{\eta}_{ij} \equiv \log(\eta_{ij})$ and $\tilde{\eta}_j \equiv \log(\eta_j)$. As for a random variable X with lognormal distribution, $\tilde{X} = \log(X)$ follows a normal distribution, the mean weight of the arc $\mu_{\tilde{w}_{ij}}$ and the variance $\sigma^2_{\tilde{w}_{ij}}$ can be straightforwardly obtained through [Montgomery and Runger, 2010]

$$\mu_{\tilde{w}_{ij}} = \mu_{\tilde{\eta}_{ij}} - \mu_{\tilde{\eta}_j} \tag{4.2}$$

and

$$\sigma^2_{\tilde{w}_{ij}} = \sigma^2_{\tilde{\eta}_{ij}} + \sigma^2_{\tilde{\eta}_j}, \tag{4.3}$$

with $\mu_{\tilde{\eta}_{ij}}$ and $\sigma^2_{\tilde{\eta}_{ij}}$ denoting the mean and the variance of $\tilde{\eta}_{ij}$, and $\mu_{\tilde{\eta}_j}$ and $\sigma^2_{\tilde{\eta}_j}$ standing for the mean and the variance of $\tilde{\eta}_j$. Let X correspond to η_{ij} or η_j and $\tilde{X} = \log(X)$ to $\tilde{\eta}_{ij}$ or $\tilde{\eta}_j$. The logarithmic means $\mu_{\tilde{\eta}_{ij}}$, $\mu_{\tilde{\eta}_j}$, and variances $\sigma^2_{\tilde{\eta}_{ij}}$, $\sigma^2_{\tilde{\eta}_j}$ can be computed from $\mu_{\eta_{ij}}$, μ_{η_j}, $\sigma^2_{\eta_{ij}}$ and $\sigma^2_{\eta_j}$ taking into account that

$$\mu_{\tilde{X}} = \log\left(\mu_X \Big/ \sqrt{1 + \frac{\sigma^2_X}{\mu^2_X}}\right) \tag{4.4}$$

and

$$\sigma^2_{\tilde{X}} = \log\left(1 + \frac{\sigma^2_X}{\mu^2_X}\right). \tag{4.5}$$

Finally note that making use of the logarithmic transformation, the weight of a path p^n_{ij} in (2.51) becomes

$$\tilde{w}_{i\ldots j} = \tilde{w}_{ih_1} + \tilde{w}_{h_1h_2} + \cdots + \tilde{w}_{h_{n-1}j} \equiv \tilde{w}\left(p^n_{ij}\right) \tag{4.6}$$

and its mean value $\mu_{\tilde{w}_{i\ldots j}}$ and variance $\sigma^2_{\tilde{w}_{i\ldots j}}$ can be computed as,

$$\mu_{\tilde{w}_{i\ldots j}} = \mu_{\tilde{w}_{ih_1}} + \mu_{\tilde{w}_{h_1h_2}} + \cdots + \mu_{\tilde{w}_{h_{n-1}j}} \tag{4.7}$$

and

$$\sigma^2_{\tilde{w}_{i\ldots j}} = \sigma^2_{\tilde{w}_{ih_1}} + \sigma^2_{\tilde{w}_{h_1h_2}} + \cdots + \sigma^2_{\tilde{w}_{h_{n-1}j}}, \tag{4.8}$$

the weight of the path hence following a normal distribution.

4.2.3 *The set of K dominant energy transmission paths in a stochastic SEA graph*

Once it is known how to weight stochastic biparametric SEA graphs and how to compute the mean and variance weights of any path connecting two arbitrary nodes in such a graph, a criterion for comparing paths is needed prior designing an algorithm for their classification. This implies defining a dominance condition between paths [Huckenbeck, 1997]. Note that the question of whether a path transmits more energy than another is of immediate answer in the case of a deterministic SEA graph; a path $p_{ij,1}$ from i to j dominates another path from i to j, $p_{ij,2}$, (i.e. it transmits more energy) whenever (3.1) is fulfilled. However, the answer is not so trivial for a stochastic SEA graph given that the weight of a path depends on its mean $\mu_{\tilde{w}_{i\ldots j}}$ as well as on its variance $\sigma^2_{\tilde{w}_{i\ldots j}}$. Both terms should be included when defining the dominance condition between paths.

One possible way to address this issue is by means of defining an appropriate cost function [Hutson and Shier, 2009; Ji, 2005; Loui, 1983; Murthy and Sarkar, 1997] $\Phi\left(p_{ij}\right)$ such as,

$$\Phi\left(p_{ij}\right) = \mu_{\tilde{w}_{i\ldots j}} + \phi\left(\sigma^2_{\tilde{w}_{i\ldots j}}\right), \tag{4.9}$$

where $\phi\left(\sigma^2_{\tilde{w}_{i\ldots j}}\right)$ is a function (presumably nonlinear) that accounts for the incidence of the variance. If normal pdfs are involved (as shown in the previous subsection), one typically chooses $\phi\left(\sigma^2_{\tilde{w}_{i\ldots j}}\right) = -N\sqrt{\sigma^2_{\tilde{w}_{i\ldots j}}}$ to consider the most restrictive situation [Deng and Wong, 2006] (see examples in forthcoming Sections). For instance, if $N = 3$ we get $\Phi\left(p_{ij}\right) = \mu_{\tilde{w}_{i\ldots j}} - 3\sigma_{\tilde{w}_{i\ldots j}}$ and it is guaranteed that for a path weight $\tilde{w}\left(p^n_{ij}\right)$ having a Gaussian distribution, the probability P of the weight lying between $\mu_{\tilde{w}_{i\ldots j}} \pm 3\sigma_{\tilde{w}_{i\ldots j}}$ is greater than 0.99. The cost function in (4.9) provides one way to compare paths, so that a path $p_{ij,1}$ is said to be more dominant than $p_{ij,2}$ whenever $\Phi\left(p_{ij,1}\right) > \Phi\left(p_{ij,2}\right)$.

Let us denote by $\mathcal{P}_{st}$ the set of infinite transmission paths from a source subsystem s, where external energy is being input, to a target subsystem t. As described in [Guasch and Aragonès, 2011], in many cases of practical interest most energy is transmitted through a finite group of K dominant paths in $\mathcal{P}_{st}$, say $\mathcal{P}_{st,K}$. Therefore, analogous to the Problem 1 in Chapter 3 and [Guasch and Aragonès, 2011] of finding the most dominant energy transmission paths in a deterministic SEA graph, the problem of finding and ranking the most dominant paths in a biparametric stochastic SEA graph can be posed as follows.

Problem 1 Given two nodes s and t in a biparametric stochastic SEA graph and a cost function $\Phi\left(p_{ab}\right)$ assigned to every path in $\mathcal{P}_{st}$, we intend to find the finite set $\mathcal{P}_{st,K} = \{p_{st,1}, p_{st,2}, \ldots, p_{st,K}\} \subseteq \mathcal{P}_{st}$ such that

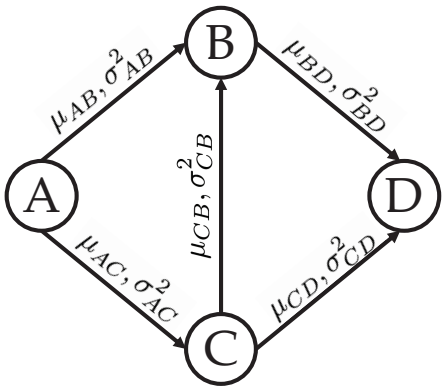

Figure 4.2: Failure of the optimality principle

- $\Phi(p_{st,k}) \geq \Phi(p_{st,k+1}) \forall k \in \{1, \ldots, K-1\}$,
- $\Phi(p_{st,K}) \geq \Phi(q_{st}) \forall q_{st} \in \mathcal{P}_{st} - \mathcal{P}_{st,K}$,
- $p_{st,k}$ is found just before $p_{st,k+1} \forall k \in \{1, \ldots, K-1\}$.

That is to say our goal is to find a set of K paths fulfilling that the k-th path dominates the $k+1$-path (first item), that the paths in $\mathcal{P}_{st,K}$ dominate any path outside the set (second item) and that all paths are obtained sequentially, starting with the most dominant one (third item).

4.3 ALGORITHM TO FIND THE MOST DOMINANT PATHS IN A STOCHASTIC SEA GRAPH

4.3.1 *Description of the algorithm*

An efficient way to classify of dominant paths in a deterministic SEA graph was presented in Chapter 3 by resorting to the MPS algorithm [Martins et al., 1999]. This algorithm relies on first computing the tree of maximum energy transmission paths $\mathcal{T}_t^*$ between nodes in the graph (using e.g., Dijkstra's algorithm [Dijkstra, 1959]) and then computing deviation paths of extremal paths [Eppstein, 1998]. This procedure relies in turn on the fulfilment of the optimality principle [Huckenbeck, 1997], which states than any extremal path is built from extremal subpaths. For instance, if the maximum energy transmission path from node A to D in Fig. 4.1b was $p_{AD} = \{A, B, C, D\}$, this would mean that the maximum energy transmission path from A to C would be $p_{AC} = \{A, B, C\}$ and not $p_{AC} = \{A, C\}$. Unfortunately, the very effective MPS algorithm cannot be used for stochastic graphs because the optimality principle is not fulfilled for them (see e.g., [Guasch and Aragonès, 2010] and references therein).

Let us illustrate this fact with the example on Figure 4.2. We want to find the path from A to D which maximizes the cost function $\Phi(p_{AD}) = \mu_{\tilde{w}_{AD}} - 0.5\sigma_{\tilde{w}_{AD}}$. The values of the averages, variances and cost functions of every first order path in the graph are shown in Table 4.1. The weights of the arcs in the

opposite directions, not appearing in Figure 4.2, are assumed to be positive but approximately 0 to simplify the explanation. There are three paths from A to D, $p_{AD,1} = \{A, B, D\}$, $p_{AD,2} = \{A, C, B, D\}$ and $p_{AD,3} = \{A, C, D\}$. According to the optimality principle, the most dominant one should be $p_{AD,1}$ since the most dominant arc departing from A is p_{AB} and next, there is a single arc leaving from B which is the direct path to D. However, when computing the cost function values for the three paths one can observe that the one that maximizes it is $p_{AD,2}$ (see Table 4.2). Therefore, this example proves that when the cost function is not linear, the optimality principle may not be satisfied.

Yet, a possible solution can be found for this problem following the proposal in [Deng and Wong, 2006], which consists in precisely transforming the biparametric stochastic SEA graph into an *extended* uniparametric deterministic SEA graph. The MPS algorithm could then be applied to this extended graph.

p_{ij}	$\mu_{\bar{w}_{ij}}$	$\sigma^2_{\bar{w}_{ij}}$	$\Phi(p_{ij})$
p_{AB}	3.55	0.8	3.51
p_{AC}	2.1	0.75	2.06
p_{CB}	2.1	0.75	2.06
p_{BD}	1.0	0.2	0.98
p_{CD}	0.5	0.5	0.46

Table 4.1: *Arc weights and first order path cost functions for the graph in Fig. 4.2*

$p_{AD,i}$	$\Phi(p_{AD,i})$
$p_{AD,1} = \{A, B, D\}$	4.05
$p_{AD,2} = \{A, C, B, D\}$	4.55
$p_{AD,3} = \{A, C, D\}$	2.04

Table 4.2: *Cost function values for the p_{AD} paths in Fig. 4.2*

A process leading to the solution of Problem 1 in the preceding section can then be designed that consists of the four blocks summarized in Algorithm 4.1. In the first one the transformation of the stochastic SEA graph into the extended deterministic graph is carried out. The nodes in the extended graph that do not connect the source to the target are deleted in the second block, to reduce the computational cost. Then, in the third block, the Dijkstra algorithm is used to compute the tree of maximum paths, which contains the most dominant paths from every node in the extended graph to the target subsystem. In the fourth block, the MPS algorithm is finally applied to rank the K most dominant paths. In what follows the first two blocks in Algorithm 4.1 will be described in some detail, blocks third and fourth having already been described in 3.

Algorithm 4.1 *Pseudocode for ranking the most dominant energy transmission paths in a stochastic SEA graph*

1: Build extended SEA graph
   Input: $B, \sigma^2_{\tilde{p}_{st},\max}, G = \left(\tilde{\boldsymbol{\mathcal{W}}}_{\mu}, \tilde{\boldsymbol{\mathcal{W}}}_{\sigma^2}\right), source, target$
   Output: G', vs, vt
2: Delete unconnected nodes
   Input: G', vs, vt
   Output: G', vs, vt
3: Dijkstra tree
   Input: G', vs, vt
   Output: $\mathcal{T}^*$
4: MPS algorithm
   Input: $K, vs, vt, \mathcal{T}^*$
   Output: K *dominant paths*

A pseudocode with the steps leading to the transformation of the stochastic SEA graph, say G, into the extended deterministic SEA one, say G', is provided in Algorithm 4.2. First, and due to specifications of the MPS algorithm [Martins et al., 1999], a virtual source node vs connected to the original one s, and a virtual target node vt connected to t are created. This is so, because, as stated in Chapter 3, for the MPS algorithm to work properly it is necessary that no arc in the graph points to the source and that no arc in the graph leaves the target. The arc connecting vs with s is assigned null variance. Next, remember that two weighting matrices $\tilde{\boldsymbol{\mathcal{W}}}_{\mu}$ and $\tilde{\boldsymbol{\mathcal{W}}}_{\sigma^2}$ are required to characterize the stochastic graph G. In order to build an uniparametric graph, the stochastic graph G is extended by generating new nodes, and the variance information is transferred to them. This is done in the following manner [Deng and Wong, 2006]. A threshold value for the maximum admitted variance in a path $\sigma^2_{\tilde{w}_{s\ldots t},\max}$ is first chosen and an integer value is assigned to it. Let us denote this value by B. Then, the continuous interval of variances $\left[0, \sigma^2_{\tilde{w}_{s\ldots t},\max}\right]$ is mapped into a discrete interval of indexes $\{0, 1, \ldots, i, \ldots, B\}$. This quantization mapping will be denoted by $Q\left(\sigma^2_{\tilde{w}_{s\ldots t}}\right)$; in particular note that $Q\left(0\right) = 0$ and $Q\left(\sigma^2_{\tilde{w}_{s\ldots t},\max}\right) = B$. The type of quantization can be selected depending on the size of the graph and the range of values of the variance. The simplest one is the uniform quantization, where all the quantization steps have the same size. However, if the quantization step is very small and long paths are to be considered, this results in a large value of B, and thus in a very large extended graph G' (see below); in contrast, very large quantization steps would result in poor accuracy. Therefore, depending on the characteristics and the dimensions of the graph it may be convenient to consider non-uniform quantization as well.

Once the quantization operation has been defined, every node u in the original graph G is split into $B+1$ clones $\{u_0, u_1, \ldots, u_B\}$ in G' (see Fig. 4.3a). Each clone u_i represents the original subsystem u but its subscript i indicates a variance

Algorithm 4.2 *Algorithm function: 1. Building the extended graph.*

```
Generate virtual source and virtual target
Map variance interval from [0, σ²_{w̃_{s...t},max}] to [0, B]
for all u ∈ {G − vs} do
    Create B + 1 nodes {u_0, ..., u_B} in G'
    for all e = (u, v) ∈ G do
        for all u_i do
            j = i + Q(σ²_ẽ)
            if j ≤ B then
                Create arc (u_i, v_j) in G'
                w(u_i, v_j) = W̃_μ(u, v)
            end if
            Create vt in G'
            for all t_i do
                Connect t_i to vt
                w(t_i, vt) = φ(i)
            end for
        end for
    end for
end for
```

value. In particular, it is the total variance that any path reaching that node would have. Say it in other words, every path ending at node u_i has a total variance of i (remind that i is a discrete number obtained through quantization of a continuous value of $\sigma^2_{\tilde{e}}$).

The nodes in G' are connected as follows. If the nodes u and v were already connected in G, i.e., if there existed an arc $e = (u, v)$, with a mean weight $\mu_{\tilde{e}} = \tilde{\mathcal{W}}_{\mu}(u, v)$ and a variance weight $\sigma^2_{\tilde{e}} = \tilde{\mathcal{W}}_{\sigma^2}(u, v)$, every clone $u_i \in G'$ is connected to $v_j \in G'$ with $j = i + Q\left(\sigma^2_{\tilde{e}}\right)$. If the value of j is higher than B, no further connection is established given that there is no v_j node with $j > B$. The new arcs between clones u_i and v_j in G' are assigned a single weight, the mean value $\mu_{\tilde{e}}$ between u and v in G (see Fig. 4.3b). Note that with this procedure the variance information has been transferred to nodes and only one weighting parameter is assigned to every arc in G'.

Finally, the information of the variance is returned back to some arcs in G' to allow computing the cost functions of paths (see Eq. (4.9)). This is done at the connections between the target subsystem clones and the virtual target node. Every clone of the target t_i has an associated variance value i, which means that every path reaching it has a total variance of i; its mean value being given by the summation of the mean values of the arcs composing the path, see Eq. (4.7). The connection between a clone t_i and the virtual target vt is then weighted with the value of the variance term of the cost function in (4.9), i.e., $w_{t_i vt} = \phi(i)$, to be added to its mean value to get the cost of the path Φ (see Fig. 4.3c).

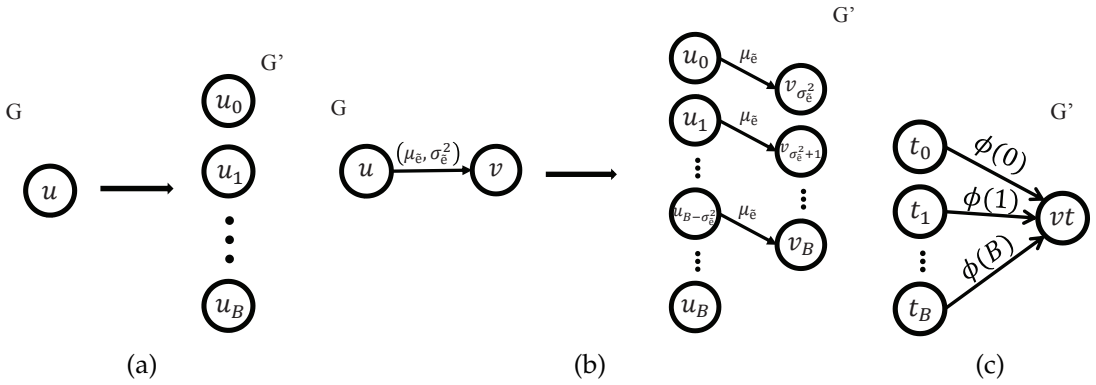

Figure 4.3: (a) Splitting of the nodes in G to G′. (b) Transfer of the variance to the new graph. (c) Application of the cost function to the final arcs.

Once the extended graph G' has been built, an important operation (see second block in Algorithm 4.1) is that of deleting unconnected nodes in G', or nodes that do not belong to any path connecting the virtual source with the virtual target. This process is important as it can drastically reduce the size of G'. Once it is finished, the uniparametric extended graph where to apply the MPS algorithm is already available (blocks three and four in Algorithm 4.1). As mentioned above, first the the Dijkstra algorithm is used to compute the tree of maximum paths $\mathcal{T}_t^*$ from every node to vt, and then the MPS algorithm can be used to find and classify the set of K dominant paths from vs to vt. At this point, it should be noted that there are two basic differences with the application of the MPS in Chapter 3. In the current work summations are used to compute the weights of paths instead of products and a different condition of dominance for path comparison is employed. Apart from this, the MPS algorithm basis remains the same.

4.3.2 *Benchmark example*

For a better comprehension of the above detailed procedure, it will be next applied to the simple 4-node graph G in Fig. 4.4a, node S corresponding to the source and node T to the target. The mean $\mu_{w_{ij}}$ and variance $\sigma^2_{w_{ij}}$ values of the weights of the arcs as well as their corresponding logarithmic transformed values $\mu_{\tilde{w}_{ij}}$ and $\sigma^2_{\tilde{w}_{ij}}$ are given in Table 4.3.

The extended graph G' is built as follows. The value of B is chosen to be 3 so every node gets split into 4 clones. The quantization step is set to the minimum variance value in the graph ($\sigma^2_{\tilde{w}_{ij},\text{min}} = 1.23$, see Table 4.3). Given that the subscript index i of every node corresponds to i times the quantization step, all paths reaching e.g., S_2, have variance 2.46, whilst the maximum admitted variance for a path becomes $\sigma^2_{\tilde{w}_{s\ldots t},\text{max}} = B \times \sigma^2_{\tilde{w}_{ij},\text{min}} = 3.69$. A virtual source vs is also created and connected to S_0 with zero weight. Taking into account that a virtual target vt is also generated, the new graph G' has 18 nodes. Next, the

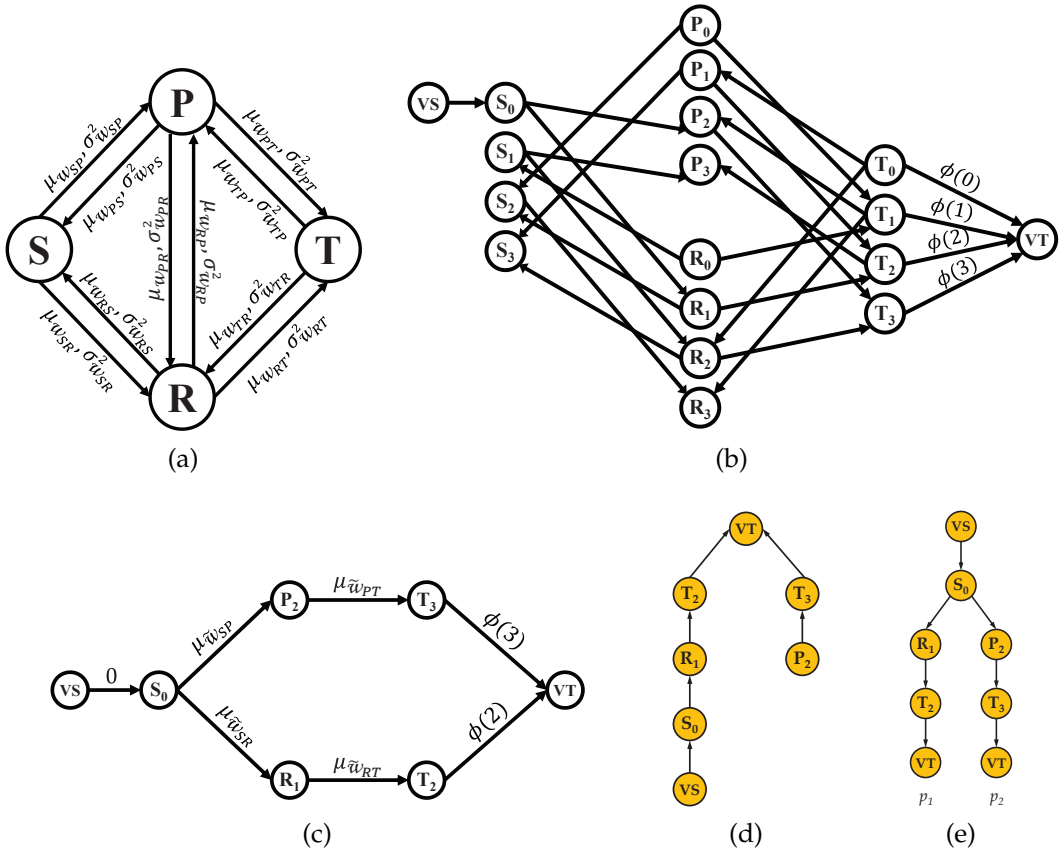

Figure 4.4: Example of building an extended graph. (a) Original graph. (b) Extended graph with all the nodes (c) Extended graph after deleting unconnected nodes. (d) Tree of the maximum paths from every node to the target. (e) First 2 most dominant transmission paths.

connection between nodes is carried out. For example, since the variance of the arc (S, P), $\sigma^2_{\tilde{w}_{SP}} = 2.46$ is twice the quantization step, S_0 is connected to P_2 and the arc is weighted with $\mu_{\tilde{w}_{SP}}$. S_1 is connected to P_3 with identical weight but S_2 and S_3 cannot be connected because P_4 and P_5 do not exist, as they would have variances larger than $B = 3$. The process is repeated for all nodes in G'. At the end, the arcs between the clones of the target T_m and the virtual target vt are created. Each one of these arcs (T_m, vt) is weighted with $\phi(m)$. Since the variables included in the computation of the weight of the paths are Gaussian, the cost function is selected to follow the three sigma rule (see subsection 2.3). Then, $\phi(m) = -3\sqrt{m\sigma^2_{\tilde{w}_{ij},\min}}$.

The resulting graph G' once all nodes have been connected is shown in Fig. 4.4b. The next step consists in deleting those nodes that are not accessible from vs or vt. As it can be observed in Fig. 4.4c, the size of the graph gets strongly reduced. Afterwards, the Dijkstra algorithm is applied and the tree of the maximum paths $\mathcal{T}_t^*$ is obtained (see Fig. 4.4d). $\mathcal{T}_t^*$ contains all maximum transmission paths from any node to vt. For instance, the maximum path from the source vs to the target vt is $p_1 = \{vs, S_0, R_1, T_2, vt\}$. p_1 is finally used in

the MPS algorithm to compute deviation paths and thus obtain the set of ranked K dominant paths from the source to the target in G'. In this case there are only two valid paths (i.e., with $B \leq 3$) connecting the source and the target, which are depicted in Fig. 4.4e. The cost function for the first path is $\Phi(p_1) = \mu_{\tilde{w}_{SR}} + \mu_{\tilde{w}_{RT}} - 3\sqrt{2\sigma^2_{\tilde{w}_{ij},\min}} = -10.22$ and for the second, $\Phi(p_2) = \mu_{\tilde{w}_{SP}} + \mu_{\tilde{w}_{PT}} - 3\sqrt{3\sigma^2_{\tilde{w}_{ij},\min}} = -18.14$, so that $\Phi(p_1) > \Phi(p_2)$.

Arc (i,j)	μ_{ij}	σ^2_{ij}	$\mu_{\tilde{w}_{ij}}$	$\sigma^2_{\tilde{w}_{ij}}$
(S,P)	8.94×10^{-4}	1.17×10^{-6}	$\mu_{\tilde{w}_{SP}} = -8.25$	$\sigma^2_{\tilde{w}_{SP}} = 2.46$
(S,R)	5.41×10^{-1}	6.72×10^{-2}	$\mu_{\tilde{w}_{SR}} = -1.23$	$\sigma^2_{\tilde{w}_{SR}} = 1.23$
(P,S)	4.70×10^{-3}	3.23×10^{-5}	$\mu_{\tilde{w}_{PS}} = -6.59$	$\sigma^2_{\tilde{w}_{PS}} = 2.46$
(P,T)	2.97×10^{-2}	2.04×10^{-4}	$\mu_{\tilde{w}_{PT}} = -4.13$	$\sigma^2_{\tilde{w}_{PT}} = 1.23$
(R,S)	5.57×10^{-1}	7.14×10^{-2}	$\mu_{\tilde{w}_{RS}} = -1.20$	$\sigma^2_{\tilde{w}_{RS}} = 1.23$
(R,T)	2.56×10^{-2}	1.51×10^{-4}	$\mu_{\tilde{w}_{RT}} = -4.28$	$\sigma^2_{\tilde{w}_{RT}} = 1.23$
(T,P)	1.32×10^{-2}	4.03×10^{-5}	$\mu_{\tilde{w}_{TP}} = -4.94$	$\sigma^2_{\tilde{w}_{TP}} = 1.23$
(T,R)	1.10×10^{-1}	1.76×10^{-2}	$\mu_{\tilde{w}_{TR}} = -3.44$	$\sigma^2_{\tilde{w}_{TR}} = 2.46$

Table 4.3: *Weights for the graph in Fig. 4.4a.*

4.4 TEST CASES

In what follows, the developments in the previous sections will be applied to two more realistic cases namely, a simplified model of a building and a satellite's mock-up. In the first one, there exists a small group of dominant paths that transmits most of the energy from the source to the target, whereas in the second one the energy becomes more equipartitioned between a large number of paths.

4.4.1 *Test case I: Building*

A six floor building with four rooms per floor is considered [Aragonès and Guasch, 2012] (see Fig. 4.5). The materials used for walls, floors and ceilings, together with their physical properties are listed in Table 4.4. Only bending waves are considered in the SEA model of the building, which consists of a total of 124 subsystems. An airborne source is located in a room of the fourth floor and the air cavity in its adjacent room is chosen as the target subsystem, as in common scenarios of noise regulations between dwellings (see Fig. 4.5). Results are presented for the 1kHz octave frequency band. The 500 most dominant paths between source and target are first computed for the deterministic SEA graph [Guasch and Aragonès, 2011], i.e. considering only the mean values of the loss factors, and then for the stochastic SEA graph, i.e. taking also into account

the information on variances. Random variances ranging from 0.5 to 3 dB are assigned to the edges of the stochastic SEA graph for illustrative purposes. Besides, the cost function in (4.9) is defined again to follow the three sigma rule, $\phi\left(\sigma^2\right) = -3\sigma$. As mentioned, the negative sign is used to consider the most restrictive situation [Deng and Wong, 2006].

Element	Walls	Floors and ceilings
Material	Hollow brick	Concrete
Thickness	0.07 m	0.15 m
Density	770 kg/m^3	2300 kg/m^3
Young modulus	3.5 GPa	28.1 GPa
Internal Loss Factor	0.006	0.006

Table 4.4: *Properties of the materials used for the model of the building.*

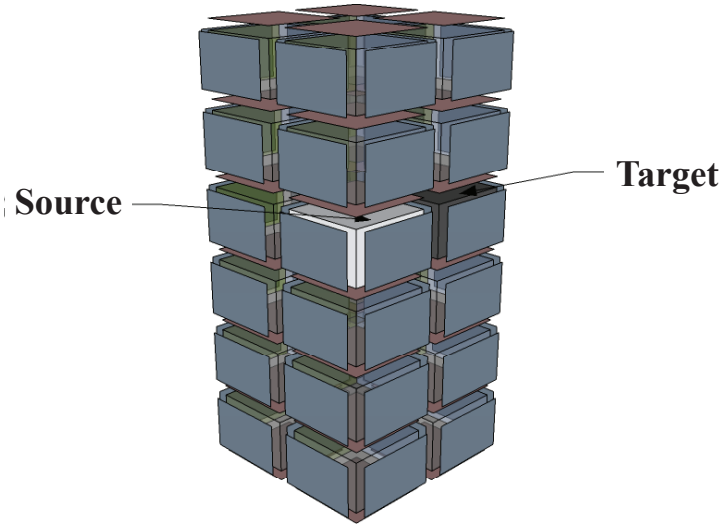

Figure 4.5: Building example.

This example is representative of a case in which a limited set of dominant paths is responsible for most energy transmission. As it can be observed in Fig. 4.6, the first dominant path supplies almost 36% of the energy at the target. This is the second order path passing through the partition wall. 70% of the target energy is achieved by considering only the 10 most dominant paths. For such a scenario, one could hardly expect considerable changes in the ranking of the stronger dominant transmission paths, even when considering high variance values.

This is analyzed in Fig. 4.7, where a comparison is established between the ranking of paths resulting from the deterministic and the stochastic SEA graphs. The X-axis in the figure represents the position of the paths in the ranking arising

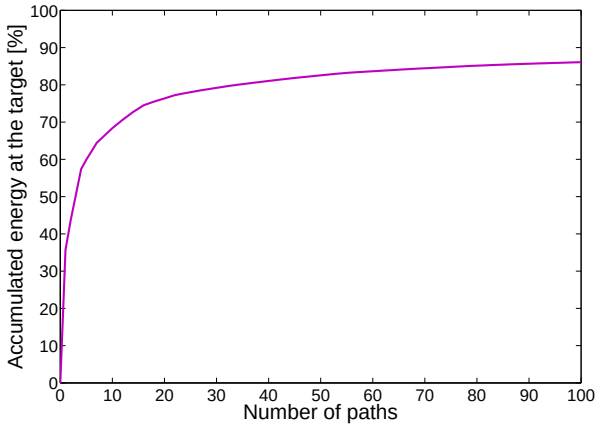

Figure 4.6: Building example. Accumulated energy at the target for the first 100 paths in the deterministic graph.

from the stochastic graph and the Y-axis represents the ranking arising from the deterministic graph. The continuous line indicates the position that the paths in the stochastic graph would have in the deterministic one. For instance, the 10-th path in the stochastic ranking would have been the 8-th path in the classification if only the mean values of the loss factors were considered (see zoom in Fig. 4.7). The dashed line represents the hypothetical case in which all variances were zero and the rankings from the stochastic and deterministic graphs coincide.

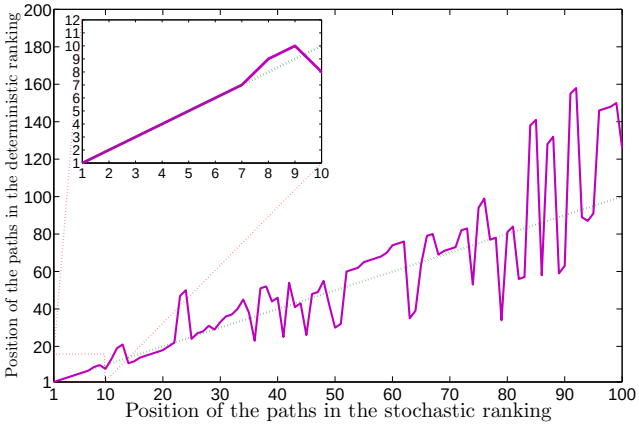

Figure 4.7: Building example. Position of the paths obtained in the deterministic ranking versus the position of the same paths in the stochastic ranking.

As expected, no substantial changes are appreciated in the ranking of the first few dominant paths. However beyond the eighth path and up to the 100-th only four paths have the same ranking position in both classifications. This is reasonable since as long as the contribution of the paths diminishes, they become more sensitive to the influence of the variance, and differences in ranking position become more apparent. One can also observe that if only the

deterministic case was considered, some paths arising from the stochastic case would be missing, e.g., from the 85-th path to the 100-th path.

4.4.2 *Test case II: Satellite's mock-up*

The system depicted in Fig. 4.8 is next considered. It corresponds to the mock-up of a typical structure of a satellite and has been taken from [Roibás-Millán et al., 2012]. The structure consists of a lower platform and an upper platform, six lateral faces, two external solar arrays and an adapter cone to the launcher. The solar arrays are attached to their corresponding lateral faces through three connection beams. Both, the solar arrays and their corresponding faces are divided in three panels each, up, mid, and low, the connection beams being placed at the common vertices (depicted as T4-T6 in the zoom of Fig.4.8). The materials and dimensions of all elements are specified in Table 4.5 and 4.6. The SEA model has 130 subsystems consisting of plates, beams and the air cavity inside the satellite. Bending (F), shear (S) and longitudinal (E) modes have been considered for the plates, whereas bending in the x (X) and y (Y) directions, extension (E) and torsion (T) have been taken into account for beams (see [Roibás-Millán et al., 2012] for details). Results will be presented for the 4kHz octave frequency band.

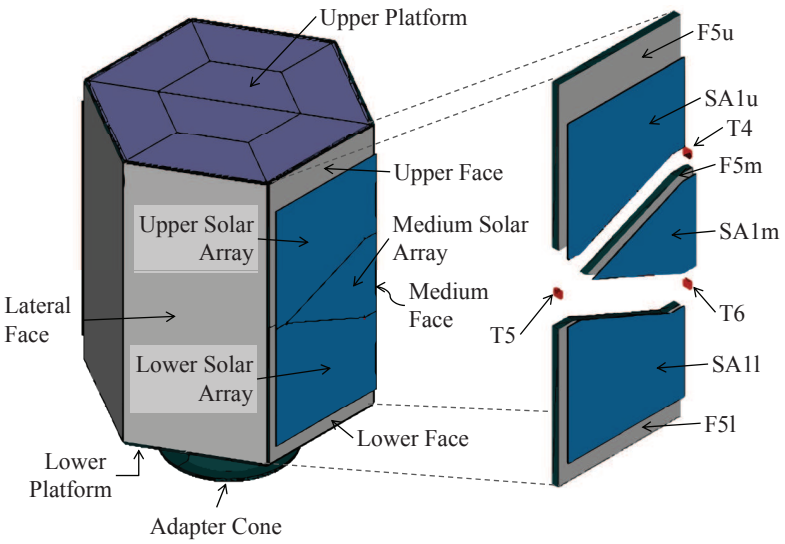

Figure 4.8: Satellite example.

It is worthwhile noting that vibroacoustics plays an important role in space missions, specially at the launch time during rocket engine ignition. For instance, excessive vibration levels can result in damage of the solar arrays. It becomes then essential to understand the importance of airborne and structure borne paths through the satellite structure and payload bay. Let us next focus on the very limited case of analyzing the vibration transmission from the plate in the upper lateral face, F5uF (source), to the upper solar array, SA1uF (target), see Fig. 4.8). The values for the variances and the cost function have been respectively

Elements	Material	Thickness [mm]
Upper platform	Aluminium	1
Lower platform	Aluminium	10
Lateral faces	Methacrylate	6
Solar arrays	Aluminium	1
Adapter cone	Aluminium	4
Connectors	Aluminium	Dimensions [mm]: 3×5

Table 4.5: *Materials and thicknesses of the elements of the system in Fig. 4.8*

Material	Aluminium	Methacrylate
Density	2700 kg/m^3	1216 kg/m^3
Young modulus	71 GPa	3.559 GPa
Internal Loss Factor	0.01	0.01

Table 4.6: *Properties of the materials introduced on Table 4.5.*

generated and defined as in the previous building example, and 500 paths have been computed using both, the deterministic and stochastic approaches.

As for the building case, the accumulated energy is plotted for the first 100 paths (see Fig. 4.9). However, the situation is quite different now, the individual contributions of paths being rather small. The most dominant path is the second order path going through subsystem T4E, i.e. the extensional modes of the connection beam T4, and it only justifies 13% of the energy at the target; only 55% of the target energy becomes justified from the contributions of the first 100 paths.

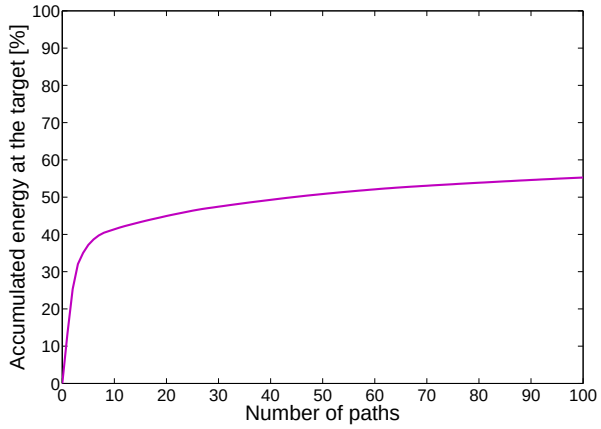

Figure 4.9: Satellite example. Accumulated energy at the target for the first 100 paths in the deterministic graph.

Given that the first paths have similar mean contributions (favored by the high symmetry of the model) but different variances, their positions in the stochastic case strongly differ from those in the deterministic ranking. This can be observed in Fig. 4.10, where the curve is much more irregular than its corresponding one in Fig. 4.7. In fact, only five paths in Fig. 4.10 show the same position in both rankings; note that even the first path swaps its position with the second one. From then on, the average difference in positions between the two rankings is 30, with a maximum difference of 174 (the 259th path in the deterministic ranking becomes the 85th path in the stochastic one).

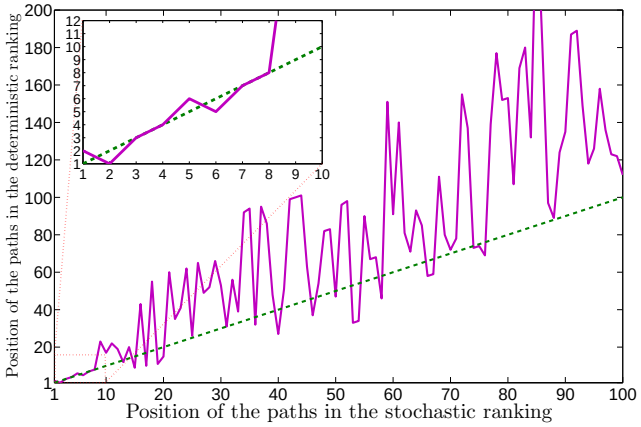

Figure 4.10: Satellite example. Position of the paths obtained in the deterministic ranking versus the position of the same paths in the stochastic ranking.

Though one would be tempted to conclude that a path analysis makes no sense for such a situation because the are no clear dominant paths, still some valuable information can be gathered from the analysis. For instance, in Fig. 4.11 the incidence of the subsystems in the deterministic (purple) and stochastic (green) rankings of the first 500 paths is presented, thus revealing those subsystems appearing in most transmission paths. The two highest bars obviously correspond to the source (F5UF) and the target (SA1uF) subsystems which belong to all paths. These are followed by the mid lateral face plate (F5mF) and then by the two connection beams (T4E, T5E) between the upper lateral face and the upper solar array. This is logical given that the mid lateral face plate will play a determinant role in all paths with order larger than two, passing through the connection beams. The extensional modes of the latter are the dominant ones in this case, as being excited by the panel bending waves. Had the connection beams been placed in an angular disposition, the path analysis could have served e.g., to determine the relative influence of bending and extensional mode influence on energy transmission. Besides, note that some strong differences can be appreciated between the stochastic and deterministic cases for some subsystems such as the solar array mid and low plates (SA1mF, SA1lF). This can be attributed to the strong variance that has been arbitrarily assigned to these subsystems.

Though identifying relevant subsystems in a simple model such as the satellite could be done relying on intuition and/or experience, this could be not so easy for more complex structures, or when determining, as mentioned, the influence of different types of modes in vibroacoustic transmission, making path analysis and graph cut strategies [Guasch et al., 2011] useful. If the effects of variance are to be included, the difficulty increases and intuition may easily fail.

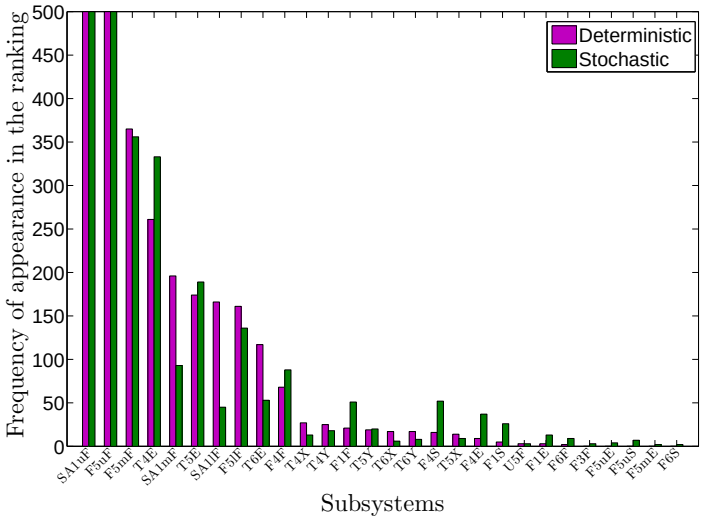

Figure 4.11: Satellite example. Incidence of subsystems in the first 500 paths for the deterministic and stochastic rankings.

4.4.3 *Computation times*

The execution times for the two cases in a regular PC (Intel Core 2 Quad CPU q9400 @2.66 GHz) are gathered in Table 4.7. The same number of paths has been computed for both cases, however, the large amount of subsystems in the satellite system increases considerably the computation time, to approximately 12.5 hours. It must be taken into account that the code has been developed in Matlab and optimization and conversion to other languages could be developed in order to improve the performance.

	Building of Extended Graph	Tree of maximum paths	Sorted Forward Star Form	MPS Algorithm	Post-processing functions	Total
Building example	188.84 s	184.09 s	5.54 s	335.46 s	1.86 s	715.79 s
Satellite's mock-up	2064.9 s	254.55 s	36.29 s	42407.1 s	50.3 s	44813.4 s

Table 4.7: *Computation times of test cases I and II.*

4.5 CONCLUSIONS

Including variance information in SEA transmission path analysis poses several difficulties, namely, assigning variance values to each first order path connecting two subsystems, determining a method to compare path energies and developing an efficient algorithm for the computation and classification of paths. In this chapter, a possible solution to these issues has been provided. First, it has been show how deterministic SEA graphs are no longer valid for the system description and have to be substituted by biparametric stochastic SEA graphs, in which arcs (i.e. first order paths) are assigned both a mean and variance value. Variances for arcs can be obtained assuming lognormal probability density functions for the loss factors and resorting to a logarithmic transformation. Second, a cost function that accounts not only for the path mean energy but also for its variance has been defined and used to compare energy transmission through different paths. Third, biparametric stochastic SEA graphs have the problem of not fulfilling the optimality principle so that efficient deterministic classification algorithms cannot be applied to them. However, it has been shown that it is possible to build deterministic extended graphs from stochastic ones, by transferring the variance information to new created nodes. Deterministic ranking algorithms like the MPS can then be applied to these extended graphs to classify paths according to the previously specified cost function.

The importance of taking into account the stochastic nature of loss factors in SEA path classification has been made apparent by means of two examples consisting of the SEA model of a building and a satellite's mock-up. It has been shown that even in the case of having a clear set of dominant paths, important differences can arise between a pure deterministic classification that only considers the mean energy of paths and a stochastic ranking that also includes path variances. Moreover, it has been shown that path analysis could prove useful even in situations where there is not a clear set of dominant transmission paths.

Finally, it is to be noted that several hypotheses have been made in order to solve the problem of SEA energy path classification, such as assuming certain probability density functions for the loss factors, or choosing a particular cost function to compare path contributions. Obviously, selecting e.g. a different cost function may result in a different path ranking. In this sense, the present work is to be viewed as actually providing a general framework where to solve the stochastic path classification problem, rather than giving an absolute and definite solution to it. Besides, though the procedure may look intricate, it could work as a black box for the vibroacoustic engineer, who only needs to select the source and target subsystems and provide the SEA loss factor matrix; all path computations being carried out by an appropriate software.

5

CONDITIONS FOR TRANSMISSION PATH ANALYSIS IN ENERGY DISTRIBUTION MODELS

Summary. In this chapter, we explore under which conditions transmission path analysis (TPA) developed for statistical energy analysis (SEA) can be applied to the less restrictive energy distribution (ED) models. It is shown that TPA can be extended without problems to proper-SEA systems whereas the situation is not so clear for quasi-SEA systems. In the general case, it has been found that a TPA can always be performed on an ED model if its inverse influence energy coefficient (EIC) matrix turns to have negative off-diagonal entries. If this condition is satisfied, it can be shown that the inverse EIC matrix automatically becomes an M-matrix. An ED graph can then be defined for it and use can be made of graph theory ranking path algorithms, previously developed for SEA systems, to classify dominant paths in ED models. A small mechanical system consisting of connected plates has been used to illustrate some of the exposed theoretical results.

This chapter is based on the following work

- À. Aragonès and O. Guasch. Conditions for transmission path analysis in energy distribution models. *Mechanical Systems and Signal Processing* , Submitted, 2015b [Aragonès and Guasch, 2015b]

5.1 INTRODUCTION

Transmission path analysis (TPA) in statistical energy analysis (SEA) relies on Craik's definition of energy transmission path [Craik, 1990]. TPA is usually carried out for vibroacoustics remedial purposes as it provides information on energy flow paths from a source subsystem, where external energy is being input, to a target subsystem where energy is to be reduced [Craik, 1996]. Performing a TPA basically makes sense whenever the energy transmission is dominated by a limited set of paths. However, computing and ranking transmission paths in an efficient way is not a straightforward task for complex SEA models, as seen in Chapters 2 and 3.

As introduced in Chapter 2, given that a mechanical system and its inputs have to satisfy some rather restrictive conditions in order to be modelled by SEA, namely large population of modes, high modal overlap and weak coupling

among others as seen in Chapter 2 (see e.g., [Le Bot and Cotoni, 2010]), it is the main goal of this chapter to determine under which conditions a SEA-like TPA could be extended to the more general energy distribution (ED) models. In an ED model, the mechanical system also becomes split into a set of subsystems, and the energy at any of them when submitting some part of the system to a broadband excitation is characterized by means of the so called energy influence coefficients (EICs) ([Guyader et al., 1982], see also [Fredö, 1997; Mace and Shorter, 2000]). They are not submitted to the restrictive conditions demanded to SEA coupling loss factors. Actually, a question of interest is that of determining under which circumstances the EICs are such that the resulting ED matrix system can be identified with a SEA system [C.H Hodges, P. Nash and J. Woodhouse, 1987]. This let to the definition of quasi and proper SEA systems in [Mace, 2003, 2005]. We will explore in this chapter whether it is possible or not to apply a TPA to quasi and proper SEA models, and thus make use of ED graphs to compute and rank transmission paths for them.

The chapter is organized as follows. In Section 5.2 we give a possible definition for transmission paths in ED models and justify it in terms of the series expansion of the subsystem energy vector. Then, we determine under which conditions this expansion will converge making ED TPA possible in some cases. A small ED consisting of six steel plates is used in Section 5.3 to show how a TPA can be performed for a system that does not admit SEA modelling. Finally, the conclusions close the chapter in Section 5.4.

5.2 TRANSMISSION PATH ANALYSIS IN ENERGY DISTRIBUTION MODELS

5.2.1 *Definition of transmission paths*

As commented in the Introduction, the aim of this chapter is to explore under which conditions transmission path analysis becomes possible in an ED model, so that the graph algorithms developed in Chapter 3 can be applied to it. It will be shown that this depends on some properties of $\boldsymbol{X}$, though no direct one to one correspondence has been found between them and those involved in the above definitions of SEA-like matrices. We will see that transmission path analysis makes sense for proper-SEA matrices as well as for any other $\boldsymbol{X}$ matrix that can be shown to be an M-matrix (reciprocally, for any EIC matrix $\boldsymbol{A}$ that can be shown to be an *inverse* M-matrix).

In Chapter 2 we have seen that an energy path between two arbitrary subsystems in a SEA system is made of the concatenation of first order paths between adjacent subsystems. The weight of a first order path from subsystem i to j is given by η_{ij}/η_j (η_{ij} standing for the coupling loss factor and η_j for the total loss factor) [Guasch, 2011]. The definition of a first order path actually relies on the notion of direct or blocked transmissibilities (see e.g. [Guasch, 2009; Guasch and Magrans, 2004; Magrans, 1981]). That is to say η_{ij}/η_j is nothing but the ratio of energies E_j/E_i when a unit input power is applied to i and all the remaining

SEA subsystem energies are set to zero i.e., $E_k = 0,\ \forall\ k \neq i, j$. If we proceed similarly for (2.18), in order to try to define a first order energy transmission path for an ED model, we get,

$$\begin{pmatrix} X_{ii} & X_{ij} \\ X_{ji} & X_{jj} \end{pmatrix} \begin{pmatrix} E_i \\ E_j \end{pmatrix} = \begin{pmatrix} 1 \\ 0 \end{pmatrix} \tag{5.1}$$

which once solved, results in

$$\frac{E_j}{E_i} = -\frac{X_{ji}}{X_{jj}} =: F_{ji}. \tag{5.2}$$

Given that F_{ji} represents a quotient of energies $\forall\ i, j$, it it is clear that the diagonal and off-diagonal entries in $\boldsymbol{X}$ should have opposite sign. Let us assume, for the moment, that this is the case. This allows us to define energy transmission paths between subsystems in an ED model by concatenating first order paths, as done in SEA. That is to say, the weight of an n-th order path p_{ij}^n between subsystems i and j will be given by

$$w\left(p_{ij}^n\right) = F_{h_1 i} F_{h_2 h_1} F_{h_3 h_2} \cdots F_{j h_{n-1}}. \tag{5.3}$$

At this point we should notice that the above procedure can be carried out despite of whether the matrix entries linking two subsystems simply involve the connected pair, as it is the case of η_{ij} in SEA, or the response of the whole system, as it is the case of the EICs A_{ij} in ED models (and therefore that of X_{ij} and F_{ij}). Another issue is to which extent a path like (5.3) may represent a physical energy transmission path from i to j. In an SEA model with no indirect coupling this is certainly the case, though links between non-physically connected subsystems are commonly employed in SEA to represent non-resonant transmission paths [Craik, 1996; Lyon and DeJong, 1998]. This does not prevent Craik's definition of SEA transmission path to be valid. Similarly, in ED models indirect paths may exist and denote failure of the CPP hypothesis [Mace, 1994, 2003, 2005], but again this does not invalidate the path definition usefulness in (5.3). In fact, there is an additional point which provides the key justification for defining energy paths in ED and SEA models. For the path definition to make sense, it has to be possible to factorize the energy at any target subsystem of an ED model as the summation of the energies transmitted through the infinite number of paths connecting subsystems where external power is being input, to the target one. This will be the topic of the next subsection.

5.2.2 *Series expansion of the subsystem energies and definition of the ED graph*

Let us rewrite equation (2.18) as

$$[\boldsymbol{I} - \boldsymbol{I} + \mathrm{d}iag(1/X_{ii})\boldsymbol{X}]\boldsymbol{E} = \mathrm{d}iag(1/X_{ii})\boldsymbol{P} =: \boldsymbol{P}', \tag{5.4}$$

with $\boldsymbol{I}$ standing for the identity matrix. Defining $\boldsymbol{F} := \boldsymbol{I} - \mathrm{d}iag(1/X_{ii})\boldsymbol{X}$ we get

$$F_{ij} = \begin{cases} -X_{ij}/X_{ii} & \mathrm{if} \quad i \neq j, \\ 0 & \mathrm{if} \quad i = j, \end{cases} \tag{5.5}$$

the physical meaning of F_{ij} as a first order transmission path between j and i being already established in (5.2). It follows from (5.4) that the subsystem energies in the ED model can be computed from

$$\boldsymbol{E} = (\boldsymbol{I} - \boldsymbol{F})^{-1}\boldsymbol{P}'. \tag{5.6}$$

Whenever the spectral radius of matrix $\boldsymbol{F}$, $\rho(\boldsymbol{F})$, is less than unity, (5.6) admits a convergent series expansion

$$\boldsymbol{E} = (\boldsymbol{I} - \boldsymbol{F})^{-1}\,\boldsymbol{P'} = \left(\sum_{k=0}^{\infty} \boldsymbol{F}^k\right)\boldsymbol{P}' = \left(\boldsymbol{I} + \boldsymbol{F} + \boldsymbol{F}^2 + ...\right)\boldsymbol{P}'. \tag{5.7}$$

As discussed in Chapter 2, a power expansion like (5.7) was first proposed for SEA systems in [Magrans, 1993]. As for a SEA model [Guasch and Cortés, 2009; Magrans, 1993], the k-th power of the generating matrix $\boldsymbol{F}$ contains the contributions from all k-th order paths connecting the source subsystems, where P'_i is injected, with the target ones. Therefore, the series expansion (5.7) allows to recover the energy at any target subsystem as the infinite summation of all paths linking the source to it. Assuming the convergence of (5.7) and that F_{ij} is positive $\forall\ i \neq j$ (see Section 5.2.1), it is possible to identify the transpose of $\boldsymbol{F}$, i.e. $\boldsymbol{F}^\top$, with the weighting matrix of an ED graph, and to apply the graph algorithms presented in [Aragonès and Guasch, 2015a; Guasch and Aragonès, 2011] to efficiently rank energy path contributions in an ED model. Obviously, the remaining task at this point is that of determining under which circumstances the two former conditions for $\boldsymbol{F}$ will be satisfied.

5.2.3 *Conditions on the inverse energy influence coefficient matrix for transmission path analysis*

A sufficient condition for the inverse EIC matrix $\boldsymbol{X}$ to allow fulfillment of $\rho(\boldsymbol{F}) < 1$ and positiveness of $F_{ij}\ \forall\ i \neq j$ is that of $\boldsymbol{X}$ being an M-matrix (reciprocally that of the EIC matrix $\boldsymbol{A}$ being an inverse M-matrix). Let us recall that a real $n \times n$ matrix $\boldsymbol{B}$ is said to be an M-matrix whenever it is non-singular, its off-diagonal entries $B_{ij} < 0$ and its inverse satisfies $\boldsymbol{B}^{-1} \geq \boldsymbol{0}$ (see e.g. [Varga, 1962]). Here $\boldsymbol{0}$ denotes an $n \times n$ matrix of zeros so the last condition expresses that all elements in $\boldsymbol{B}^{-1}$ are non-negative. This implies, in our case, that we just need requiring $X_{ij} < 0$ for $\boldsymbol{X}$ to be an M-matrix, given that we already know that $\boldsymbol{X}^{-1} = \boldsymbol{A} \geq \boldsymbol{0}$ because $\boldsymbol{A}$ is an EIC matrix, and all its entries A_{ij} are positive. Besides, it can be proved that if $\boldsymbol{B}$ is an M-matrix then the matrix $\boldsymbol{G} := \boldsymbol{I} - \mathrm{d}iag(1/B_{ii})\boldsymbol{B}$ is non-negative, irreducible and convergent (see

Theorem 3.11, pg. 84 in [Varga, 1962]). As a consequence, for the present case if $X_{ij} < 0$ then $\boldsymbol{X}$ will be an M-matrix and $\boldsymbol{F}$ will automatically converge.

It is clear that an SEA matrix of loss factors is an M-matrix. It is nonsingular, its off-diagonal entries are given by $-\eta_{ij} < 0$ and its inverse is a particular case of an EIC matrix and thus will have positive entries. Consequently the analogous series expansion (5.7) for SEA in (2.34) will always converge. An alternative proof of convergence following very different argumentation lines based on graph theory considerations can be found in Chapter 3 [Guasch and Aragonès, 2011].

With regard to proper-SEA systems, we closely follow the developments in [Mace, 2005], where expressions for the EIC matrix were derived in terms of the system modes. First, the inverse EIC matrix can be rewritten as

$$\boldsymbol{X} = \omega\eta\boldsymbol{I} + \omega\boldsymbol{C}, \tag{5.8}$$

where η represents the system damping loss factor and $\boldsymbol{C}$ is a matrix of coupling loss factors. The EIC matrix $\boldsymbol{A}$ can be set as

$$\boldsymbol{A} = \frac{1}{\omega\eta}\left(\boldsymbol{I} - \boldsymbol{\alpha}\right), \tag{5.9}$$

the definition of $\boldsymbol{\alpha}$ being implicit in (5.9). Since the EICs are always nonnegative, the elements of $\boldsymbol{\alpha}$ fulfill

$$\alpha_{ij} = \begin{cases} 0 < \alpha_{ii} < 1 & \text{if} \quad i = j \\ \alpha_{ij} \leq 0 & \text{if} \quad i \neq j. \end{cases} \tag{5.10}$$

Then again, if the spectral radius of $\boldsymbol{\alpha}$ is less than unity, $\boldsymbol{C}$ can be written as

$$\boldsymbol{C} = \eta\boldsymbol{\alpha}\left(\boldsymbol{I} - \boldsymbol{\alpha}\right)^{-1} = \eta\left(\boldsymbol{\alpha} + \boldsymbol{\alpha}^2 + \boldsymbol{\alpha}^3 + ...\right). \tag{5.11}$$

For high modal overlap or when all the system modes are local (i.e., basically restricted to subsystems), the coefficients α_{ij} can be proved to be small which makes the powers of $\boldsymbol{\alpha}$ negligible [Mace, 2005]. The series in (5.11) can then be truncated to first order

$$\boldsymbol{C} \approx \eta\boldsymbol{\alpha} \tag{5.12}$$

which results in

$$\boldsymbol{X} \approx \omega\eta\left(\boldsymbol{I} + \boldsymbol{\alpha}\right). \tag{5.13}$$

Therefore, it becomes always possible to perform a transmission path analysis for proper-SEA systems given that all diagonal terms in (5.13) will be positive and the off-diagonal ones will be negative. $\boldsymbol{X}$ will then be an M-matrix and, as a consequence, it will make sense to perform a TPA.

In the case of quasi-SEA systems or for general ED systems the situation becomes more intricate and it should be checked at each occurrence that $X_{ij} < 0$, to guarantee that a TPA is feasible. Yet it is to be noted that in the case of low modal overlap and global modes $\boldsymbol{X}$ could hardly be an M-matrix. Actually, for the limiting case of energy equipartition $\boldsymbol{A}$ becomes singular so that $\boldsymbol{X}$ does not even exist [Mace, 2005].

5.3 NUMERICAL EXAMPLE

In this section, an energy transmission path analysis is performed for the ED model of a simple mechanical system inspired on that in [Zhang et al., 2003]. The system is depicted in Fig. 5.1, and consists of 6 steel (Density $\rho = 7800$ kg/m^3, Young modulus $E = 2.1 \times 10^{11}$ Pa, Poisson's ratio $\mu = 0.3125$) plates whose dimensions are listed in Table 5.1. The damping loss factor of every plate has been taken as 0.05. An ED model of the system has been built using a finite element approach with the commercial software VA-ONE. Subsystems have been identified with the physical plates in Fig. 5.1. To obtain each EIC A_{ij} in $\boldsymbol{A}$, the average energy at plate i resulting from rain-on-the-roof excitation of plate j has been calculated. A minimum of 6 elements per wavelength have been considered for the computations in all subsystems. The analysis has been carried out for 20 bands ranging from 100 Hz to 2000 Hz, with a constant bandwidth of 100 Hz. For illustrative purposes, only the results for the 500 Hz and 2000 Hz central frequency bands will be presented.

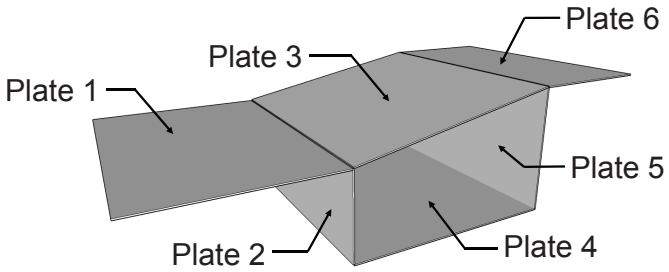

Figure 5.1: Tested mechanical system.

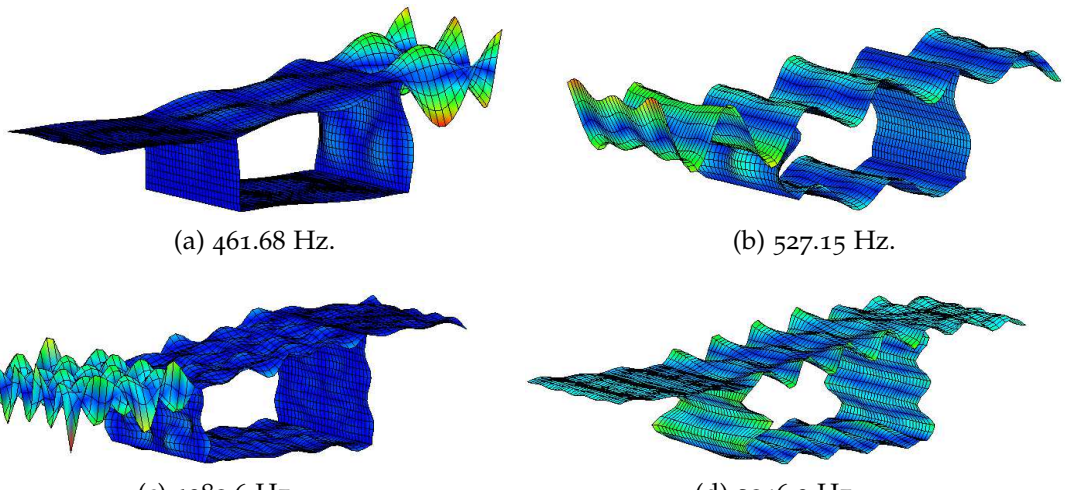

(a) 461.68 Hz. (b) 527.15 Hz.

(c) 1980.6 Hz. (d) 2046.9 Hz.

Figure 5.2: Local and global modes belonging to the 500 Hz and 2000 Hz central frequency bands.

		500 Hz		2000 Hz	
Subsystem	Dimensions[mm]	N	M	N	M
Plate 1	$600 \times 400 \times 3$	2	0.5	3	3
Plate 2	$600 \times 200 \times 3$	1	0.25	2	2
Plate 3	$600 \times 510 \times 3$	3	0.75	5	5
Plate 4	$600 \times 500 \times 3$	2	0.5	1	1
Plate 5	$600 \times 300 \times 3$	4	1	1	1
Plate 6	$600 \times 300 \times 3$	4	1	1	1

Table 5.1: *Plate dimensions, number of modes per band (N) and modal overlap (M) of the model in Fig. 5.1*

It is well known that fulfillment of the SEA conditions require both, the modal overlap M and the number of modes N in a band, to be higher than unity (see Chapter 2, Section 2.1). We briefly remember that the modal overlap is defined as $M = n\eta\omega$, with $n = N/\Delta\omega$ being the modal density, $\Delta\omega$ the bandwidth, η the damping loss factor and ω the band central frequency. In Table 5.1, we show the values for M and N corresponding to the two central frequency bands of 500 Hz and 2000 Hz. As observed, the modal overlaps and the number of modes per band are far from the requirements of SEA (note in particular that M and N coincide at 2000 Hz, since $\eta\omega/\Delta\omega = 1$). Actually, if we have a look at the modes in these bands we will observe that global modes still coexist with local modes. Some of them are presented in Fig. 5.2. In the left column of the figure (Figs. 5.2a and 5.2c) localized modes at plates #6 and #1 are respectively observed for the 500 Hz and 2000 Hz bands, whereas global modes for the same bands are shown in the right column (Figs. 5.2b and 5.2d). In fact, it turns out for the present case that not only SEA cannot be applied to it, but that the ED model is not even a quasi-SEA model (it can be checked that indirect coupling exists between the entries of the inverse EIC matrix $\boldsymbol{X}$, and that $\boldsymbol{X}$ does not satisfy the CPP relation). However, it follows that $X_{ij} < 0$ so $\boldsymbol{X}$ turns to be an M-matrix. Therefore, a transmission path analysis can be carried out for this ED model and we can associate an ED graph to it, whose adjacency matrix is given by the transpose of the generating matrix $\boldsymbol{F}$.

The ED graph corresponding to the mechanical system in Fig. 5.1 is presented in Fig. 5.3. For simplicity we have only plotted one edge between linked subsystems but each edge has two side end arrows indicating that the connection exists in both directions (ED and SEA graphs are strongly connected graphs). It can be observed that several indirect couplings exist, which have been indicated using dashed lines. In order to perform a transmission path analysis making use of this ED graph, we have applied the algorithm in Chapter 3 to compute and rank all dominant paths between the input subsystem #1, and the target

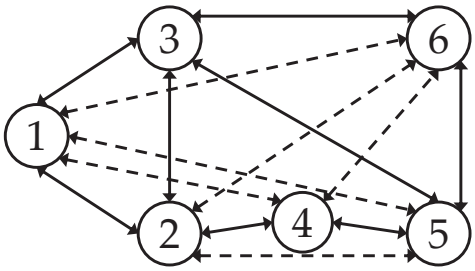

Figure 5.3: ED graph corresponding to the model in Fig. 5.1

subsystem #6. The computation time in a regular PC (Intel Core 2 Quad CPU q9400 @2.66 GHz) for this case are shown in Table 5.2.

Tree of max. paths	Sorted Forward Star Form	MPS Algorithm	Post-processing functions	Total
0.43 s	0.12 s	1.25 s	0.40 s	2.21 s

Table 5.2: *Computation times of the mechanical example in Figure 5.1*

Path	500 Hz	2000 Hz
p_1	$P1 \to P3 \to P6$	$P1 \to P3 \to P6$
p_2	$P1 \to P6$	$P1 \to P6$
p_3	$P1 \to P2 \to P6$	$P1 \to P5 \to P6$
p_4	$P1 \to P2 \to P3 \to P6$	$P1 \to P3 \to P5 \to P6$
p_5	$P1 \to P4 \to P5 \to P6$	$P1 \to P2 \to P3 \to P6$
p_6	$P1 \to P3 \to P5 \to P6$	$P1 \to P4 \to P5 \to P6$
p_7	$P1 \to P4 \to P6$	$P1 \to P2 \to P4 \to P5 \to P6$
p_8	$P1 \to P2 \to P4 \to P5 \to P6$	$P1 \to P4 \to P6$
p_9	$P1 \to P2 \to P4 \to P6$	$P1 \to P3 \to P6 \to P3 \to P6$
p_10	$P1 \to P2 \to P5 \to P6$	$P1 \to P3 \to P6 \to P5 \to P6$

Table 5.3: *Most dominant energy transmission paths from subsystem* #1 *to subsystem* #6 *at* 500 *Hz and* 2000 *Hz.*

The results have been listed in Table 5.3. For both frequency bands, 500 Hz and 2000 Hz, the first dominant path is the shortest path between the source and the target, which only involves direct connections (see Figs. 5.1 and 5.3). Again for both frequencies, the second path involves the indirect coupling from the source to the target. For the third dominant paths, differences appear for the 500 Hz and 2000 Hz bands because the former involves subsystem #2 whilst the second involves subsystem #5. Both paths involve again indirect couplings. Finally, we

note that differences become apparent between the 500 Hz and 2000 Hz path ranking from the third path in the lists of Table 5.3.

5.4 CONCLUSIONS

An extension of the definition of a SEA transmission path has been proposed for ED models, which finds its key justification in the power series development for the subsystem energy vector. Whenever this series converges it becomes possible to perform a TPA analysis between source and target subsystems of an ED model. The convergence of the series depends on the properties of the inverse EIC matrix of the ED system. It has been shown that the TPA can be carried out without problems if that matrix corresponds to a proper-SEA matrix, but for quasi-SEA or more general ED matrices this will not always be the case. Actually, it has been shown that for a general ED model the proposed TPA will be feasible whenever the off-diagonals entries of the inverse EIC matrix of the system are negative, as in this case the inverse EIC matrix turns to be an M-matrix.

For the convergent cases, one can build an ED graph and apply graph theory algorithms, previously developed for transmission path classification in SEA, to ED models. A small six steel plate system that cannot be properly modelled with SEA has served as a simple example to show that a TPA can be performed on ED models, which satisfy the conditions specified in the previous paragraph.

6

A GRAPH THEORY APPROACH TO IDENTIFY RESONANT AND NON-RESONANT TRANSMISSION PATHS IN STATISTICAL MODAL ENERGY DISTRIBUTION ANALYSIS

Summary. Statistical modal energy distribution analysis (SmEdA) extends classical statistical energy analysis (SEA) to the mid frequency range by establishing power balance equations between modes in different subsystems. This circumvents the SEA requirement of modal energy equipartition and enables applying SmEdA to the cases of low modal overlap, locally excited subsystems and to deal with complex heterogeneous subsystems as well. Yet, widening the range of application of SEA is done at a price with large models because the number of modes per subsystem can become considerable when the frequency increases. Therefore, it would be worthwhile to have at one's disposal tools for a quick identification and ranking of the resonant and non-resonant paths involved in modal energy transmission between subsystems. It will be shown that the graph theory algorithms for transmission path analysis (TPA) in SEA developed in the previous chapters can be adapted to SmEdA and prove useful for that purpose. The case of airborne transmission between two cavities separated apart by homogeneous and ribbed plates will be first addressed to illustrate the potential of the graph approach. A more complex case representing transmission between non-contiguous cavities in a shipbuilding structure will be also presented.

This chapter is based on the following work

- À. Aragonès, L. Maxit, and O. Guasch. A graph theory approach to identify resonant and non-resonant transmission paths in statistical modal energy distribution analysis. *Journal of Sound and Vibration*, 350(0):91 – 110, 2015b. ISSN 0022-460X [Aragonès et al., 2015b]

- À. Aragonès, L. Maxit, and O. Guasch. Computation of modal energy transmission paths in SmEdA using graph theory algorithms. In *NOVEM2015: Dubrovnik (Croatia), 13-15 April, Noise and Vibration: Emerging Methods*, 2015a [Aragonès et al., 2015a]

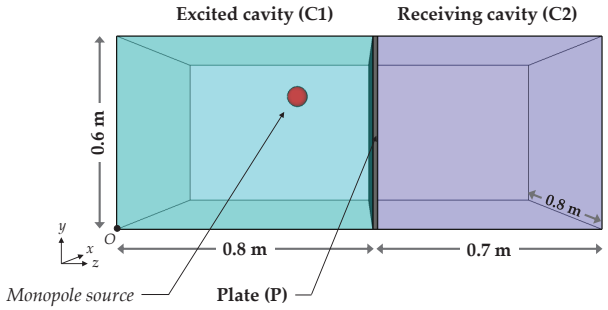

Figure 6.1: Cavity-panel-cavity system.

6.1 INTRODUCTION

Though SmEdA may offer several advantages when compared to SEA, the price to be paid is that of dealing with large matrix systems (yet much smaller than those encountered in deterministic methods like FEM, which can involve millions of degrees of freedom). This makes the analysis of the obtained results difficult. For instance, determining which modes play a predominant role in the energy transmission between subsystems for even simple cases, such as two cavities separated by a homogeneous wall, may implicate hundreds of modes at mid-frequencies. A thorough analysis of the interaction of modal works and involved modal coupling loss factors then becomes necessary to find the dominant modal energy transmission paths between the excited cavity and the receiver one [Maxit et al., 2014]. It is the goal of this chapter to try to lighten this process by resorting to an alternative approach. In particular, it will be shown that path graph algorithms can also be applied to SmEdA models to identify and rank the relevant modes governing the energy transmission between subsystems.

The chapter is organized as follows. In section 6.2 the inclusion of non-resonant transmission in a SmEdA model is presented. In section 6.3 it is exposed how to define a SmEdA graph, and the notion of modal energy transmission paths becomes introduced. Two benchmark examples involving resonant and non-resonant energy transmission between two adjacent cavities separated apart by homogeneous and ribbed plates are presented in section 6.4. It is shown how the graph theory approach can provide very valuable information in a quicker and more efficient way than when attempting a conventional analysis of the SmEdA results. A more complex case dealing with vibrational and acoustic energy transmission in a shipbuilding built-up structure is addressed in section 6.5. Conclusions close the article in section 6.6.

6.2 RESONANT AND NON-RESONANT TRANSMISSION IN A THREE-SUBSYSTEM SMEDA MODEL

In Section 2.4, a review on the basic concepts of SmEdA has been given. The SmEdA modelling of a physical system consisting of two subsystems has been described. A slightly more involved case is next considered which consists of a system made of three subsystems. This will allow one to inspect how non-resonant transmission can be accounted for in SmEdA, a topic that has only been addressed very recently [Maxit et al., 2014]. For the ease of exposition and without loss of generality, suppose that the system is made of two cavities separated by a panel, as the one depicted in Figure 6.1. Subsystems 1 and 3 are identified with the cavities and subsystem 2 with the panel (this system will be re-encountered in the benchmark examples of Section 6.4). The sets of resonant modes for the cavities in the frequency range of interest will be denoted by $\hat{P}$ and $\hat{R}$, $\hat{Q}$ standing for the set of panel resonant modes. The SmEdA matrix formulation analogous to (2.24) if external input power is supplied to the first cavity, will be given by

$$\begin{pmatrix} \boldsymbol{\beta_{11}} & -\boldsymbol{\beta_{12}} & \mathbf{0} \\ -\boldsymbol{\beta_{12}}^{\top} & \boldsymbol{\beta'_{22}} & -\boldsymbol{\beta_{23}} \\ \mathbf{0} & -\boldsymbol{\beta_{23}}^{\top} & \boldsymbol{\beta_{33}} \end{pmatrix} \begin{pmatrix} \boldsymbol{E_1} \\ \boldsymbol{E_2} \\ \boldsymbol{E_3} \end{pmatrix} = \begin{pmatrix} \boldsymbol{\Pi_1} \\ \mathbf{0} \\ \mathbf{0} \end{pmatrix}, \tag{6.1}$$

with $\boldsymbol{E_1}$, $\boldsymbol{E_2}$ and $\boldsymbol{E_3}$ respectively standing for the modal energy vectors of the first cavity, panel and second cavity.

Two remarks should be made with regard to (6.1). First, the diagonal matrix $\boldsymbol{\beta'_{22}}$ is different from $\boldsymbol{\beta_{22}}$ in (2.24) because it incorporates the coupling with subsystem 3. Its expression becomes

$$\boldsymbol{\beta'_{22}} = \mathrm{d}iag\left(\omega_q \eta_q + \sum_{p\in\hat{P}} \beta_{pq} + \sum_{r\in\hat{R}} \beta_{qr}\right)_{N_Q \times N_Q}. \tag{6.2}$$

Second, the null blocks $\mathbf{0}$ in (6.1) indicate that there is no direct coupling between the resonant modes of both cavities, given that they are not physically connected. However, it is well known that resonant transmission, as described by the standard SmEdA approach (6.1), cannot correctly represent the whole acoustic transmission through the panel below the critical frequency, which is governed by the mass law. To tackle with this problem it was proposed in [Maxit et al., 2014] to include the panel non-resonant modes in the analysis. Although the frequencies of these non-resonant panel modes do not coincide with those of the cavity resonant modes, the modes are strongly coupled one to another because of spatial matching. If one incorporates non-resonant transmission in the DMF equations, it turns out that after matrix condensation the former can be accounted for by establishing a direct coupling between the modes of both cavities (even though not being physically connected). The coupling factors β_{pr}

between modes in $\hat{P}$ and $\hat{R}$ are characterized by spring connections rather than gyroscopic ones. The stiffness of the spring connection can be related to the intermodal works between the resonant cavity modes and the non-resonant panel modes (see [Maxit et al., 2014] for details).

As a consequence, when non-resonant paths are considered (6.1) transforms to

$$\begin{pmatrix} \boldsymbol{\beta''_{11}} & -\boldsymbol{\beta_{12}} & -\boldsymbol{\beta_{13}} \\ -\boldsymbol{\beta_{12}}^{\top} & \boldsymbol{\beta'_{22}} & -\boldsymbol{\beta_{23}} \\ -\boldsymbol{\beta_{13}}^{\top} & -\boldsymbol{\beta_{23}}^{\top} & \boldsymbol{\beta''_{33}} \end{pmatrix} \begin{pmatrix} \boldsymbol{E_1} \\ \boldsymbol{E_2} \\ \boldsymbol{E_3} \end{pmatrix} = \begin{pmatrix} \boldsymbol{\Pi_1} \\ \mathbf{0} \\ \mathbf{0} \end{pmatrix}, \tag{6.3}$$

where the block $\boldsymbol{\beta_{13}} = \left(\beta_{pr}\right)_{N_P \times N_R}$ is no longer zero. Note that the matrices $\boldsymbol{\beta''_{11}}$ and $\boldsymbol{\beta''_{33}}$ differ from $\boldsymbol{\beta_{11}}$ and $\boldsymbol{\beta_{33}}$ in (6.3) because they include the terms corresponding to the direct connections between cavities, characterized by $\boldsymbol{\beta_{13}}$. Numerical validations on test cases [Maxit et al., 2014] had shown the ability of this SmEdA approach to describe the non-resonant transmission through the panel, and in particular, the mass law behaviour. However, determining which cavity and panel modes play a relevant role in the transmission through spatial matching may be rather lengthy and intricate. A fast way to do so by resorting to graph theory will be presented for the cavity-panel-cavity system in Section 6.4.

6.3 MODAL ENERGY TRANSMISSION PATHS AND SMEDA GRAPHS

6.3.1 *Modal energy transmission paths in SmEdA*

The definition of energy transmission paths between subsystems in SEA models has been introduced in Chapter 2. As quoted in [Guasch, 2011], the notion of transmission paths between two adjacent subsystems relies on the concept of blocked transmissibility [Guasch, 2009; Guasch and Magrans, 2004; Magrans, 1981]; the energy transmitted from an arbitrary subsystem i to a neighboring subsystem j is given by the quotient of energies E_j/E_i when i is excited and all energies in the SEA model but i and j are set to zero. This results in $E_j/E_i = \eta_{ij}/\eta_j$, η_{ij} standing for the SEA coupling loss factor between i and j, and η_j for the total loss factor of subsystem j. Therefore η_{ij}/η_j can be interpreted as the fraction of energy at j that directly comes from i, and thus identified with the weight of a first order transmission path connecting subsystems i and j i.e., $w(p^1_{ij}) = \eta_{ij}/\eta_j$. A second order path p^2_{st} linking e.g., subsystem s with t through a third subsystem j could be built concatenating the first order paths p^1_{sj} and p^1_{jt}, with weight $w(p^2_{st}) = (\eta_{sj}/\eta_j)(\eta_{jt}/\eta_t)$. Following this procedure arbitrary n-order paths linking $n+1$ subsystems can be built having weights $w(p^n_{st}) = \Pi^{n-1}_{h_i=1}(\eta_{h_i h_{i+1}}/\eta_{h_i})$ (s being identified with h_1 and t with h_{n-1}).The same line of reasoning can be pursued to define energy transmission in SmEdA, from an arbitrary mode p in a subsystem P to a mode q in subsystem Q. The

weight of the first order order transmission path, p^1_{pq}, from mode $p \in \hat{P}$ to $q \in \hat{Q}$, in the case of subsystems P and Q being adjacent, will be given by

$$w(p^1_{pq}) = \frac{\beta_{pq}}{\beta_q}. \tag{6.4}$$

A general n-th order path between a mode $s \in \hat{S}$ and a mode $t \in \hat{T}$ in the SmEdA system can then be built by concatenation as

$$w(p^n_{st}) = \frac{\beta_{sh_1}}{\beta_{h_1}} \frac{\beta_{h_1h_2}}{\beta_{h_2}} \cdots \frac{\beta_{h_{n-1}t}}{\beta_t}. \tag{6.5}$$

Note from the considerations in Section 2.4 that (6.5) makes sense given that $\beta_{h_ih_{i+1}} \geq 0$ and $\beta_{h_i} > 0$, $\forall\ h_i \in \hat{P}$, $h_{i+1} \in \hat{Q}$. Note also that, as specified, no transmission is allowed from a mode in one subsystem to another mode in the same subsystem. However, a path going from one mode, say $p_1 \in \hat{P}$ to $q \in \hat{Q}$ and then back to $p_2 \in \hat{P}$, or even $p_1 \in \hat{P}$, is perfectly feasible.

A transmission path, as defined in (6.5), allows one to know the energy that has been transmitted from a particular source mode, where the external energy is input, to a target mode in a different subsystem, involving a particular set of intermediate modes. As it will be shown in Section 6.4, the fast and efficient computation of such paths will prove very useful to determine which modes play a significant role in resonant and non-resonant transmission in SmEdA models. However, it should be remarked that in order for transmission path analysis to be a well-posed problem from a mathematical and physical point of view, an additional condition has to be satisfied. It has to be possible to recover the overall energy at any target mode as the summation of the energy contributions of all transmission paths linking the source mode with the target one (see Section 2.5 and [Guasch and Aragonès, 2011] for a detailed explanation in the case of SEA). Assuming fulfillment of that condition, a transmission path analysis makes sense from a practical point of view whenever the energy transmission is justified by a small set of dominant paths, so that one could act on their constituent modes/subsystems for remedial action.

Let us next see that transmission path analysis in SmEdA is in fact a well-posed problem. Define the matrix $\boldsymbol{B} := \boldsymbol{I} - \mathrm{d}iag(1/\beta_{ii})\boldsymbol{\beta}$ whose diagonal is null and its off-diagonal entries non-negative. This matrix is also irreducible, i.e. it cannot be made similar to a block upper triangular matrix via a permutation. This amounts to saying that the adjacency matrix associated to $\boldsymbol{B}$ is that of a strongly connected directed graph (this is actually the case, see next section). Next one can make use of the Perron-Frobenius theorem (see e.g., [Varga, 1962]) and easily show that the spectral radius of $\boldsymbol{B}$, $\rho(\boldsymbol{B}) < 1$. As a consequence $\boldsymbol{B}$ is convergent, i.e., the series of matrices $\boldsymbol{B}^m$, $m = 0, 1, 2 \ldots$, converge to the null matrix. Defining $\boldsymbol{\Pi'} = \mathrm{d}iag\,(1/\beta_{ii})\,\boldsymbol{\Pi}$ permits rewriting (2.26) as

$$(\boldsymbol{I} - \boldsymbol{B})\boldsymbol{E} = \boldsymbol{\Pi'} \tag{6.6}$$

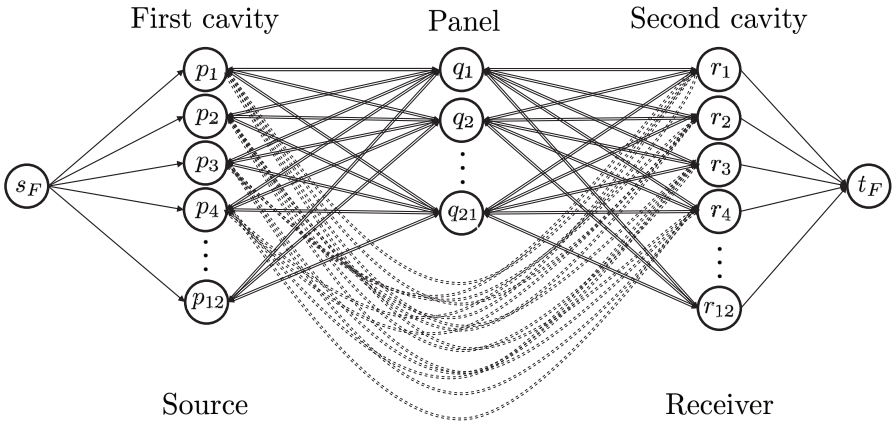

Figure 6.2: SmEdA graph corresponding to the cavity-panel-cavity model in Fig. 6.1

so that

$$\boldsymbol{E} = (\boldsymbol{I} - \boldsymbol{B})^{-1} \boldsymbol{\Pi}' = \left(\sum_{n=0}^{\infty} \boldsymbol{B}^n \right) \boldsymbol{\Pi}'. \tag{6.7}$$

This proves that the energy at any mode can effectively be recovered as the infinite summation of the energy contributions of the transmission paths linking the SmEdA system source modes with the target ones. The entries in $\boldsymbol{B}^\top$ correspond to the energy contribution of the first order paths between pairs of modes; note that $B_{pq} = \beta_{pq}/\beta_p$, $p \neq q$, which according to (6.4) corresponds to a path from q to p (v. $\beta_{pq} = \beta_{qp}$). Thus B_{qp} will be the entry for a path from p to q. In the same way, the transposed of $\boldsymbol{B}^n$ includes the total contribution of the n-th order paths linking modes in the SmEdA system. As the paths get longer their contribution decreases because as said $n \to \infty \Rightarrow \boldsymbol{B}^n \to \boldsymbol{0}$. As stated in Chapter 2, a series like (6.7) was first proposed for SEA systems in [Magrans, 1993], see also [Craik, 1996; Guasch and Cortés, 2009; Magrans, 1993; Tanner, 2009]. As will be shown next, (6.7) constitutes the key to link SmEdA with graph theory.

6.3.2 *The SmEdA graph*

Succinctly, a graph $G = (U, E)$ consists of two sets of elements, U being the set of nodes and E the set of arcs, or edges, connecting the nodes. The arcs in E can be assigned numerical values which can be gathered in the so called weighting matrix of the graph (see Section 2.6,[Carré, B.A., 1979]). A SmEdA graph can be built by defining all subsystem modes as the nodes of the graph and identifying the arcs with the first order paths connecting them. The arcs are then assigned the weights of these first order paths. Note that this would come down to identifying the transpose of the generating matrix in (6.5), $\boldsymbol{B}^\top$, as the weighting matrix of a strongly connected directed SmEdA graph, analogously to what is done in SEA (see Section 2.7 and [Guasch and Aragonès, 2011; Guasch and Cortés, 2009]). The graph is strongly connected because for any two arbitrary nodes in the graph there always exists a path connecting them.

For the correct definition of a SmEdA graph an additional subtle point has to be considered. In practice it is not possible to excite a particular mode of a given subsystem; standard mechanisms excite the whole subsystem at once. Moreover, one is usually interested in knowing the influence of a given transmission path to the whole target subsystem energy, not to one of its modes. To take into account these two facts, the SmEdA graph has to be enlarged with two fictitious nodes (not corresponding to system modes), one connected to the source subsystem modes, and the other one to the target subsystem modes. With regard to the former, one of the advantages of SmEdA is precisely that it can deal with both, localized and rain on the roof excitations. Let us denote the source subsystem as P with modes $p \in \hat{P}$. A fictitious source node s_F will be included in the graph with one-direction connections to every $p \in \hat{P}$. The weights of these connections will depend on the excitation being point-like or distributed. The power balance equation for a mode in the source subsystem P, when setting all remaining SmEdA system modal energies to zero, provides

$$\Pi_{inj}^{p} = \beta_p E_p. \tag{6.8}$$

In the case of a rain on the roof excitation Π_{inj}^{p} will be constant for all $p \in \hat{P}$. As opposes to this, in the case e.g. of a monopole source term, $\Pi_{inj}^{p} \approx (\pi/4)\bar{S}_{Q_p}$, with $\bar{S}_{Q_p}$ standing for the power spectral density of the monopole, as stated in (2.22). The following weights will be thus assigned to the edges linking s_F to every $p \in \hat{P}$,

$$w_{s_F p} = \frac{\Pi_{inj}^{p}}{\beta_p}. \tag{6.9}$$

With regard to the target or receiver subsystem, say R, another fictitious node t_F is included in the graph. All modes $r \in \hat{R}$ become connected to it through arcs with unitary weights $w_{rt_F} = 1$. The energy at the target subsystem can be recovered from the summation of the energy of all its modes, $E_T = \sum_{r \in \hat{R}} E_t$.

To summarize, a SmEdA graph will consist of $(N + 2)$ nodes, where N is the total number of the SmEdA system modes. The two additional nodes are a fictitious source node s_F, which is connected to all the modes in the source subsystem with the weight in (6.9), and a fictitious target node to which all target subsystem modes become connected with unit weight. As an example of SmEdA graph, in Fig. 6.2 that corresponding to the cavity-panel-cavity example in Section 6.2 is presented, which will also be referred to in the forthcoming Section 6.4 (see also Fig. 6.1). The arcs plotted in solid lines correspond to resonant first order paths while the dashed line arcs correspond to non-resonant first order paths. The source is placed in the first cavity and the second cavity corresponds to the target subsystem. Therefore, the node s_F is connected to all nodes in the first cavity, whereas all nodes in the second cavity become connected to t_F.

Once a SmEdA graph has been generated, use can be made of previously developed algorithms in graph theory for the computation of transmission paths

linking the source and the target subsystems. In particular, it suffices to apply the adaptation of the MPS algorithm [Martins, 1984; Martins et al., 1999] to SEA that has been done in Chapter 3, to compute a list of dominant transmission paths in SmEdA systems. With a brief post-process, it will be also possible to automatically identify the modes more often appearing in the dominant paths. This will considerably facilitate the cumbersome task of detecting those modes regulating the energy transmission between subsystems.

6.4 APPLICATION TO CAVITY-PANEL-CAVITY MODELS

In this section, the above developments will be applied to cavity-panel-cavity models. Most conclusions in [Maxit et al., 2014] with regard to modal energy transmission between cavities will be validated, but now following a totally different and faster approach. The models under analysis consist of two cavities separated apart by a panel, as shown in Fig. 6.1. It will be assumed that energy transmission only takes place through the dividing panel, the remaining cavity walls being totally rigid. In a first example a homogeneous panel will be considered. This comprises of a steel plate with dimensions 0.8 m $\times$ 0.6 m $\times$ 0.001 m, mass density $\rho = 7800$ kg/m^3, Young modulus E $= 2 \times 10^{11}$ Pa and damping loss factor $\eta = 0.01$. The panel is supposed to be simply-supported on its four edges. In the second example, the steel plate will be stiffened with the addition of some ribs, as detailed in Section 6.4.2.

The dimensions of the source cavity C1, are 0.8 m $\times$ 0.6 m $\times$ 0.8 m, and those of the receiver cavity C2, 0.8 m $\times$ 0.6 m $\times$ 0.7 m. The cavities are filled with air (mass density $\rho_0 = 1.29$ kg/m^3, speed of sound $c_0 = 340$ m/s and damping loss factors $\eta_{C1} = \eta_{C2} = 0.01$). $C1$ will be excited with a monopole source of unit strength located at the point $(0.24, 0.42, 0.54)$ m, according to the coordinate system $[O; x, y, z]$ in Fig. 6.1. In forthcoming explanations, the particular i-th mode belonging to the source cavity C1 will be referred to as $p_i \in \hat{P}$, the i-th mode belonging to the plate as $q_i \in \hat{Q}$ and the i-th mode in the receiver cavity C2 as $r_i \in \hat{R}$. For both examples, the most dominant modal energy transmission paths have been computed for the one third octave bands ranging from 400 Hz to 4000 Hz central frequencies. Tables 6.1 and 6.2 show respectively the computation times for both cases in a regular computer (Intel Core 2 Quad CPU q9400 @2.66 GHz).

6.4.1 *Cavity – bare plate – cavity*

In this case, the subsystem modal information required in SmEdA can be calculated analytically for both, the natural frequencies and the interaction modal works (i.e. integral of the product between the pressure cavity modes and the displacement panel modes). In Table 6.3, a first overview on how modal energy transmission takes place for every analyzed 1/3 octave band is presented (first column in the table). The results are built from the outputs of the the

Band [Hz]	Tree of max. paths	Sorted Forward Star Form	MPS Algorithm	Post-processing functions	Total
400	5.5×10^{-3} s	3.4×10^{-4} s	0.71 s	0.19 s	0.91 s
500	6.1×10^{-3} s	2.7×10^{-4} s	0.66 s	0.17 s	0.83 s
630	8.8×10^{-3} s	4.02×10^{-4} s	0.64 s	0.15 s	0.81 s
800	11.6×10^{-3} s	5.62×10^{-4} s	0.71 s	0.13 s	0.85 s
1000	15.5×10^{-3} s	8.62×10^{-4} s	1.78 s	0.28 s	2.07 s
1250	31×10^{-3} s	1.9×10^{-3} s	7.07 s	0.70 s	7.80 s
1600	61.5×10^{-3} s	49.1×10^{-3} s	25.43 s	1.51 s	27.05 s
2000	0.13 s	0.02 s	26.51 s	1.42 s	28.09 s
2500	0.40 s	0.08 s	101.59 s	3.31 s	105.38 s
3150	1.27 s	0.33 s	605.86 s	12.11 s	619.57 s
4000	4.46 s	1.22 s	2774.52 s	43.12 s	2823.32 s

Table 6.1: *Computation times of the bare plate example in Section 6.4.1*

Band [Hz]	Tree of max. paths	Sorted Forward Star Form	MPS Algorithm	Post-processing functions	Total
400	47.6×10^{-3} s	0.03 s	1.16 s	0.43 s	1.67 s
500	7.4×10^{-3} s	2.6×10^{-3} s	0.92 s	0.18 s	1.11 s
630	9.2×10^{-3} s	6.31×10^{-4} s	2.06 s	0.33 s	2.40 s
800	11.4×10^{-3} s	9.46×10^{-4} s	1.86 s	0.30 s	2.17 s
1000	27.2×10^{-3} s	8.6×10^{-3} s	3.49 s	0.45 s	3.97 s
1250	56.6×10^{-3} s	37×10^{-3} s	27.81 s	1.69 s	29.59 s
1600	0.10 s	35.2×10^{-3} s	106.31 s	4.54 s	111.00 s
2000	0.26 s	0.14 s	108.50 s	3.75 s	112.66 s
2500	0.92 s	0.42 s	621.28 s	13.12 s	635.75 s
3150	2.88 s	1.53 s	2651.29 s	38.17 s	2693.87 s
4000	70.44 s	8.03 s	3546.43 s	39.41 s	3664.31 s

Table 6.2: *Computation times of the ribbed plate example in Section 6.4.2*

MPS algorithm as implemented in Chapter 3. The second column in the table contains the overall energy at the receiver cavity C2. The third one indicates the total number of paths that have been computed for each band and the fourth and fifth columns show the contributions of the computed paths, respectively in percentage and decibels, to the energy at C2. Next, the type of paths that participate in the energy transmission from C1 to C2 are indicated (tri-block sixth column). The acronym PNR stands for purely non-resonant paths, herein identified with paths that only involve the bare plate non-resonant modes, whereas PR stands for purely resonant paths, i.e. paths only involving the plate resonant modes. M denotes mixed transmission paths that contain both, resonant and non-resonant plate modes. The contributions in percentage and decibels of the various types of paths is exposed in the tri-block columns seven and eight.

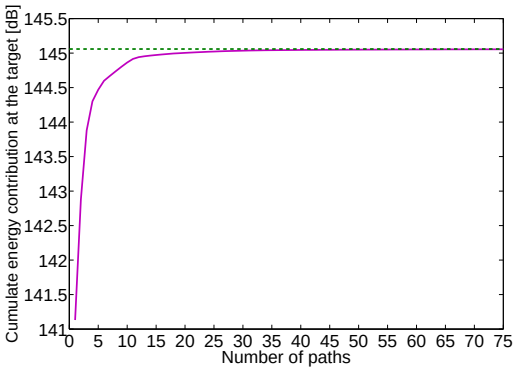

Figure 6.3: Cumulative path energy contribution at the receiver cavity C2 versus number of considered dominant paths, for the cavity - bare plate - cavity example at 630 Hz. Continuous purple line: cumulative energy contribution, dashed green line: total energy at the receiver C2.

As observed in the table, though the number of resonant paths is large and for several bands surpass that of non-resonant paths, their contribution to the energy level at C2 becomes negligible when compared to the non-resonant one, as one would expect for the behaviour of a homogeneous plate well below the critical frequency f_c ($f_c \sim 11$ kHz in the present example). Let us next focus, for the ease of exposition, on the results of the 630 Hz one-third octave band. There are 12 resonant modes for the source cavity C1 and for the receiver cavity C2 in this band. In what concerns the plate, it has 21 resonant modes and 75 non-resonant modes in the band. As explained, the latter do not result in extra nodes in the SmEdA graph but in additional edges directly connecting the modes of the two cavities. The SmEdA graph for the problem at hand will thus contain 47 nodes, 45 arising from all resonant modes in the system, plus two nodes corresponding to the fictitious source and target nodes (see Fig. 6.2).

In Fig. 6.3, the cumulative contribution of the first 75 paths has been plotted. The dashed line represents the total energy at the receiver cavity which has a value of 145.06 dB ref. 10^{-12} J, whereas the purple solid line corresponds to the cumulative energy contribution when increasing the number of considered paths. It can readily be checked, for instance, that the first 5 paths had an overall contribution of 144.47 dB whereas the first 75 paths supply 145.05 dB of energy (99.9% of the overall energy at the target). At this point, it should be remarked that for practical applications in vibroacoustic problems differences of less than 1 dB become almost negligible (this constitutes in fact an eligible criteria to make a decision on the number of paths to be computed for each graph). Therefore, it can be observed that with the sole contribution of the five most dominant transmission paths it becomes possible to justify the whole transmission of energy from C1 to C2.

More insight can be gained by having a look at the results in Table 6.4. Its first column contains the number of transmission paths taken into account in the analysis, their cumulative energy contribution to the target subsystems in dB

Band [Hz]	Cavity C2 Energy	Number of Paths	Accum. Contr. [%]	Accum. Contr. [dB]	Type of paths [%]			Accum. Contr. [%]			Accum. Contr. [dB]		
					PNR	PR	M	PNR	PR	M	PNR	PR	M
400	148.06	100	100.00	148.06	16.00	33.00	51.00	93.96	5.31	0.73	147.79	135.32	126.69
500	136.57	100	100.00	136.57	10.00	50.00	40.00	80.16	18.89	0.96	135.61	129.33	116.37
630	145.06	100	99.95	145.06	29.00	69.00	2.00	95.91	4.02	0.02	144.88	131.11	107.39
800	143.72	100	99.38	143.69	41.00	57.00	2.00	84.57	14.76	0.05	142.99	135.41	110.86
1000	142.08	200	98.69	142.02	39.50	60.50	0.00	87.57	11.12	0.00	141.50	132.54	$-\infty$
1250	141.90	500	98.57	141.84	39.00	60.20	0.80	86.15	12.40	0.02	141.25	132.83	105.14
1600	140.87	1000	97.79	140.77	39.90	60.10	0.00	91.41	6.38	0.00	140.48	128.92	$-\infty$
2000	140.87	1000	95.83	140.68	65.10	34.90	0.00	92.56	3.26	0.00	140.53	126.00	$-\infty$
2500	140.33	2000	93.72	140.04	69.75	30.25	0.00	90.02	3.69	0.00	139.87	126.00	$-\infty$
3150	140.21	5000	93.10	139.90	67.10	32.90	0.00	89.97	3.13	0.00	139.75	125.16	$-\infty$
4000	139.29	10000	91.39	138.90	71.58	28.42	0.00	88.76	2.64	0.00	138.77	123.50	$-\infty$

Table 6.3: *Cavity - bare plate - cavity example. Contributions of resonant, non-resonant and mixed transmission paths for the considered 1/3 octave frequency bands.*

Number of paths	Accumulated contribution [dB]	Accumulated contribution [%]	$\hat{P}$	$\hat{Q}^R$	$\hat{R}$	Total involved modes	Missing modes
∞	145.06	100.00	12	21	12	45	0
75	145.05	99.91	12	14	12	38	7
25	145.02	99.16	12	5	10	27	18
10	144.86	95.59	7	1	7	15	30
8	144.73	92.82	7	0	7	14	31

Table 6.4: *Cavity - bare plate - cavity example. Transmission path analysis and involved modes for the* 630 *Hz* 1/3 *octave band.*

and percentage respectively being presented in columns two and three. The next three columns include the number of resonant modes of each subsystem (C1, panel and C2) that are involved in the corresponding paths of the first column, followed by the total summation of resonant modes in column number seven. Finally, the last column of the table indicates the difference between the total number of modes in the system and the number of modes appearing in the paths of the first column.

With regard to the row information in the table, the first row is a reference containing all data involved in the exact transmission process from source to target. The second row shows the results when considering 75 dominant paths, which justify, as said, 99.9% of the energy at the receiver cavity. 38 modes from the 45 modes of the complete problem still play a role in the energy transmission process. However, by simply considering 25 paths, the accumulated contribution is 99.16%, which leads to a negligible difference in terms of decibels compared

to the reference (less than 0.04 dB) and only 27 modes become involved in the transmission. Focusing on the 8 most dominant paths, it can be observed that the difference in dB is still insignificant (less than 1 dB) and that only 14 modes are of importance. There is also a very important point to note in this case. As opposed to the preceding ones, it can be appreciated that no plate resonant mode intervenes. In other words, the energy transmission between the two cavities at the 630 one-third octave band is mainly non-resonant, as already noticed from the analysis of the results in Table 6.3. The proposed graph approach not only allows one to corroborate this well-known point, but to determine which are the most important non-resonant modes dominating the transmission. In Table 6.5, the ranking of the 10 stronger dominant paths has been listed. Non-resonant paths can be easily identified as they do not contain any q_i element. As seen in the table, the first eight transmission paths are completely non-resonant, being the ninth path the first one to include a q_i mode (in particular q_{21}).

Path	Cavity – Homogenous plate – cavity
1	$S \to p_6 \to r_7 \to T$
2	$S \to p_{10} \to r_{10} \to T$
3	$S \to p_{12} \to r_{11} \to T$
4	$S \to p_1 \to r_3 \to T$
5	$S \to p_4 \to r_5 \to T$
6	$S \to p_3 \to r_6 \to T$
7	$S \to p_6 \to r_{10} \to T$
8	$S \to p_7 \to r_9 \to T$
9	$S \to p_{12} \to q_{21} \to r_{11} \to T$
10	$S \to p_{10} \to r_7 \to T$

Table 6.5: *Cavity - bare plate - cavity example. Ranking of the* 10 *most dominant modal energy paths from a total of* 75 *computed paths for the* 630 *Hz* 1/3 *octave band*

It should be remarked that obtaining the type of information in Tables 6.3, 6.4 and 6.5 is a straightforward task from the output of the MPS algorithm. As opposed to this, trying to get this kind of information directly from the analysis of the whole SmEdA system is a rather intricate and lengthy task that involves several simplifying hypotheses [Maxit et al., 2014]. This can be realized when trying to determine the first two or three dominant paths in the SmEdA model following the procedure in [Maxit et al., 2014]. To do so, the SmEdA model has to be first simplified assuming weak coupling and taking advantage of the fact that the three subsystems are connected in series. Then, it may be expected that the modal energies of the excited subsystem $C1$ will be much higher than those of the homogeneous plate, which in turn will be higher than those in the receiving cavity $C2$. The simplified SmEdA model relates the modal energies of $C2$ with the modal injected powers through non-resonant and resonant paths, by means of equations (51) and (52) in [Maxit et al., 2014], respectively. Inspecting

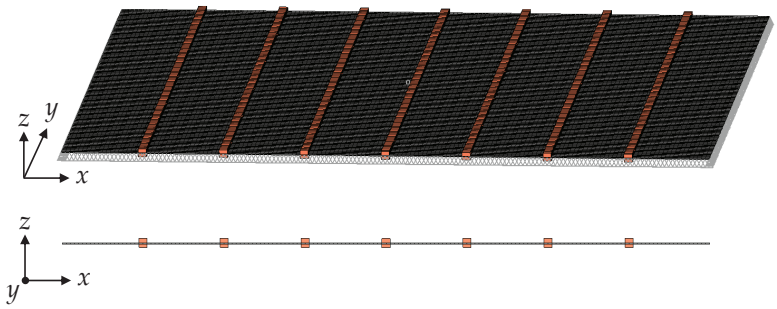

Figure 6.4: Ribbed plate finite element model

the values of the analytical factors relating these quantities, it becomes possible to determine the two or three most dominant paths, which coincide with those in the ranking of Table 6.5. Therefore, one can resort to the procedure in [Maxit et al., 2014] to validate the first paths resulting from the application of the MPS algorithm, but it should be emphasized that by no means is it possible to apply that procedure to generate an automatic list of dominant paths. Moreover, the approach in [Maxit et al., 2014] only works under some restrictive assumptions which may not be valid in the case of complex SmEdA models. As seen, such difficulties can be overcome by resorting to the MPS algorithm.

6.4.2 *Cavity – ribbed plate – cavity*

In this second example the homogeneous bare plate becomes stiffened with some ribs. The ribs are regularly placed 100 mm apart parallel to the plate y-axis and have a cross section of 10 mm $\times$ 10 mm, see Fig. 6.4. It is well-known that the acoustic transmission of a ribbed plate differs from that of a bare plate because its stiffness becomes increased in the rib direction. As a first approximation for low frequencies, the ribbed plate may be considered equivalent to an orthotropic plate. Whereas the bare plate has a single critical frequency ($\sim$ 11 kHz in the previous example), an orthotropic plate is characterized by having two critical frequencies. The lowest one is that corresponding to the coincidence of waves traveling in the plate stiffest direction (rib direction) with acoustic waves. In our case, this first critical frequency occurs at $\sim$ 1.7 kHz (the second being that of the bare plate at $\sim$ 11 kHz). Therefore and contrary to the bare plate, for which resonant plate modes are only in spatial coincidence with the acoustic modes beyond 11 kHz, the stiffened plate may have some resonant modes in spatial coincidence with the acoustic ones for frequencies well below 11 kHz. One would then expect the resonant paths to play a more important role in the acoustic transmission than the one they played for the bare plate. It is however difficult to make an a priori estimation of the importance of the resonant paths compared to the non-resonant ones. As it will be shown below the graph theory approach can substantially ease this task.

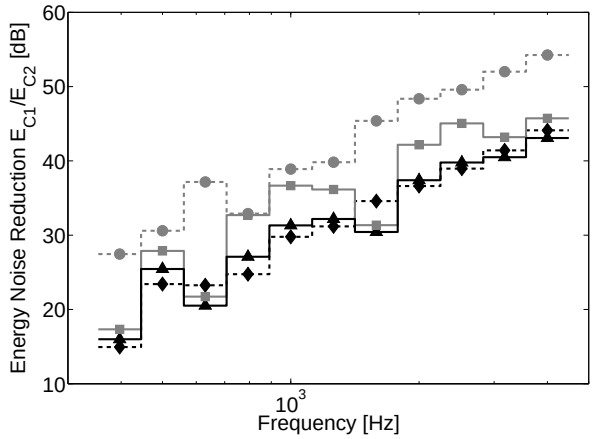

Figure 6.5: Energy noise reduction between the two cavities. - -●- - (grey) bare plate with only resonant transmission, - -◆- - (black) bare plate with resonant and non-resonant transmission, —■— (grey) ribbed plate with only resonant transmission —▲— (black) ribbed plate with resonant and non-resonant transmission.

In order to build the SmEdA matrix for this case, the subsystem modes of the ribbed plate have been calculated with FEM. The plate has been modelled with 19200 quadrilateral shell elements while 900 one-dimensional beam elements have been used for the ribs (see Fig. 6.4). Uncoupled extensional (in-plane) and bending (out-plane) motions have been considered for the thin plate whereas bending, extensional and torsional motions have been taken into account for the beam-like stiffeners. Based on the classical FEM sampling criterion of using six elements per wavelength in the generated mesh, the results are expected to be valid up to 10 kHz. The normal modes have been computed using the SDTools code [Balmes et al., 2011]. Besides, the cavity modes have been calculated analytically as in the cavity-bare plate-cavity example of the preceding subsection.

As expected, the energy transmission no longer presents two distinct ranges of behaviour like for the bare plate. This can be first observed in Table 6.6, built again from the outputs of the MPS algorithm, which is the analogous to Table 6.3 but for the ribbed case. As seen, it is no longer true that the contribution to the energy level at C2 becomes dominated by non-resonant paths, the resonant ones playing a determinant role for several $1/3$ octave bands. More graphically, this can be appreciated when analyzing the energy noise reduction (ENR) between cavities [Maxit et al., 2014]. The ENR is defined as $ENR = 10\log_{10}(E_{C1}/E_{C2})$, with E_{C1} and E_{C2} respectively standing for the time averaged total energies at cavities C1 and C2 respectively. In Fig. 6.5 the ENR has been plotted in one-third octave bands for both, the bare plate of the previous example (dashed lines) and the ribbed one (solid lines). For each case two ENRs have been considered, the first one only considers resonant modes in the transmission (grey lines) whereas the second one takes into account resonant and non-resonant transmission as well (black lines).

Band [Hz]	Cavity C2 Energy	Number of Paths	Accum. Contr. [%]	Accum. Contr. [dB]	Type of paths [%]			Accum. Contr. [%]			Accum. Contr. [dB]		
					PNR	PR	M	PNR	PR	M	PNR	PR	M
400	146.84	100	99.84	146.83	7.00	68.00	25.00	25.83	73.28	0.73	140.96	145.49	125.45
500	133.89	100	99.93	133.89	6.00	75.00	19.00	42.60	56.89	0.44	130.19	131.44	110.37
630	147.46	200	99.65	147.44	11.50	83.50	5.00	24.36	75.24	0.05	141.33	146.22	114.63
800	141.37	200	99.49	141.36	23.00	75.50	1.50	72.43	27.04	0.03	139.97	135.69	105.93
1000	140.53	300	99.48	140.51	27.00	72.00	1.00	70.77	28.69	0.02	139.03	135.11	104.14
1250	140.88	1000	98.79	140.83	17.70	82.10	0.20	59.76	39.03	0.01	138.64	136.79	98.38
1600	144.98	2000	98.55	144.91	16.00	83.55	0.45	18.92	79.62	0.02	137.74	143.99	107.25
2000	140.07	2000	94.89	139.84	33.35	66.65	0.00	66.07	28.82	0.00	138.27	134.67	$-\infty$
2500	139.50	5000	92.79	139.17	35.08	64.92	0.00	69.51	23.29	0.00	137.92	133.17	$-\infty$
3150	141.12	10000	82.84	140.30	27.56	72.44	0.00	44.81	38.03	0.00	137.63	136.92	$-\infty$
4000	140.32	10000	78.70	139.28	42.98	57.02	0.00	42.66	36.05	0.00	136.62	135.89	$-\infty$

Table 6.6: *Cavity - ribbed plate - cavity example. Contributions of resonant, non-resonant and mixed transmission paths for the considered 1/3 octave frequency bands.*

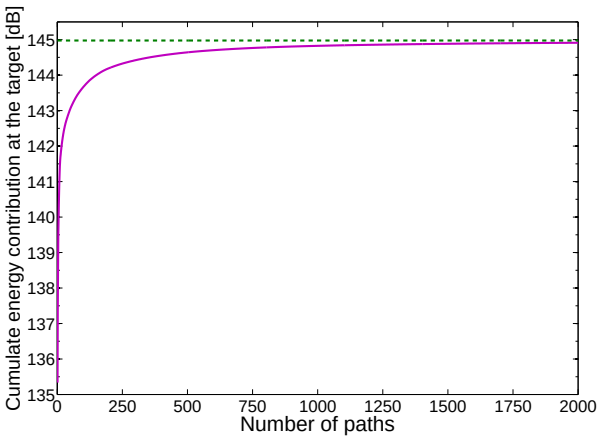

Figure 6.6: Cumulative path energy contribution at the receiver cavity C2 versus number of considered dominant paths, for the cavity - ribbed plate - cavity example for the 1600 Hz 1/3 octave band. Continuous purple line: cumulative energy contribution, Dashed green line: total energy at the receiver C2.

Given that the maximum frequency limit in the figure is 4KHz, which is well below the critical frequency of the bare plate, the resonant transmission ENR (dashed grey line) is clearer higher than the resonant plus non-resonant ENR (dashed black line) because, as explained in Section 6.4.1 (see Table 6.3), transmission is mainly dominated by non-resonant modes at this frequency range. However, when comparing the ENRs for the ribbed plate, there is no clear dominance from one type of transmission or another. Besides, note from Fig. 6.5 that the ENR of the ribbed plate considering all type of paths is generally higher than that of the bare plate, except for the 630 Hz and 1600 Hz bands. At these frequencies, the transmission seems to be mainly resonant for the ribbed plate,

since the grey and black solid lines have really close values and there are two dips in the ENR curves. This is confirmed by the results in Table 6.6.

If the transmission is mostly resonant, one could suspect that there is a group of modes of the cavities and the plate which exhibit spatial and frequency coincidences, i.e. a group involving a path of the type $p_i \rightarrow q_i \rightarrow r_i$. One could then be tempted to check from all possible combinations of three modes which of them present a high intermodal work W_{ij} (to account for the spatial matching) or which are closer in frequency (to account for the frequency matching), to try to determine which modes control the energy coupling. However, this is not a very good option because the effects of spatial and frequency coincidence are studied separately. To determine modal energy transmission it is better to focus the analysis on the modal coupling factors, see (2.23), which include the spatial and frequency coincidence effects at the same time. Inspecting the values of these factors between the excited cavity and the ribbed panel on the one side, and between the ribbed panel and the receiving cavity on the other side, it is possible to identify the most dominant paths between each pair of coupled subsystems. However, it still becomes very difficult to identify the most dominant paths when considering the coupling of all three subsystems together. For example, one plate mode could be strongly coupled with a mode of the excited cavity whereas poorly coupled with the modes of the receiving cavity. Such a mode could exchange much less energy than another one being moderately coupled with the modes of both cavities. The analysis of the modal coupling may be a lengthy and time consuming manual procedure which cannot fully guarantee that the inspected modes will be the ones dominating energy transmission. Alternatively, resorting to graph theory allows one to gather this type of information.

Path	Cavity – Ribbed plate – cavity
1	$S \rightarrow p_{49} \rightarrow q_{20} \rightarrow r_{49} \rightarrow T$
2	$S \rightarrow p_{7} \rightarrow q_{1} \rightarrow r_{13} \rightarrow T$
3	$S \rightarrow p_{14} \rightarrow q_{5} \rightarrow r_{12} \rightarrow T$
4	$S \rightarrow p_{82} \rightarrow q_{31} \rightarrow r_{72} \rightarrow T$
5	$S \rightarrow p_{82} \rightarrow q_{31} \rightarrow r_{55} \rightarrow T$
6	$S \rightarrow p_{78} \rightarrow q_{20} \rightarrow r_{49} \rightarrow T$
7	$S \rightarrow p_{49} \rightarrow q_{20} \rightarrow r_{30} \rightarrow T$
8	$S \rightarrow p_{141} \rightarrow q_{57} \rightarrow r_{129} \rightarrow T$
9	$S \rightarrow p_{82} \rightarrow q_{31} \rightarrow r_{81} \rightarrow T$
10	$S \rightarrow p_{33} \rightarrow q_{20} \rightarrow r_{49} \rightarrow T$

Table 6.7: *Cavity - ribbed plate - cavity example. Ranking of the* 10 *most dominant modal energy paths from a total of* 2000 *computed paths for the* 1600 *Hz* 1/3 *octave band.*

It is interesting to focus on the 1600 Hz frequency band for which resonant modes play a significant role. In Fig. 6.6 the cumulative energy contribution of

the first 2000 paths in this band is depicted. The total energy at the receiver cavity is 144.97 dB and the contribution e.g., of the first 250 paths already provides 144.32 dB, which is fairly close to the total value (less than 1 dB). Therefore, it becomes feasible to circumscribe the analysis to the ranking of the first 250 paths. For every mode, the number of appearances in the list of the 250 paths and the number of paths that contain it have been counted. The results are presented in Fig. 6.7. It can be observed that for every subsystem, there is a relatively small group of outstanding modes, whose maxima can respectively be identified as p_{49}, q_{20} and r_{49}. One may presume that these modes will play a predominant role in energy transmission. Actually, if one inspects the ranking of the 250 paths (see Table 6.7 for the first 10 paths), it precisely follows that the preeminent path is $p_{49} \rightarrow q_{20} \rightarrow r_{49}$ which contributes 135.36 dB to the energy at the receiver cavity. The natural frequencies of these modes are 1547 Hz for p_{49}, 1549 Hz for q_{20}, and 1565 Hz for r_{49}. These modes are relatively close in frequency but for the receiving cavity, other modes closer to q_{20} than r_{49} can be found. For example, r_{42} has a frequency of 1547 Hz. Thus, the matching in frequency cannot explain in itself why $p_{49} \rightarrow q_{20} \rightarrow r_{49}$ dominates.

It is worth examining this point in more detail. In Fig. 6.8 the spatial distribution (pressure for cavity modes and displacement for the ribbed plate) on

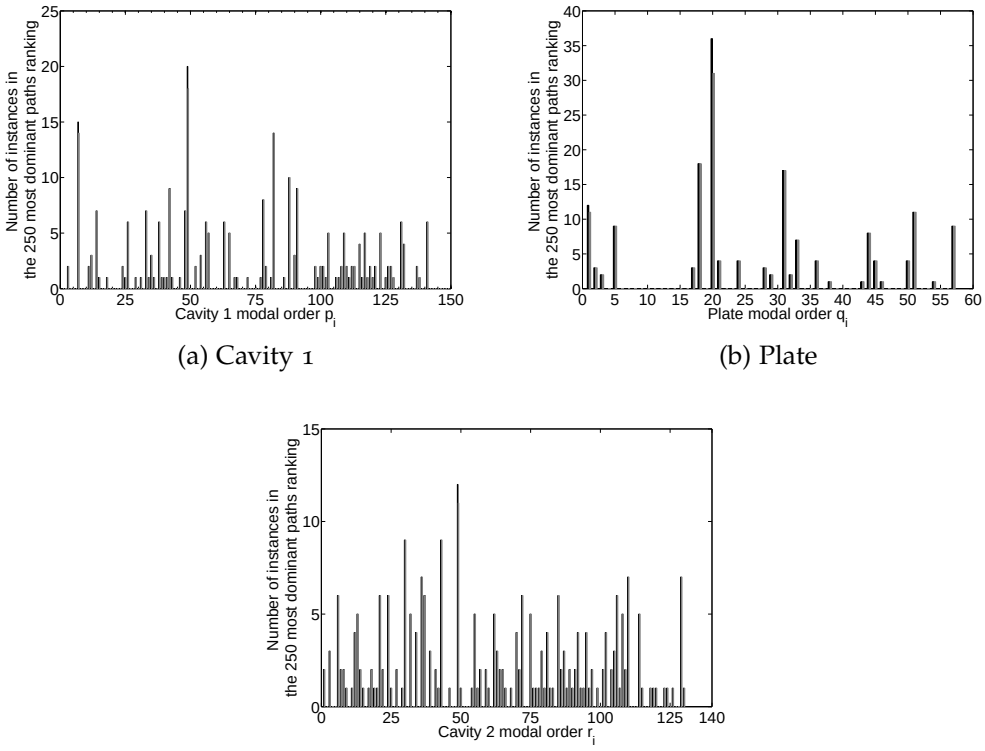

(a) Cavity 1

(b) Plate

(c) Cavity 2

Figure 6.7: Number of instances of every mode in the 250 most dominant paths ranking. Black columns: total number of instances in the path ranking. Grey columns: number of paths containing a particular mode.

the plate surface is plotted, for the three involved modes. Although the natural flexural wavelength of the plate is ~ 0.08 m at 1.5 kHz, a wavelength for mode q_{20} along the y-direction can be appreciated well above this value, which is comparable to the wavelengths of acoustic modes. This is due to the stiffness effect of the ribs and it leads to a spatial matching between this plate mode and the acoustic modes p_{49} and r_{49} in the the y-direction. The intermodal works between p_{49} and q_{20}, and q_{20} and r_{49} are, respectively, 66.7 J and 71.4 J and their modal coupling factors turn out to be 22.5 Hz and 12.8 Hz. The latter is lower than the former whereas the opposite happens for the intermodal works. This can be simply explained by the fact that p_{49} and q_{20} are closer in frequency than q_{20} and r_{49}. The spatial matching is here the key phenomenon which leads the path $p_{49} \rightarrow q_{20} \rightarrow r_{49}$ to be the most dominant one, as identified by the MPS algorithm.

In order to give the reader a point for comparison, an analysis is made of the interactions in the path $p_{34} \rightarrow q_{14} \rightarrow r_{33}$ which does not appear in the MPS ranking of the first 250 paths, though its modes have very close natural frequencies (1514.2 Hz, 1512.0 Hz, 1512.6 Hz, respectively). The pressure and displacement spatial patterns of those modes on the plate surface have

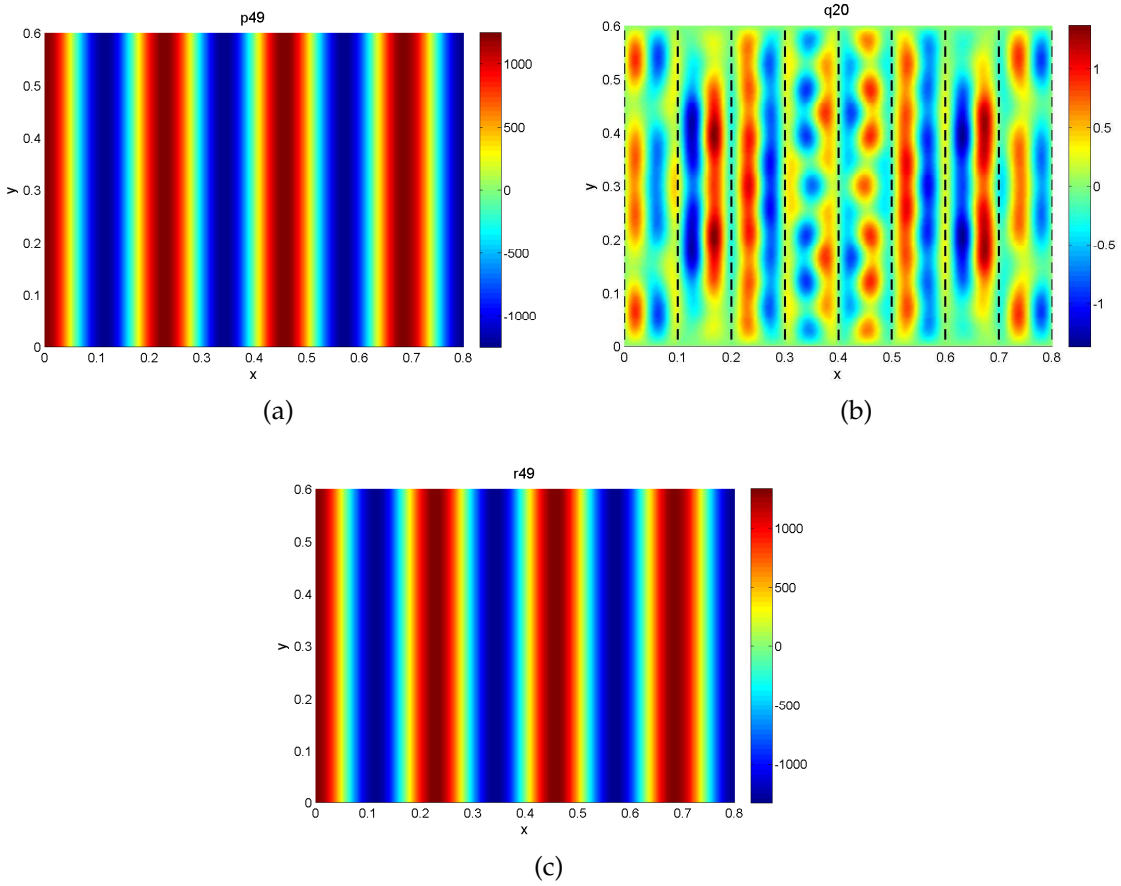

Figure 6.8: Magnitudes of the mode spatial shapes on the coupling surface: (a)p_{49}; (b) q_{20} (Vertical dashed line: rib positions); (c) r_{49}.

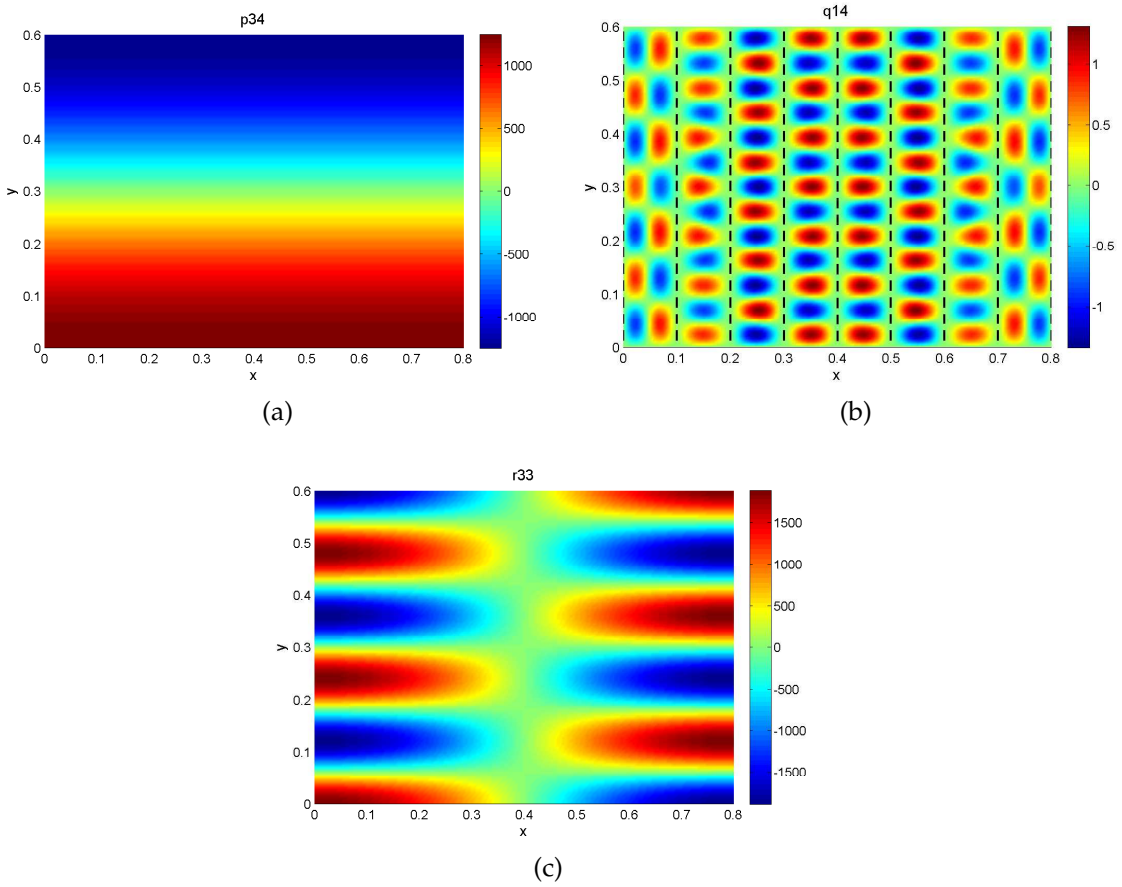

Figure 6.9: Magnitudes of the mode spatial shapes on the coupling surface: (a) p_{34}; (b) q_{14} (Vertical dashed lines: rib positions); (c) r_{33}.

been plotted in Fig. 6.9 to be compared with those in Fig. 6.8. As observed, the plate mode q_{14} presents short wavelengths along the x and y directions compared to the wavelengths of the acoustic modes. This results in low values for the intermodal works (1.9×10^{-7} J between p_{34} and q_{14} and 8.7×10^{-7} J between q_{14} and r_{33}) and in very low values for the modal coupling factors (1.9×10^{-16} Hz between p_{34} and q_{14} and 3.9×10^{-17} Hz between q_{14} and r_{33}), despite the frequency matching. Hence, it becomes clear that the main difference between the paths $p_{49} \rightarrow q_{20} \rightarrow r_{49}$ and $p_{34} \rightarrow q_{14} \rightarrow r_{33}$ is the effect of spatial matching. The former path is the most dominant one and this is a consequence of the rib effects which lead to a low energy noise reduction in comparison to that of the bare plate for the 1600 Hz third octave band (see Fig. 6.5). Therefore, it becomes clear again how from an automatic and quick inspection of the outputs of the MPS algorithm it is possible to identify those modes responsible of a sudden decrease in the ENR curves, and act upon them if necessary. Otherwise, one could waste lots of time analysing paths with good frequency matching but no relevant energy contribution such as $p_{34} \rightarrow q_{14} \rightarrow r_{33}$.

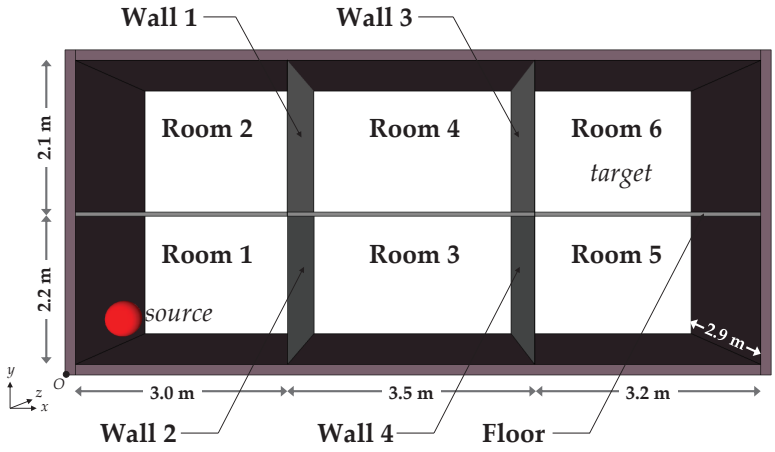

Figure 6.10: Sketch of the shipbuilding built-up structure model

6.5 APPLICATION TO A SHIPBUILDING STRUCTURE

6.5.1 *Path analysis in SmEdA*

The above developments will be applied in this section to a more complex case consisting of a shipbuilding structure made of 6 rooms distributed in two decks (see Fig. 6.10). The floor between decks and the vertical walls between rooms are made of steel ($\rho = 7800$ kg/m^3, Young modulus $E = 2 \times 10^{11}$ Pa and internal damping $\eta = 0.01$). The thicknesses of the panels are 6 mm for the floor and 2 mm for the walls. The floor and the walls are stiffened with 6 T-shaped ribs. These ribs are regularly spaced along the floor's longest edge and along the vertical wall edges. The rib spacing is 0.4 m and the first and the last ribs are respectively placed at 0.46 m and 0.44 m from the edges. The T-cross section dimensions are $[80 \times 8]$ mm^2 / $[80 \times 8]$ mm^2 for the floor ribs and $[60 \times 5]$ mm^2 / $[60 \times 5]$ mm^2 for the wall ones (see Figure 6.11). Besides, to deal with a more amenable model the external walls and floors of the structure have been assumed rigid. The rooms are filled with air (mass density $\rho_0 = 1.29$ kg/m^3, wavespeed $c_0 = 340$ m/s, damping loss factors $\eta = 0.01$). Overall, this results in a model with eleven subsystems: six rooms $R1 - R6$, the floor F and four separating walls $W1 - W4$ (see Fig. 6.10).

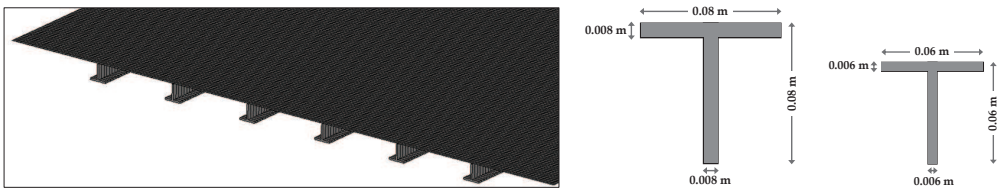

(a) (b) (c)

Figure 6.11: (a) Zoom view of the floor in the shipbuilding structure of Fig. 6.10. (b) Section of the floor ribs. (c) Section of the wall ribs.

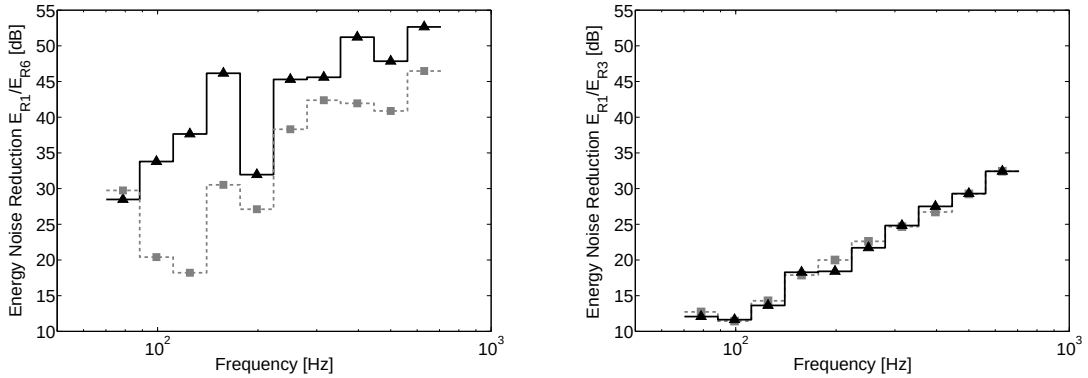

Figure 6.12: (a) Energy Noise Reduction E_{R6}/E_{R1} between Room 1 and Room 6. —▲— (black) SmEdA results. - -■- - (grey) SEA results. (b) Energy Noise Reduction E_{R3}/E_{R1} between Room 1 and Room 3. —▲— (black) SmEdA results. - -■- - (grey) SEA results.

In this case, to build the SmEdA model only flexural vibration modes have been considered for the panels. Different studies on ship structures [Hynna et al., 1995; Nilsson, 1977] showed that this type of vibration transmission is predominant in the low and mid frequency range. For high frequencies (several kHz for typical naval frames), in-plane modes may be of importance for some one third octave bands. Actually, it has been noticed that in-plane longitudinal and shear motions may have significant contributions on the energy transmitted to a subsystem far away from the excited one [Lyon, 1986; Tratch, 1985]. However, given that the frequency range of analysis has been fixed to [80 Hz–500 Hz], which is below the first in-plane mode of the floor (616 Hz), contemplating only bending motions is a fair enough approximation. The modes of the floor and walls have been computed with FEM and the SDTool code [Balmes et al., 2011], whereas the cavity modes have been calculated analytically, like in the previous examples.

An acoustic monopole has been located at point $M_0 = (0.8, 0.9, 0.7)$ m in Room 1 (source subsystem), with unit power spectral density. Room 6 is considered as the receiver. In Fig. 6.12a the ENR between R1 and R6 has been plotted, whereas the ENR for the two adjacent rooms R1 and R3 is also presented in Fig. 6.12b for comparison. As observed, the energy reduction between R1 and R6 is considerably high except for the 200 Hz band where strong energy transmission takes place. One may then wonder which modes are responsible for the transmission at this frequency band to act upon them e.g., by increasing their damping and thus reducing the energy level at the receiver.

In Table 6.8 a path analysis is presented for the shipbuilding built-up structure, analogous to that in Table 6.4 for the cavity-homogeneous plate-cavity system. As seen from the table, there are a total of 326 modes involved in the 200 Hz band, the overall energy at the receiver subsystem being 45.06 dB (first row). Considering 1000 paths 93.77% of the energy at the receiver can be recovered,

with a drastic reduction in the number of involved modes (from 326 to 112). The strongest reduction of modes takes place for subsystems $R2$, $R3$ and $W1 - W4$, which is logical. With the sole consideration of 25 paths the reconstructed energy at the receiver is less than one dB of its overall value, which may suffice for the analysis of the vibroacoustic behaviour of the structure. The computation times for the path analysis in a regular PC (Intel Core 2 Quad CPU q9400 @2.66 GHz) are included in Table 6.9.

Computing the number of instances of every mode in the ranking of paths (see Fig. 6.13) reveals that the dominant modes of the floor are f_{22} and f_{23}. This can also be appreciated in the ranking list of Table 6.10 for the first seven dominating transmission paths. These paths contribute 58.11% of the energy at the receiver and only contain modes belonging to the source room, the receiver room and the floor. This indicates that energy is mainly transmitted along the floor separating the two decks.

Similarly to what occurred for the cavity - ribbed plate - cavity example, a close inspection of modes f_{22} and f_{23} shows that they present high wavelengths in the floor's stiffest direction, which results in good spatial matching with the cavity modes (see Figures 6.14a and 6.14b). Despite the amplitudes of the mode shapes being smaller in the junction area with room 1 than with room 6, there is still good spatial matching of f_{22} and f_{23} with the cavity modes of the former. In contrast, mode f_{25}, for example, exhibits lower vibration values in the junction areas with rooms 1 and 6 than in the junction with room 2, and also presents shorter wavelengths than f_{22} and f_{23} (see Figure 6.14c). This explains the lack of spatial matching leading to destructive interference between the floor mode and the cavity modes. In turn, that results in low intermodal works within room 1 and room 6 modes.

Number of paths	Accum. Contr. [dB]	Accum. Contr. [%]	$\hat{R}1$	$\hat{R}2$	$\hat{R}3$	$\hat{R}4$	$\hat{R}5$	$\hat{R}6$	$\hat{F}$	$\hat{W}1$	$\hat{W}2$	$\hat{W}3$	$\hat{W}4$	Total involved modes	Missing modes
∞	45.06	100.00	15	14	18	18	17	17	65	42	40	40	40	326	0
1000	44.78	93.77	12	5	6	13	8	17	37	2	5	7	0	112	214
500	44.67	91.39	11	5	3	8	4	15	30	1	3	5	0	85	241
100	44.44	81.67	8	3	3	4	3	12	14	0	0	2	0	49	277
25	44.18	70.85	3	1	0	0	1	5	6	0	0	0	0	16	310
7	42.70	58.11	1	0	0	0	0	3	3	0	0	0	0	7	319

Table 6.8: *Shipbuilding structure. Transmission path analysis and involved modes.*

Tree of max. paths	Sorted Forward Star Form	MPS Algorithm	Post-processing functions	Total
0.89 s	0.15 s	36.05 s	1.12 s	40.40 s

Table 6.9: *Shipbuilding structure example. Computation times of the path analysis.*

Path	Shipbuilding
1	$S \rightarrow r1_6 \rightarrow f_{22} \rightarrow r6_5 \rightarrow T$
2	$S \rightarrow r1_6 \rightarrow f_{22} \rightarrow r6_6 \rightarrow T$
3	$S \rightarrow r1_6 \rightarrow f_{23} \rightarrow r6_5 \rightarrow T$
4	$S \rightarrow r1_6 \rightarrow f_{23} \rightarrow r6_6 \rightarrow T$
5	$S \rightarrow r1_6 \rightarrow f_{22} \rightarrow r6_7 \rightarrow T$
6	$S \rightarrow r1_6 \rightarrow f_{21} \rightarrow r6_5 \rightarrow T$
7	$S \rightarrow r1_6 \rightarrow f_{23} \rightarrow r1_6 \rightarrow f_{22} \rightarrow r6_5 \rightarrow T$

Table 6.10: *Shipbuilding structure example. Ranking of the* 10 *most dominant modal energy paths from a total of* 1000 *computed paths*

As a consequence, one could attempt to increase the damping of modes f_{22} and f_{23} in order to diminish the energy level in the receiver room. This has been simulated by setting their new internal damping values to $\eta_{22} = \eta_{23} = 0.1$, which has resulted in a 5.0 dB reduction of the transmitted energy. Of course this structural modification is only theoretical, but it confirms that the structural modes on which one should intervene for controlling the noise transmission have been well identified. In practice, viscoelastic layers can be used for increasing the modal damping. In order to optimize the increase of damping of a given mode the layers should be placed at the positions of maximum strain energy according to the mode shape [Kumar and Singh, 2010]. The damping factors of all modes in the considered structure will be obviously influenced by these viscoelastic layers. They could be estimated using the Modal Strain Energy (MSE) method [Hwang et al., 2014; Koruk and Sanliturk, 2011; Ungar and Kerwin Jr, 1962].

To summarize, the MPS algorithm has allowed for a quick identification of the two most critical modes determining the energy transmission between source and receiver in the SmEdA model of the shipbuilding built-up structure, which contains a total of 326 modes. The sole modification of the damping loss factors

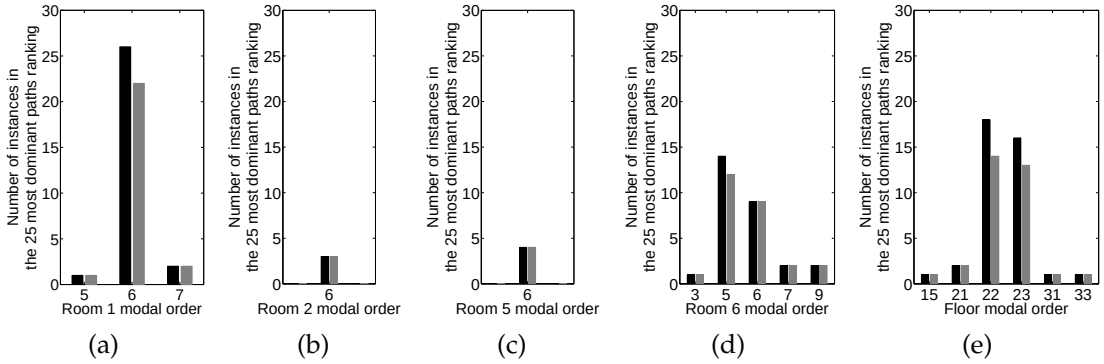

Figure 6.13: Number of instances of every mode in the 25 most dominant paths ranking. Black columns: total number of instances in the path ranking. Grey columns: number of paths containing a particular mode.

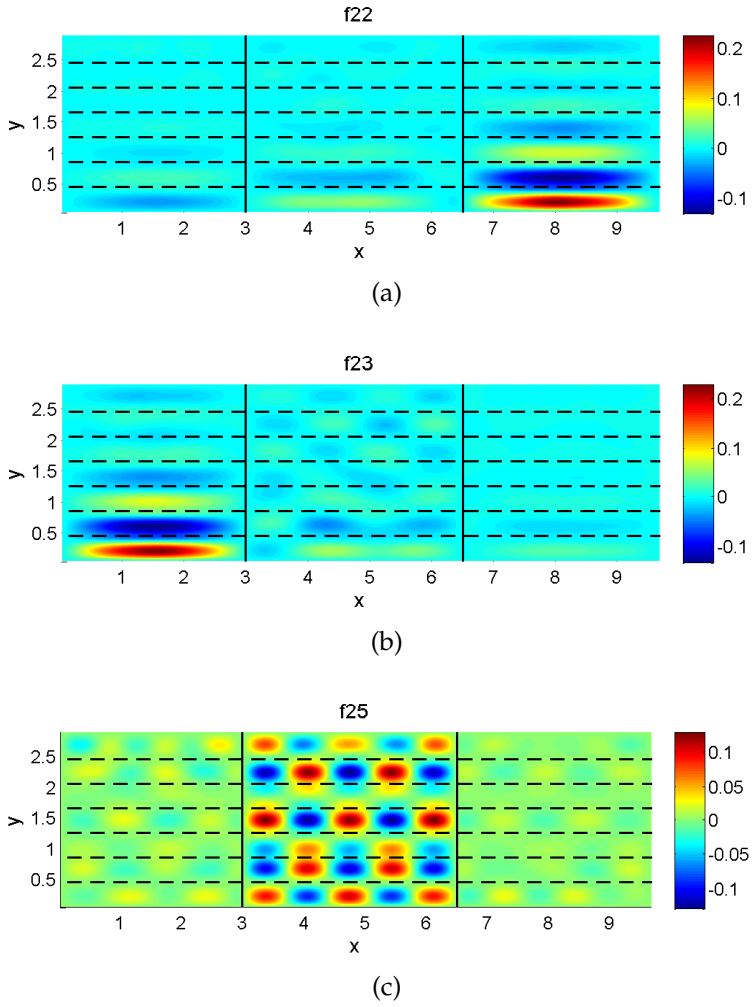

Figure 6.14: Magnitudes of the mode spatial shapes on the coupling surface (Horizontal dashed lines: rib positions): (a) f_{22}; (b) f_{23} ; (c) f_{25}.

of two modes, from 65 modes in the floor, has resulted in a noise reduction of 5 dB.

All in all, it would be feasible to think of drawing a process for any built-up structure, which could start with the identification of the most dominant modal transmission paths from source to receiver subsystems, using the graph theory approach depicted heretofore. An analysis could then be made of the mode shapes having the most significant participation in noise transmission (like modes f_{22} and f_{23}), and then one could try to reduce their energy contribution at the receiver by increasing their damping. A target noise reduction value could be fixed for the receiver (like the 5 dB in room 6) and appropriate values for the problematic mode damping (like 0.1 for f_{22} and f_{23}) could be derived to reach that goal. Damping layers could judiciously be placed to reach the objective and determined according to the MSE method. A final SmEdA simulation would verify the performance of the solution in terms of noise reduction. A similar automatized procedure in the easier case of SEA is developed in the framework

of graph theory in Chapter 7. The development of an analogous process for SmEdA as described is, however, outside the scope of this thesis.

6.5.2 *Comparison with SEA results*

A comparison with the results that can be obtained from a SEA model of the shipbuilding structure instead of the SmEdA one will be finally presented to highlight some of the advantages of the latter. A SEA system can be directly deduced from a SmEdA one by assuming modal energy equipartition, see [Maxit and Guyader, 2001a, 2003]. The SEA coupling loss factors (CLF) and injected power can be related, respectively, to the SmEdA modal coupling factors and modal injected powers. For the basic case of two coupled subsystems considered in Section 2.4.1, the CLF between subsystems 1 and 2, η_{12}, can be computed as

$$\eta_{12} = \frac{\sum_{p\in\hat{P}} \sum_{q\in\hat{Q}} \beta_{pq}}{\omega_c N_p}, \tag{6.10}$$

and the injected power in subsystem 1 as

$$\Pi^1 = \sum_{p\in\hat{P}} \Pi^p_{inj}. \tag{6.11}$$

These expressions can be easily generalized in the case of having more subsystems.

When the subsystem modal overlap is high (typically greater than one), energy equipartition takes place to a good extent so that SEA and SmEdA provide similar results. However, for low modal overlap, modal energy equipartition is no longer satisfied for subsystems located far away from the excited one, which leads SEA to overestimate energy transmission [Maxit and Guyader, 2003]. This can be observed in Figs. 6.12a and (b) for the ENR values between rooms 1 and 6 and rooms 1 and 3. In the case of adjacent rooms SEA and SmEdA yield fairly close results. As opposed to this, in the case of rooms 1 and 6 which are at considerable distance apart (see Fig. 6.10) a strong discrepancy can be observed between the predictions of SmEdA and SEA. The latter gives a lower ENR value and thus a higher energy level at the receiver room 6.

In Table 6.11, the ranking for the 10 dominant energy transmission paths between rooms 1 and 6 in the SEA model is presented. As observed the first path clearly involves energy transmission through the floor. Table 6.12 shows the presence of the subsystems in every path ranking. However, and contrary to the results in Table 6.10, in this case no information at all is available on which modes are responsible for this transmission.

6.6 CONCLUSIONS

Energy interchange between modes in subsystems rather than between subsystems (groups of modes) themselves, it is at the very core of SmEdA. As

Path	Shipbuilding SEA
1	$S \to r1 \to f \to r6 \to T$
2	$S \to r1 \to f \to r4 \to r6 \to T$
3	$S \to r1 \to w2 \to f \to r6 \to T$
4	$S \to r1 \to r3 \to f \to r6 \to T$
5	$S \to r1 \to f \to w3 \to r6 \to T$
6	$S \to r1 \to f \to r4 \to f \to r6 \to T$
7	$S \to r1 \to f \to r3 \to f \to r6 \to T$
8	$S \to r1 \to r2 \to f \to r6 \to T$
9	$S \to r1 \to f \to r5 \to r6 \to T$
10	$S \to r1 \to f \to r6 \to f \to r6 \to T$

Table 6.11: *Shipbuilding structure example. Ranking of the* 10 *most dominant energy SEA paths from a total of* 100 *computed paths for the* 200 *Hz* 1/3 *octave band.*

Number of paths	Accum. Contr. [dB]	Accum. Contr. [%]	Presence of the subsystem										
			R1	R2	R3	R4	R5	R6	F	W1	W2	W3	W4
∞	49.73	100.00	✓	✓	✓	✓	✓	✓	✓	✓	✓	✓	✓
100	49.73	99.93	✓	✓	✓	✓	✓	✓	✓	✓	✓	✓	✓
20	49.72	99.73	✓	✓	✓	✓	✓	✓	✓	×	✓	✓	×
10	49.68	98.72	✓	✓	✓	✓	✓	✓	✓	×	✓	✓	×
1	49.47	94.12	✓	×	×	×	×	✓	✓	×	×	×	×

Table 6.12: *Shipbuilding structure. Transmission path analysis in the SEA model.*

seen, avoiding modal energy equipartition allows one to extend classical SEA to the mid frequency range and dealing with low modal overlap and/or locally excited subsystems, as well as with complex geometry subsystems. However, given that many modes are considered within subsystems, the dimensions of SmEdA matrices become considerably large even for medium sized systems, like those representing sound transmission between two adjacent cavities. Energy transmission in such type of systems is more often caused not so much by mode frequency matching as by mode spatial matching. If one aims at vibroacoustic remedial actions, identifying those resonant and non-resonant modes that play an essential role in energy transmission becomes a must. However, direct mode by mode inspection may become a never-ending task even in the occurrence of frequency matching, as shown for some of the analyzed examples.

It has been proved that graph theory offers a way out to this problem. Analogously to what was previously done in SEA, and for some energy distribution models as well, it becomes possible to define a SmEdA graph associated to any SmEdA model and apply a ranking path algorithm to it. The latter results

in a sorted list of modal energy transmission paths from source to receiver subsystems, which allows for the straightforward identification of the modes that dominate the transmission process. Then one could focus on analyzing the spatial matching of the modes in that dominating paths and see whether an increase of damping, a structure reinforcement, or whatever action deemed appropriate, may result in a decrease of the noise transmitted to the receiver. The validity of the graph approach to ease the analysis of SmEdA systems has been demonstrated for different examples, consisting of the transmission of sound between cavities separated by both bare and ribbed plates, as well as for the more complex case of a shipbuilding structure.

7

A GRAPH CUT STRATEGY FOR TRANSMISSION PATH PROBLEMS IN STATISTICAL ENERGY ANALYSIS

Summary. In this chapter, it is shown how a strategy based on algorithms for computing cuts in undirected networks, can be applied to reduce energy transmission in realistic statistical energy analysis (SEA) models, with the sole modification of a limited number of internal and coupling loss factors. The frequency dependent case of SEA systems with multiple sources and targets is considered. A mathematical justification for the strategy is also provided, which relies on an analysis of the series expansion of the energy vector, in terms of the powers of the SEA graph adjacency matrix. A numerical example of vibroacoustic transmission in a simple test building has been included to show the performance of the approach.

This chapter is based on the following work

- O. Guasch, À. Aragonès, and M. Janer. A graph cut strategy for transmission path problems in statistical energy analysis. *Mechanical Systems and Signal Processing* , 30:343–355, 2011 [Guasch et al., 2011]
- O. Guasch, À. Aragonès, and M. Janer. Graph cuts to reduce energy transmission in the sea model of a building. In *Proceedings of Inter-Noise 2010, June 13-16, Lisbon (Portugal)*, 2010 [Guasch et al., 2010]
- O. Guasch, L. Cortés, and À. Aragonès. Graph cuts applied to transmission path problems in Statistical Energy Analysis models. In B.R. Mace, N.S. Ferguson, and E. Rustighi, editors, *NOVEM2009, on the CD-ROM: Oxford (UK), 5-8 April, Noise and Vibration: Emerging Methods*, 2009 [Guasch et al., 2009]

7.1 INTRODUCTION

Let us consider an N-dimensional statistical energy analysis (SEA) model. Assume that external energy is being input at a limited number of say, N_s subsystems, whereas restrictions are posed on the energy another set of N_t subsystems should not surpass. Henceforth, let us term the former as *source* or *input* subsystems, while the latter subsystems, whose energy is to be reduced, will be

referred to as the *target* or *output* subsystems. A common problem of noise and vibration control in SEA models is that of reducing the energy level at the N_t targets modifying as few SEA system parameters (internal and coupling loss factors) as possible. In other words, one aims at diminishing the vibration or noise levels at the target locations of the modelled physical system, carrying out a minimum number of design modifications.

The above control problem has been not addressed until recently, as seen throughout this thesis, and a few options have been considered to solve it. If no information is available on which are the loss factors having more influence on the target subsystem energies, one can always resort to Monte Carlo and related approaches [Dinsmore and Unglenieks, 2005]. The values of a limited set of loss factors are randomly changed to new admissible values, and the subsystem energies become recomputed for each modification, until the desired energy goals at the targets are obtained. The use of genetic algorithms [He et al., 2005] can improve the final solution although they still not provide direct information on the explicit dependence of the target subsystem energies on the system parameters.

To remedy this situation and gain more insight on the SEA model behaviour, a more classical approach was followed in [Bartosch and Eggner, 2007; Büssow and Petersson, 2007] that consists in performing a first-order Taylor expansion of the energies at the target subsystems, in terms of the system loss factors. Then, an optimization problem can be posed expressing the target subsystem energies as an objective function to be minimized by appropriate modification of the SEA system parameters. Obviously, the optimum solution would imply modifying a large number of loss factors, which could be infeasible for a real industrial case. Consequently, a sensitivity analysis has to be performed to assess the influence on the targets of the variations in the loss factors. As a result, modifications are only attempted for the most sensitive loss factors. A similar approach was followed in [Chavan and Manik, 2005] for a SISO (single input / single output) SEA system, the main difference being in the definition of the cost function to be minimized. The latter was expressed as the summation of the contributions of several transmission paths [Craik, 1979, 1996] linking the source with the target. The method consequently depends on the number of paths taken into account, that rapidly increases when considering high order paths.

A third and totally different approach to the SEA vibroacoustic control problem is presented in this chapter. Actually, the key idea of the method was already proposed in [Guasch and Cortés, 2009]. It was shown in that reference that besides the ranking path problem, other noise and vibration transmission path problems could be posed in the general framework of graph theory. In the previous chapters, the link between SEA and graph theory has been widely discussed. Thanks to the definition of the SEA graph, it has been shown how valuable information on the SEA system energy transmission paths can be obtained by means of the adaptation of algorithms intended to solve path problems in graphs.

On the other hand, one of the main topics addressed in [Guasch and Cortés, 2009] was the SISO control problem of trying to reduce the energy at a target subsystem that had been input to the SEA model through a single source subsystem. A strategy was developed that relies on the use of graph cut algorithms [Nagamochi et al., 1997; Stoer and Wagner, 1997; Subramanian, 1995]. Given that all transmission paths from the source to the target have to cross a cutset [Carré, B.A., 1979; Diestel, 2005; Gross and Yellen, 1999] between them, it was proposed to find the cutset having minimum size and to modify the loss factors associated to it. If the desired energy reduction at the target was not achieved, cutsets of higher size were considered until the expected final energy level at the output was reached.

In this chapter, we aim at pushing forward the graph cut strategy outlined in [Guasch and Cortés, 2009]. Whereas only low dimensional benchmark SISO graphs at a single frequency band were presented in [Guasch and Cortés, 2009], the first goal of this chapter will be that of extending the graph cut strategy to large MIMO (multiple input / multiple output) SEA graphs covering as much frequency bands as demanded. It will be shown that the MIMO case presents some important particularities. For instance, when cutting the graph, the subsets containing the sources and targets are not necessarily connected subgraphs, which allows to automatically recover the well-known noise control strategy of acting near the sources to reduce the emitted noise and vibrations. If this possibility is not good enough, the strategy automatically looks for alternatives, detecting structure bottlenecks where it may be worthwhile acting.

The second goal of the present work is to provide a mathematical justification for the key step of the graph cut strategy. The justification relies on resorting the SEA system series solution in terms of the contributions of the paths between sources and receivers that cross the cutset, and then proceed to minimize the energy at the latter. Finally, the third goal of this chapter is to show how the graph cut strategy could be applied in a realistic problem. The case of noise transmission between two rooms in a dwelling is addressed for this purpose.

When compared to other methods, the graph cut strategy could be helpful in solving some of their weakness, and actually it can be sought as an alternative but also as a complimentary method for them, in order to face SEA vibroacoustic control problems. For instance, a typical difficulty of the Monte Carlo method solutions is that they involve making design modifications on several disperse and disconnected locations of the structure, which are impractical in real life situations. In contrast, the subsystems to be modified are usually located in small areas for the graph cut approach, given that it automatically detects energy transmission bottlenecks [Guasch and Cortés, 2009]. This point is further reinforced by the fact shown in this work, that subsets from a SEA graph partition are not necessarily connected subgraphs, which allows for instance, to automatically check for solutions involving subsystems located near the sources and the targets. In what concerns optimization plus sensitivity analysis (see e.g., [Bartosch and Eggner, 2007; Büssow and Petersson, 2007] and references

therein), the graph cut strategy could perform superior in those cases in which the internal loss factors of specially sensitive subsystems could not be drastically increased. In such situations, the SEA system energy will tend to redistribute and reach the target subsystems through other transmission paths, all of them being addressed in the graph cut case. However, the latter has the drawback that maybe a subsystem that will be worthwhile modifying is left apart if it does not belong to any computed cutset. Therefore, it is also worthwhile noting that the graph cut strategy could also be implemented in combination with optimization plus sensitivity analyses, or with Monte Carlo approaches. In the former case, this will ensure that no subsystem upon which it would be worthwhile to act is ignored. Concerning the latter, one could compute a small size graph cut and make a Monte Carlo computation on a reduced sample space. This will ease the computational cost and yield a less disperse solution. However, these combined possibilities will be not addressed in this work and are left for future developments.

The chapter is organized as follows. In Section 7.2, a brief review of some basic SEA and graph theory topics that will be needed for the remaining of the chapter is given for completeness. In particular, emphasis is put on the series solution of the SEA matrix system, on the notion of SEA graph and on some connectivity issues belonging to graph theory. In Section 7.3, the general MIMO strategy for energy reduction at the target subsystems is first explained. Then a benchmark example is presented to highlight some features of the method and a mathematical justification is provided to support its key step. Two numerical examples to show how the graph cut strategy could operate in a realistic situation are given in Section 7.4. The problem of vibroacoustic transmission between separated rooms in the simple SEA model of a building is addressed. Final considerations conclude the chapter in Section 7.5.

7.2 SEA AND GRAPH THEORY PRELIMINARY RESULTS

7.2.1 *Series solution for the SEA system*

Throughout sections 7.2 and 7.3 we will deal with a general N-dimensional SEA model characterized by an $N \times N$ loss factor matrix $\boldsymbol{\mathcal{H}}$. As usual, the unknown subsystem energies will be grouped into an $N \times 1$ energy column vector $\boldsymbol{E}$ and our interest will focus on reducing the energy at a set of N_t target subsystems. The external power input into the SEA model at each subsystem will be represented by means of the $N \times 1$ column vector $\boldsymbol{W}$. As outlined in the Introduction section, the subsystems corresponding to the N_s non zero entries of $\boldsymbol{W}$ will be referred to as *source* or *input* subsystems. In many cases of practical interest it happens that $N_s, N_t << N$ and that the target subsystems do not coincide with the source ones i.e., there is no energy input at the targets.

7.2.2 *Connectivity and cuts in SEA graphs*

As defined in Section 2.6, a kth order path on a graph from a node u_{i_0} to a node u_{i_k} is defined by the edge sequence $p^k_{i_0 i_k} = \left\{ \left(u_{i_0}, u_{i_1}\right), \left(u_{i_1}, u_{i_2}\right), \ldots \left(u_{i_{k-1}}, u_{i_k}\right) \right\}$. For the SEA graphs to be considered in this chapter, the weight of a path is given by the product of all edge weights in the path, i.e., $w\left(p^k_{i_0 i_k}\right) = \prod_{n=0}^{k-1} w_{i_n i_{n+1}}$ (see (2.51)). Hence, the weight of a path in G_{SEA} will be given by (2.51) whereas the weight of a path in B_{SEA} will have always a unit value.

Going back to the series expansion in (2.34), it is clear that it represents how energy is transmitted from the source subsystems to the target ones in the SEA graph, via the various order paths connecting them. Therefore, if we would like that no energy at all becomes transmitted from the sources to the targets, we could aim at somehow cutting the SEA graph into two parts, one containing the source subsystems, and the other one the targets. This naturally yields the notion of graph *cuts* or *cutsets*.

Let us first consider the SISO case of a SEA graph containing one single *source* node s and one single *target* node t, and let us focus, for example, on the graph B_{SEA}. Next, consider a partition $\{U^u_s, U^u_t\}$ of U^u_{SEA} (i.e., $U^u_{SEA} = U^u_s \cup U^u_t$, $U^u_s \cap U^u_t = \varnothing$) with U^u_s and U^u_t being proper subsets respectively containing the source and target nodes. The set of all edges with initial nodes at U^u_s and end nodes at U^u_t is then termed an $s-t$ *cutset* or an $s-t$*-cut* of B_{SEA}. We will use the notation $\langle U^u_s, U^u_t \rangle := \left\{ \left(u_i, u_j\right) \in E^u_{SEA} \middle| u_i \in U^u_s, u_j \in U^u_t \right\}$ to identify an $s-t$ cutset. For the MISO case (multiple sources / single target), the partition will be such that all sources $\{s_i\}$ will be contained in the corresponding U^u_S (note the upper case letter S), and we will then talk of an $\{s_i\} - t$ cutset. The latter will be identified as $\left\langle U^u_S, U^u_t \right\rangle$. Analogously, for the SIMO case (single source / multiple targets) we will have $\left\langle U^u_s, U^u_T \right\rangle$, $s - \{t_i\}$ cutsets. Finally, for the general MIMO case (multiple sources / multiple targets) to be addressed in this chapter, we will deal with $\{s_i\} - \{t_j\}$ cutsets represented by $\left\langle U^u_S, U^u_T \right\rangle := \left\{ \left(u_i, u_j\right) \in E^u_{SEA} \middle| u_i \in U^u_S, u_j \in U^u_T \right\}$. Given an $\{s_i\} - \{t_j\}$ cutset with cardinality L, its weight will be obtained from the summation of the weights of its edges, $w\left(\left\langle U^u_S, U^u_T, \right\rangle\right) = \sum_{l=1}^{L} w_{ij}$ with $\left(u_i, u_j\right) \in \left\langle U^u_S, U^u_T \right\rangle$. For the boolean SEA graph being considered B_{SEA}, all the edge weights have a unity value. Therefore, the weight of the cut will coincide with its cardinality. A cutset with cardinality L will often be referred to as a cutset of size L or as an L-cutset.

Several algorithms to find graph cutsets were developed in the past century. Originally, most of them relied on $\max - \min$ duality arguments that corresponded to variations of the well-known Menger's theorem [Menger, 1927]. This is the case for example, of the celebrated Ford-Fulkerson algorithm [Ford and Fulkerson, 1956]. In the nineties, however, new approaches to the problem were developed that resulted in the generation of deterministic algorithms to find cutsets. The strategy for energy reduction at the target subsystems of a SEA model, to be presented in next section, makes use of one of them. In particular, the algorithm in [Nagamochi et al., 1997] to find all small cuts in an

undirected network of weights less than a chosen value has been adopted. The algorithm was briefly outlined in [Guasch and Cortés, 2009], but the reader is referred to the original work [Nagamochi et al., 1997] for full technical details and explanations.

7.3 THE GRAPH CUT STRATEGY

7.3.1 *Description*

In this section we will push forward the graph cut strategy for SISO benchmark problems in [Guasch and Cortés, 2009], to account for more general and realistic frequency dependent MIMO situations. Hence, a general MIMO N-dimensional SEA graph will be considered with N_s sources, where external energy is being input, and with N_t targets whose energy is to be reduced. The main idea is to find the graph cutsets separating the sources from the targets and reduce, as far as possible, the weights (coupling loss factors) of their edges, as well as increase the internal loss factors of their initial and end nodes. Such a procedure guarantees that all energy transmission paths from the sources to the targets become modified. The idea is to start with cutsets of minimum size to limit the number of design modifications to be made, and then, if necessary, proceed increasing the size of the cutsets to involve more changes until the desired goal energy at the targets is achieved.

The graph cut strategy closely resembles the SISO case one, but various particularities are required to adapt it to the MIMO situation. Actually, several alternatives could have been chosen for the latter. For example, one could have addressed the MIMO problem as a combination of MISO problems. That is to say, suppose that we have two target subsystems $\{t_1, t_2\}$ and N_s sources. Then we could have decided to find the MISO cutsets $\left\langle U_S^u, U_{t_1}^u \right\rangle$, $\left\langle U_S^u, U_{t_2}^u \right\rangle$ and perform modifications on $\left\langle U_S^u, U_{t_1}^u \right\rangle \cup \left\langle U_S^u, U_{t_2}^u \right\rangle$. However, the latter does not correspond to a partition of the graph and generally its size is bigger than the corresponding MIMO cutset $\langle U_S^u, U_T^u \rangle$ with $t_1, t_2 \in U_T^u$. Numerical tests carried out insofar support this point and clearly indicate that directly working with MIMO cutsets is advantageous.

A pseudocode for the graph cut strategy is presented in algorithmic form in Algorithm 7.1. The code starts with a loop over the frequency range to be considered. It is assumed that modifications of the loss factors at a given frequency band will not affect the loss factors at all other frequencies (see the discussion below). The main steps have been numbered from 1 to 7 in the pseudocode and a succinct description for them is as follows:

1. First, the new goal values for the energy at the target subsystems are selected. For a set of N_t targets $\{t_i\}$ we will have $\{E_{t_i}^g\}$ goal values with corresponding goal energy levels $\{L_{Eti}^g\}$ that can be grouped in an $N_t \times 1$ vector $\boldsymbol{L}_{ET}^g$. If $\boldsymbol{L}_{ET}$ designates the vector of initial energy levels at the

Algorithm 7.1 *Pseudocode for the graph cut strategy to reduce the energy levels at the target subsystems*

for all frequency bands over frequency range **do**
  Assign the goal values $\{L^g_{Eti}\}$ and compute $\Delta \boldsymbol{L}^g_{ET}$ (alternatively, assign α_i, and compute ΔL^g_{ET})
  Assign the lower threshold values for η^{low}_{ij} and upper threshold values for η^{up}_{id}. Build the groups $\{\eta_{ij}\}$ and $\{\eta_{id}\}$
  Build SEA graphs G_{SEA} and B_{SEA}
  Compute B_{SEA} graph $\{s_i\} - \{t_i\}$ cuts $\{\langle U_S, U_T\rangle_k\}$ up to selected size M
  Set $L = \min\{\text{card}\,\langle U_S, U_T\rangle_k\}$, $r = 0$
  while $\{L^r_{Eti}\} > \{L^g_{Eti}\}$ **or** $L \leq M$ **do**
    Compute R as summation of possible disjoint unions $\{\cup_k \langle U_S, U_T\rangle_k\} \mid \text{card}\,\{\cup_k \langle U_S, U_T\rangle_k\}_r = L$ and L-cutsets
    Set $r = 1$
    while $\{L^r_{Eti}\} > \{L^g_{Eti}\}$ **and** $r \leq R$ **do**
      Compute $\{\cup_k \langle U_S, U_T\rangle_k\}^L_r$
      Set $\eta_{ij} \longrightarrow \eta^{\text{low}}_{ij}$ and $\eta_{id} \longrightarrow \eta^{\text{up}}_{id}$ in $\{\cup_k \langle U_S, U_T\rangle_k\}^L_r$ and in $\{\eta_{ij}\}$, $\{\eta_{id}\}$, and then compute $\{L^r_{Eti}\}$
      $r = r + 1$
    end while
    $L = L + 1$
  end while
  Output: $\{L^{\min}_{Eti}\}$ and $\{\cup_k \langle U_S, U_T\rangle_k\}^{\min}$
end for
Output: $\cup_\omega \{\cup_k \langle U_S, U_T\rangle_k (\omega)\}^{\min}$ and $\{L^{\min}_{Eti}\}$

target subsystems, we aim at a reduction of $\Delta \boldsymbol{L}_{ET}^{g} = \boldsymbol{L}_{ET} - \boldsymbol{L}_{ET}^{g}$. However, sometimes this condition may be too stringent and one could smooth it by defining some averaged, or weighted, reduction to be achieved. For instance, we could define $\Delta L_{ET}^{g} = \sum_{i}^{N_t} \alpha_i \Delta L_{Eti}^{g}$ as the goal to be reached, with $\alpha_i \in (0,1)$. In the case of all α_i being zero except one, a MISO situation is recovered. If $\alpha_i = 1,\ \forall\ i = 1 \ldots N_t$, the subsystems with large reductions demands become more important than those with small reductions demands (the summation involves decibels). Hence, by assigning different values to α_i a combined overall energy level reduction at the targets can be reached, the importance of the reduction at each target being somehow stated by its corresponding value of α_i. Obviously, other possibilities could be considered.

2. Next, the new admissible threshold values for the loss factors are chosen according to the design modification possibilities. It is shown in the mathematical proof of Section 7.3.3, that maximum energy reduction is achieved whenever coupling loss factors are diminished as much as possible, whereas the opposite occurs for the internal loss factors. We will therefore respectively denote these new values by η_{ij}^{low} and η_{id}^{up} . In subsequent steps of the strategy, if the edge (u_i, u_j) belongs to a cutset, its corresponding coupling loss factor will be reduced to η_{ij}^{low}, and the internal loss factors of u_i and u_j will be increased to η_{id}^{up} and η_{jd}^{up}. On the other hand, it is sometimes convenient to modify a group of subsystems instead of just one (e.g., a group of stiffeners or panels). We can then define sets of coupling and internal loss factors $\{\eta_{ij}\}$, $\{\eta_{id}\}$ so that all loss factors belonging to them have to be replaced by their new threshold values simultaneously (see Section 7.4.1.2 for further explanations).

3. The two SEA graphs G_{SEA} and B_{SEA} described in Section 2.7 are built. The adjacency matrix of the first one, $\mathcal{A}_S$, can be used for standard SEA matrix system computations, while the adjacency matrix $\mathcal{A}_B$ of the undirected boolean graph B_{SEA}, will be used to compute the cutsets separating source and target subsystems.

4. The algorithm in [Nagamochi et al., 1997] is used to compute all B_{SEA} $\{s_i\} - \{t_i\}$ cuts up to a preselected size M. In this way, a collection of MIMO cutsets $\{\langle U_S, U_T \rangle_k\}$ is obtained that separate the sources from the targets. The index L is initialized as the minimum size of these cutsets, i.e., $L = \min \{\text{card}\, \langle U_S, U_T \rangle_k\}$, whereas $M = \max \{\text{card}\, \langle U_S, U_T \rangle_k\}$.

5. Once the collection of MIMO cutsets $\{\langle U_S, U_T \rangle_k\}$ has been computed, we start the loop to reduce the energy level at the target subsystems. For a given cardinality L, all MIMO cutsets of this size are considered, as well as unions of cutsets of lower cardinality such that their combination results in a set of size L, i.e., we calculate $\{\cup_k \langle U_S, U_T \rangle_k\} \mid \text{card}\, \{\cup_k \langle U_S, U_T \rangle_k\}_r = L$.

Index r is used to designate individual cutsets and cutsets combinations of size L. We will denote their set as $\{\cup_k \langle U_S, U_T\rangle_k\}^L$ assuming that cutsets of size L are also included in this set. The cutsets and combined cutsets in $\{\cup_k \langle U_S, U_T\rangle_k\}^L$ can be sorted, for instance, according to their weights. The latter can be defined in terms of their capacity to diminish the SEA system energy. For example, one could define a cutset weight as the summation of the internal loss factors associated to the initial and end nodes of all edges belonging to the cut, as an alternative to the standard weight of a cutset given in the last section. Next, for every $\{\cup_k \langle U_S, U_T\rangle_k\}_r^L$ the new admissible threshold weights η_{ij}^{low} and η_{id}^{up} are used to replace the old ones. If any of the edges $\{\cup_k \langle U_S, U_T\rangle_k\}_r^L$ belong to the groups $\{\eta_{ij}\}$ and/or $\{\eta_{id}\}$, replacements are also carried out for the remaining elements in the group. Then, the new energy levels at the targets $\boldsymbol{L}_{ET}^r$ are computed from the standard SEA matrix system defined by G_{SEA}, and compared to the goals $\boldsymbol{L}_{ET}^g$. If the expected energy reduction is not achieved with any of the cutsets in $\{\cup_k \langle U_S, U_T\rangle_k\}_r^L$, the cardinality gets increased and the elements in $\{\cup_k \langle U_S, U_T\rangle_k\}_r^{L+1}$ become analysed next. The loop continues until we get the expected goal energy reduction at the targets, or until the maximum considered cutset size M is reached.

6. The first output of the graph cut strategy, for every considered frequency band with central frequency ω, consists in giving the final reduced energy levels at the targets $\{L_{Eti}^{\min}(\omega)\}$ (together with the remaining subsystem energies in G_{SEA}), and the list of edges in $\{\cup_k \langle U_S, U_T\rangle_k(\omega)\}^{\min}$ whose weights have been modified.

7. Finally, the complete list of elements to be modified in the SEA system will be obtained from the union of all the cutsets obtained at each frequency band, i.e., $\cup_\omega \{\cup_k \langle U_S, U_T\rangle_k(\omega)\}^{\min}$. The energy levels resulting from this union cutset will be the final solution we were looking for. Note that frequency dependence has not been explicitly written neither for the variables in Algorithm 7.1 nor in the above explanations, to ease the notation.

7.3.2 *A MIMO benchmark problem*

In this subsection we will present a first numerical benchmark example to figure out an important characteristic of graph cuts, which turns out to be specially valuable when addressing MIMO transmission path problems in SEA models. Considerations regarding possible application of the strategy to more realistic problems are left for Section 7.4, where the case of noise and vibration transmission in the SEA model of a building is addressed.

The basic point we would like to stress with the following MIMO benchmark example is the fact that the proper source and target subsets U_S and U_T re-

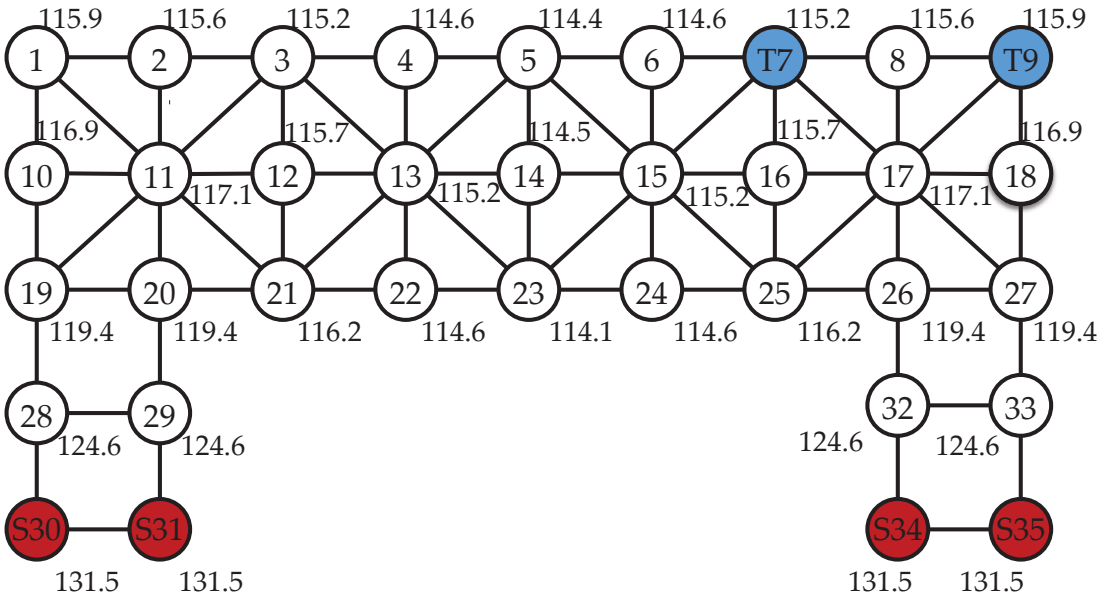

Figure 7.1: MIMO benchmark SEA graph with initial energy values in dB.

sulting from the partition of a MIMO SEA graph are not necessarily connected subgraphs. In other words, if two sources are quite separated apart, U_S does not necessarily contain a path linking them. This ensures that the logical noise control engineering option of trying to make modifications near the sources (read also targets) can be automatically taken into account in the graph cut strategy.

Let us consider for this purpose the graph shown in Fig. 7.1, which consists of 35 subsystems connected by means of 70 edges. Sources are placed on subsystems $S30$, $S31$, $S34$ and $S35$, whilst $T7$ and $T9$ are identified with the targets. Although a graph draw does not need to have any similarity with the SEA model it represents, for the ease of exposition we could thing of the graph in Fig. 7.1 as standing for the model of a "two-dimensional" railway coach at a given frequency band, with the source subsystems corresponding to the wheels and the target subsystems to some panels of the coach, whose energy is to be reduced.

Unit external energy is input at the wheels resulting in the energy levels provided in Fig. 7.1, for every subsystem in the graph. The symmetry of the obtained energy values is a direct consequence of the internal and coupling loss factors that have been chosen for the SEA graph. For simplicity, the same properties have been assigned to every subsystem belonging to a given row in the graph. That is to say for example, that nodes 1 to 9 (first row) have the same internal loss factor η_{id}, that a unique value has been assigned to all the coupling loss factors of the horizontal edges in the row, $\eta_{ij}-$, and so for the vertical edges $\eta_{ij}|$ and cross edges $\eta_{ij}\times$, linking rows 1 and 2. On the other hand, we assume that these loss factors can be modified in quantities $\Delta\eta_{id}$, $\Delta\eta_{ij}-$, $\Delta\eta_{ij}|$ and $\Delta\eta_{ij}\times$ to obtain η_{id}^{up} and $\eta_{ij}^{\text{low}} - |\times$ (e.g., $\eta_{ij}^{\text{low}}| = \eta_{ij}| - \Delta\eta_{ij}|$ and $\eta_{id}^{\text{up}} = \eta_{id} + \Delta\eta_{id}$),

Table 7.1: *Values used for the MIMO benchmark example.*

Row	$\eta_{id} \times 10^{-3}$	$\Delta\eta_{id} \times 10^{-3}$	n_i	$\eta_{ij} - \times 10^{-3}$	$\Delta\eta_{ij} - \times 10^{-3}$	$\eta_{ij}\vert \times 10^{-3}$	$\Delta\eta_{ij}\vert \times 10^{-3}$	$\eta_{ij} \times 10^{-3}$	$\Delta\eta_{ij} \times 10^{-3}$
First	5.9	2.3	1	58.7	17.6	25.1	7.5	48	14.4
Second	27.9	11.2	0.86	67.6	20.2	28.9	8.6	55.3	16.6
Third	18.2	7.2	1.03	56.5	16.9	24.2	7.2		
Fourth and Fifth	56	22.4	1.28	45.5	13.6	19.5	5.8		

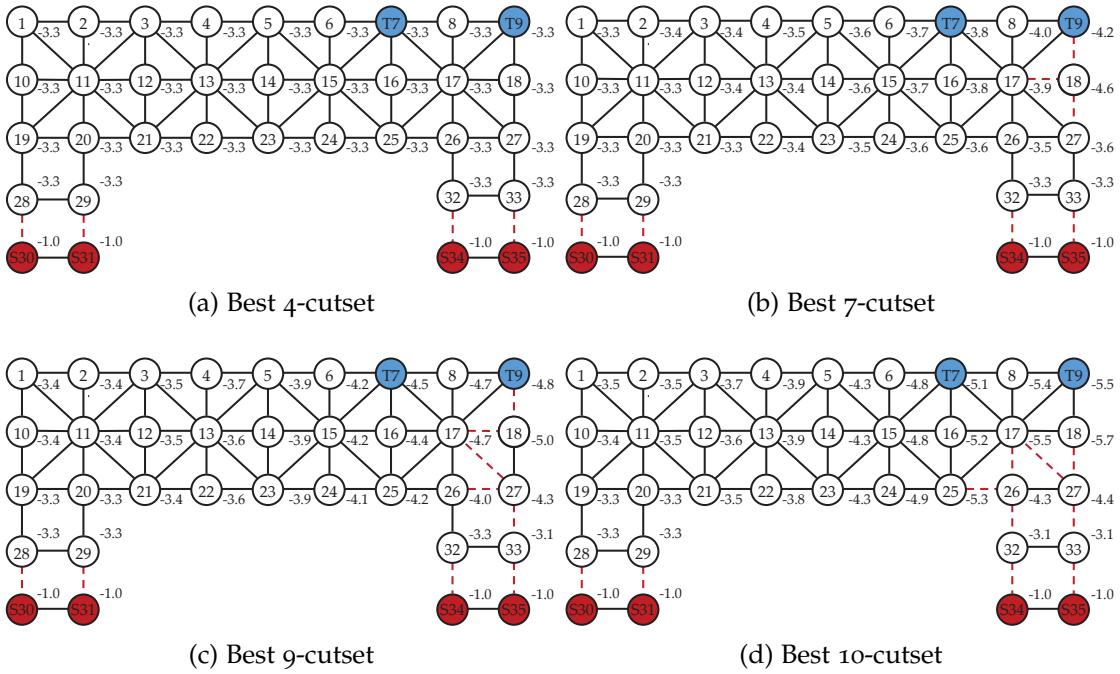

(a) Best 4-cutset

(b) Best 7-cutset

(c) Best 9-cutset

(d) Best 10-cutset

Figure 7.2: $\{s_i\} - \{t_j\}$ cutsets (dashed lines) with energy reduction achieved at each subsystem in dB.

whenever they become affected by a cutset. The numerical values for all the loss factors and allowed modifications in the graph are given in Table 7.1.

In Fig. 7.2, we show the energy reduction at all subsystems in the SEA graph for the best fourth, seventh, ninth and tenth size cutsets separating the sources (wheels) from the targets, once applied the graph cut strategy. As observed in Fig. 7.2a, the 4-cutset separates the sources from the targets with $U_S = \{S30, S31, S34, S35\}$, the wheels $S30$ and $S31$ not being connected with the wheels $S34$ and $S35$. As mentioned above, this is clearly a desirable property given that a golden rule in noise and vibration control is to act near the sources whenever this is possible. However, in the opposite case, for instance, of all subsystems in row 1 being sources, and all subsystems in row 5 being targets, the same cutset would have been found, indicating that the less intrusive approach in such situation would have been to act near the targets.

The 4-cutset provides an energy reduction at the target of 3.3 dB, see Fig. 7.2a. If larger energy reductions are desired, one has to resort to the higher cardinality cutsets in Fig. 7.2b, 7.2c and 7.2d. As seen, for the 7-, 9- and 10-cutsets the respective energy reductions at $T7$ become 3.8, 4.5 and 5.1 dB, and at $T9$ 4.2, 4.8 and 5.5 dB. It is interesting to have a look at the edges involved in these cutsets. They include the edges separating the wheels from the remaining of the coach already found in the 4-cutset, but they also begin to include edges located near target $T9$ (note that $T9$ has less connections with the coach than $T7$). The 9- and 10-cutsets also involve edges located in-between sources $S34$ and $S35$ and the targets. These sources are closer to the targets than sources $S30$ and $S31$ and will have a stronger influence on the target energy levels. Edges near $T7$ would appear in cutsets involving more than ten edges. In case of a 5 dB energy reduction at the targets sufficing for the noise control engineer in the present example, the 10-cutset would be the appropriate solution provided by the graph cut strategy. This would result in a final 110.1 dB energy level at $T7$, whereas we will have 110.4 dB at $T9$.

7.3.3 *Mathematical justification*

In what follows a mathematical justification for the key step of the above presented graph cut strategy will be presented. We will basically focus on the SISO case for the ease of exposition, the generalization to the MIMO case being quite straightforward. Let us consider a SEA system where external energy $E'_0(s)$ is input at a source subystem s and transmitted to a target subsystem t, whose energy is to be reduced. According to Eqs. (2.34), (2.50) and assuming that no external energy is being input at the target, the resulting energy at the latter, transmitted from source s, can be expressed as

$$\begin{aligned} E(t) &= E'_0(s) \sum_{k=1}^{\infty} \mathcal{S}^k(t,s) \approx E'_0(s) \sum_{k=1}^{K} \mathcal{S}^k(t,s) \\ &= E'_0(s) \sum_{k=1}^{K} \sum_{sh_1 \ldots h_{k-1}t}^{N_k} w_{sh_1} w_{h_1 h_2} \ldots w_{h_{k-1}t}. \end{aligned} \tag{7.1}$$

In (7.1), the weights are those of (2.50), $w_{ij} = \eta_{ij}/\eta_j$, and K stands for the truncating value of the series (i.e., only paths of order up to K between s and t are taken into account). N_k denotes the overall number of paths of order k linking s and t, which can be obtained from the corresponding element of the kth power of the adjacency matrix $\mathcal{A}_{\mathcal{B}}(t,s)$, defined in (2.52) [Guasch and Cortés, 2009; Magrans, 1993].

The summation in (7.1) can be rearranged by enumerating the set of N_k paths $p^k_{st} = \left\{ (s, u_{h_1}), (u_{h_1}, u_{h_2}), \ldots \left(u_{h_{k-1}}, t\right) \right\}$ of order k. We recall that the weight

corresponding to the nth path $P^k_{st,n}$ is denoted by $w\left(P^k_{st,n}\right) = w_{sh_1}w_{h_1h_2}\ldots w_{h_{k-1}t}$, with index n running from 1 to N_k. Consequently, we can rewrite Eq. (7.1) as

$$E(t) \approx E'_0(s)\sum_{k=1}^{K}\sum_{n=1}^{N_k} P^k_{st,n}. \tag{7.2}$$

As it has already been mentioned, the graph cut strategy is based on the fact that any transmission path linking a source s and a target t has to cross any $s-t$ cutset between them. Hence, consider an $s-t$ cutset $\langle U_s, U_t\rangle$ of G_{SEA}, with cardinality L, and denote the weights of its edges by $w^*_{ij} = \eta^*_{ji}/\eta^*_i := \left\{w_{ij}\middle|\,(u_i,u_j)\in\langle U_s,U_t\rangle\right\}$. Taking into account that any of the N_k kth order paths $p^k_{st,n}$ will have at least one of its edges belonging to the cutset, we can rewrite their weights $P^k_{st,n}$ as

$$w\left(P^k_{st,n}\right) = w^*_{h_ih_{i+1}}w\left(P^{k-1}_{st,n}\right) \tag{7.3}$$

with

$$w\left(P^{k-1}_{st,n}\right) = w_{sh_1}\ldots w_{h_{i-2}h_{i-1}}w_{h_{i+2}h_{i+3}}\ldots w_{h_{k-1t}}. \tag{7.4}$$

In the case of $p^k_{st,n}$ crossing more than once the cutset, there will be further elements in (7.4) corresponding to edges in the cut. In such situations, the term $w^*_{h_ih_{i+1}}$ in decomposition (7.3) will correspond to the weight of the edge in the cutset that path $p^k_{st,n}$ crosses for the first time.

We can next enumerate the edges in $\langle U_s, U_t\rangle$ from $l=1$ to L, and rewrite their corresponding weights as $w^{l*}_{h_ih_{i+1}}$ to account for the indexing. Then, the summation of the weights of all N_k kth order paths from the source to the target can be expressed as

$$\sum_{n=1}^{N_k} w\left(P^k_{st,n}\right) = \sum_{l=1}^{L} w^{l*}_{h_ih_{i+1}}\sum_{n=1}^{N_k} w\left(P^{k-1}_{st,n}\right)\delta_{ln}, \tag{7.5}$$

with δ_{ln} standing for the Kronecker's delta that has value 1 if the nth path $p^k_{st,n}$ crosses the lth edge $\left(u_{h_i},u_{h_{i+1}}\right)_l$ in the $s-t$ cut, and zero otherwise. Substituting (7.5) in (7.2) yields the following result for the energy at the target subsystem

$$E(t) \approx E'_0(s)\sum_{l=1}^{L} w^{l*}_{h_ih_{i+1}}\sum_{k=1}^{K}\sum_{n=1}^{N_k} w\left(P^{k-1}_{st,n}\right)\delta_{ln}. \tag{7.6}$$

The meaning of the above series expansion is apparent: it expresses the energy at the target sorted as the energy transmitted from the source s to t through any path that first crosses the first ($l=1$) edge in the $s-t$ cutset, plus the energy transmitted from s to t through any path that first crosses the second ($l=2$) edge in the $s-t$ cutset, and so on to the contributions of paths that first cross the last ($l=L$) edge of the cut.

From (7.6), the graph cut strategy can be more clearly justified: replacing all $s-t$ cutset edge weights w^{l*}_{ij} by new admissible values we guarantee that all

energy transmission paths from the source to the target become modified. This can mitigate energy redistribution through secondary paths, which can occur if individual and non connected system loss factors are changed.

To simplify the analysis, let us consider for the moment that the transmission paths between source and target only cross the cutset once. This may be a reasonable approximation in some practical cases, given that paths crossing forwards and backwards the cutsets will usually have a much longer length than those that only cross it once. Therefore, and according to (2.32), the former will carry much less energy than the latter.

The edge weights in the cutset are given by

$$w_{ij}^{l*} = \frac{\eta_{ij}^{l*}}{\eta_{j}^{l*}} = \frac{\eta_{ij}^{l*}}{\eta_{jd}^{l*} + \sum_{k \neq j} \frac{n_k}{n_j} \eta_{kj}}, \tag{7.7}$$

where we have used the consistency relation to make η_{ij}^{*} explicitly appear in the summation of the denominator. We can then wonder how η_{ij}^{l*} and η_{jd}^{l*} should be modified to reduce $E(t)$ in (7.6) as much as possible. Let us denote by $\partial_x f$ the partial derivative of a function f with respect to a variable x, and assume, as mentioned, that all transmission paths only cross the cutset once. The partial derivative $\partial_{\eta_{ij}^{l*}} E(t)$ will be given by

$$\partial_{\eta_{ij}^{l*}} E(t) \approx E_0'(s)\, \partial_{\eta_{ij}^{l*}} w_{ij}^{l*} \sum_{k=1}^{K} \sum_{n=1}^{N_k} w\left(P_{st,n}^{k-1}\right) \delta_{ln}, \tag{7.8}$$

with

$$\partial_{\eta_{ij}^{l*}} w_{ij}^{l*} = \frac{\eta_{jd}^{l*} + B}{\left(\eta_{jd}^{l*} + B + \frac{n_j}{n_i}\eta_{ij}^{l*}\right)^2} = \frac{\eta_{j}^{l*} - \eta_{ji}^{l*}}{\left(\eta_{j}^{l*}\right)^2}, \tag{7.9}$$

$$B = \sum_{k \neq i,j} \frac{n_k}{n_j} \eta_{kj}. \tag{7.10}$$

Note that (7.9) is a decreasing but always positive function for increasing η_{ij}^{l*} and so it will be (7.8). Consequently, the energy at the target (7.6) will be a monotonic increasing function with respect to increasing η_{ij}^{l*} and will achieve its lowest value at the inferior boundary of the domain of variation of η_{ij}^{l*}. This result could have also been obtained by direct inspection of (7.7), and justifies replacing η_{ij}^{l*} by $\eta_{ij}^{l*\text{low}}$ in the graph cut strategy of the previous section (see Algorithm 7.1).

We can follow an analogous procedure to see the dependence of $E(t)$ with respect to the internal loss factor η_{jd}^{l*}. The expressions analogous to Eqs. (7.8)-(7.9) are

$$\partial_{\eta_{jd}^{l*}} E(t) \approx E_0'(s)\, \partial_{\eta_{jd}^{l*}} w_{ij}^{l*} \sum_{k=1}^{K} \sum_{n=1}^{N_k} w\left(P_{st,n}^{k-1}\right) \delta_{ln}, \tag{7.11}$$

with

$$\partial_{\eta_{jd}^{l*}} w_{ij}^{l*} = \frac{-\eta_{ji}^{l*}}{\left(\eta_{jd}^{l*} + \sum_{k\neq j} \frac{n_k}{n_j}\eta_{kj}\right)^2} = \frac{-\eta_{ij}^{l*}}{\left(\eta_j^{l*}\right)^2}. \tag{7.12}$$

Looking at (7.12) it is clear that (7.11) will be always negative and that the energy at the target in this case will be a monotonic decreasing function with respect to increasing η_{jd}^{l*}. Therefore, $E(t)$ will reach its lowest value at the superior boundary of the domain of variation of η_{jd}^{l*}, which justifies replacing η_{jd}^{l*} by $\eta_{jd}^{l*\text{up}}$ in the graph cut strategy.

In the case of a path crossing the same edge of the cutset, say m times, its weight will involve the mth power of this edge's weight $\left(w_{ij}^{l*}\right)^m$. Consequently, (7.8) and (7.11) will include terms of the type $m\left(w_{ij}^{l*}\right)^{m-1}\partial_{\eta_{ij}^{l*}} w_{ij}^{l*}$ and $m\left(w_{ij}^{l*}\right)^{m-1}\partial_{\eta_{jd}^{l*}} w_{ij}^{l*}$. Therefore, the same conclusions previously found for the easiest situation of just crossing the cutset once, will still apply.

If MISO and MIMO problems are considered, very similar results to those presented above are obtained, except for the fact that $\langle U_S, U_t\rangle$ and $\langle U_S, U_T\rangle$ cutsets are to be respectively taken into account. For instance, in a MISO case having N_s sources we will compute an $\{s_i\} - t$ cutset to separate the sources from the receiver. An analogous reasoning to that used for the SISO situation yields the following expansion for the energy at the latter

$$E(t) \approx \sum_{l=1}^{L} w_{h_i h_{i+1}}^{l*} \sum_{k=1}^{K}\sum_{n=1}^{N_k}\sum_{i=1}^{N_s} P_{s_i t,n}^{k-1}\delta_{ln} E_0'(s_i)\,. \tag{7.13}$$

Next, proceeding again as for the SISO case, it can be easily checked that the maximum energy reduction at the receiver will be achieved by replacing $\eta_{ij}^{l*} \longrightarrow \eta_{ij}^{l*\text{low}}$ and $\eta_{jd}^{l*} \longrightarrow \eta_{jd}^{l*\text{up}}$ in the weights of the $\{s_i\} - t$ cutset. These results also apply individually for any target in a MIMO problem if an $\{s_i\} - \{t_i\}$ cutset is considered. Moreover, similar conclusions can be derived if any linear combination of the energies at the targets is considered as the goal function to be decreased. The situation does not change if energy levels are used instead of energies, given that the logarithm is a monotonically increasing function.

7.4 NUMERICAL EXAMPLES: TWO MIMO CASES IN THE SEA MODELS OF TWO TEST BUILDINGS

7.4.1 *Case A*

7.4.1.1 *Model description and problem statement*

In this section we will consider a simplified SEA model of a building in order to test the performance of the previously described graph cut strategy in a more

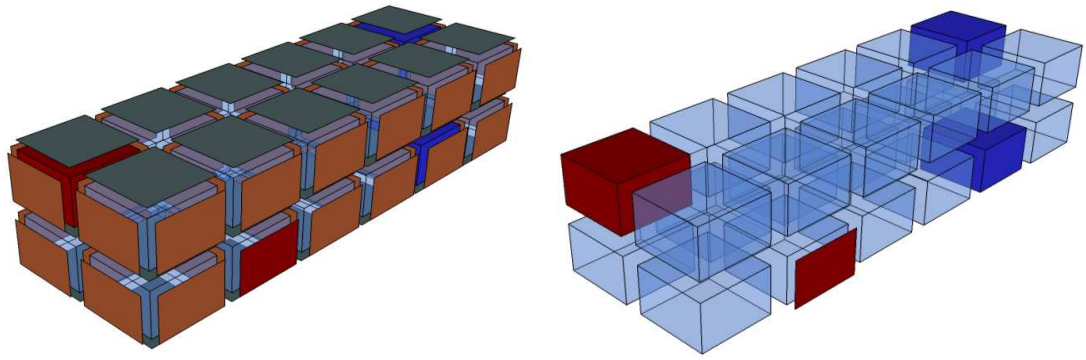

(a) SEA model subsystems (b) Source (left) and target (right) subsystems

Figure 7.3: Case A: 24 room building design modelled with SEA.

realistic situation. This model has been also used in Chapter 3 to test a procedure to rank energy transmission paths in SEA systems. The model (see Fig. 7.3a) consists of 24 identical rooms with dimensions $4 \times 4 \times 2.5$ (length$\times$width$\times$height). The room walls are made of a 7 cm hollow brick while the floors and roofs are made of a 15 cm concrete slab. Material properties are given in Table 3.2. For simplicity, no beams have been taken into account and the only structural waves that have been considered for plates (walls, floors and roofs) are bending waves. Therefore, each wall, floor and roof has been modelled as a single SEA subsystem. The SEA model has been built using the commercial software VA ONE.

We have considered the MIMO situation of having two source subsystems and two target subsystems. Concerning the former, two different type of sources have been taken into account: the first one corresponds to airborne excitation of a corner room placed at the second floor, and the second one corresponds to structure-borne excitation of a wall in the first floor (see Fig. 7.3b). The goal is to achieve at least a 10 dB reduction of the sound pressure level L_p at the two target room subsystems (see Fig. 7.3b), for each octave frequency band comprising the range from 125 Hz to 2 KHz.

7.4.1.2 *Graph cut approach and output results*

Once the new goal values for the sound pressure level at the two target rooms have been established, the next step for the noise control engineer is to consider which elements could be modified to achieve such results. That is to say the engineer has to define the various types of noise control treatments (NCT) that could be introduced in the model. This will allow to compute the new admissible threshold values for the loss factors η_{ij}^{low} and η_{id}^{up}. For the present example, the following NCTs have been considered.

Whenever a $\{s_i\} - \{t_j\}$ cutset involves an edge connecting two plates, the NCT will consist in inserting an elastic linear junction between them. The junction is made of an elasticized expanded polystyrene EEPS and its properties are listed

Table 7.2: *Material properties for noise control treatments (NCT)*

NCT	Thick-ness [m]	Width [m]	Dynamic stiffness [MN/m^3]	Poisson ratio
Elastic linear junction EEPS	0.0015	0.09	7	0.4

NCT	Surface density [kg/m^2]	Internal loss factor
Wall: PL(13)+GW(45)	11.25	0.01
Floor: PL(13)+GW(50)+AC(137)	11.35	0.01

in Table 7.2. The plate internal loss factors will not be modified. Although the NCT for plates may look rather unrealistic for a real building application, due to installation complexities, it will serve the purpose of illustrating the graph strategy performance.

On the other hand, an important practical point is to be noted concerning the above type of NCT, because the insertion of an elastic junction not only affects the coupling loss factors of the two connected plates in the graph cutset, but also the coupling loss factors of all other plates sharing the same linear junction. However, this problem can be easily solved by defining groups of loss factors $\{\eta_{ij}\}$ to be modified together. This has been the option implemented in this work; whenever a cutset affects one loss factor in the group, all remaining loss factors in the group get assigned their new admissible values. This situation will be quite common in practical cases and it is not only restricted to particular types of NCTs, such as the linear junction one. For instance, an acoustic engineer will rarely make use of different stiffeners for the acoustic floating floor of a railway coach or use different type of acoustic glasses for its windows, due to installation and economical constraints. Consequently, if it is recommendable to change some of them because they belong to a cutset, they can all be modified together.

In the case of the cutset involving an edge linking a plate and an air cavity, the noise control treatments to modify the coupling loss factors have consisted in building a double wall partition. A leaf made of plasterboard (PL) and glasswool (GW) has been assembled to the original plate, the solution being slightly different for the plate being a wall or a floor/roof (the latter also includes an acoustic chamber (AC)). Details for these NCTs are provided in Table 7.2, the number in parenthesis after the materials indicating their thickness in mm. In what concerns the modification of subsystem internal loss factors, it is assumed that the mean absorption coefficient of the rooms can be increased from 0.16 to 0.3.

Deciding the type and number of modifications that could be applied to a given SEA model will be, in general, strongly case dependent. In several realistic situations, the type of modifications to be carried out are quite limited and

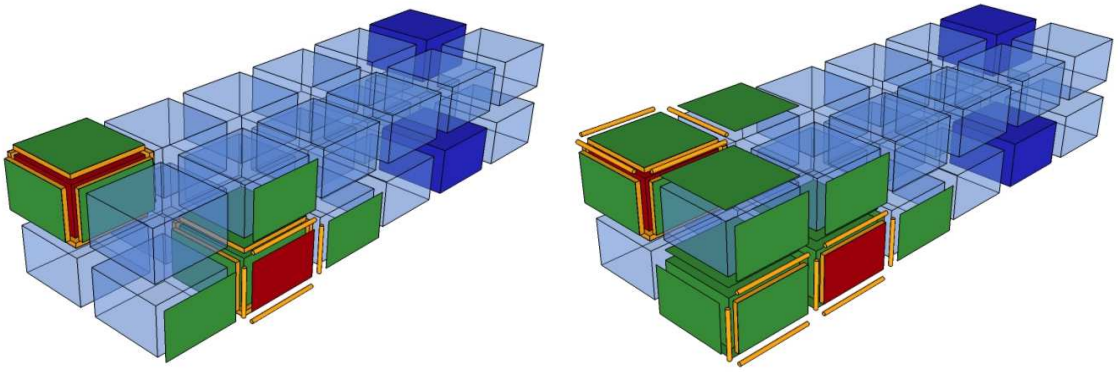

(a) Best union 18-cutset (15 NCTs involved) (b) Best union 26-cutset (19 NCTs involved)

Figure 7.4: Case A: $\{s_i\} - \{t_j\}$ cutsets with all subsystems involved and noise control treatments (NCT) included.

they can be easily determined a priori. However, in rather complex systems involving structural elements of a very different nature, it may be more difficult to determine a priori which modifications should be performed. For such cases, one could run the graph cut algorithm for the boolean SEA graph, without making any modification, and see which edges do appear in most cutsets. This will give a rough initial estimation on which subsystems will be worth acting upon.

All the above described NCTs will result in new admissible frequency dependent threshold values for the SEA model loss factors. The graph cut strategy then proceeds to find the cutsets for the SEA graphs associated to each frequency band that guarantee the expected 10 dB reduction for every band, and provides the results for the union of all them, as explained in the description of the graph cut strategy of subsection 3.1. The computation times in a regular PC (Intel Core 2 Quad CPU q9400 @2.66 GHz) for every band in analysis are shown in Table 7.3.

Band	Time
125 Hz	170.17 s
250 Hz	168.44 s
500 Hz	172.36 s
1000 Hz	166.50 s
2000 Hz	171.15 s

Table 7.3: *Computation times of Case A.*

The application of the graph cut strategy to the above described problem results in a final union cutset (see step 7 in Algorithm 7.1) of size 18, which supplies the desired sound pressure level reduction at the target subsystems. In

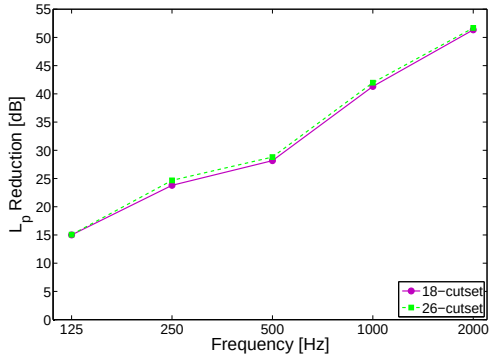

(a) L_p reduction at the first floor target subsystem

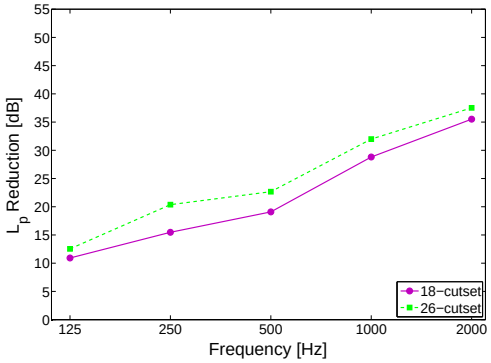

(b) L_p reduction at the second floor target subsystem

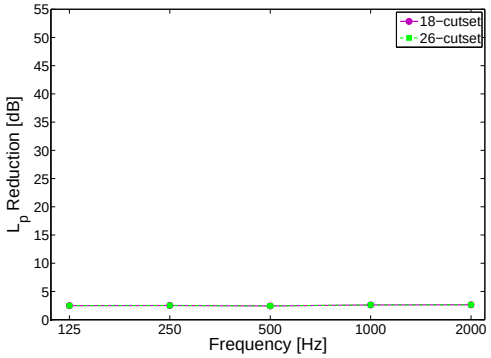

(c) L_p reduction at the airborne source subsystem

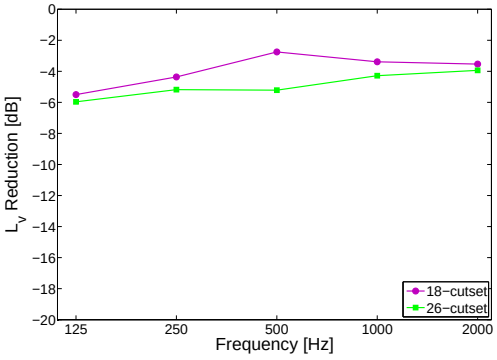

(d) L_v reduction at the structure-borne source subsystem

Figure 7.5: Case A: Reduction in dB at target and source subsystems with two different $\{s_i\} - \{t_j\}$ cutsets.

Fig. 7.4a we have plotted the subsystems in the building whose coupling and/or internal loss factors have become modified by this cutset. The corresponding noise control treatments have been also drawn. As observed, the cutset involves subsystems near the sources but these are not connected one to the other as it was the case for the sources in the numerical example of Section 7.3.2. On the other hand, given that the L_p reduction for one of the targets at 125 Hz hardly exceeds 10 dB (see Fig. 7.5b), we have also shown the results of the next higher order cutset for comparison. This is the 26-cutset plotted in Fig. 7.4b. It can be noticed from Fig. 7.4 that the size of a cutset does not necessarily coincide with the number of NCTs to be made. This is so because the size of a cutset is given by half the number of the modified coupling loss factors, whereas a single NCT may involve changing several pairs of coupling loss factors (e.g., a line junction). For instance, the 18-cutset in Fig. 7.4a involves 15 NCTs (11 double wall partitions + 4 elastic line junctions), while the 26-cutset in Fig. 7.4b involves 19 NCTs (8 double wall partitions + 11 elastic line junctions).

The sound pressure level L_p and velocity level L_v reductions obtained for the target and source subsystems, once made the modifications of the SEA graph cutset, are given in Fig. 7.5. Fig. 7.5a presents the L_p reduction obtained at the target room in the first floor. As observed, both the 18 and 26-cutsets yield very similar results, the latter being only slightly superior. The reduction increases from almost 15 dB at the 125 Hz octave band to 50 dB at the 2KHz octave band (note that this concerns the present simplified example, in a real situation such strong reductions may not be achieved). The L_p reduction for the target subsystem in the second floor is shown in Fig. 7.5b. In this case the 26-cutset performs clearly better than the 18-cutset and ensures a reduction larger than 10 dB for every octave band. Therefore, both, the 18 and 26-cutset suffice to achieve the goal of diminishing the L_p more than 10 dB for every target and at every frequency.

In what concerns the source subsystems, we can observe for the airborne one that the L_p in the corresponding room subsystem also diminishes. This is due to the fact that it is included in the cutset and consequently, its absorption is increased to 0.3. Given that the acoustic treatment in the source room is almost identical for the 18 and 26-cutsets, the obtained reduction is the same for both cases, having an almost constant value between two and three dB (see Fig. 7.5c). Regarding the structure-borne source, it is to be noted that its velocity level L_v increases (negative reduction, see Fig. 7.5d and note that the vertical axis contains negative values) once the NCTs have been applied. This is due to the fact that elastic linear junctions are placed at all boundaries of the source wall. Thus, a strong percentage of the external energy input at the wall cannot be transmitted to contiguous subsystems. As we have not included the possibility of increasing the internal loss factor of plates, this energy cannot be dissipated and, as a result, the L_v of the source wall increases. The increase in velocity level is stronger (more negative) for the 26-cutset than for the 18-cutset as shown in Fig. 7.5d, because the former is more efficient than the second.

7.4.2 *Case B*

In this case, the characteristics of the building are the same than in the previous case but the rooms are disposed in a different configuration. As it can be observed in Figure 7.6, the building consists of a pair of two floor blocks with four rooms per floor, connected by means of two additional rooms at the first level. The rooms have the same dimensions and properties than in Case A (see Table 3.2).

Our goal is to diminish the SPL (Sound Pressure Level) at two target rooms of the right hand side block in Figure 1, when noise is generated at two rooms of the left hand side block (see Figure 7.7 for source and target locations). We would like to achieve at least a 30 dB SPL reduction at the targets for each octave frequency band from 125 Hz to 2 KHz. The applicable noise control treatments are again those of the previous case, listed in Table 7.2. The algorithm

is performed in the selected frequency bands and the computation times are gathered in Table 7.4.

Band	Time
125 Hz	61.01 s
250 Hz	61.16 s
500 Hz	60.38 s
1000 Hz	61.89 s
2000 Hz	171.15 s

Table 7.4: *Computation times of Case B*

As a result of the strategy, a 9-cutset has been obtained that results in the expected SPL reduction at the target. The cutset involves five NCTs that can be observed in Figure 7.8a. The NCTs consist in inserting five elastic junctions at the borders of the wall separating the two block connection rooms, as well as treating the right hand side one. The plot in Figure 7.8a highlights all subsystems involved in the cutset. Although the 9-cutset already fulfills the expectative of reducing at least 30 dB for each octave frequency band, further cutsets have been computed for completeness. In Figure 7.8b, for example, we have plotted the best union 22-cutset which involves fourteen NCTs.

It can be observed in Figure 7.8 that the plotted cutsets directly involve the structure bottleneck (two connection rooms). Acting on it looks apparent for the present model if few subsystems are to be modified. However, bottlenecks may not be so easy to identify in more complex systems, and the graph cut strategy provides an automatic way to find them.

In Figures 7.9a and 7.9b the SPL reduction at both target rooms for the considered frequency range have been plotted. The first target Figure 7.9a is the room above the row including the connection rooms. For each room, the results corresponding to three different cutsets have been included. These correspond to the best union 9, 22 and 27-cutsets, the best results being obtained

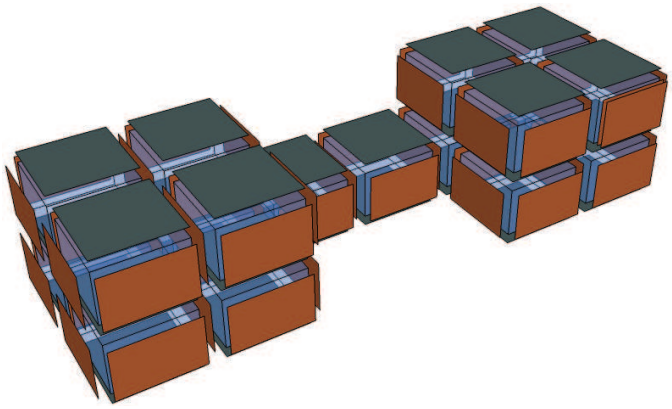

Figure 7.6: Case B: 18 room building design modelled with SEA.

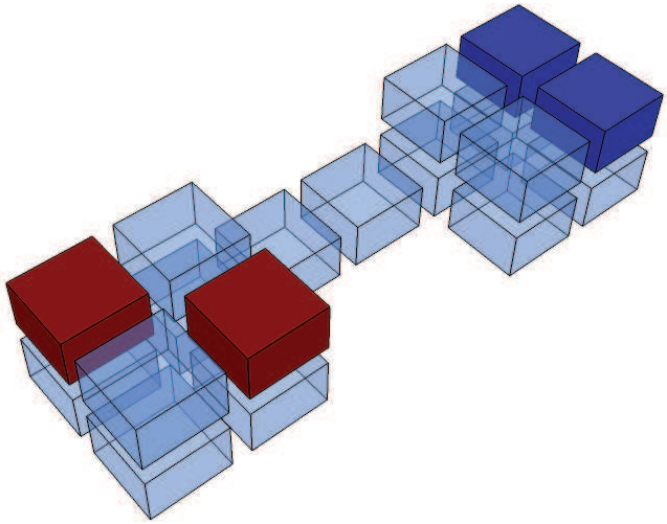

Figure 7.7: Case B: Source (red) and target (blue) room locations.

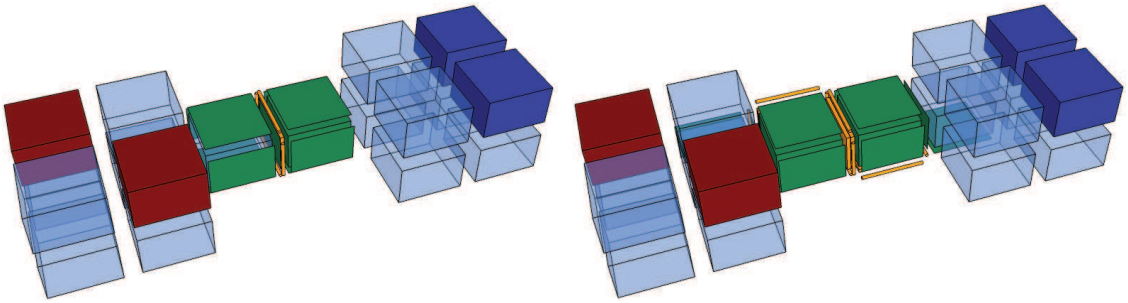

(a) Best union 9-cutset (5 NCTs involved) (b) Best union 22-cutset (14 NCTs involved)

Figure 7.8: Case B: $\{s_i\} - \{t_j\}$ cutsets with all subsystems involved and noise control treatments (NCT) included.

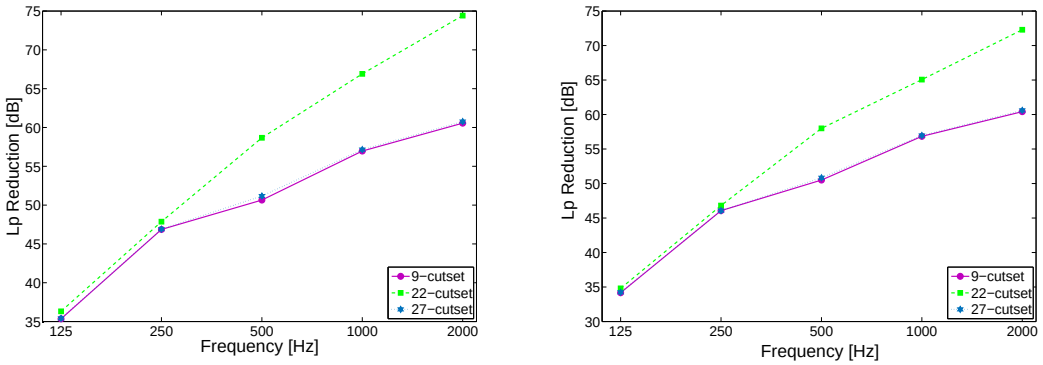

(a) L_p reduction at the first target subsystem (b) L_p reduction at the second target subsystem

Figure 7.9: Case B: Reduction in dB at the target subsystems with different $\{s_i\} - \{t_j\}$ cutsets.

by means of the 22-cutset for both targets (see Figure 7.9b). The fact that the

27-cutset performs worst than the 22-cutset is not strange with initial cutsets (see Section 7.4.1 and [Guasch and Cortés, 2009]), although the tendency is that higher reductions will be obtained as long as the size of the cutsets increase (the number of modified loss factors grows). As observed, the SPL reduction for the 22-cutset increases from 35 dB at the 125 Hz octave band to 73 dB at the 2 KHz octave band for the first target room. Similar results are obtained for the second target room.

7.5 CONCLUSIONS

Results from graph theory have been applied in this chapter to solve problems related to energy transmission paths in SEA models. In particular, it has been shown how a strategy based on the computation of graph cuts of increasing sizes can be adapted to diminish the energy transmitted from a set of source subsystems, to a set of target subsystems, in realistic frequency dependent SEA models. The key point of the strategy relies on the fact that all paths linking the sources and the targets have to cross a cutset. Therefore, the modification of the loss factors of all edges belonging to the cutset ensures that we are acting on all possible energy links between sources and targets. A mathematical justification for the performance of the strategy has been also provided.

To show the potential of the proposed approach for practical implementations, the vibroacoustic energy transmission in two simple but rather realistic SEA models of two buildings have been analysed. In the first case, the fact that the source and target subsets resulting from the partition of a SEA graph are not necessarily connected, allows to automatically modify loss factors from subsystems near the sources, even if these are quite separated apart. In the second case, the results show the possibility to detect bottlenecks in complex structures. This automatic selection of key subsystems in the energy transmission process can make the strategy very useful for noise control engineering in complex SEA systems.

8 CONCLUSIONS AND FURTHER WORK

8.1 CONCLUSIONS

In general terms, this dissertation has proposed an alternative computational approach to identify energy transmission paths in the vibroacoustic model of a mechanical system by means of graph theory algorithms. Numerical methods allow one to predict a system dynamic response but they do not describe how energy is propagated throughout it. By performing a transmission path analysis, one can determine how energy, injected by an external vibroacoustic source, is transmitted to every part of the system. This makes possible identifying how a possible noise and vibration problem in the system should be addressed.

The main outputs obtained throughout the development of this thesis are listed as follows.

- A link between graph theory and SEA has been established thanks to the definition of the SEA graph which accurately represents the SEA system.
- In some situations, a finite group of paths governs the energy transmission between a source subsystem and a target subsystem. In such cases, the energy at the target subsystem can be approximated by the total contribution of a finite set of say, K dominant paths. The MPS graph algorithm has been adapted to efficiently rank the K most dominant energy transmission paths between a source subsystem and a target subsystem in a SEA model.
- The stochastic nature of SEA parameters has been taken into account when ranking energy transmission paths thanks to the introduction of the stochastic SEA graph.

  The stochastic SEA graph is a biparametric graph since it includes mean and variance values for every arc. This fact has implied performing some before the MPS algorithm can be applied to it.

  - A dominance condition has been stated in order to compare stochastic path contributions. This has required the using an utility function which involves both mean and variance values.
  - The biparametric graph has been transformed to an extended uniparametric graph in order to fulfill the optimality principle.

By means of two test cases, it has been shown that ignoring the stochastic nature of the loss factors in the path ranking can lead to the omission of not only important paths but also, influent subsystems.

- The graph theory path transmission approach has been extended to Energy Distribution models. The conditions that the inverse of the EIC matrix has to fulfill for this purpose have been evaluated. For the favourable cases, an ED graph has been defined.

- The graph approach has been also extended to SmEdA models. A definition of modal energy transmission paths in a SmEdA model has been proposed and the SmEdA graph has been characterized.

  The MPS algorithm has been applied to some SmEdA models. The evaluation of the list of the most dominant modal energy transmission paths has provided for instance, information on which kind of transmission, either resonant or non-resonant, predominates in a model; as well as the group of modes that contribute the most to the energy transmission.

- An automatic strategy to reduce the energy at a group of target subsystems in a SEA system by using graph cut algorithms has been developed. The algorithm provides the small number of modifications to apply in a system in order to obtain the desired energy reduction.

To conclude, the connection between graph theory and vibroacoustic models has shown to be a useful tool to resolve noise and vibration problems. The main advantage is that it provides direct methods to solve problems that up to the moment, had to be solved by means of intuition, expertise or laborious tasks.

8.2 FURTHER WORK

The use of graph theory in vibroacoustics is quite recent and therefore, the possible future work lines are numerous and spread in several directions. Some of them are next itemized.

- The algorithm to obtain the most dominant paths performs relatively fast for graphs of the order of some hundreds nodes, such as SEA and ED graphs. However, the construction of the tree of maximum paths based on the Dijsktra algorithm, becomes considerably slow for larger graphs (of the order of some thousands of nodes) such as the SmEdA graphs and the extended uniparametric graphs obtained from the stochastic SEA graphs. The algorithm should be optimized for these cases.

- The inclusion of the stochastic nature of the parameters should be considered also for SmEdA and ED models, since these are also statistical approaches.

- The utility functions used to determine the dominance condition of the transmission paths in the stochastic SEA graph have been chosen under gaussian probability density function assumptions. This might not be always the best choice and further investigation should be carried out.
- The loss factors in the stochastic SEA system have been assumed to be independent random variables to simplify the definition of the mean and variance values of the path contribution. The errors committed by this assumption should be evaluated and if non-admissible, better approximations of the probability density functions for these parameters should be used.
- The TPA algorithm which was initially developed for SEA systems, has been extended to ED and SmEdA models. However, the variety of mid-frequency methods is much wider. The feasibility of applying the graph theory approach to, for instance, hybrid FE-SEA models, should be evaluated.
- The graph cut strategy could be combined with other approaches, like classical sensitivity analysis, to avoid dealing with very big cut-sets.
- Algorithms to find cutsets constrained to pass through the set of higher sensitive subsystems in a SEA model could be also derived, to avoid undesirably energy redistribution.

8.3 PUBLICATIONS

8.3.1 *Academic journals*

- À. Aragonès and O. Guasch. Conditions for transmission path analysis in energy distribution models. *Mechanical Systems and Signal Processing* , Submitted, 2015b [Aragonès and Guasch, 2015b]
- À. Aragonès, L. Maxit, and O. Guasch. A graph theory approach to identify resonant and non-resonant transmission paths in statistical modal energy distribution analysis. *Journal of Sound and Vibration*, 350(0):91 – 110, 2015b. ISSN 0022-460X [Aragonès et al., 2015b]
- À. Aragonès and O. Guasch. Ranking paths in statistical energy analysis models with non-deterministic loss factors. *Mechanical Systems and Signal Processing* , 52–53:741–753, 2015a [Aragonès and Guasch, 2015a]
- O. Guasch, À. Aragonès, and M. Janer. A graph cut strategy for transmission path problems in statistical energy analysis. *Mechanical Systems and Signal Processing* , 30:343–355, 2011 [Guasch et al., 2011]

- O. Guasch and À. Aragonès. Finding the dominant energy transmission paths in statistical energy analysis. *Journal of Sound and Vibration*, 330(10): 2325 – 2338, 2011 [Guasch and Aragonès, 2011]

8.3.2 *Conference proceedings*

- À. Aragonès, L. Maxit, and O. Guasch. Computation of modal energy transmission paths in SmEdA using graph theory algorithms. In *NOVEM2015: Dubrovnik (Croatia), 13-15 April, Noise and Vibration: Emerging Methods*, 2015a [Aragonès et al., 2015a]

- O. Guasch and À. Aragonès. Graph theory applications for noise and vibration transmission path problems in Statistical Energy Analysis models. In *Acústica 2012: VIII Congresso Ibero-americano de Acústica, October 1-3, Évora (Portugal)*, 2012 [Guasch and Aragonès, 2012]

- À. Aragonès and O. Guasch. Considering the stochastic nature of loss factors to classify energy transmission paths in SEA. In *Proceedings of the Nineteenth International Congress on Sound and Vibration ICSV19, Vilnius, Lithuania, 2012.*, July 2012 [Aragonès and Guasch, 2012]

- O. Guasch and À. Aragonès. Ranking energy paths in a SEA model. In *Proceedings of 20th International Congress on Acoustics ICA 2010, Sidney, Australia, 2010*, 2010 [Guasch and Aragonès, 2010]

- O. Guasch, À. Aragonès, and M. Janer. Graph cuts to reduce energy transmission in the sea model of a building. In *Proceedings of Inter-Noise 2010, June 13-16, Lisbon (Portugal)*, 2010 [Guasch et al., 2010]

- O. Guasch, L. Cortés, and À. Aragonès. Graph cuts applied to transmission path problems in Statistical Energy Analysis models. In B.R. Mace, N.S. Ferguson, and E. Rustighi, editors, *NOVEM2009, on the CD-ROM: Oxford (UK), 5-8 April, Noise and Vibration: Emerging Methods*, 2009 [Guasch et al., 2009]

BIBLIOGRAPHY

À. Aragonès and O. Guasch. Considering the stochastic nature of loss factors to classify energy transmission paths in SEA. In *Proceedings of the Nineteenth International Congress on Sound and Vibration ICSV19, Vilnius, Lithuania, 2012.*, July 2012.

À. Aragonès and O. Guasch. Ranking paths in statistical energy analysis models with non-deterministic loss factors. *Mechanical Systems and Signal Processing* , 52–53:741–753, 2015a.

À. Aragonès and O. Guasch. Conditions for transmission path analysis in energy distribution models. *Mechanical Systems and Signal Processing* , Submitted, 2015b.

À. Aragonès, L. Maxit, and O. Guasch. Computation of modal energy transmission paths in SmEdA using graph theory algorithms. In *NOVEM2015: Dubrovnik (Croatia), 13-15 April, Noise and Vibration: Emerging Methods*, 2015a.

À. Aragonès, L. Maxit, and O. Guasch. A graph theory approach to identify resonant and non-resonant transmission paths in statistical modal energy distribution analysis. *Journal of Sound and Vibration*, 350(0):91 – 110, 2015b. ISSN 0022-460X.

J. Azevedo, M. E. O. Santos Costa, J. E. Silvestre Madeira, and E. Vieira Martins. An algorithm for the ranking of shortest paths. *European Journal of Operational Research*, 69(1):97–106, 1993.

E. Balmes, J. Bianchi, and J. Leclère. Structural dynamics toolbox & FEMLink, User's guide. *SDTools, Vibration Software and Consulting*, 2011.

T. Bartosch and T. Eggner. Engine noise potential analysis for a trimmed vehicle body: Optimization using analytical SEA gradient computation technique. *Journal of Sound and Vibration*, 300 (1-2):1–12, 2007.

N. Beaulieu, A. Abu-Dayya, and P. McLane. Estimating the distribution of a sum of independent lognormal random variables. *IEEE Transactions on Communications*, 43(12):2869, 1995.

J. Bendat. System identification from multiple input/output data. *Journal of Sound and Vibration*, 49(3):293 – 308, 1976a.

J. Bendat. Solutions for the multiple input/output poblem. *Journal of Sound and Vibration*, 44(3):311 – 325, 1976b.

M. Beshara and A. Keane. Statistical energy analysis of multiple, non-conservatively coupled systems. *Journal of sound and vibration*, 198(1):95–122, 1996.

D. Bies and S. Hamid. In situ determination of loss and coupling loss factor by the power injection method. *Journal of Sound and Vibration*, 70 (2):187–204, 1980.

C. B. Burroughs, R. W. Fischer, and F. R. Kern. An introduction to statistical energy analysis. *The Journal of the Acoustical Society of America*, 101(4):1779–1789, 1997.

R. Büssow and B. Petersson. Path sensitivity and uncertainty propagation in SEA. *Journal of Sound and Vibration*, 300 (3-5):479–489, 2007.

Carré, B.A. *Graphs and Networks*. Oxford Applied Mathematics and Computing Science Series, Oxford University Press, Oxford, 1979.

C.H Hodges, P. Nash and J. Woodhouse. Measurement of coupling loss factors by matrix fitting: an investigation of numerical procedures. *Applied Acoustics*, 22:47–69, 1987.

A. Chavan and D. Manik. Design sensitivity analysis of statistical energy analysis models using Transfer Path Approach. *Electronic Journal "Technical Acoustics" <http://www.ejta.org>*, 3, 2005.

V. Cotoni, R. Langley, and M. Kidner. Numerical and experimental validation of variance prediction in the statistical energy analysis of built-up systems. *Journal of Sound and Vibration*, 288(3):701–728, 2005.

V. Cotoni, P. Shorter, and R. Langley. Numerical and experimental validation of a hybrid finite element-statistical energy analysis method. *The Journal of the Acoustical Society of America*, 122(1):259–270, 2007.

R. Craik. The noise reduction of the acoustic paths between two rooms interconnected by a ventilation duct. *Applied Acoustics*, 12(3):161–179, 1979.

R. Craik. Sound transmission paths through a Statistical Energy Analysis model. *Applied Acoustics*, 30:45–55, 1990.

R. Craik. *Sound Transmission Trough Buildings Using Statistical Energy Analysis*. Gower, London, 1996.

R. Craik. The contribution of long flanking paths to sound transmission in buildings. *Applied Acoustics*, 62:29–46, 2001.

A. Culla, W. D'Ambrogio, and A. Fregolent. Parametric approaches for uncertainty propagation in SEA. *Mechanical Systems and Signal Processing* , 25(1): 193–204, 2011.

Davis, E.B. . By air by sea. In *Noise-Con 04, on the CD-ROM: Dearborn, Michigan, July 28-20, The 2008 National Conference on Noise Control Engineering (ISBN: Nc08, available from INCE-USA)*, 2008.

S. De Rosa and F. Franco. A scaling procedure for the response of an isolated system with high modal overlap factor. *Mechanical Systems and Signal Processing*, 22(7):1549 – 1565, 2008.

S. De Rosa and F. Franco. On the use of the asymptotic scaled modal analysis for time-harmonic structural analysis and for the prediction of coupling loss factors for similar systems. *Mechanical Systems and Signal Processing*, 24(2): 455–480, 2010.

E. Deckers, O. Atak, L. Coox, R. D'Amico, H. Devriendt, S. Jonckheere, K. Koo, B. Pluymers, D. Vandepitte, and W. Desmet. The wave based method: An overview of 15 years of research. *Wave Motion*, 51(4):550 – 565, 2014. Innovations in Wave Modelling.

E. Denardo and B. Fox. Shortest route methods: reaching, pruning and buckets. *Operations Research*, 27:161–186, 1979.

L. Deng and M. Wong. An exact algorithm for the statistical shortest path problem. In *Asia and South Pacific Conference on Design Automation, Yokohama, Japan, 2006.*, 2006.

N. Deo and C. Pang. Shortest path algorithms: taxonomy and annotation. *Networks*, 9:275–323, 1979.

W. Desmet. *A wave based prediction technique for coupled vibro-acoustic analysis*. PhD thesis, Katholieke Universiteit Leuven, Belgique, 1998.

C. Díaz-Cereceda. *Efficient models for building acoustics: combining deterministic and statistical methods*. PhD thesis, Universitat Politècnica de Catalunya, November 2013.

C. Díaz-Cereceda, J. Poblet-Puig, and A. Rodríguez-Ferran. Automatic subsystem identification in statistical energy analysis. *Mechanical Systems and Signal Processing*, 54 - 55(0):182 – 194, 2015.

R. Diestel. *Graph Theory*. Graduate Texts in Mathematics. Springer-Verlag, Heidelberg, 2005.

E. Dijkstra. A note on two problems in connection with graphs. *Num. Math.*, 1: 269–271, 1959.

M. Dinsmore and R. Unglenieks. Acoustical optimization using quasi-Monte Carlo methods and SEA modelling. In *SAE 2005 Noise and Vibration Conference and Exhibition, May 2005, Grand Traverse, MI, USA, Paper 2005-01-2431 (available online at www.sae.org/technical/papers/2005-01-2431, date last viewed 04/30/2009)*, 2005.

C. Dodds and J. Robson. Partial coherence in multivariate random processes. *Journal of Sound and Vibration*, 42(2):243 – 249, 1975.

S. Dreyfus. An appraisal of some shortest path algorithms. *Operations Research*, 17:395–412, 1969.

D. Eppstein. Finding the k shortest paths. *SIAM Journal on computing*, 28:652–673, 1998.

F. Fahy. An alternative to the SEA coupling loss factor: rationale and method for experimental determination. *Journal of Sound and Vibration*, 214(2):261 – 267, 1998.

F. Fahy and A. Mohammed. A study of uncertainty in applications of SEA to coupled beam and plate systems, part I: computational experiments. *Journal of Sound and Vibration*, 158(1):45–67, 1992.

L. Ford and D. Fulkerson. Maximal flow through a network. *Canadian Journal of Mathematics*, 8:399–404, 1956.

M. Fredman and R. Tarjan. Fibonacci heaps and their uses in improved network optimization algorithms. *Journal of the ACM*, 34:596–615, 1987.

C. Fredö. A sea-like approach for the derivation of energy flow coefficients with a finite element model. *Journal of Sound and Vibration*, 199(4):645–666, 1997.

L. Galbrun. The prediction of airborne sound transmission between two rooms using first-order flanking paths. *Applied Acoustics*, 69 (12):1332–1342, 2008.

J. Gross and J. Yellen. *Graph theory and its applications*. CRC Press series on discrete mathematics and its applications, Boca Raton, Florida, 1999.

J. L. Gross, J. Yellen, and P. Zhang. *Handbook of Graph Theory*. CRC Press, 2013.

O. Guasch. Direct transfer functions and path blocking in a discrete mechanical system. *Journal of Sound and Vibration*, 321 (3-5):854–874, 2009.

O. Guasch. A direct transmissibility formulation for experimental statistical energy analysis with no input power measurements. *Journal of Sound and Vibration*, 330(25):6223–6236, Dec. 2011.

O. Guasch and À. Aragonès. Ranking energy paths in a SEA model. In *Proceedings of 20th International Congress on Acoustics ICA 2010, Sidney, Australia, 2010*, 2010.

O. Guasch and À. Aragonès. Finding the dominant energy transmission paths in statistical energy analysis. *Journal of Sound and Vibration*, 330(10):2325 – 2338, 2011.

O. Guasch and À. Aragonès. Graph theory applications for noise and vibration transmission path problems in Statistical Energy Analysis models. In *Acústica 2012: VIII Congresso Ibero-americano de Acústica, October 1-3, Évora (Portugal)*, 2012.

O. Guasch and L. Cortés. Graph theory applied to noise and vibration control in statistical energy analysis models. *The Journal of the Acoustical Society of America*, 125 (6):3657–3672, 2009.

O. Guasch and F. Magrans. The Global Transfer Direct Transfer method applied to a finite simply supported elastic beam. *Journal of Sound and Vibration*, 276 (1-2):335–359, 2004.

O. Guasch, L. Cortés, and À. Aragonès. Graph cuts applied to transmission path problems in Statistical Energy Analysis models. In B.R. Mace, N.S. Ferguson, and E. Rustighi, editors, *NOVEM2009, on the CD-ROM: Oxford (UK), 5-8 April, Noise and Vibration: Emerging Methods*, 2009.

O. Guasch, À. Aragonès, and M. Janer. Graph cuts to reduce energy transmission in the sea model of a building. In *Proceedings of Inter-Noise 2010, June 13-16, Lisbon (Portugal)*, 2010.

O. Guasch, À. Aragonès, and M. Janer. A graph cut strategy for transmission path problems in statistical energy analysis. *Mechanical Systems and Signal Processing* , 30:343–355, 2011.

J. Guyader, C. Boisson, and C. Lesueur. Energy transmission in finite coupled plates, part I: theory. *Journal of Sound and Vibration*, 81(1):81–92, 1982.

H. He, J. Pan, and A. Luebke. From complex vehicle requirements to component design - A case study of sound package early development using SEA genetic optimization and system engineering. In *SAE 2005 Noise and Vibration Conference and Exhibition, May 2005, Grand Traverse, MI, USA, Paper 2005-01-2434 (available online at www.sae.org/technical/papers/2005-01-2434, date last viewed 04/30/2009)*, 2005.

C. H. Hodges and J. Woodhouse. Confinement of vibration by one-dimensional disorder, I: theory of ensemble averaging. *Journal of Sound and Vibration*, 130 (2):237–251, 1989.

C. Hopkins. Statistical energy analysis of coupled plate systems with low modal density and low modal overlap. *Journal of Sound and Vibration*, 251(2):193–214, 2002.

C. Hopkins. *Sound Insulation*. Butterworth-Heinemann, 2007.

C. Hopkins. Experimental statistical energy analysis of coupled plates with wave conversion at the junction. *Journal of Sound and Vibration*, 322:155–166, 2009.

U. Huckenbeck. *Extremal paths in graphs: foundations, search strategies, and related topics*. Akademie Verlag, Berlin, 1997. ISBN 9783055016585.

T. J. Hughes. *The Finite Element Method: Linear Static and Dynamic Finite Element Analysis*. Courier Corporation, 2000.

K. R. Hutson and D. R. Shier. Extended dominance and a stochastic shortest path problem. *Computers and Operations Research*, 36(2):584–596, 2009.

H. D. Hwang, K. Ege, L. Maxit, N. Totaro, and J. Guyader. Equivalent damping modelling in the framework of SmEdA. In *Proceedings of XIX-th symposium VIbrations, SHocks & NOise (VISHNO)*, Aix en Provence, France, June 2014.

P. Hynna, P. Klinge, and J. Vuoksinen. Prediction of structure-borne sound transmission in large welded ship structures using statistical energy analysis. *Journal of Sound and Vibration*, 180(4):583–607, 1995.

F. Ihlenburg. *Finite element analysis of acoustic scattering*, volume 132. Springer Science & Business Media, 1998.

X. Ji. Models and algorithm for stochastic shortest path problem. *Applied Mathematics and Computation*, 170(1):503–514, 2005.

H. Koruk and K. Sanliturk. Assesment of the complex eigenvalue and the modal strain energy methods for damping predictions. In *Proceedings of 18th International Congress on Sound and Vibration*, Rio De Janerio, Brazil, 2011.

N. Kumar and S. Singh. Experimental study on vibration and damping of curved panel treated with constrained viscoelastic layer. *Composite Structures*, 92(2):233 – 243, 2010.

T. Lafont, N. Totaro, and A. Le Bot. Review of statistical energy analysis hypotheses in vibroacoustics. *Proceedings of the Royal Society A: Mathematical, Physical and Engineering Science*, 470(2162):20130515, 2014.

R. Langley. A general derivation of the statistical energy analysis equations for coupled dynamic systems. *Journal of Sound and Vibration*, 135(3):499–508, 1989.

R. Langley and V. Cotoni. Response variance prediction in the Statistical Energy Analysis of built-up systems. *The Journal of the Acoustical Society of America*, 115:706–718, 2004.

R. Langley and K. Heron. Elastic wave transmission through plate/beam junctions. *Journal of Sound and Vibration*, 143(2):241 – 253, 1990.

R. Langley, J. Legault, J. Woodhouse, and E. Reynders. On the applicability of the lognormal distribution in random dynamical systems. *Journal of Sound and Vibration*, 332(13):3289–3302, June 2013.

R. S. Langley and J. A. Cordioli. Hybrid deterministic-statistical analysis of vibro-acoustic systems with domain couplings on statistical components. *Journal of Sound and Vibration*, 321(3–5):893 – 912, 2009.

R. S. Langley and P. J. Shorter. The wave transmission coefficients and coupling loss factors of point connected structures. *The Journal of the Acoustical Society of America*, 113(4):1947–1964, 2003.

A. Le Bot and V. Cotoni. Validity diagrams of statistical energy analysis. *Journal of Sound and Vibration*, 329:221–235, 2010.

M. Lenzi, G. Stigliano, S. Donders, B. Pluymers, and W. Desmet. New insights of an energy flow visualization into vehicle design. In *Proceedings of the ISMA2010 International Conference on Noise and Vibration Engineering*, pages 2025–2038, 2010.

R. Loui. Optimal paths in graphs with stochastic or multidimensional weights. *Communications of the ACM*, 26:670–676, 1983.

R. Lyon. In-plane contribution to structural noise transmission. *Noise Control Engineering Journal*, 26(1):22–27, 1986.

R. Lyon and R. DeJong. *Theory and Application of Statistical Energy Analysis*. RH Lyon Corp, Cambridge MA, 2nd Edition, 1998.

B. Mace. On the statistical energy analysis hypothesis of coupling power proportionality and some implications of its failure. *Journal of Sound and Vibration*, 178(1):95–112, 1994.

B. Mace. Statistical energy analysis, energy distribution models and system modes. *Journal of Sound and Vibration*, 264:391–409, 2003.

B. Mace. Statistical energy analysis: coupling loss factors, indirect coupling and system modes. *Journal of Sound and Vibration*, 279(1):141–170, 2005.

B. Mace and P. Shorter. Energy flow models from finite element analysis. *Journal of Sound and Vibration*, 233(3):369–389, 2000.

F. Magrans. Method of measuring transmission paths. *Journal of Sound and Vibration*, 74 (3):311–330, 1981.

F. X. Magrans. Definition and calculation of transmission paths within a SEA framework. *Journal of Sound and Vibration*, 165 (2):277–283, 1993.

C. Manohar and A. Keane. Statistics of energy flows in spring-coupled one-dimensional subsystems. *Philosophical Transactions of the Royal Society of London A: Mathematical, Physical and Engineering Sciences A*, 346(1681):525–542, 1994.

E. Martins. Deviation algorithms for ranking shortest paths. *European Journal of Operational Research*, 18:123–130, 1984.

E. Martins, M. Pascoal, and J. Santos. Deviation algorithms for ranking shortest paths. *International Journal of Foundations of Computer Science*, 10(3):247–261, 1999.

L. Maxit. *Extension et reformulation du modèle SEA par la prise en compte de la répartition des énergies modales (Extension and reformulation of SEA models considering the modal energy distribution)*. Ph.D. Thesis 2000 INSAL 0016, Institut National des Sciences Appliquées de Lyon, March 2000.

L. Maxit and J. Guyader. Estimation of SEA coupling loss factors using a dual formulations and FEM modal information – Part I: Theory. *Journal of Sound and Vibration*, 239(5):907 – 930, 2001a.

L. Maxit and J. Guyader. Estimation of SEA coupling loss factors using a dual formulations and FEM modal information – Part II: Numerical applications. *Journal of Sound and Vibration*, 239(5):931 – 948, 2001b.

L. Maxit and J. Guyader. Extension of SEA model to subsystems with non-uniform modal energy distribution. *Journal of Sound and Vibration*, 265(2):337 – 358, 2003.

L. Maxit, K. Ege, N. Totaro, and J. Guyader. Non resonant transmission modelling with statistical modal energy distribution analysis. *Journal of Sound and Vibration*, 333(2):499 – 519, 2014.

K. Menger. Zur allgemeinen Kurventheorie (On the general theory of curves). *Fundamenta Mathematicae*, 10(1):96–115, 1927.

S. Miaou and S. Chin. Computing *k*-shortest paths for nuclear spent fuel highway transportation. *European Journal of Operational Research*, 53:64–80, 1991.

D. C. Montgomery and G. C. Runger. *Applied Statistics and Probability for Engineers*. John Wiley & Sons, Hoboken, Mar. 2010.

I. Murthy and S. Sarkar. Exact algorithms for the stochastic shortest path problem with a decreasing deadline utility function. *European Journal of Operational Research*, 103(1):209–229, 1997.

H. Nagamochi, K. Nishimura, and T. Ibaraki. Computing all small cuts in an undirected network. *SIAM J. Discr. Math.*, 10(3):469–481, 1997.

A. Nilsson. Attenuation of structure-borne sound in superstructures on ships. *Journal of Sound and Vibration*, 55(1):71–91, 1977.

W. Park, D. Thompson, and N. Ferguson. Variability of the coupling loss factor between two coupled plates. *Journal of Sound and Vibration*, 279(3–5):557–579, 2005.

M. Petyt. *Introduction to finite element vibration analysis*. Cambridge university press, 2010.

R. Potter. Matrix formulation of multiple and partial coherence. *The Journal of the Acoustical Society of America*, 61(3):776 – 781, 1977.

R. Ming. An experimental comparison of the sea power injection method and the power coefficient method. *Journal of Sound and Vibration*, 282:1009–1023, 2005.

E. Roibás-Millán, M. Chimeno-Manguán, B. Martínez-Calvo, and J. López-Díez. Criteria for mathematical model selection for satellite vibro-acoustic analysis depending on frequency range. In *Proceedings of 12th European Conference on Space Structures, Materials and Enviromental Testing, Noordwijk, The Netherlands, 2012*, 2012.

J. Santos. K shortest path algorithms. In *The Ninth DIMACS Implementation Challenge: The Shortest Path Problem, DIMACS Center, Rutgers University, Piscataway, NJ (available online at www.dis.uniroma1.it/ challenge9/papers/santos.pdf, date last viewed 11/02/2010)*, 2006.

M. Sheng, M. Wang, and J. Sun. Effective internal loss factors and coupling loss factors for non-conservatively coupled systems. *Journal of Sound and Vibration*, 209(4):685 – 694, 1998.

P. Shorter and R. Langley. Vibro-acoustic analysis of complex systems. *Journal of Sound and Vibration*, 288(3):669 – 699, 2005.

P. W. Smith. Statistical models of coupled dynamical systems and the transition from weak to strong coupling. *The Journal of the Acoustical Society of America*, 65(3):695–698, 1979.

W. Stahel, R. Van Ligten, and J. Gillard. Measuring method to obtain the transmission paths and simultaneous real force contributions in a mechanical linear system. Technical report, 1980.

M. Stoer and F. Wagner. A simple min-cut algorithm. *Journal of the ACM*, 44(4): 585–591, 1997.

A. Subramanian. Two recent algorithms for the global minimum cut problem. *ACM SIGACT News*, 26(2):78–87, 1995.

G. Tanner. Dynamical energy analysis - determining wave energy distributions in vibro-acoustical structures in the high-frequency regime. *Journal of Sound and Vibration*, 320(45):1023 – 1038, 2009.

A. Thite and B. Mace. Robust estimation of coupling loss factors from finite element analysis. *Journal of Sound and Vibration*, 303(3 - 5):814 – 831, 2007.

A. Thite and B. Mace. The effects of design modifications on the apparent coupling loss factors in SEA-like analysis. *Journal of Sound and Vibration*, 329 (24):5194–5208, 2010.

N. Totaro and J. Guyader. SEA substructuring using cluster analysis: The MIR index. *Journal of Sound and Vibration*, 290(1 - 2):264 – 289, 2006.

N. Totaro and J. Guyader. Extension of the statistical modal energy distribution analysis for estimating energy density in coupled subsystems. *Journal of Sound and Vibration*, 331(13):3114 – 3129, 2012.

J. Tratch. Vibration transmission through machinery foundation and ship bottom structure. Master's thesis, Dep. Of Mech. Eng., Massachusetts Institute of Technology, 1985.

H. Tschudi. The force transmission path method: an interesting alternative concerning demounting tests. In *Unikeller Conference*, volume 91, page 1991, 1991.

E. Ungar and E. Kerwin Jr. Loss factors of viscoelastic systems in terms of energy concepts. *The Journal of the Acoustical Society of America*, 34(7):954–957, 1962.

R. S. Varga. *Matrix iterative analysis*, volume 1. Prentice Hall Series in Automatic Computations, Englewood Cliffs: Prentice-Hall, 1962.

J. W. Verheij. *Multi-path sound transfer from resiliently mounted shipboard machinery: experimental methods for analyzing and improving noise control*. PhD thesis, TU Delft, Delft University of Technology, 1982.

E. Wester and B. Mace. Statistical energy analysis of two edge-coupled rectangular plates: ensemble averages. *Journal of Sound and Vibration*, 193(4):793–822, 1996.

Wikipedia contributors. Tudor dynasty, 2015. URL `http://en.wikipedia.org/w/index.php?title=Tudor_dynasty&oldid=655158551`.

T. Wu. *Boundary element acoustics: Fundamentals and computer codes*, volume 7. Wit Pr/Computational Mechanics, 2000.

J. Yen. An algorithm for finding shortest routes from all source nodes to a given destination in general networks. *Quarterly of Applied Mathematics*, 27:526–530, 1970.

J. Yen. Finding the k shortest loopless paths in a network. *Management Science*, 17:712–716, 1971.

Q. Zhang and M. Sainsbury. The energy flow method for strongly coupled systems. In *Proceedings - SPIE The International Society for Optical Engineering*, volume 2, pages 1839–1845, 1999.

Q. Zhang, C. Wang, D. Wang, M. Qian, W. Nack, and P. Pamidi. Energy flow method for mid-frequency vibration analysis. Technical report, SAE Technical Paper, 2003.

Universitat Ramon Llull

Aquesta Tesi Doctoral ha estat defensada el dia ____ d _____ de ____

al Centre **Escola Tècnica Superior d'Enginyeria Electrònica i Informàtica La Salle**

de la Universitat Ramon Llull

davant el Tribunal format pels Doctors sotasignants, havent obtingut la qualificació:

President/a

_____

Vocal

_____

Vocal

_____

Vocal

_____

Secretari/ària

_____

Doctorand/a
Àngels Aragonès Martín

C. Claravall, 1-3
08022 Barcelona
Tel. 936 022 200
Fax 936 022 249
E-mail: urlsc@sec.url.es
www.url.es